The Use of Biomarker and Stable Isotope Analyses in Palaeopedology

Reconstruction of Middle and Late Quaternary Environmental and Climate History, with Examples from Mt. Kilimanjaro, NE Siberia and NE Argentina

Dissertation

zur Erlangung des Grades

Doktor der Naturwissenschaften

(Dr. rer. nat.)

an der

Fakultät Biologie/Chemie/Geowissenschaften

der Universität Bayreuth

vorgelegt von

Michael Zech

geb. am 13.05.1977 in Rosenheim

Bayreuth, Oktober 2006

Vollständiger Abdruck der von der Fakultät für Chemie, Biologie und Geowissenschaften der Universität Bayreuth genehmigten Dissertation zur Erlangung des Grades eines Doktors der Naturwissenschaften (Dr. rer. nat.).

Die Arbeiten zur vorliegenden Dissertation wurden im Zeitraum von Juni 2003 bis Oktober 2006 am Lehrstühl Geomorphologie (unter Leitung von Prof. Dr. L. Zöller) und an der Abteilungen für Bodenphysik (unter Betreuung von PD Dr. B. Glaser) der Universität Bayreuth durchgeführt.

Einreichung der Dissertation:	10. Oktober 2006
Tag des wissenschaftlichen Kolloquims:	29. Januar 2007

Erstgutachter:	Prof. Dr. L. Zöller
Zweitgutachter:	PD Dr. B. Glaser

Prüfungsausschuss:	Prof. Dr. G. Gebauer (Vorsitz)
	Prof. Dr. L. Zöller
	PD Dr. B. Glaser
	Prof. Dr. Y. Kuzyakov
	Prof. Dr. E. Matzner

Kontakt/communications: michael_zech@gmx.de

Verfügbar als PDF unter/available as PDF at: http://opus.up.uni-bayreuth.de

Dedicated to

my friends in need

Contents

I. Extended Summary

II. Cumulative Study

Study 1: Evidence for Late Pleistocene climate changes from buried soils on the southern slopes of Mt. Kilimanjaro, Tanzania

Study 2: Multi-proxy analytical characterization and palaeoclimatic interpretation of the Tumara Palaeosol Sequence, NE Siberia

Study 3: A 240,000-year stable carbon and nitrogen isotope record from a loess-like palaeosol sequence in the Tumara Valley, Northeast Siberia

Study 4: Reconstruction of NE Siberian vegetation history based on cuticular lipid biomarker and pollen analyses

Study 5: Late Quaternary environmental changes in Misiones, subtropical NE Argentina, deduced from multi-proxy geochemical analyses in a palaeosol-sediment sequence

Study 6: Improved compound-specific δ¹³C analysis of n-alkanes for the application in palaeoenvironmental studies

List of Tables

List of Figures

List of Abbreviations

^{12}C	stable carbon atom with atomic mass 12
^{13}C	stable carbon atom with atomic mass 13
^{14}C	radioactive carbon atom with atomic mass 14
^{14}N	stable nitrogen atom with atomic mass 14
^{15}N	stable nitrogen atom with atomic mass 15
a.s.l.	above see level
Ab horizon	buried topsoil horizon
Ah horizon	humic-rich mineral topsoil horizon
Arg. D4	the investigated sediment core, which was taken in a shallow basin in the Province of Misiones, NE Argentina
ASE	Accelerated Solvent Extraction
Asp	aspartic acid (amino acid)
BC	Black carbon
BP	before present (1950)
C3	photosynthetic pathway of trees and most grasses and herbs in temperate and boreal environments
C4	photosynthetic pathway of many savanna grasses
CAM	Crassulacean Acid Metabolism
CF-IRMS	Continuous-Flow Isotope Ratio Mass Spectrometry
CSIA	Compound-Specific Isotope Analysis
D-/L-amino acid	chiral amino acid enantiomers (dextro/levo)
d_{42}-n-C_{20}	deuterated n-eicosane (alkane) standard
d_{50}-n-C_{24}	deuterated n-tetracosane (alkane) standard
F	correction factor for amount dependence
FID	Flame Ionization Detector
GC-C-IRMS	Gas Chromatography-Combustion-Isotope Ratio Mass Spectrometer
GC-MS	Gas Chromatography-Mass Spectrometer
H	humins (alkali insoluble substances)
HA	humic acids (alkali soluble substances)
HI	Hydrogen Index
ITCZ	InterTropical Convergence Zone

IPCC	International Panel of Climate Change
IRSL	InfraRed Stimulated Luminescence
KOH	sodium hydroxid
LGM	Last Glacial Maximum
Lys	lysine (amino acid)
MeOH	methanol
MIS	Marine Isotope Stage
m/z	mass/charge
n-alkane	unbranched hydrocarbon
nC_{xy}	unbranched alkane with xy carbon atoms
NGRIP	North GReenland Icecore Project
OEP	Odd-over-Even Preference
OI	Oxygen Index
OM	Organic Matter
R	correlation coefficient
R_{sample} and $R_{standard}$	ratio of a heavier to a lighter isotope in a sample or a standard, respectively
SASM	South American Summer Monsoon
SOM	Soil Organic Matter
TOC	Total Organic Carbon
TPS	the investigated loess-like palaeosol sequence in the Tumara Valley, NE Siberia
$\delta^{13}C$	natural abundance of ^{13}C
$\delta^{13}C_{TOC}$	natural abundance of ^{13}C in bulk soil organic matter
$\delta^{15}N$	natural abundance of ^{15}N

Summary

Palaeosols are important terrestrial archives for the reconstruction of the Quaternary landscape and climate history. In order to derive reliable information from these archives about sedimentation, vegetation and climate history, various methods and proxies are traditionally applied, e.g. texture analysis, numeric dating methods and mineral analysis. The aim of this dissertation is to evaluate the potential of biomarker and stable isotope analyzes. Specifically, I focused on plant leaf wax-derived n-alkanes, amino acid enantiomers, stable carbon and nitrogen isotopes ($\delta^{13}C_{TOC}$ and $\delta^{15}N$) in bulk soil organic matter (SOM) and on compound-specific isotope analysis (CSIA) of n-alkanes. The respective methods were partly optimized and then applied in multi-proxy analytical approaches to three selected different palaeosol records, representing different ecological environments: (i) The palaeosol sequences on the southern slopes of Mt. Kilimanjaro, Tanzania, (ii) a loess-like palaeosol sequence in the Tumara Valley (Tumara Palaeosol Sequence = TPS) in the forelands of the Verkhoyansk Mountains, NE Siberia, and (iii) a palaeosol sediment sequence (Arg. D4) sampled in a small basin in the Province of Misiones, subtropical NE Argentina.

In all three study areas, long-chain n-alkane ratios, nC_{31}/nC_{27} and $(nC_{31} + nC_{29})/nC_{27}$, respectively, proved to be straightforward biomarker proxies for the reconstruction of the terrestrial palaeovegetation at plant community level (especially grasses and herbs versus trees). On the contrary, the short- and mid-chain n-alkanes ($nC_{17} - nC_{19}$ and $nC_{20} - nC_{25}$, respectively) were successfully used for detecting algal- and aquatic macrophyte-derived organic matter (OM) in the sediment core Arg. D4, pointing to lacustrine conditions having prevailed temporarily before ~40 ka BP and during the Late Glacial.

Amino acid enantiomers as nitrogen (N) biomarkers allowed a further characterization of the SOM in the Tumara Palaeosol Sequence: On the one hand, the depth functions of D/L-aspartic acid (Asp) and D/L-lysine (Lys) could be roughly described by exponential fits, reflecting SOM aging. On the other hand, brown interglacial/-stadial palaeosols generally revealed higher D/L-ratios than dark gray glacial palaeosols. This finding suggests that D/L-aspartic acid and D/L-lysine may serve as palaeotemperature proxies.

In the Arg. D4 record, $\delta^{13}C_{TOC}$ varied in a wide range (from -30.1‰ to -17.4‰), indicating C3-C4 vegetation changes and hence allowing a reconstruction of the palaeovegetation. However, the natural abundance of ^{13}C was no straightforward proxy for the interpretation of the palaeosol sequences on Mt. Kilimanjaro and in the Tumara Valley. There, the interpretation of smaller $\delta^{13}C_{TOC}$ variations – assumed to be independent of C3-C4

vegetation changes – needed multi-proxy analytical approaches for disentangling the various possibly influencing environmental factors: On Mt. Kilimanjaro, $\delta^{13}C_{TOC}$ is higher in palaeosols, which developed under ericaceous vegetation ($\sim$ -25‰) compared to those developed under tropical montane forests ($\sim$ -27‰), suggesting that such vegetation changes are responsible for the observed $\delta^{13}C_{TOC}$ pattern. In the Tumara Palaeosol Sequence, $\delta^{13}C_{TOC}$ correlates negatively with total organic carbon (TOC) and TOC/N. As both parameters may serve as proxies for SOM decomposition, it is assumed that degradation processes have contributed significantly to this $\delta^{13}C_{TOC}$ record. Furthermore, also changing water stress conditions for the plants could have played a crucial role for $\delta^{13}C_{TOC}$ in the Tumara Palaeosol Sequence.

In contrast to $\delta^{13}C_{TOC}$, $\delta^{15}N$ in the Tumara Palaeosol Sequence does not correlate with any of the other SOM characterizing parameters (TOC, TOC/N and $\delta^{13}C_{TOC}$). Although other processes than SOM decomposition like (i) denitrification, (ii) N fixation, (iii) N losses by frequent fire events, and (iv) changes in the atmospheric ^{15}N deposition are discussed as factors contributing to an open N cycle, $\delta^{15}N$ in the Tumara Palaeosol Sequence seems not to be a straightforward proxy.

The compound-specific $\delta^{13}C$ analysis (CSIA) of n-alkanes was optimized and applied to selected samples from the Arg. D4 record. The highly significant correlations of the compound-specific isotope results (for long-chain n-alkanes) with $\delta^{13}C_{TOC}$ corroborate the reliability of the $\delta^{13}C_{TOC}$ vegetation proxy. Furthermore, the increasing $\delta^{13}C$ amplitudes from nC_{27} to nC_{33} validate the origin of these biomarker molecules, with nC_{27} and nC_{29} mainly deriving from C3 trees and shrubs and nC_{31} and nC_{33} mainly deriving from C3 or C4 grasses and herbs.

In summary, multi-proxy analytical approaches (especially biomarker and stable isotope analyzes in combination with numeric data) enabled detailed reconstructions of the Middle and Late Quaternary palaeoenvironmental changes in the three climatically different study areas:

Accordingly, the deep black palaeosols on the southern slopes of Mt. Kilimanjaro reflect periods of climatic deterioration during the Last Glacial Maximum (LGM) and the Late Glacial, which coincided with a descent of the ericaceous vegetation belt. Even older palaeosols document that such events also occurred during the Marine Isotope Stages (MIS) 3 and 4.

The palaeopedologic findings from the Tumara Palaeosol Sequence suggest that the dark gray and brown stratigraphic units of this record describe alternating glacial and interglacial/-stadial periods. Despite of uncertainties concerning the numeric data, the comparison with other northern hemispheric records and the regional glacial and geomorphologic history indicate that the Tumara Palaeosol Sequence spans the last ~240 ka.

The stratigraphic units of the Arg. D4 record reflect (i) a wet phase before ~40 ka BP (Unit C), presumably corresponding with the 'Inca Huasi' event on the Bolivian Altiplano, (ii) the LGM and the wet Late Glacial (Unit B), which is recently discussed in the literature in terms of an intensified palaeo-South American Summer Monsoon (SASM), and (iii) the Holocene (Unit A) with its deposits possibly being influenced by human activity.

Zusammenfassung

Paläoböden sind wichtige terrestrische Archive zur Rekonstruktion der quartären Landschafts- und Klimageschichte. Dazu werden sie konventionellerweise z.B. mittels Texturanalyse, Elementaranalyse, Tonmineralanalyse, Mikromorphologie und numerischen Datierungen untersucht. Oft lassen die Ergebnisse Rückschlüsse auf bodenbildende Faktoren wie Klima, Vegetation und Relief zu. Das Ziel der vorliegenden Dissertation ist es zu prüfen, ob innovative Methoden wie die Biomarker- und Stabilisotopen-Analytik wesentliche zusätzliche Informationen für die Interpretation von Paläoböden liefern können. In meiner Arbeit konzentrierte ich mich insbesondere auf pflanzenwachsbürtige Alkane, Aminosäure-Enantiomere, stabile Kohlenstoff- und Stickstoffisotope in der Feinerde ($\delta^{13}C_{org}$ und $\delta^{15}N$) und auf die substanzspezifische Isotopenanalyse von Alkanen. Die entsprechenden Methoden mussten zum Teil optimiert werden. Da nicht auszuschließen ist, dass Biomarker und Stabilisotope unter verschiedenen Klimabedingungen unterschiedlich reagieren, prüfte ich deren Eignung anhand von Paläoböden aus drei verschiedenen Klimazonen: (i) an „tropischen" Paläoböden entlang den Südwesthängen des Kilimandscharo, Tansania, (ii) an „subtropischen" Paläoböden (Arg. D4) erbohrt in einer Senke in Misiones, Nordost Argentinien und (iii) an einer „borealen" löss-ähnlichen Paläoboden-Sequenz (TPS) im Tumara Tal im Vorland des Werchojansker Gebirges, Nordost Sibirien.

In allen drei Untersuchungsgebieten erwiesen sich die Quotienten langkettiger Alkane, wie nC_{31}/nC_{27} beziehungsweise $(nC_{31} + nC_{29})/nC_{27}$, als geeignete Biomarker Proxies, die insbesondere eine deutliche Unterscheidung von Grass- und Gehölzgesellschaften ermöglichten, was paläoklimatisch von hoher Relevanz ist. Zusätzlich eigneten sich kurz- und mittelkettige Alkane zur Kennzeichnung lakustriner organischer Substanz und lieferten damit einen wichtigen Hinweis auf humidere Klimaperioden.

In der „borealen" Paläoboden-Sequenz untersuchte ich Aminosäure Enantiomere als Stickstoff- (N-)Biomarker. Es zeigte sich, dass die D/L-Verhältnisse der Asparaginsäure und des Lysins annähernd exponentiell mit zunehmender Tiefe weiter werden, was auf den Alterungsprozess der organischen Bodensubstanz zurückzuführen ist. Zum anderen waren die D/L-Verhältnisse in den als „warmzeitlich" interpretierten braunen Paläoböden stets weiter als in den „kaltzeitlichen" dunkelgrauen Paläoböden. Dies lässt sich mit einer temperaturbedingten beschleunigten Razemisierung in den interglazialen braunen Paläoböden erklären.

Im „subtropischen" Bohrkern Arg. D4 variierte $\delta^{13}C_{org}$ eindeutig zwischen den für C3-und C4-Pflanzen typischen Werten (~ -27‰ und ~ -14‰). Aus paläobotanischer Sicht ist dies ein klarer Beleg für den Wechsel von Gehölz- (und evtl. C3-Gras-)fluren und Grassavannen (und evtl. CAM-Pflanzen). Dagegen dürften Änderungen des Photosyntheseweges in den hochgelegenen (> 2000 m ü. NN) Paläoboden-Sequenzen am Kilimandscharo und in Nordost-Sibirien keine wesentliche Rolle für die dort gemessenen kleineren Schwankungen in der natürlichen Isotopenhäufigkeit gespielt haben. Die geringfügig positiveren $\delta^{13}C_{org}$ -Werte in den unter Ericaceaen-Vegetation (im Vergleich zur Bergregenwaldvegetation) entstandenen schwarzen Paläoböden am Kilimandscharo belegen die Tieferwanderung des Ericaceaen-Gürtels während kalter Klimate. In der nordost-sibirischen Paläoboden-Sequenz korreliert $\delta^{13}C_{org}$ negativ mit dem Gesamtkohlenstoff (TOC) und mit dem TOC/N-Verhältnis (R = -0,70 bzw. R = -0,71). Da letztere die unterschiedlich starke Degradation der organischen Bodensubstanz widerspiegeln, liegt es nahe, auch die Variationen der $\delta^{13}C_{org}$ -Werte mit unterschiedlich starker Humusdegradation zu erklären. Nicht auszuschließen ist, dass die geringfügigen Schwankungen der $\delta^{13}C_{org}$ -Werte in diesen Paläoböden auch durch Wasserstress im Zusammenhang mit Trockenperioden beeinflusst sind.

Im Gegensatz zu $\delta^{13}C_{org}$ korreliert $\delta^{15}N$ in der nordost-sibirischen Paläoboden-Sequenz mit keinem anderen organischen Parameter (TOC, TOC/N and $\delta^{13}C_{org}$). Eine eindeutige paläoökologische Interpretation der $\delta^{15}N$-Befunde war nicht möglich, obwohl ich jene Prozesse, die maßgeblich die natürliche Isotopenhäufigkeit beeinflussen können, in Betracht zog. Dazu zählen: N-Mineralisation, Denitrifikation, N-Fixierung, N-Verluste durch Feuerereignisse und atmosphärische N-Deposition.

Die substanzspezifische Stabilkohlenstoff-Analytik für n-Alkane wurde optimiert und auf ausgewählte Proben des Arg. D4-Bohrkerns angewandt. Die $\delta^{13}C$-Werte der pflanzenbürtigen Alkane korrelierten hochsignifikant mit $\delta^{13}C_{org}$. Dies bestätigt, dass $\delta^{13}C_{org}$ in dieser „subtropischen" Paläoboden-Sediment-Abfolge sich bestens für die Rekonstruktion der Paläovegetation eignet. Darüber hinaus verifizieren die von nC_{27} bis nC_{33} zunehmenden $\delta^{13}C$ Amplituden die Herkunft dieser Biomarker Moleküle; während nC_{27} und nC_{29} hauptsächlich von C3-Bäumen und Sträuchern stammen, haben nC_{31} und nC_{33} ihren Ursprung hauptsächlich in C3- oder C4-Gräsern und Kräutern.

In Verbindung mit den Ergebnissen weiterer analytischer Methoden (insbesondere jenen numerischer Datierungen) tragen die Biomarker- und Stabilkohlenstoff-

Isotopenergebnisse wesentlich zur Rekonstruktion und zum besseren Verständnis der mittel- und spätquartären Landschaftsgeschichte in den drei klimatisch unterschiedlichen Untersuchungsgebieten bei:

Die tiefschwarzen Paäoböden an den Südhängen des Kilimandscharo spiegeln Phasen der Klimaverschlechterung während des letzten globalen Temperaturminimums (LGM) und des Spätglazials wider. Kälte und Trockenheit führten zum Zurückweichen des montanen tropischen Bergregenwaldes und zur Tieferwanderung des Ericaceaen-Gürtels. Die paläopedologischen Befunde belegen, dass derartige Ereignisse bereits im Marinen Isotopen Stadium (MIS) 3 und 4 stattgefunden haben.

Die Ergebnisse aus Nordost Sibirien lassen vermuten, dass die Abfolge dunkelgrauer und brauner Paläoböden in der Tumara-Paläoboden-Sequenz den Wechsel von Glazialen und Interglazialen/-stadialen widerspiegelt. Trotz vorhandener Unsicherheiten in der numerischen Datierung macht der Vergleich mit anderen nordhemisphärischen Klimaarchiven und der regionalen Glazialchronologie wahrscheinlich, dass diese Paläoboden-Sequenz die letzten ~ 240 ka repräsentiert.

Die stratigraphischen Einheiten des nordost-argentinischen Bohrkerns Arg. D4 korrelieren mit (i) einer Feuchtphase um 40 ka BP, die vermutlich dem humiden „Inca Huasi"-Ereignis auf dem Bolivianischen Altiplano entspricht, (ii) dem LGM und der spätglazialen Feuchtphase, die in der jüngeren Literatur mit einem verstärktem Paläo-Südamerikanischem Sommermonsun erklärt wird, und (iii) dem Holozän, während dem die Sedimentation bereits vom Menschen beeinflusst erscheint.

The Use of Biomarker and Stable Isotope Analyses in Palaeopedology

Reconstruction of Middle and Late Quaternary Environmental and Climate History, with Examples from Mt. Kilimanjaro, NE Siberia and NE Argentina

(Zum Einsatz der Biomarker- und Stabilisotopen-Analytik in der Palaeopedologie

Rekonstruktion mittel- und spätquartärer Landschafts- und Klimageschichte, mit Beispielen vom Kilimandscharo, aus NE Sibirien und NE Argentinien)

Extended Summary

1. Introduction

1.1 Rationale

In order to better predict how different climate and ecosystems will react on accelerating global warming (IPCC, 2001) it is essential to understand their dynamics during the past. Whereas sediment and ice cores from the deep sea, Greenland and Antarctica allow climate reconstruction at high temporal resolution and on a mainly global scale (e.g. Mangerud, 1989; NGRIP members, 2004; Petit et al., 1999; Shackleton et al., 2000), soils and sediments (e.g. palaeosol-loess sequences) are considered as important terrestrial counterparts (e.g. Kukla, 1987; Rousseau et al., 2002; Zöller et al., 2004). If reliable proxies can be developed for such archives, they may provide valuable information about regional palaeoenvironments. Various analytical methods have already been applied successfully in palaeopedological studies, e.g. mineralogy, texture, micromorphology, palaeoenvironmental magnetism, luminescence dating and palynology (e.g. Andreev et al., 2004; Gallet et al., 1998; Machalett et al., 2006; Muhs et al., 2004; Nugteren et al., 2004). During the last decades also biomarkers, stable isotopes and the combination of both have got more and more in the focus of palaeoecologists (e.g. Amelung, 2003; Boutton, 1996; Glaser, 2005; Zhang et al., 2006).

1.2 Biomarkers in palaeopedology

Biomarkers are organic compounds with a known origin, which are preserved in archives and store information about their source organisms (Eganhouse, 1997). For instance, long-chain n-alkanes (nC_{27}-nC_{33}) with a strong odd-over-even predominance (OEP) are well known to be important constituents of epicuticular plant leaf waxes (Kolattukudy, 1976; Rieley et al., 1991). On the contrary, short- and mid-chain n-alkanes ($nC_{15} - nC_{19}$ and $nC_{20} - nC_{25}$, respectively) are predominantly found in lacustrine organisms (Ficken et al., 2000; Zhang et al., 2004). As alkanes are assumed to be relatively resistant to degradation (Cranwell, 1981; Meyers and Ishiwatari, 1993), the contribution of terrestrial versus lacustrine organic matter (OM) in sediments can be assessed (Bourbonniere et al., 1997; Glaser and Zech, 2005). This is of high relevance for the understanding of landscape evolution as terrestrial OM in lake sediments indicate the intensity of erosion in catchments. Furthermore, terrestrial plants partly reveal different long-chain n-alkane patterns and have therefore been used for reconstructing vegetation changes (Cranwell, 1973; Nott et al., 2000; Schwark et al.,

2002; Zhang et al., 2006). However, such biomarker results are not always in agreement with palynological findings (Farrimond and Flanagan, 1996a; Ficken et al., 1998).

Like n-alkanes, amino acids in soils and sediments originate from living organisms. Mainly bound in proteins, they constitute an important nitrogen (N) pool in soils and may serve as N biomarkers (Amelung, 2003): Containing a chiral carbon (C) atom, they can occur either in the left-handed form (L-enantiomer) or in the right-handed form (D-enantiomer) with living organisms primarily producing the L-enantiomers. The D-amino acids are then generated by racemization – a mainly time-, temperature- and pH-dependent abiotic reaction – from their respective L-enantiomers (Bada, 1985). It has therefore been suggested that D/L-ratios of amino acids can be used for dating. Mahaney and Rutter (1989), for instance, found the ratio D/L-aspartic acid to be a suitable geochronometer in buried soils on Mt. Kenya.

1.3 Stable carbon and nitrogen isotopes in palaeopedology

Concerning stable isotopes, the natural abundance of ^{15}N ($\delta^{15}N$) is already used in palaeolimnological (e.g. Talbot, 2001 and references therein) and in ecological studies (Eshetu and Högberg, 2000; Gebauer and Meyer, 2003; Nadelhoffer and Fry, 1994; Schulze et al., 1994), but it was not yet investigated in palaeosols. On the contrary, the natural abundance of ^{13}C ($\delta^{13}C$) is intensively applied in palaeoecological/-pedological studies since the availability of automated continuous-flow isotope ratio mass spectrometry (CF-IRMS, e.g. in Barrie and Prosser, 1996). However, $\delta^{13}C$ variations in terrestrial archives can be interpreted very differently: On the one hand, $\delta^{13}C$ is often used for reconstructing vegetation changes in tropical and subtropical records (Aucour et al., 1999; Collatz et al., 1998; Freitas et al., 2001; Liu et al., 2005c; Pessenda et al., 1998; Wang et al., 2000) as it is well known that plants using the C4 metabolic pathway (many savannah grasses) are enriched in ^{13}C ($\delta^{13}C = \sim$ -14‰) in comparison to C3 plants (trees and C3 grasses, $\delta^{13}C = \sim$ -27‰). On the other hand, $\delta^{13}C$ is also used for reconstructing palaeoprecipitation in records, where C4 contribution can be excluded (Hatté and Guiot, 2005), as it is also well known that smaller $\delta^{13}C$ variations within the C3 metabolic pathway depend on environmental conditions, especially on water use efficiency of plants (Farquhar et al., 1982; Liu et al., 2005a; O'Leary, 1995; Stevenson et al., 2005). Finally, ^{13}C enrichment in soils (up to several per mil) is also attributed to soil organic matter (SOM) decomposition (Balesdent et al., 1993; Bol et al., 1999; Chen et al., 2002; Krull et al., 2002; Nadelhoffer and Fry, 1988; Xie et al., 2004), challenging the reliability of reconstructed palaeovegetation and –precipitation.

In search of responsible mechanisms for the observed isotope fractionation during SOM decomposition, Balesdent and Mariotti (1996) suggested a model, in which ^{13}C-depleted/-enriched C pools are differently prone to decay. Hence, more reliable δ^{13}C input signals may be derived from individual C pools as performed by compound-specific isotope analysis (CSIA). This was shown to be especially promising when focusing on plant-derived biomarkers like lignin phenols, sugars or alkanes (Glaser and Zech, 2005; Liu et al., 2005b; Street-Perrott et al., 2004).

1.4 Objectives

The here presented dissertation is part of an effort to establish innovative analytical methods for the palaeoenvironmental research at the Faculty for Geosciences, University of Bayreuth. The specific methodological objectives of my work were:

- to optimize the n-alkane analysis for both quantification and compound-specific isotope analysis (CSIA),
- to evaluate the potential of n-alkane analysis for the reconstruction of palaeoenvironments in different ecosystems,
- to test the applicability of amino acid enantiomers as N biomarkers in palaeosols,
- to compare the applicability of δ^{13}C in different palaeoenvironmental studies,
- to compare δ^{13}C of bulk SOM ($\delta^{13}C_{TOC}$) with δ^{13}C of plant-derived n-alkanes, and
- to evaluate the potential of δ^{15}N in palaeosols

In order to address these objectives, I selected three promising records, located in the tropics, in the subtropics, and in the boreal continental zone:

- the palaeosol sequences on the southern slopes of Mt. Kilimanjaro, Tanzania,
- a palaeosol sediment sequence in a small basin in the Province of Misiones, NE Argentina, and
- a loess-like permafrost palaeosol sequence in the forelands of the Verkhoyansk Mountains, NE Siberia

The above-mentioned biomarker and stable isotope methods were then applied in the context of multi-proxy analytical approaches to the selected case studies. As superior

objective, I thus also aimed at reconstructing the respective regional or even over-regional palaeoenvironmental and climate histories of the study areas.

2. Study areas

2.1 Mt. Kilimanjaro, Equatorial East Africa (Study 1)

The ancient volcano Mt. Kilimanjaro (5895 m a.s.l.) is located in Equatorial East Africa (~ 3°S , 37°E) on the territory of Tanzania close to the border to Kenya. Climate greatly varies within this altitudinal range and with exposure (Rohr and Killingtveit, 2003), the southern slopes being generally more humid than the northern ones. Climatic factors and topography heavily influence the vegetational zonation, which is similarly differentiated as in many other East African mountains (Hedberg, 1951; Klotz, 1989). An overview of the vegetation zones of Mt. Kilimanjaro is given by Morris (1970) and Hemp et al. (2006; 1998). Characteristically and of special relevance for my study, the "subalpine" zone, forming the transition between the broad-leaf tropical montane forest (below ~2800 m a.s.l.) and the alpine *Helichrysum* scrub vegetation (above ~3500 m a.s.l.), is dominated by fire-tolerant *Erica* species like *Erica excelsa, E. arborea, E. trimera, Protea caffra* and *Euryops dacrydioides* (Hemp and Beck, 2001). Whereas glacial chronologies have already been established (e.g. Osmaston, 1989; Shanahan and Zreda, 2000) for Mt. Kilimanjaro, no reliable data are available about vegetation shifts during the Quaternary.

In March 2001 a soil catena was established along the Machame Route, which leads from Machame Gate (1825 m a.s.l.) to the Shira Plateau (about 4000 m a.s.l.). In the montane zone, the middle and lower parts of the soil profiles are often characterized by sequences of buried black, brown and mottled gray horizons and reddish iron pans (Schrumpf, 2004). Deduced from field observations and especially from the morphological resemblance of the buried black horizons in the montane zone with the deep black topsoils in the "ericaceous belt", Study 1 is structured around the following hypotheses:

  (i)   the buried black horizons in the montane zone are buried topsoils (Ab horizons),
  (ii)   they developed under ericaceous vegetation, and thus
  (iii)   represent periods with significant changes of the climate regime and the vegetation belts.

In order to verify these working hypotheses, I studied in detail a key soil profile (TS01/2250) at 2250 m a.s.l., being representative for the montane forest belt. Furthermore, litter and plant samples as well as further soil samples for radiocarbon dating were taken.

Both n-alkane and stable carbon isotope analyses were applied to evaluate their potential for contributing to the reconstruction of the palaeoenvironment on the southern slopes of Mt. Kilimanjaro.

2.2 Forelands of the Verkhoyansk Mountains, Northeast Siberia (Studies 2, 3 and 4)

The Verkhoyansk Mountains are located in NE Siberia and are characterized by boreal continental climate, i.e. short, warm summers and long, cold winters (Müller, 1980). In Jakutsk, about 300 km south of the Verkhoyansk Mountains, maximum and minimum temperatures are 30 to 38°C and -60 to -70°C, respectively. Westerlies prevail and provide moisture from the Atlantic Ocean with annual precipitation being less than 300 mm (Jakutsk: 213 mm/a, Verkhoyansk: 155 mm/a). The extreme continental conditions in this study area are responsible for the formation of 400 – 600 m thick permafrost and the absence of big glaciers today. Large moraine arcs, however, dominating the landscape in the forelands west and southwest of the Verkhoyansk Mountains, document several former and extensive piedmont glaciations (Grinenko and Kamaletdinov, 1993; Stauch et al., 2006). About 10 km South of the outermost moraine arc a 50 - 60 m high cliff is exposed on the orographically right bank of the Tumara River, which drains the southern part of the Verkhoyansk Mountains. The uppermost 15 m overly fluvio-glacial sandy gravels and are built up by frozen dark gray loess-like sediments intercalated by brown soil horizons. They were sampled at high resolution (n = 117) and are referred to as "Tumara Palaeosol Sequence" (TPS).

A detailed profile description and discussion of the chronology is the focus of Study 2. Dealing with a multi-proxy analytical approach (geochemistry, texture, SOM characterization) and testing the amino acid enantiomers as biomarker proxy for palaeotemperature, it forms the sedimentological and palaeoclimatic framework for ongoing more specific studies: The potential of both stable carbon and nitrogen isotopes for the palaeoenvironmental reconstruction is evaluated in Study 3, whereas the n-alkane biomarker results are compared with pollen results in Study 4 in order to reconstruct the palaeobotany.

2.3 Misiones, subtropical Northeast Argentina (Studies 5 and 6)

The Province of Misiones in subtropical NE Argentina (25 – 28°S, 53 – 56°W , 100 – 800 m a.s.l.) lies between the Rivers Paraná and Uruguay and receives the highest rainfalls of the country (mean annual precipitation ~1700 mm) except for the Southern Cordillera (Cerveny, 1998). This is caused by the combined influence of both the SE trades, which advect moisture to regions near the Atlantic coast (NE Argentina, Uruguay and SE Brazil)

and the only recently discussed circulation regime of the South American Summer Monsoon (SASM, in Gan et al., 2004; Vera et al., 2002; Zhou and Lau, 1998). The original vegetation cover in Misiones mainly consists of mesophytic subtropical forests with large proportions of evergreen species (Hueck and Seibert, 1972). According to Iriondo and Kröhling (2004), loess of Late Pleistocene-Holocene age (the so-called Oberá Formation) mantles the study area with a typical thickness between 3 and 8 m. On the contrary, Morrás et al. (2005) suggested that in situ weathered mesozoic basalt rather than eolian silt is the dominant soil parent material.

In September 2004, a 4.5 m long sediment core ('Arg. D4') was taken with a piston corer from a weakly flooded small basin located northeast of the city Oberá (27°23'35''S; 55°31'52''W; 330 m a.s.l.). Again, I used a multi-proxy analytical approach to reconstruct the sedimentation history. Both n-alkane biomarker and stable carbon isotope analyses were applied in order to evaluate their potential for the reconstruction of the palaeoenvironmental evolution in the study area (Study 5). Furthermore, I determined compound-specific δ^{13}C values for individual biomarkers by optimizing the method for n-alkanes and compared these results with bulk δ^{13}C$_{TOC}$ values (Study 6).

3. Analytical methods

All soil, plant and litter samples were air-dried, sieved (<2 mm) or cut to small pieces, respectively, and finely ground.

3.1 Biomarker analyses

The analytical procedure for the isolation of the n-alkanes was adopted from Bourbonniere et al. (1997). After optimization, which is discussed in detail in Study 6, it comprised (i) addition of deuterated n-tetracosane (d$_{50}$-n-C$_{24}$) as internal standard, (ii) lipid extraction with azeotropic toluene/methanol using accelerated solvent extraction (ASE), (iii) concentration of the extract and saponification of co-eluted esters with 0.5M KOH in MeOH, (iv) fractionation of different lipid classes on aluminum oxide/silica gel (both 5% deactivated) columns with hexane/toluene (85:15) as eluent, (v) addition of deuterated n-eicosane (d$_{42}$-n-C$_{20}$, recovery standard) to the eluted and concentrated hydrocarbon fraction, and (v) separation and quantification of the n-alkanes on an HP 6890 GC equipped with a flame ionization detector (FID).

Amino acid enantiomers for 10 selected samples from the Tumara Palaeosol Sequence (Study 2) were determined in replication according to the method proposed by Amelung and Zhang (2001). Sample preparation comprised pre-extraction of free and water-soluble amino acids, hydrolysis of protein-bound amino acids, purification with strongly acid cation exchange resin columns (Dowex W X8) and conversion to N-pentafluoro-propionyl-iso-propyl esters. Quantification was carried out on a Saturn GC-MS Workstation at the Institute of Soil Science and Soil Ecology, University of Bonn. Although over 25 amino acid enantiomers were quantified, I only used the results obtained for aspartic acid (Asp) and lysine (Lys), which proved to be most suitable for dating purposes in soils (Amelung, 2003).

3.2 Stable carbon and nitrogen analyses

The $\delta^{13}C$ and $\delta^{15}N$ values of bulk SOM were measured using dry combustion of a 40 mg decalcified sub-sample with a Carlo Erba NC 2500 elemental analyzer coupled to a Delta^{plus} continuous flow isotope ratio mass spectrometer (IRMS) via a Conflow II interface (Thermo Finnigan MAT, Bremen, Germany). Sucrose (CH-6, IAEA, Vienna, Austria), $CaCO_3$ (NBS 19, Gaithersburg, USA) and ammoniumsulfate (N1 and N2, both IAEA, Vienna, Austria) were used as calibration standards. Natural abundances of stable carbon and nitrogen isotopes are expressed in the usual δ-scale in parts per thousand according to the equation:

$$\delta_{sample}\ (‰) = \left(\frac{R_{sample} - R_{standard}}{R_{standard}} \right) \times 1000,$$

where R_{sample} and $R_{standard}$ are the $^{13}C/^{12}C$ or $^{15}N/^{14}N$ abundance ratios of a sample or a standard, respectively. Precision was determined by measuring known standards in replication ($\sim$ 0,15‰ for $\delta^{13}C$ and 0.25‰ for $\delta^{15}N$).

3.3 Compound-specific isotope analysis

The compound-specific $\delta^{13}C$ values of individual n-alkanes were determined by GC-C–IRMS using a Trace GC 2000 equipped with a split–splitless injector coupled via a Combustion III interface to a Delta^{plus} continuous flow IRMS (all Thermo Finnigan MAT, Bremen, Germany). All measured $\delta^{13}C$ values were (i) drift-corrected using regularly discharged pulses of pure CO_2 as reference gas, (ii) corrected for amount-dependency by co-analyzing standards with increasing analyte amounts (Glaser and Amelung, 2002; Schmitt et al., 2003), and (iii) finally calibrated against two internal standards.

4. Results and Discussion

4.1 Biomarkers

4.1.1 n-Alkanes in the three investigated ecosystems (Studies 1, 4 and 5)

All investigated plants, litter samples and Ab horizons were dominated by long-chain homologs (nC_{27}-nC_{33}) with a strong odd-over-even predominance. Such alkane distribution patterns are typical for plant leaf waxes (Kolattukudy, 1976). Palaeoecologically important, further differentiations are often possible and allow distinguishing between plant communities in the ecosystems under study:

On Mt. Kilimanjaro (Study 1), samples from the broad-leaved tropical montane forest zone are clearly dominated by nC_{27} and nC_{29}. On the contrary, nC_{31} is the most abundant homolog in almost all samples from the ericaceous belt. This finding was recently corroborated in a transect study by Hörold (unpublished data). The alkane ratio nC_{31}/nC_{27} is
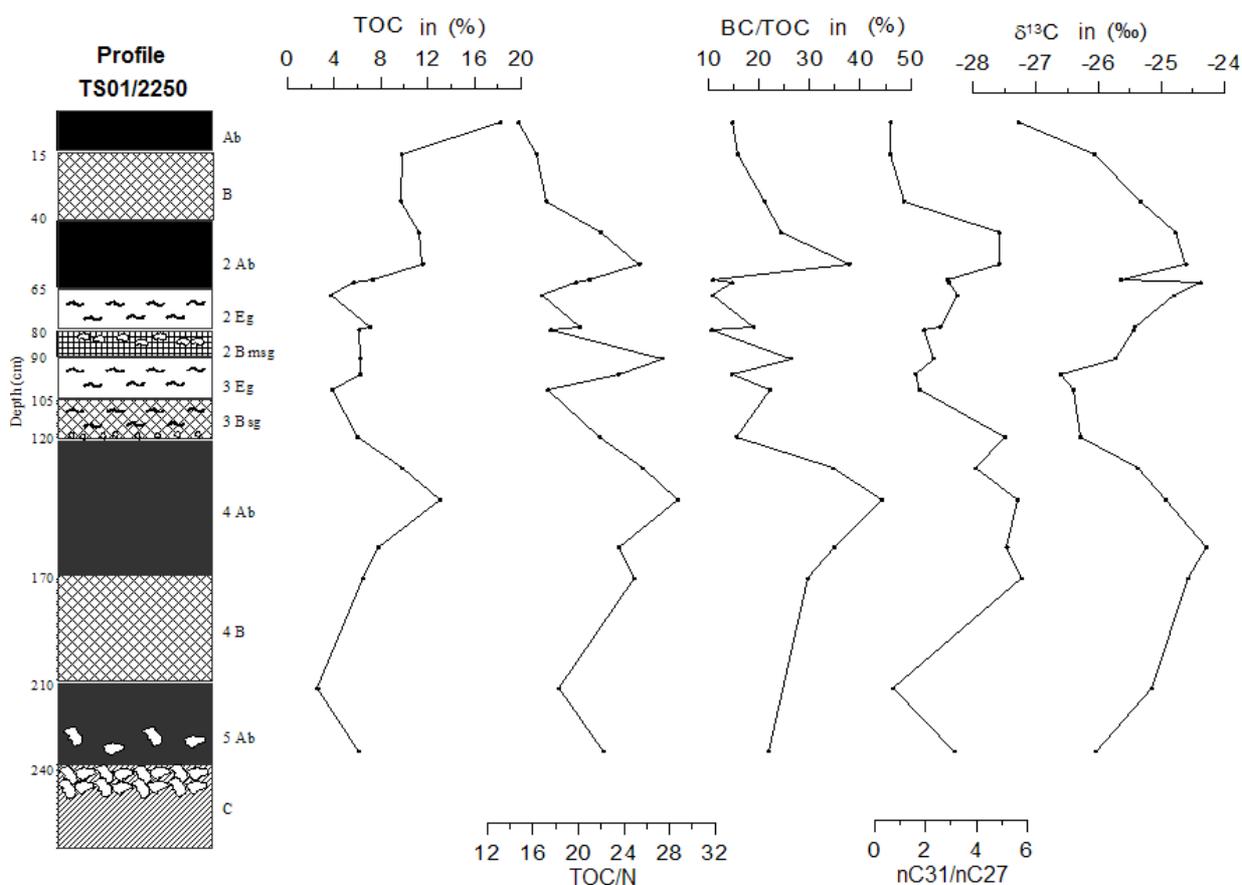
Fig. I: Stratigraphy and geochemical results of profile TS01/2250. Black horizons reveal higher TOC contents and are therefore referred to as Ab horizons. Especially the 2 Ab and 4 Ab horizon are characterized by high TOC/N ratios, maxima in BC, high nC_{31}/nC_{27} ratios and more positive $\delta^{13}C$ values, indicating that these horizons developed under ericaceous vegetation.

therefore used in Study 1 as biomarker proxy for detecting buried palaeosols, which developed during the past under ericaceous vegetation (Fig. I). This interpretation of the palaeosols 2 Ab, 4 Ab and 5 Ab in profile TS01/2250 is further corroborated by (i) high TOC/N ratios, (ii) high black carbon (BC) contents, and (iii) palynological analyses from Schlütz (personal communication), who found mainly *Erica excelsa* pollen (> 80%) in the 4 Ab horizon. Unfortunately, pollen are intensively corroded in most other horizons and a thorough comparison with our biomarker results is hence not possible in this record.

On the contrary, pollen data are available for many stratigraphic units of the Tumara Palaeosol Sequence and allow a direct comparison between the biomarker and the respective pollen results in the NE Siberian study area. As discussed in Study 4, both methods have advantages but also limitations and thus have the potential to complement each other. Again, a biomarker proxy, $(nC_{31} + nC_{29})/nC_{27}$, could successfully trace the origin of plant remains in the palaeosols: Most grasses and herbs typically cluster close to nC_{31} or nC_{29} (*Carex*) in ternary diagrams, whereas nC_{27} predominates in trees and shrubs. This proxy was applied to the loess-like palaeosol sequence in the Tumara Valley and informs about the contribution of trees/shrubs versus grasses/herbs to the SOM (Fig. II). Results indicate that the lower half of the Tumara Palaeosol Sequence developed under tree-dominated vegetation. A transition to grass/herb dominance is recorded in the middle part of the sequence. Reforestation started again at ~2.3 m depth during the Late Glacial but experienced a marked temporary retreat in the uppermost meter. This interpretation is generally well in agreement with the palynological findings. Although the latter allow a better differentiation between former plant communities, pollen are intensively corroded in the middle part of the profile. The seemingly discrepancy between the reconstructed palaeovegetation and the basic climatic stratigraphy (Fig. II) will be discussed later on.

Also in subtropical NE Argentina vegetation changes during the Late Quaternary are supposed to have been accompanied with alternations of forests and grasslands. Like on Mt. Kilimanjaro, the nC_{31}/nC_{27} ratio turned out to be the most informative biomarker proxy for the reconstruction of the palaeovegetation (Fig. III): In the sediment core Arg. D4 it allows assessing the varying contributions of grasses/herbs versus trees/shrubs (Study 5). Unfortunately, pollen results for this record were not yet available when the respective manuscript was submitted. However, the unpublished pollen data confirm the palaeovegetational interpretation derived from the biomarkers: Accordingly, a mixed
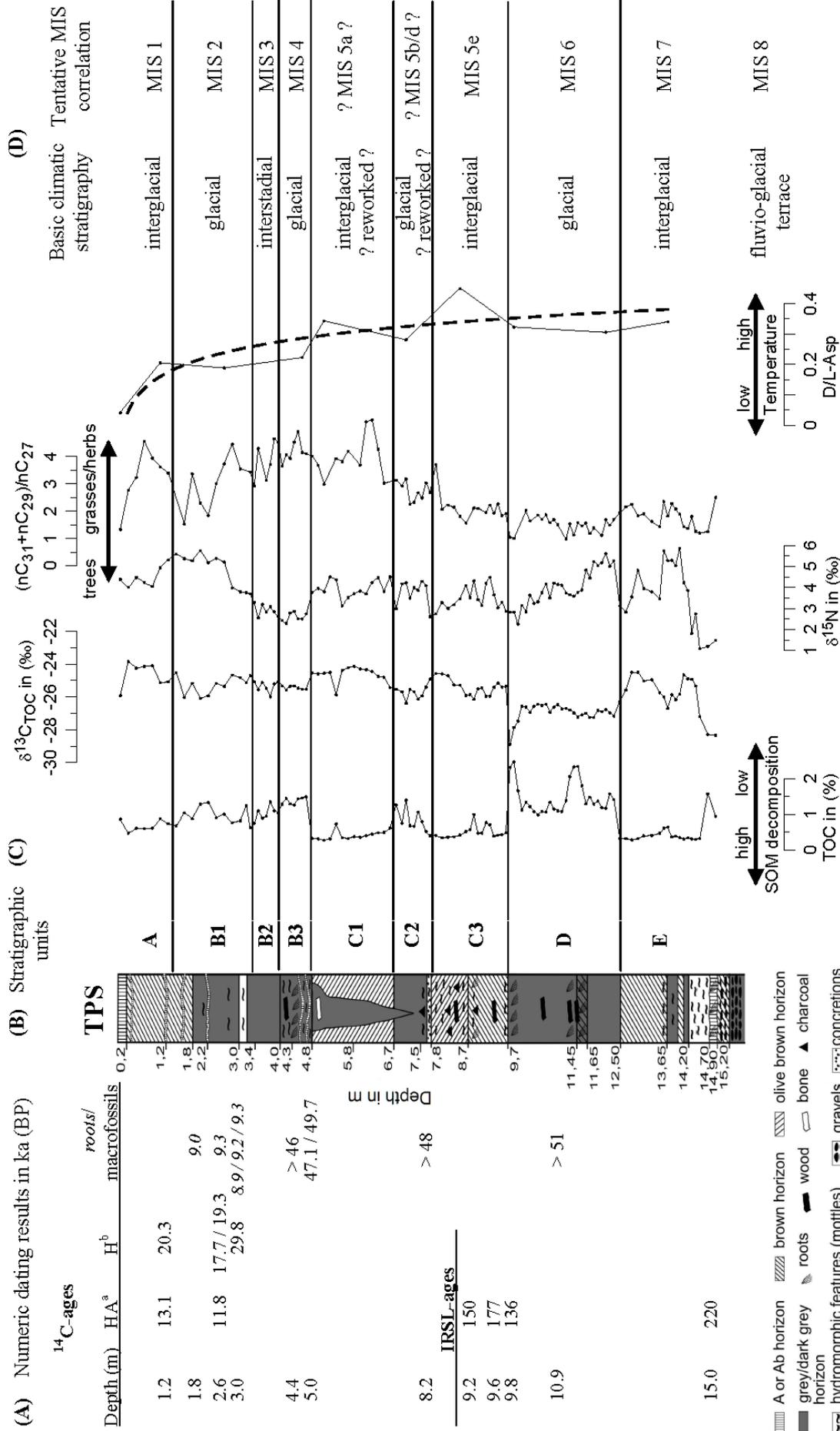
Fig. II: (A) Numeric dating results, (B) TPS stratigraphy and legend, (C) depth profiles of the palaeoenvironmental and palaeoclimatic proxies as inferred from the analytical results and (D) basic climatic stratigraphy and tentative MIS correlation. [a] HA = alkali soluble substances (humic acids), [b] H = alkali insoluble substances (humins), dotted line = exponential fit.
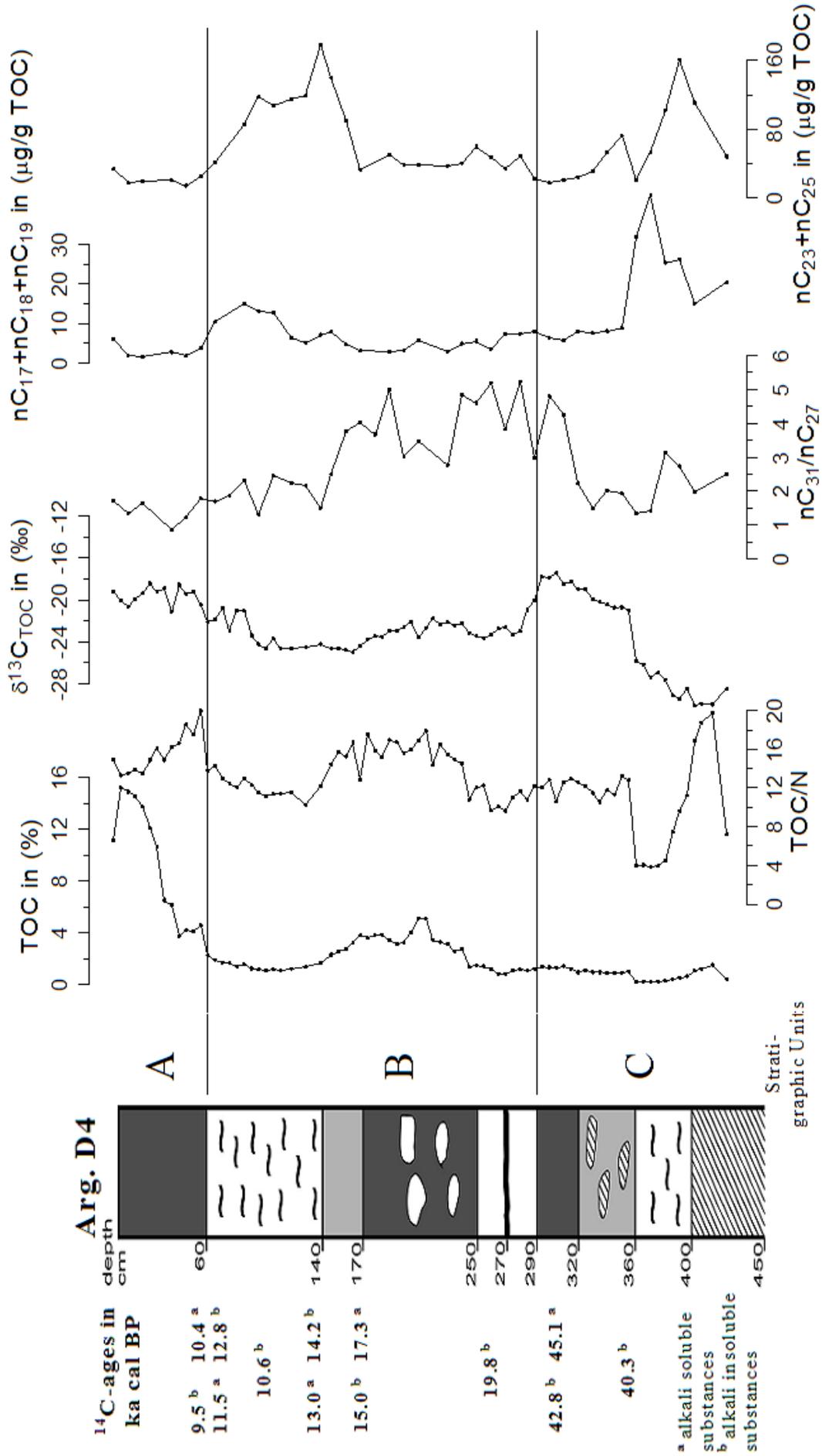
Fig. III: Left: Schematic stratigraphy and numeric dating results for the sediment core Arg. D4 and stratigraphic subdivision. Right: Depth-functions for TOC, TOC/N, $\delta^{13}C_{TOC}$, and the biomarker proxies nC_{31}/nC_{27}, $nC_{17}+nC_{18}+nC_{19}$ and $nC_{23}+nC_{25}$.

tree/grass vegetation covered the study area before ~40 ka BP. Grasses dominated during formation of the upper part of Unit C. Reforestation is recorded during the Late Glacial in the upper part of Unit B and in Unit A.

Whereas the long-chain n-alkanes allow the reconstruction of the terrestrial vegetation history, the short- and mid-chain n-alkanes are used as biomarkers to provide evidence for the temporary existence of lacustrine conditions in the investigated small basin in Misiones (Fig. III and Study 5): The n-alkanes $nC_{17} - nC_{19}$ are well known to be mainly algal-derived (Bourbonniere et al., 1997; Meyers and Ishiwatari, 1993) and the mid-chain homologs nC_{23} and nC_{25} were recently demonstrated to predominate in lacustrine plants (Ficken et al., 2000; Zhang et al., 2004). Plotted versus depth, the sums of these alkanes independently reveal that two sections of the Arg. D4 record received significant amounts of lacustrine organic matter before ~40 ka BP and during the Late Glacial.

4.1.2 Amino acid enantiomers in the Tumara Palaeosol Sequence (Study 2)

In contrast to n-alkanes, which store information by being poorly altered during SOM degradation, amino acids were suggested to be of use in palaeoenvironmental studies because the primarily produced L-enantiomers are converted by the mainly time- and temperature-dependent racemization reaction into their respective D-enantiomers (Amelung, 2003). The D/L-ratios obtained for aspartic acid and lysine from selected samples of the Tumara Palaeosol Sequence can roughly be described by exponential fits (Fig. II and Study 2). Latter ones are expected if only SOM aging influences racemization of the N biomarkers. Furthermore, the results show that the racemization rate is lower for lysine than for aspartic acid (the latter have higher D/L-ratios), which is in agreement with findings from Amelung (2003). In addition, the brown stratigraphic units are generally characterized by higher D/L-ratios than the dark gray units, suggesting that higher temperatures may have prevailed in the respective palaeosols (Fig. II). This interpretation is corroborated by other proxies developed for the Tumara Palaeosol Sequence in order to establish a basic climatic stratigraphy with alternating glacial versus interglacial/-stadial palaeosols (Study 2).

4.2 Stable isotope results

4.2.1 Natural abundance of ^{13}C in the three investigated palaeosol records (Studies 1, 3 and 5)

The $\delta^{13}C_{TOC}$ values of the key soil profile TS01/2250 on Mt. Kilimanjaro (Study 1) are well within the range typical for the C3 photosynthetic pathway (-27,3‰ to -24,3‰) and give

no rise for C4 plant abundance (Fig. I). Nevertheless, $\delta^{13}C_{TOC}$ shifts to more positive values in the buried A horizons correlate significantly with other palaeovegetationally relevant proxies like nC_{31}/nC_{29} (R = 0.81) and nC_{31}/nC_{27} (R = 0.57), respectively. As also the horizons A and 2 Abg of the further uphill located soil profile TS01/3150 are characterized by more positive $\delta^{13}C_{TOC}$ values (-25,6‰) than the A horizon of profile TS01/2250 (-27,3‰), these results further corroborate hypothesis (ii) that the buried deep black palaeosols in the tropical montane zone developed under ericaceous vegetation. Although an isotope enrichment due to SOM decomposition certainly also occurred during the formation of the palaeosols, it is difficult to quantify this effect. However, all recent Ah horizons are enriched by about 1‰ compared to the litter independently of the altitude above see level suggesting that SOM decomposition is of minor importance for the observed $\delta^{13}C_{TOC}$ variations in these palaeosol sequences.

Like on Mt. Kilimanjaro, photosynthetic pathway changes can also be neglected in the NE Siberian study area (Study 3). Nevertheless, $\delta^{13}C_{TOC}$ in the Tumara Palaeosol Sequence – ranging from −28.9‰ to −23.9‰ – displays systematic variations throughout the profile with more negative values coinciding with TOC and TOC/N maxima in the dark gray Units B, C2 and D (Fig. II). As TOC in the Tumara Palaeosol Sequence may serve as proxy for SOM decomposition (Study 2), the observed negative correlations of $\delta^{13}C_{TOC}$ with TOC and TOC/N (R = -0.70 and R = -0.71, respectively; n = 117) indicate that also $\delta^{13}C_{TOC}$ may be influenced by the degree of SOM decomposition. This idea is corroborated by studies revealing that in temperate and boreal environments soils generally become enriched up to 2 – 3‰ with depth, which is attributed to SOM decomposition (e.g. Balesdent et al., 1993; Bol et al., 1999; Nadelhoffer and Fry, 1988). However, also other palaeoenvironmental factors like (i) the atmospheric CO_2 concentration and its isotope signal, and (ii) water stress have to be considered when interpreting $\delta^{13}C_{TOC}$ in soils. Recently, Hatté and Guiot (2005) used these relationships to reconstruct palaeoprecipitation quantitatively from $\delta^{13}C_{TOC}$ in the Nußloch loess sequence (Rhine Valley, Germany). Applied to the Tumara Palaeosol Sequence, more positive $\delta^{13}C_{TOC}$ values could indicate increased water stress in the brown Units A, C1, C3 and E and more negative values in the dark gray Units B, C2 and D could indicate abundant water supply for plants during formation of these palaeosols. This interpretation is in agreement with the palaeoclimatic stratigraphy (Fig. II and Study 2) correlating the latter units with glacial periods: Firstly, glaciations can be assumed to be triggered by increased precipitation in the strongly continental climate of NE Siberia, secondly, glaciations should

have coincided with a worsened drainage and increased water logging of the topsoils due to a thinner active permafrost layer and reduced evapotranspiration.

In contrast to the palaeosol sequences on Mt. Kilimanjaro and in the Tumara Valley, the sediment core Arg. D4 reveals large $\delta^{13}C_{TOC}$ variations (-30.1‰ to -17.4‰), which can not be explained with SOM decomposition and/or water stress alone, but only with C3-C4 vegetation changes (Fig. III and Study 5). Accordingly, C3 vegetation was replaced by C4-dominated vegetation in Unit C after ~40 ka BP. Whereas the C3 photosynthetic pathway dominated again in the lower and middle part of Unit B (Last Glacial Maximum and early Late Glacial), savannah grasses (often C4) and/or CAM plants started to expand in the upper part of Unit B and in Unit A. Although other palaeoenvironmental factors than photosynthetic pathway changes probably also influenced the Arg. D4 isotope record, the reconstructed C3-C4 vegetation history is further corroborated by compound-specific isotope analysis of plant-derived n-alkanes.

4.2.2 Compound-specific $\delta^{13}C$ results (Study 6)

Compound-specific $\delta^{13}C$ results are available for the Arg. D4 record (Fig. IV and Study 6): Accordingly, the $\delta^{13}C$ values of the individual long-chain n-alkanes corroborate the major $\delta^{13}C_{TOC}$ variations with correlation coefficients ranging from 0.82 (nC_{27}) to 0.89 (nC_{33}). This is in agreement with findings from Liu et al. (2005b) in loess-palaeosol sequences and suggests that $\delta^{13}C_{TOC}$ in the Arg. D4 record is poorly adulterated by SOM decomposition. This finding corroborates the reliability of $\delta^{13}C_{TOC}$ as proxy for C3-C4 vegetation changes (Study 5). Furthermore, the compound-specific isotope results reveal that plant-derived n-alkanes are an isotopically depleted C pool compared to bulk SOM. Also this is in agreement with findings from other authors (Glaser, 2005; van Dongen et al., 2002) and confirms that a selective removal of certain enriched or depleted C pools has to be considered when interpreting $\delta^{13}C_{TOC}$ variations in soils (Balesdent and Mariotti, 1996). Finally, it is noteworthy that $\delta^{13}C$ of the individual long-chain n-alkanes have variable amplitudes: $\delta^{13}C$ (nC_{27}) ranges from ~ -25‰ to -35‰, $\delta^{13}C$ (nC_{29}) from ~ -20‰ to -35‰ and $\delta^{13}C$ (nC_{31}) and $\delta^{13}C$ (nC_{33}) vary within a range of almost 20‰. This is explained in Study 6 with different origins of the n-alkanes and at the same time validates the long-chain n-alkanes as plant-derived biomarkers: nC_{27} and nC_{29} mainly derive from trees and shrubs, i.e. from C3 plants, whereas nC_{31} and nC_{33} mainly derive from grasses and herbs, i.e. from C3 and/or C4 plants. The longer-chain n-alkanes are therefore particularly sensitive biomarkers for detecting C3-C4 vegetation changes.
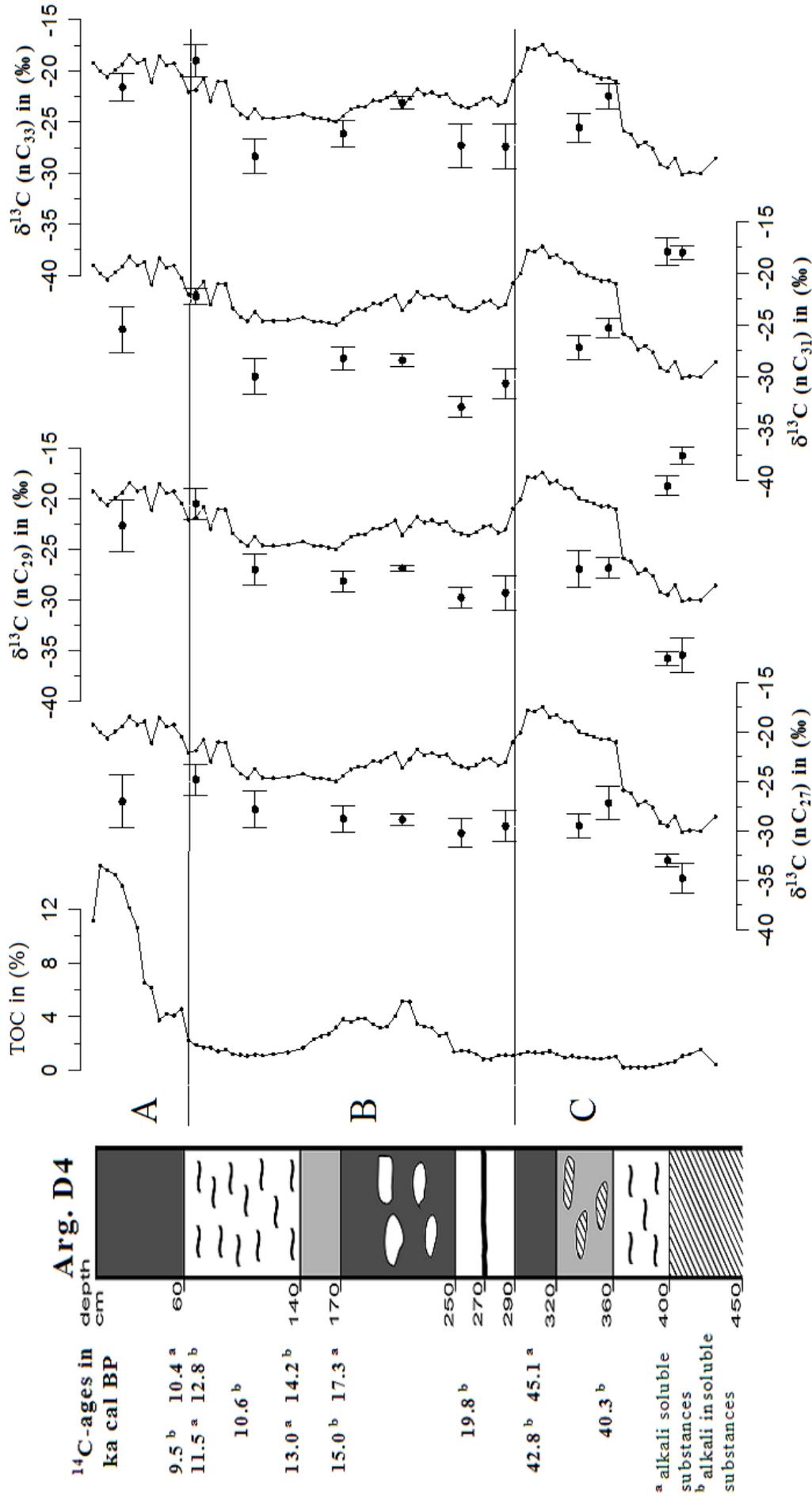
Fig. IV: Stratigraphy of the sediment core Arg. D4 and $\delta^{13}C$ values of individual terrestrial plant-derived n-alkanes (circles with error bars) in comparison with $\delta^{13}C_{TOC}$ (solid lines). Capital letters to the right of the profile indicate stratigraphic units..

4.2.3 Natural abundance of ^{15}N in the Tumara Palaeosol Sequence (Study 3)

In order to evaluate the potential of δ^{15}N in palaeopedology, Study 3 focuses not only on δ^{13}C$_{TOC}$ but also on δ^{15}N (Fig. II). Values vary from +1‰ and +6‰ and are well within the range typically found in soils (Nadelhoffer and Fry, 1988). The Units A and C generally reveal smaller δ^{15}N fluctuations around +4‰, whereas distinct long-term trends occur in the organic-rich Units B and D. The largest variations occur in the lowermost Unit E.

In both soil ecological and palaeolimnological studies, ^{15}N enrichment/depletion is generally interpreted in terms of closed or opened N cycles, respectively (e.g. Eshetu and Högberg, 2000; Talbot, 2001): More positive δ^{15}N values in soils and sediments are mainly attributed to nitrogen losses, whereas closed N cycles lead to more negative δ^{15}N values. Interestingly, δ^{15}N in the Tumara Palaeosol Sequence does neither vary in concert with other parameters (TOC, TOC/N and δ^{13}C$_{TOC}$) nor does it reveal uniform patterns in the individual stratigraphic units. Thus, although SOM decomposition should have influenced the δ^{15}N record, it did not exert a dominant control on it and other processes of the N cycle have to be considered. Especially denitrification might have played an important role in isotopically enriched palaeosols as this process leads to losses of depleted N. From a palaeoenvironmental point of view, increased denitrification could have been triggered by extraordinarily frequent freeze-thaw cycles (Papen and Butterbach-Bahl, 1999). On the contrary, N fixation is well known to cause more negative δ^{15}N of the biomass and hence also of the SOM. Furthermore, one may speculate that frequent fire events could have contributed significantly to an open N cycle and thus to a preferential loss of isotopically lighter plant OM. Finally, also changes in the nitrogen input by dry and wet atmospheric deposition are discussed in Study 3: Rain contains significant amounts of dissolved nitrogen (as NO_3^-, NO_2^- and NH_4^+) with relatively low δ^{15}N values (Heaton, 1987; Paerl and Fogel, 1994), whereas eolian dust containing SOM should be relatively enriched in ^{15}N.

4.3 Reconstruction of the palaeoenvironmental and climate history of the three ecosystems under study

4.3.1 Mt. Kilimanjaro (Study 1)

Both biomarker and stable carbon isotope results presented in Fig. I and Study 1 indicate together with other proxies that the frequently occurring buried black A horizons in the tropical montane forest belt have developed under ericaceous vegetation. Since *Erica* species are not abundant at this altitude nowadays but are characteristic for the subalpine zone (above 2800 m a.s.l.), the palaeosols reflect palaeoclimatically driven fluctuations and

changes of the vegetation zones on Mt. Kilimanjaro. This interpretation is in agreement with palynological studies on East African mountains suggesting that altitudinal shifts of the vegetation belts took place during the past and were mainly controlled by climatic factors like temperature and precipitation (Flenley, 1979b; Hamilton, 1982; Lamb et al., 2003). According to the numeric dating results obtained for the catena under study, the descent of the ericaceous belt coincided with cold and dry periods: Above 2700 m a.s.l., the development of buried A horizons correlates with Late Glacial and Early Holocene glacial re-advances around 16.5 ka BP, during the Younger Dryas and at about 7.6 ka BP (Shanahan and Zreda, 2000). Additionally, the lower members of the soil catena between 2090 m and 2290 m a.s.l. reveal black Ab horizons, which developed during the LGM, about 35 ka BP, and even before.

4.3.2 Forelands of the Verkhoyansk Mountains (Studies 2, 3 and 4)

The sedimentology of the Tumara Palaeosol Sequence is discussed in detail in Study 2. The there presented multi-proxy analytical approach (geochemical composition, texture, SOM characterization, numeric dating) suggests creating a basic climatic stratigraphy with alternating glacial and interglacial/-stadial palaeosols (Fig. II). Although it is difficult to disentangle the contributions of SOM decomposition and water stress to the observed $\delta^{13}C_{TOC}$ variations (Study 3), $\delta^{13}C_{TOC}$ confirms this stratigraphy. Accordingly, the loess-like sediments of the Tumara Palaeosol Sequence started to accumulate on fluvio-glacial sandy gravels deposited during Marine Isotope Stage (MIS) 8 and spans the last ~ 240 ka. The stratigraphic units can be correlated with MIS stages and the cold mode ones (Unit B1, B3, C2 and D) with the last four glaciations recently described for Northern Eurasia (Svendsen et al., 2004).

The vegetation history of the Tumara Valley is reconstructed in Study 4 based on both biomarker and pollen analyses: Accordingly, the lower half of the Tumara Palaeosol Sequence developed under tree/shrub vegetation, whereas grass/herb-derived pollen and n-alkanes predominate in the upper half. Reforestation started again at ~2.3 m depth with a marked temporary retreat being documented in the uppermost meter. The best modern analogue (BMA) method, which was applied recently for quantitative Late Pleistocene and Holocene pollen-based climatic reconstruction in Arctic Russia (Andreev et al., 2004; Andreev et al., 2003a; Andreev et al., 2003b), can be used to derive qualitative palaeoclimatic information from the reconstructed vegetation. However, these results are not in agreement with the chronostratigraphy developed in Study 2. For instance, the palaeopedologic proxies suggest correlating Unit D with a glacial period (Fig. II). But both biomarker and pollen indicate tree dominance, which is generally interpreted as interglacial vegetation.

A differentiated view on the climatic factors triggering palaeobotany and glacial history, respectively, could help reconciling the seemingly contradicting results and is proposed in Study 4: As shown e.g. by Andreev et al. (2003b) and Kaplan (2001), mean July temperature and the annual sum of days with mean temperatures above 5°C have the most definite effect on Arctic vegetation. In the extreme continental climate prevailing in the study area, both climatic factors can be assumed to be of minor relevance for the growth of glaciers. On the contrary, glaciations in the Verkhoyansk Mountains should have been principally triggered by increased precipitation. Hence, the glacial and the vegetation history in this study area could have developed partly independent from each other. For instance, it is suggested that Unit D developed during a period when glaciers advanced into the forested lowlands due to higher winter precipitation.

4.3.3 Misiones, subtropical NE Argentina (Studies 5 and 6)

Like in the preceding studies, geochemical composition, SOM characterization and numeric dating provide valuable information for understanding the sedimentological history of the Arg. D4 record. Both biomarkers and $\delta^{13}C_{TOC}$ are again straightforward proxies for reconstructing the palaeobotany with $\delta^{13}C$ of individual long-chain n-alkanes validating the bulk SOM isotope record. Accordingly, the lower part of Unit C may represent the 'Inca Huasi' wet phase on the Bolivian Altiplano (before ~40 ka BP) with lacustrine conditions having prevailed in the investigated small basin and tree dominance in the catchment. In the superjacent palaeosols C4 grasses replace the antecedent C3 vegetation, thus recording the end of the 'Inca Huasi' wet phase. A sedimentary hiatus after ~ 40 ka BP is interpreted as a pronounced pre-LGM dry period with landscape erosion/deflation. Sedimentation starts again during the LGM with C3 grass dominance. Presumably, C4 grasses were suppressed by low temperatures. In the middle part of Unit B, the ratio nC_{31}/nC_{27} documents forest expansion at the beginning of the Late Glacial wet phase. More positive $\delta^{13}C$ values in Unit A reflect the increasing contribution of C4 grasses and/or CAM plants to the SOM during the Holocene. A human impact on the formation of this unit may be possible. My results are in good agreement with other tropical/subtropical palaeoenvironmental South American records and highlight the importance and temporal variability of the palaeo-South American Summer Monsoon.

5. Conclusions

In the pedosedimentary records under study, located in the tropics (Mt. Kilimanjaro), in the subtropics (NE Argentina), and in the boreal zone (NE Siberia), long-chain n-alkane ratios (nC_{31}/nC_{27} and $(nC_{31} + nC_{29})/nC_{27}$, respectively) were shown to be straightforward biomarker proxies for the reconstruction of the palaeovegetation and thus reflect palaeoclimatic changes. Although in comparison to palynology a differentiation was only possible on the level of plant communities but not on the level of species, the presented biomarker method has distinct advantages: The leaf wax-derived n-alkanes represent the actually former standing vegetation (i) without alternations by mid- and long-distance transport, (ii) with negligibly SOM decomposition effects, and (iii) they are available even in records, which do not allow the conservation of pollen. Concerning the short- and mid-chain n-alkanes ($nC_{17} - nC_{19}$ and $nC_{20} - nC_{25}$, respectively), they were successfully used for detecting algal- and aquatic macrophyte-derived OM in the sediment core Arg. D4 in NE Argentina, pointing to lacustrine and thus more humid conditions having prevailed temporarily before ~40 ka BP and during the Late Glacial.

Amino acid enantiomers as N biomarkers allowed to further characterize the SOM in the Tumara Palaeosol Sequence. On the one hand, the depth functions of D/L-aspartic acid and D/L-lysine could be roughly described by exponential fits, reflecting SOM aging. On the other hand, brown interglacial/-stadial palaeosols generally revealed higher D/L-ratios than dark gray glacial palaeosols, suggesting that D/L-aspartic acid and D/L-lysine may serve as qualitative palaeotemperature proxies.

In the subtropical Arg. D4 record, $\delta^{13}C_{TOC}$ varied in the wide range typical for C3 and C4 vegetation changes and hence allowed a respective palaeovegetational reconstruction. However, the natural abundance of ^{13}C was no straightforward proxy in the palaeosols records from Mt. Kilimanjaro and NE Siberia. There, the interpretation of the smaller $\delta^{13}C_{TOC}$ variations – assumed to be independent of C3-C4 vegetation changes – needed multi-proxy analytical approaches for disentangling the various possibly influencing factors. On Mt. Kilimanjaro, $\delta^{13}C_{TOC}$ is more positive in buried A horizons, which developed under ericaceous vegetation compared to tropical montane forest vegetation, suggesting that such vegetation changes are responsible for the observed $\delta^{13}C_{TOC}$ pattern. Concerning $\delta^{13}C_{TOC}$ in the Tumara Palaeosol Sequence, it correlates negatively with TOC and TOC/N. As both parameters may serve as proxies for SOM decomposition, the latter may have also contributed significantly to the variations of the stable isotope composition. Furthermore, also changing

water stress conditions for the plants could have played a crucial role for $\delta^{13}C_{TOC}$ in this record.

In contrast to $\delta^{13}C_{TOC}$, $\delta^{15}N$ in the Tumara Palaeosol Sequence does not correlate with any of the other SOM characterizing parameters (TOC, TO/N and $\delta^{13}C_{TOC}$). Although other processes than SOM decomposition like (i) denitrification, (ii) N fixation, (iii) nitrogen losses by frequent fire events, and (iv) changes in the atmospheric ^{15}N deposition were discussed as factors contributing to an open N cycle, $\delta^{15}N$ turned out to be no straightforward interpretable proxy in the Tumara Palaeosol Sequence.

The compound-specific $\delta^{13}C$ analysis of n-alkanes was optimized and applied to selected samples from the Arg. D4 record. The highly significant correlations of the compound-specific isotope results (for long-chain n-alkanes) with $\delta^{13}C_{TOC}$ corroborate the reliability of the $\delta^{13}C_{TOC}$ vegetation proxy. Furthermore, the increasing $\delta^{13}C$ amplitudes from nC_{27} to nC_{33} validate the origin of these biomarker molecules, with nC_{27} and nC_{29} mainly deriving from C3 trees and shrubs and nC_{31} and nC_{33} mainly deriving from C3 or C4 grasses and herbs.

In multi-proxy analytical approaches (including biomarker and stable isotope analyses) detailed information about the Middle and Late Quaternary palaeoenvironments of the three study areas was derived and put in the respective palaeoclimatic context:

Accordingly, the deep black palaeosols on the southern slopes of Mt. Kilimanjaro reflect periods of climatic deterioration during the LGM and the Late Glacial, which coincided with a descent of the ericaceous vegetation belt. Even older palaeosols document that such events also occurred during MIS 3 and 4.

The palaeopedologic findings from the Tumara Palaeosol Sequence suggest that the brown and dark gray stratigraphic units of this palaeosol sequence describe alternating glacial and interglacial/-stadial palaeosols. Despite of uncertainties concerning the numeric data, the comparison with other northern hemispheric records and the regional glacial and geomorphologic history indicate that the Tumara Palaeosol Sequence spans the last ~240 ka.

The stratigraphic units of the Arg. D4 record reflect (i) a wet phase before ~40 ka BP (Unit C), presumably representing the 'Inca Huasi' event, (ii) the LGM and the wet late glacial period (Unit B), which is recently discussed in literature in terms of an intensified palaeo-SASM, and (iii) the Holocene (Unit A) with its deposits possibly being influenced by human activity.

Ongoing work focuses on optimizing and applying the compound-specific isotope analysis also to other biomarkers and to other elements: First palaeopedological results were already obtained for D/H ratios in alkanes and $\delta^{18}O$ in neutral sugars. Both D/H and $\delta^{18}O$ may provide valuable palaeometeorological information.

6. Contributions to the included manuscripts

In the here presented cumulative dissertation, six studies are presented. I contributed to them by preparing all manuscripts including artwork and by putting the results in the scientific context. All biomarker, stable isotope and compound-specific isotope analyses were gathered in my own work. The authors listed on the different manuscripts contributed approximately as follows:

Study 1:

M. Zech: 100 %

Study 2:

M. Zech: 59 % (laboratory work, discussion of results, manuscript preparation)

R. Zech: 15 % (field work, discussion of results, comments to improve the manuscript)

W. Zech: 15 % (field work, discussion of results, comments to improve the manuscript)

B. Glaser: 5 % (discussion of results, comments to improve the manuscript)

S. Brodowski: 3 % (laboratory support during amino acid enantiomer measurements and comments to improve the corresponding part of the manuscript)

W. Amelung: 3 % (laboratory support during amino acid enantiomer measurements and comments to improve the corresponding part of the manuscript)

Study 3:

M. Zech: 75 % (laboratory analyses, discussion of results, manuscript preparation)

R. Zech: 15 % (field work, discussion of results, comments to improve the manuscript)

B. Glaser: 10 % (discussion of results, comments to improve the manuscript)

Study 4:

M. Zech: 70 % (biomarker analyses, discussion of results, manuscript preparation)

A. Andreev: 30 % (pollen analyses, discussion of results, comments to improve the manuscript)

Study 5:

M. Zech: 75 % (laboratory analyses, discussion of results, manuscript preparation)

R. Zech: 10 % (discussion of results, comments to improve the manuscript)

B. Glaser: 7 % (discussion of results, comments to improve the manuscript)

H. de Morrás: 5 % (field work)

L. Moretti: 3 % (field work)

Study 6:

M. Zech: 80 % (analytical work, discussion of the results, manuscript preparation)

B. Glaser: 20 % (discussions on experimental design, comments to improve the

                manuscript)

References

Amelung, W., 2003. Nitrogen biomarkers and their fate in soil. Journal of Plant Nutrition and
    Soil Science, 166: 677-686.
Andreev, A.A., Grosse, G., Schirrmeister, L., Kuzmina, S.A., Novenko, E.Y., Bobrov, A.A.,
    Tarasov, P.E., Ilyashuk, B.P., Kuznetsova, T.V., Krbetschek, M., Meyer, H. and
    Kunitsky, V.V., 2004. Late Saalian and Eemian palaeoenvironmental history of the
    Bol'shoy Lyakhovsky Island (Laptev Sea region, Arctic Siberia). Boreas, 33: 319-348.
Andreev, A.A., Tarasov, P.E., Klimanov, V.A. and Hubberten, H.-W., 2003a. Russian Arctic
    lakes as climatic archives: pollen-based reconstructions of the Late Quaternary
    climate. Terra Nostra, 6: 17-21.
Andreev, A.A., Tarasov, P.E., Siegert, C., Ebel, T., Klimanov, V.A., Melles, M., Bobrov,
    A.A., Dereviagin, A.Y., Lubinski, D. and Hubberten, H.-W., 2003b. Vegetation and
    climate changes on the northern Taymyr, Russia during the Upper Pleistocene and
    Holocene reconstructed from pollen records. Boreas, 32: 484-505.
Aucour, A.-M., Hillaire-Marcel, C. and Bonnefille, R., 1999. Sources and accumulation rates
    of organic carbon in an equatorial peat bog (Burundi, East Africa) during the
    Holocene: carbon isotope constraints. Palaeogeography, Palaeoclimatology,
    Palaeoecology, 150: 179-189.
Bada, J.L., 1985. Racemization of amino acids. In: G.C. Barrett (Editor), Chemistry and
    Biochemistry of Amino Acids. Chapman and Hall, London, New York, pp. 399-414.
Balesdent, J., Girardin, C. and Mariotti, A., 1993. Site-related $\delta^{13}C$ of tree leaves and soil
    organic matter in a temperate forest. Ecology, 74(6): 1713-1721.
Balesdent, J. and Mariotti, A., 1996. Measurement of Soil Organic Matter Turnover using ^{13}C
    Natural Abundance. In: S. Yamasaki (Editor), Mass spectrometry of soils. Marcel
    Dekker, Inc., New York, pp. 83-112.
Barrie, A. and Prosser, S.J., 1996. Automated Analysis of Light-Element Stable Isotopes by
    Isotope Ratio Mass Spectrometry. In: T.W. Boutton and S. Yamasaki (Editors), Mass
    Spectrometry of Soils. Marcel Dekker, Inc., New York, pp. 1-46.
Bol, R.A., Harkness, D.D., Huang, Y. and Howard, D.M., 1999. The influence of soil
    processes on carbon isotope distribution and turnover in the British uplands. European
    Journal of Soil Science, 50: 41-51.

Bourbonniere, R.A., Telford, S.L., Ziolkowski, L.A., Lee, J., Evans, M.S. and Meyers, P.A., 1997. Biogeochemical marker profiles in cores of dated sediments from large north American lakes. In: R.P. Eganhouse (Editor), Molecular Markers in Environmental Geochemistry. Acs Symposium Series, Washington D.C., pp. 133-150.

Boutton, T.W., 1996. Stable Carbon Isotope Ratios of Soil Organic Matter and Their Use as Indicators of Vegetation and Climate Change. In: S. Yamasaki (Editor), Mass Spectrometry of Soils. Marcel Dekker, Inc., New York, pp. 47-82.

Cerveny, R.S., 1998. Present Climates of South America. In: B. H.A. (Editor), Climates of the Southern Continents: Present, Past and Future. Wiley & Sons.

Chen, Q., Shen, C., Peng, S., Sun, Y., Yi, W., Li, Z. and Jiang, M., 2002. Soil organic matter turnover in the subtropical mountainous region of south China. Soil Science, 167(6): 401-415.

Collatz, G.J., Berry, J.A. and Clark, J.S., 1998. Effects of climate and atmospheric CO_2 partial pressure on global distribution of C4 grasses: present, past and future. Oecologia, 114: 441-454.

Cranwell, P.A., 1973. Chain-length distribution of n-alkanes from lake sediments in relation to post-glacial enviromental change. Freshwater Biology, 3: 259-265.

Cranwell, P.A., 1981. Diagenesis of free and bound lipids in a terrestrial detritus deposited in a lacustrine sediment. Organic Geochemistry, 3: 79-89.

Eganhouse, R.P., 1997. Molecular Markers and Einvironmental Organic Geochemistry: An Overview. In: R.P. Eganhouse (Editor), Molecular Markers in Environmental Geochemistry. ACS Symposium Series 671, Washington, DC, pp. 1-20.

Eshetu, Z. and Högberg, P., 2000. Effects of land use on ^{15}N natural abundance of soils in Ethiopian highlands. Plant and Soil, 222: 109-117.

Farquhar, G.D., O'Leary, M.H. and Berry, J.A., 1982. On the relationship between carbon isotope discrimination and the intercellular carbon dioxide concentration in leaves. Australian Journal of Plant Physiology, 9: 121-137.

Farrimond, P. and Flanagan, R.L., 1996. Lipid stratigraphy of a Flandrian peat bed (Northumberland, UK): comparison with the pollen record. The Holocene, 6(1): 69-74.

Ficken, K.J., Barber, K.E. and Eglinton, G., 1998. Lipid biomarker, $\delta^{13}C$ and plant macrofossil stratigraphy of a Scottish montane peat bog over the last two millennia. Organic Geochemistry, 28(3/4): 217-237.

Ficken, K.J., Li, B., Swain, D.L. and Eglinton, G., 2000. An n-alkane proxy for the sedimentary input of submerged/floating freshwater aquatic macrophytes. Organic Geochemistry, 31: 745-749.

Flenley, J.R., 1979. The Late Quaternary vegetational history of the equatorial mountains. Progress in Physical Geography, 3: 488-509.

Freitas, H.A., Pessenda, L.C., Aravena, R., Gouveia, S.E., Ribeiro, A.S. and Boulet, R., 2001. Late Quaternary Vegetation Dynamics in the Southern Amazon Basin Inferred from Carbon Isotopes in Soil Organic Matter. Quaternary Research, 55: 39-46.

Gallet, S., Jahn, B., Van Vliet Lanoe, B., Dia, A. and Rossello, E., 1998. Loess geochemistry and its implications for particle origin and composition of the upper continental crust. Earth and Planetary Science Letters, 156: 157-172.

Gan, M.A., Kousky, V.E. and Ropelewski, C.F., 2004. The South American monsoon circulation and its relationship to rainfall over West-Central Brazil. Journal of Climate, 17: 47-66.

Gebauer, G. and Meyer, M., 2003. N-15 and C-13 natural abundance of autotrophic and mycoheterotrophic orchids provides insight into nitrogen and carbon gain from fungal association. New Phytologist, 160(1): 209-223.

Glaser, B., 2005. Compound-specific stable-isotope (δ^{13}C) analysis in soil science. Journal of Plant Nutrition and Soil Science, 168: 633-648.

Glaser, B. and Amelung, W., 2002. Determination of ^{13}C natural abundance of amino acid enantiomers in soil: methodological considerations and first results. Rapid Communications in Mass Spectrometry, 16: 891-898.

Glaser, B. and Zech, W., 2005. Reconstruction of climate and landscape changes in a high mountain lake catchment in the Gorkha Himal, Nepal during the Late Glacial and Holocene as deduced from radiocarbon and compound-specific stable isotope analysis of terrestrial, aquatic and microbial biomarkers. Organic Geochemistry, 36: 1086-1098.

Grinenko, V.S. and Kamaletdinov, V.A., 1993. Geological map of Yakutia (in Russian). VSEGEI, St. Petersburg.

Hamilton, A.C., 1982. Environmental History of East Africa. Academic Press.

Hastenrath, S. and Greischar, L., 1997. Glacier recession on Kilimanjaro, East Africa, 1912-89. Journal of Glaciology, 43(145): 455-459.

Hatté, C., Antoine, P., Fontugne, M., Lang, A., Rousseau, D.-D. and Zöller, L., 2001. δ^{13}C of Loess Organic Matter as a Potential Proxy for Paleoprecipitation. Quaternary Research, 55: 33-38.

Hatté, C. and Guiot, J., 2005. Palaeoprecipitation reconstruction by inverse modelling using the isotopic signal of loess organic matter: application to the Nußloch loess sequence (Rhine Valley, Germany). Climate Dynamics, 25: 315-327.

Heaton, T.H.E., 1987. ^{15}N/^{14}N ratios of nitrate and ammonium in rain at Pretoria, South Africa. Atmos. Environ., 21: 843-852.

Hedberg, O., 1951. Vegetation belts of the East African mountains. Scvensk. Bot. Tidskr., 45: 140-202.

Hemp, A., 2006. Vegetation of Kilimanjaro: hidden endemics and missing bamboo. Afrcan Journal of Ecology, 44: 305-328.

Hemp, A. and Beck, E., 2001. Erica excelsa as a fire-tolerating component of Mt. Kilimanjaro's forests. Phytocoenologia, 31(4): 449-475.

Hemp, A., Hemp, C. and Winter, J.C., 1998. Der Kilimanjaro - Lebensräume zwischen tropischer Hitze und Gletschereis. Natur und Mensch: 5-28.

Hueck, K. and Seibert, P., 1972. Vegetationskarte von Südamerika. Vegetationsmonographien der einzelnen Großräume, Band II a. Gustav Fischer Verlag, Stuttgart.

IPCC, 2001. Third Assessment Report. www.ipcc.ch.

Irion, R., 2001. The melting snows of Kilimanjaro. Science, 291(5509): 1690-1691.

Iriondo, M. and Kröhling, D.M., 2004. The parent material as the dominant factor in Holocene pedogenesis in the Uruguay River Basin. Revista Mexicana de Ciencias Geológicas, 21(1): 175-184.

Kaplan, J.O., 2001. Geophysical Applications of Vegetation Modeling. Ph.D. dissertation Thesis, University Lund. 113 pp.

Klotz, G.e.a., 1989. Hochgebirge der Erde und ihre Pflanzen- und Tierwelt. Urania - Verlag. Leipzig - Berlin.

Kolattukudy, P.E., 1976. Biochemistry of plant waxes. In: Kolattukudy (ed.), Chemistry and Biochemistry of Natural Waxes, Amsterdam: Elsevier, 290-349.

Krull, E.S., Bestland, E.A. and Gates, W.P., 2002. Soil organic matter decomposition and turnover in a tropical ultisol: evidence from δ^{13}C, δ^{15}N and geochemistry. Radiocarbon, 44(1): 93-112.

Kukla, G., 1987. Loess stratigraphy in central China. Quaternary Science Review, 6: 191-219.

Lamb, H., Darbyshire, I. and Verschuren, D., 2003. Vegetation response to rainfall variation and human impact in central Kenya during the past 1100 years. The Holocene, 13(2): 285-292.

Lehman, J.T., 1998. Environmental Change and Response in East African Lakes. Kluwer Academic Publishers.

Liu, W., Feng, X., Ning, Y., Zhang, Q., Cao, Y. and An, Z., 2005a. $\delta^{13}C$ variation of C3 and C4 plants across an Asian monsoon rainfall gradient in arid northwestern China. Global Change Biology, 11: 1094-1100.

Liu, W., Huang, Y., An, Z., Clemens, S.C., Li, L., Prell, W.L. and Ning, Y., 2005b. Summer monsoon intensity controls C_4/C_3 plant abundance during the last 35 ka in the Chinese Loess Plateau: Carbon isotope evidence from bulk organic matter and individual leaf waxes. Palaeogeography, Palaeoclimatology, Palaeoecology, 220: 243-254.

Liu, W., Yang, H., Cao, Y., Ning, Y., Li, L., Zhou, J. and An, Z., 2005c. Did an extensive forest ever develop on the Chinese Loess Plateau during the past 130 ka?: a test using soil carbon isotopic signatures. Applied Geochemistry, 20: 519-527.

Machalett, B., Frechen, M., Hambach, U., Oches, E.A., Zoller, L. and Markovic, S.B., 2006. The loess sequence from Remisowka (northern boundary of the Tien Shan Mountains, Kazakhstan) - Part I: Luminescence dating. Quaternary International, 152: 192-201.

Mahaney, W.C. and Rutter, N.W., 1989. Amino acid D/L ratio distribution in two Late Quaternary soils in the afroalpine zone of Mount Kenya, East Africa. Catena, 16: 205-214.

Mangerud, J., 1989. Correlation of the Eemian and the Weichselian with deep sea oxygen isotope stratigraphy. Quaternary International, 3/4: 13-19.

Meyers, P.A. and Ishiwatari, R., 1993. Lacustrine organic geochemistry - An overview of indicators of organic matter sources and diagenesis in lake sediments. Organic Geochemistry, 20: 867-900.

Mohammed, M.U., Bonnefille, R. and Johnson, T.C., 1995. Pollen and isotopic records in Late Holocene sediments from Lake Turkana, Kenya. Palaeogeography, Palaeoclimatology, Palaeoecology, 119: 371-383.

Morrás, H., Moretti, L., Píccolo, G. and Zech, W., 2005. New hypotheses and results about the origin of stonelines and subsurface structured horizons in ferrallitic soils of Misiones, Argentina. Geophysical Research Abstracts, 7: 05522.

Morris, B., 1970. The Zonal Vegetation of Kilimanjaro. African Wild Life, 24: 157-166.

Muhs, D.R., Ager, T.A., Bettis III, E.A., McGeehin, J., Been, J.M., Begét, J.E., Pavich, M.J., Stafford Jr., T.W. and Stevens, S.P., 2004. Stratigraphy and palaeoclimatic significance of Late Quaternary loess–palaeosol sequences of the Last Interglacial–Glacial cycle in central Alaska. Quaternary Science Reviews, 22: 1947-1986.

Müller, M.J., 1980. Handbuch ausgewählter Klimastationen der Erde. Forschungsstelle Bodenerosion. Universität Trier, Mertesdorf.

Nadelhoffer, K.J. and Fry, B., 1988. Controls on natural Nitrogen-15 and Carbon-13 abundances in soil organic matter. Soil Sci. Soc. Am. J., 52: 1633-1640.

Nadelhoffer, K.J. and Fry, B., 1994. Nitrogen isotope studies in forest ecosystems. In: R.H. Michener (Editor), Stable Isotopes in Ecology and Environmental Science. Blackwell Scientific Publications, Oxford, pp. 22-44.

NGRIP members, 2004. High-resolution record of Northern Hemisphere climate extending into the last interglacial period. Nature, 431: 147-151.

Nott, C.J., Xie, S., Avsejs, L.A., Maddy, D., Chambers, F.M. and Evershed, R.P., 2000. n-Alkane distribution in ombrotrophic mires as indicators of vegetation change related to climatic variation. Organic Geochemistry, 31: 231-235.

Nugteren, G., Vandenberghe, J., van Huissteden, J.K. and Zhisheng, A., 2004. A Quaternary climate record based on grain size analysis from the Luochuan loess section on the Central Loess Plateau, China. Global and Planetary Change, 41(3-4): 167-183.

Odada, E.O. and Olago, D.O., 2002. The East African Great Lakes: Limnology, Palaeolimnology and Biodiversity. Kluwer Academic Publishers.

O'Leary, M.H., 1995. Environmental effects on carbon isotope fractionation in terrestrial plants. In: B.D. Fry (Editor), Stable Isotopes in the Biosphere. Kyoto University Press, Japan, pp. 79-91.

Osmaston, 1989. Glaciers , glaciations and equilibrium line altitudes on Kilimanjaro. In: W.C. Mahaney (Editor), Quaternary and Environmental Research on East African Mountain. A.A.Balkema, Rotterdam/Brookfield.

Paerl, H.W. and Fogel, M.L., 1994. Isotopic characterization of atmospheric nitrogen inputs as sources of enhanced primary production in coastal Atlantic Ocean waters. Mar. Biol., 119: 635-645.

Papen, H. and Butterbach-Bahl, K., 1999. A 3-year continuous record of nitrogen trace gas fluxes from untreated and limed soil of a N-saturated spruce and beech forest ecosystem in Germany. J. Geophys. Res., 104: 18487-18503.

Pessenda, L.C., Gomes, B.M., Aravena, R., Ribeiro, A.S., Boulet, R. and Gouveia, S.E., 1998. The carbon isotope record in soils along a forest-cerrado ecosystem transect: implications for vegetation changes in the Rondonia state, southwestern Brazilian Amazon region. The Holocene, 8(5): 599-603.

Petit, J.R., Jouzel, J., Raynaud, D., Barkov, N.I., Barnola, J.-M., Basile, I., Bender, M., Chappellaz, J., Davis, M., Delaygue, G., Delmotte, M., Kotlyakov, V.M., Legrand, M., Lipenkov, V.Y., Lorius, C., Pépin, L., Ritz, C., Saltzman, E. and Stievenard, M., 1999. Climate and atmospheric history of the past 420,000 years from the Vostoc ice core, Antarctica. Nature, 399: 429-436.

Rieley, G., Collier, R.J., Jones, D.M., Eglinton, G., Eakin, P.A. and Fallick, A.E., 1991. Sources of Sedimentary Lipids Deduced from Stable Carbon Isotope Analyses of Individual Compounds. Nature, 352(6334): 425-427.

Rohr, P.C. and Killingtveit, A., 2003. Rainfall distribution on the slopes of Mt Kilimanjaro. Hydrological Sciences Journal-Journal Des Sciences Hydrologiques, 48(1): 65-77.

Rousseau, D.-D., Antoine, P., Hatté, C., Lang, A., Zöller, L., Fontugne, M., Othman, D.B., Luck, J.M., Moine, O., Labonne, M., Bentaleb, I. and Jolly, D., 2002. Abrupt millennial climatic changes from Nussloch (Germany) Upper Weichselian eolian records during the Last Glaciation. Quaternary Science Reviews, 21: 1577-1582.

Schmitt, J., Glaser, B. and Zech, W., 2003. Amount-dependent isotopic fractionation during compound-specific isotope analysis. Rapid Communications in Mass Spectrometry, 17: 970-977.

Schrumpf, M., 2004. Biochemical Investigations in Old Growth and Disturbed Forest Sites at Mount Kilimanjaro. Ph.D. Thesis, University of Bayreuth, Germany.

Schulze, E.-D., Chapin III, F.S. and Gebauer, G., 1994. Nitrogen nutrition and isotope differences among life forms at the northern treeline of Alaska. Oecologia, 100: 406-412.

Schwark, L., Zink, K. and Lechtenbeck, J., 2002. Reconstruction of postglacial to early Holocene vegetation history in terrestrial Central Europe via cuticular lipid biomarkers and pollen records from lake sediments. Geology, 30(5): 463-466.

Shackleton, N.J., Hall, M.A. and Vincent, E., 2000. Phase relationships between millennial scale events 64,000 to 24,000 years ago. Paleoceanography, 15: 565-569.

Shanahan, T.M. and Zreda, M., 2000. Chronology of quaternary glaciations in East Africa. Earth and Planetary Science Letters, 177(1-2): 23-42.

Shugart, H.H., French, N.H.F., Kasischke, E.S., Slawski, J.J., Dull, C.W., Shuchman, R.A. and Mwangi, J., 2001. Detection of vegetation change using reconnaissance imagery. Global Change Biology, 7(3): 247-252.

Stauch, G., Lehmkuhl, F. and Frechen, M., 2006. Luminescence chronology from the Verkhoyansk Mountains (North-Eastern Siberia). quaternary Geochronology, in press.

Stevenson, B.A., Kelly, E.F., McDonald, E.V. and Busacca, A.J., 2005. The stable carbon isotope composition of soil organic carbon and pedogenic carbonates along a bioclimatic gradient in the Palouse region, Washington State, USA. Geoderma, 124: 37-47.

Street, F.A. and Grove, A.T., 1979. Global Maps of Lake-Level Fluctuations since 30,000 yr B.P. Quaternary Research, 12: 83-118.

Street-Perrott, F.A., Ficken, K.J., Huang, Y. and Eglinton, G., 2004. Late Quaternary changes in carbon cycling on Mt. Kenya, East Africa: an overview of the $\delta^{13}C$ record in lacustrine organic matter. Quaternary Science Reviews, 23: 861-879.

Svendsen, J.I., Alexanderson, H., Astakhov, V.I., Demidov, I., Dowdeswell, J.A., Funder, S., Gataullin, V., Henriksen, M., Hjort, C. and Houmark-Nielsen, M.e.a., 2004. Late Quaternary ice sheet history of northern Eurasia. Quaternary Science Reviews, 23(11-13): 1229-1271.

Talbot, M.R., 2001. Nitrogen Isotopes in Palaeolimnology. In: J.P. Smol (Editor), Tracking Environmental Change Using Lake Sediments. Kluwer Academic Publishers, Dordrecht, The Netherlands, pp. 401-439.

Thompson, L.G., Mosley-Thompson, E., Davis, M.E., Henderson, K.A., Brecher, H.H., Zagorodnov, V.S., Mashiotta, T.A., Lin, P.N., Mikhalenko, V.N., Hardy, D.R. and Beer, J., 2002. Kilimanjaro ice core records: Evidence of Holocene climate change in tropical Africa. Science, 298(5593): 589-593.

Trauth, M.H., Deino, A.L., Bergner, A.G. and Strecker, M.R., 2003. East African climate change and orbital forcing during the last 175 kyr BP. Earth and Planetary Science Letters, 206: 297-313.

van Dongen, B.E., Schouten, S. and Sinninghe Damasté, J.S., 2002. Carbon isotope variability in monosaccharides and lipids of aquatic algae and terrestrial plants. Marine Ecology Progress Series, 232: 83-92.

Vera, C.S., Vigliarolo, P.K. and Berbery, E.H., 2002. Cold season synoptic-scale waves over subtropical South America. Monthly Weather Review, 130: 684-699.

Wang, H., Follmer, L.R. and Liu, C.-L.J., 2000. Isotope evidence of paleo-El Niño-Southern Oscillation cycles in loess-paleosol record in the central United States. Geology, 28(9): 771-774.

Xie, S., Guo, J., Huang, J., Chen, F., Wang, H. and Farrimond, P., 2004. Restricted utility of $\delta^{13}C$ of bulk organic matter as a record of paleovegetation in some loess–paleosol sequences in the Chinese Loess Plateau. Quaternary Research, 62: 86-93.

Zhang, Z., Zhao, M., Eglington, G., Lu, H. and Huang, C., 2006. Leaf wax lipids as paleovegetational and paleoenvironmental proxies for the Chinese Loess Plateau over the last 170 kyr. Quaternary Science Reviews, 25: 575-594.

Zhang, Z., Zhao, M., Yang, X., Wang, S., Jiang, X., Oldfield, F. and Eglinton, G., 2004. A hydrocarbon biomarker record for the last 40 kyr of plant input to Lake Heqing, southwestern China. Organic Geochemistry, 35: 595-613.

Zhou, J.Y. and Lau, K.-M., 1998. Does a monsoon climate exist over South America? Journal of Climate, 11: 1020-1040.

Zöller, L., Rousseau, D.D., Jäger, K.D. and Kukla, G., 2004. Last interglacial, Lower and Middle Weichselian - a comparative study from the Upper Rhine and Thuringian loess areas. Zeitschrift für Geomorphologie N.F., 48(1): 1-24.

The Use of Biomarker and Stable Isotope Analyses in Palaeopedology

Reconstruction of Middle and Late Quaternary Environmental and Climate History, with Examples from Mt. Kilimanjaro, NE Siberia and NE Argentina

(Zum Einsatz der Biomarker- und Stabilisotopen-Analytik in der Palaeopedologie

Rekonstruktion mittel- und spätquartärer Landschafts- und Klimageschichte, mit Beispielen vom Kilimandscharo, aus NE Sibirien und NE Argentinien)

Cumulative Study

Study 1:

Evidence for Late Pleistocene climate changes from buried soils on the southern slopes of Mt. Kilimanjaro, Tanzania

Michael Zech

Institute of Soil Science and Soil Geography, University of Bayreuth, D-95440 Bayreuth, Germany

Phone: +49 (0)921 552247; Fax: +49 (0)921 552246, Email: michael_zech@gmx.de

Abstract

The distribution of the altitudinal vegetation zones on the slopes of Mt. Kilimanjaro is well known. But no reliable data are available about the vegetation shifts during the Quaternary. Here I present palaeopedological results (elemental, biomarker, stable isotope and radiocarbon analyses), indicating that the frequently occurring buried black A horizons in the montane forest belt have developed under ericaceous vegetation. Since *Erica* species are not abundant at this altitude nowadays but are characteristic for the subalpine zone, the palaeosols reflect palaeoclimatically driven fluctuations and changes of the vegetation zones on Mt. Kilimanjaro. The downhill descent of the ericaceous belt coincided with cold and dry periods like the Late Glacial and the Last Glacial Maximum. Older palaeosols document that such events also took place during the Marine Isotope Stages 3 and 4.

1. Introduction

For a long time, the reconstruction of the East African Quaternary history was mainly based on studies about former lake level fluctuations and on glacial chronologies established for the mountains Mt. Kilimanjaro (e.g. Osmaston, 1989), Mt. Kenya, Mt. Ruwenzori and Mt. Elgon (e.g. Hamilton, 1982; Lehman, 1998; Odada and Olago, 2002; Street and Grove, 1979). New methodological approaches like exposure dating of moraine boulders with ^{36}Cl (Shanahan and Zreda, 2000) or ^{40}Ar/^{39}Ar dating of lake sediments (Trauth et al., 2003) improve our understanding of long-term climate changes. Especially for the East African Holocene, high resolution vegetation and climate records are available from peat bogs (e.g. Aucour et al., 1999), lake sediment cores (e.g. Mohammed et al., 1995) and from Kilimanjaro ice cores (Thompson et al., 2002). The actual climatic dynamics are best illustrated by the dramatic glacier recession on Mt. Kilimanjaro during the last decades (Hastenrath and Greischar, 1997; Irion, 2001) and by vegetation changes detectable in East African alpine ecosystems during the last decades (Shugart et al., 2001).

While palaeosol sequences are widely used for the reconstruction of the Quaternary landscape evolution in many parts of the world, such records are less known from tropical Africa. Mahaney et al. (1989) for instance, described buried soils on Mt. Kenya. In Rwanda, buried dark A horizons (former topsoils) frequently occur in the mountain ranges between the Congo and Nile basins at altitudes of 2200-2500 m a.s.l. (Zech and Mühle, 1989). Radiocarbon analyses indicate that they were formed around 30 ka BP before vegetation adopted to the colder and drier climate prevailing during the Last Glacial Maximum (LGM) (Flenley, 1979a).

In the present study I describe palaeosol sequences along the southern slopes of Mt. Kilimanjaro with the objective to evaluate their potential for the reconstruction of the vegetation and climate history of the highest African mountain.

2. Materials and Methods

2.1 Study area

The ancient volcano Mt. Kilimanjaro is located in equatorial East Africa (~ 3°S , 37°E) on the territory of Tanzania close to the border to Kenya. It rises from the savannah plains at about 700 m elevation to the Kibo peak with 5895 m altitude. Climate greatly varies within this altitudinal range and with exposure (Rohr and Killingtveit, 2003), the southern

slopes being generally more humid than the northern ones. Climatic factors and topography heavily influence the vegetational zonation, which is similarly differentiated for many other East African mountains, too (Hedberg, 1951; Klotz, 1989). An overview of the vegetation zones of Mt. Kilimanjaro is given by Morris (1970) and Hemp et al. (1998).

For the interpretation of my palaeopedologic results the "ericaceous belt", first described by Hedberg (1951), is of special relevance (Fig. 1-1). It corresponds closely to the term "subalpine", which is applied to the transition zone between the broad-leaf montane forest and the alpine *Helichrysum* scrub vegetation. According to Hemp and Beck (2001), the upper boundary of the broad-leaved vegetation at about 2800 m a.s.l. is often abrupt and the result of fires. Above this altitude, the fire-tolerant *Erica excelsa* is the dominant tree species. The so-called *Erica*-bush, which is mainly formed by *Erica arborea* and *E. trimera, Protea caffra* and *Euryops dacrydioides*, gradually replaces the forest between 3100 m and 3500 m.
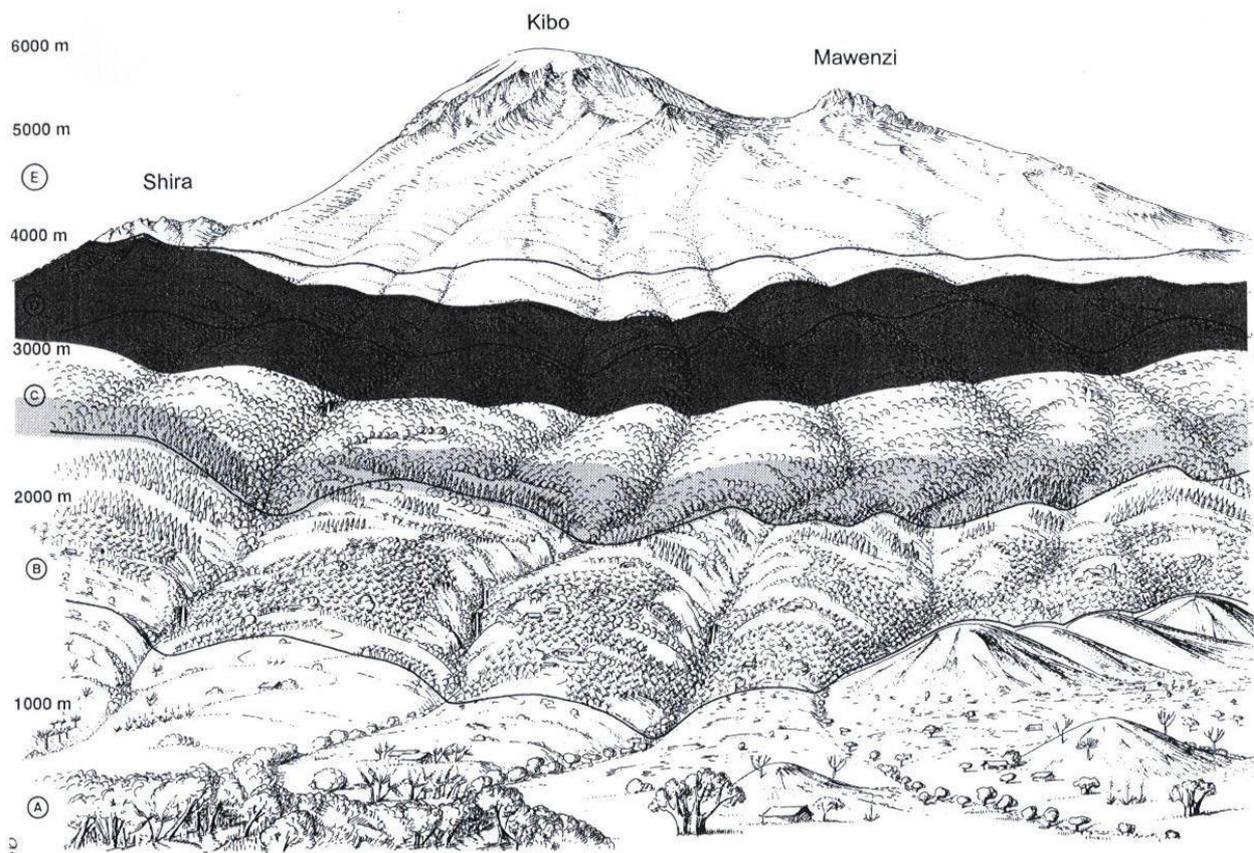
Fig. 1-1: Distribution of *Erica excelsa* over the altitudinal vegetation zones on the southern slopes of Mt. Kilimanjaro: Areas of dominant *E. e.* are marked in black. A: colline zone, B: submontane zone, C: montane zone, D: subalpine zone, E: alpine zone. From Hemp and Beck (2001).

2.2 Field work and working hypotheses

In march 2001 a soil catena was established along the Machame Route which leads from Machame Gate (1825 m a.s.l.) to the Shira Plateau (about 4000 m a.s.l.). The six soil profiles mentioned in this study are named according to their altitude above sea level, UTM coordinates are given in brackets: TS01/2090 (304971/9651216), TS01/2250 (305168/9653242), TS01/2290 (305232/9654142), TS01/2700 (306382/9656263), TS01/2900 (306836/9657131) and TS01/3150 (304868/9651133). In the montane zone the dark A topsoils typically overlie brunified B horizons. According to the Soil Taxonomy these soils can be classified as Andosols (Schrumpf, 2004; Soil Survey Staff, 2003). Middle and lower parts of the soil profiles are often characterized by sequences of buried black, brown and mottled gray horizons and reddish iron pans, indicating hydromorphic processes (Fig. 1-2).
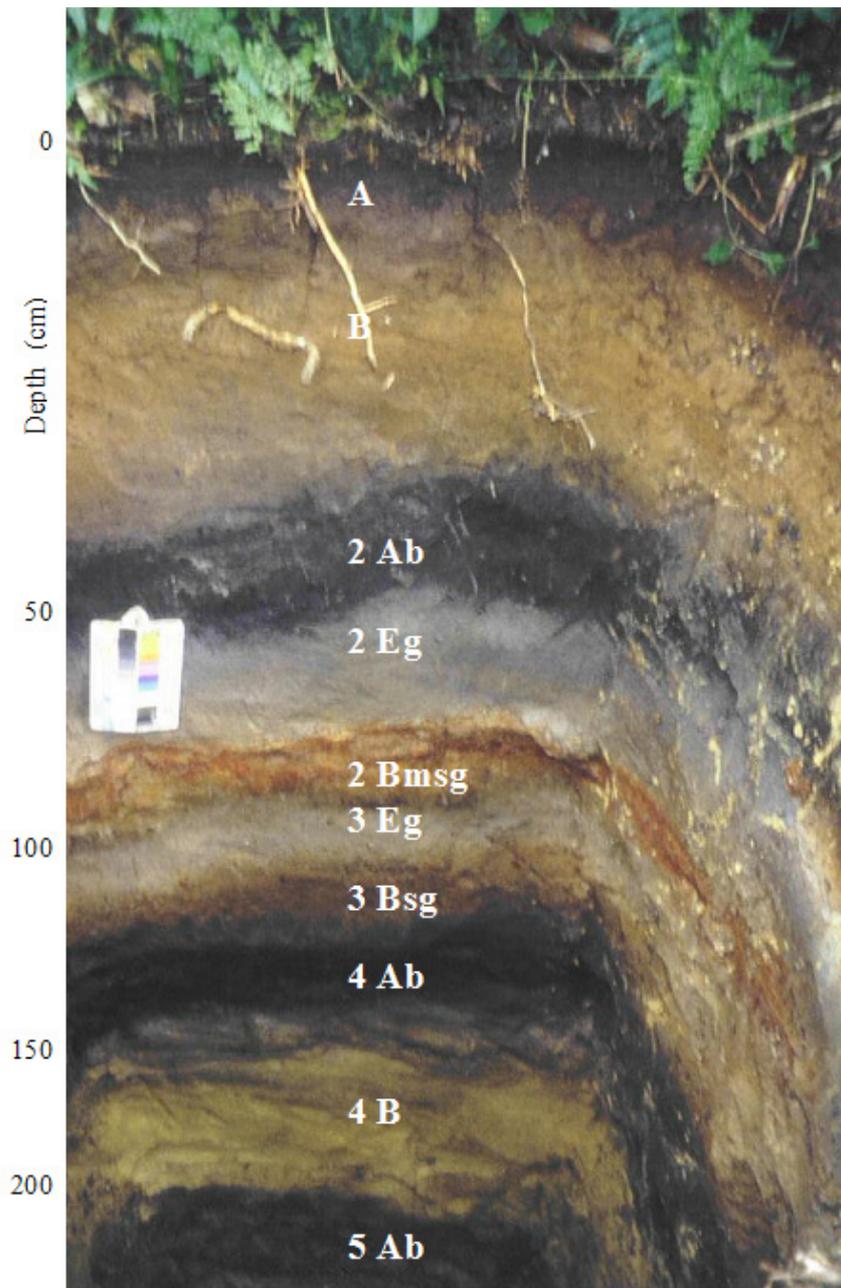
Fig. 1-2: Photo of soil profile TS01/2250 (2250 m a.s.l.) in the montane forest zone. Buried black horizons are intercalated by brown, grey and reddish layers, indicating changing pedogenetic conditions.

The basis of these palaeosol sequences is mostly formed by mottled gray clays above the volcanic parent material. Further uphill, the soils become less deep but still reveal polygenetic features up to an altitude of about 3150 m. Soils in this "ericaceous belt" are often characterized by swampy condition and the topsoils here are strikingly deep black. The alpine zone is dominated by Leptosols (A/C), which are influenced by solifluction and cryogenic processes.

Deduced from field observations and especially from the morphological resemblance of the buried black horizons in the montane zone with the deep black topsoils in the "ericaceous belt", this paper is structured around the following hypotheses:

(iv)   the buried black horizons in the montane zone are buried topsoils (Ab horizons),

(v)   they developed under ericaceous vegetation, and thus

(vi)   represent periods with significant changes of the climate regime and the vegetation belts.

In order to verify these working hypotheses, I studied in detail a key soil profile (TS01/2250) at 2250 m a.s.l., being representative for the montane forest belt, and took at least one sample from each soil horizon for geochemical analyses (n = 21) and seven samples for numeric dating. Fig. 1-2 and Fig. 1-3 illustrate the morphology and stratigraphy of soil profile TS01/2250. Within the 250 cm thick solum three buried black horizons can be identified (2 Ab, 4 Ab and 5 Ab). The intercalating mottled gray, reddish and brown layers indicate processes typical for Gleysols (diagnostic horizon: Eg) and Cambisols (B), respectively. Along the catena, additionally, litter and plant samples as well as further soil samples for radiocarbon dating were taken.

2.3 Sample preparation and laboratory analyses

Air dried and sieved samples (< 2 mm) were processed following standard laboratory procedures at the Institute of Soil Science and Soil Geography, University of Bayreuth. Total organic carbon (TOC) and nitrogen (N) were determined by dry combustion of a finely ground homogeneous 50 mg subsample followed by thermal conductivity detection on a Vario EL elemental analyser (Elementar, Hanau, Germany). $\delta^{13}C$ values of soil organic matter were obtained by dry combustion on a Carlo Erba NC 2500 elemental analyser coupled with a Delta^{plus} continuous-flow isotope ratio mass spectrometer (Thermo Finnigan MAT, Bremen, Germany) via a Conflow II interface (Thermo Finnigan MAT, Bremen, Germany). Sucrose (ANU, IAEA, Vienna, Austria) and $CaCO_3$ (NBS 19, Gaithersburg, USA) were used as

calibration standards. Natural abundance of carbon stable isotopes are expressed in the usual δ-scale in parts per thousand according to Eqn. (1),

$$\delta_{sample} \ (\text{‰}) = \left(\frac{R_{sample} - R_{standard}}{R_{standard}} \right) \ \times \ 1000, \tag{1}$$

where R_{sample} and $R_{standard}$ are the $^{13}C/^{12}C$ abundance ratios of a sample or a standard, respectively.

Black Carbon (BC) was analyzed according to Glaser et al. (1998) and Brodowski et al. (2005). For the extraction of soil lipids, an accelerated solvent extractor (Dionex ASE 200) was used. Free lipids were extracted with methanol/toluene (7/3) at 9×10^6 Pa and a temperature of 120° C, followed by n-alkane separation on columns with aluminum oxide silica gel (both 5% deactivated) and 45 ml hexane/toluene (85/15) as elution solvent. For quantification, an HP 6890 GC equipped with a flame ionization detector (FID) and deuterated n-alkanes (d_{40}-n-C_{19} and d_{50}-n-C_{24}) as internal standards were used.

Radiocarbon analyses for 18 samples were performed on the acid fraction of organic matter (HA) or of charcoal (HK) at the Physical Institute of the University of Erlangen-Nürnberg, Germany. Conventional radiocarbon ages younger than 17 ka BP were calibrated according to Stuiver et al. (1998). Both conventional and calibrated ^{14}C ages are given in Table 1-2. In the text and in Fig. 1-5 we refer to the calibrated data.

3. Results and Discussion

3.1 Elemental analyses

According to Fig. 1-3, TOC shows maxima for the three buried black horizons with TOC values of over 10% in the two upper palaeosols and over 6% in the lowermost palaeosol. This finding supports hypothesis (i) that the buried black horizons in the montane zone are humic-rich fossil topsoils.

Also the TOC/N ratios show maxima for the three Ab horizons (2 Ab = 25, 4 Ab = 28 and 5 Ab = 22). Additionally, the iron crust at 85 cm depth reveals high TOC/N ratios of 27 probably due to the accumulation of dissolved organic carbon (Fig. 1-3). These results support hypothesis (ii), because litter and vegetation samples collected above 2900 m a.s.l. in the ericaceous and alpine belt are characterized by high TOC/N ratios (> 20) (Table 1-1). On the contrary, I found TOC/N ratios around 20 and lower mainly for litter in the montane zone.

Table 1-1: TOC/N ratios of litter and some plant samples collected from along a transect on the southern slopes of Mt. Kilimanjaro. Ratios around 20 and lower are typically found in the montane forest zone and cannot explain the soil TOC/N maxima (>20) obtained for the buried A horizons in profile TS01/2250. Litter and characteristic plants of the ericaceous zone generally reveal high TOC/N ratios.

ericaceous belt		montane zone	
sample	TOC/N	sample	TOC/N
2980/litter	26,36	2030/litter	17,16
3100/litter	38,73	2140/litter	15,86
3150/litter	41,42	2250/litter	17,15
3230/litter	24,38	2350/litter	18,43
3800/litter	33,17	2550/litter	19,36
Hylocomium spec.	58,41	2650/litter	20,23
Sphagnum spec.	43,12	2780/litter	20,64
Erica spec.	35,31	*Hagenia abyssinica*	19,84
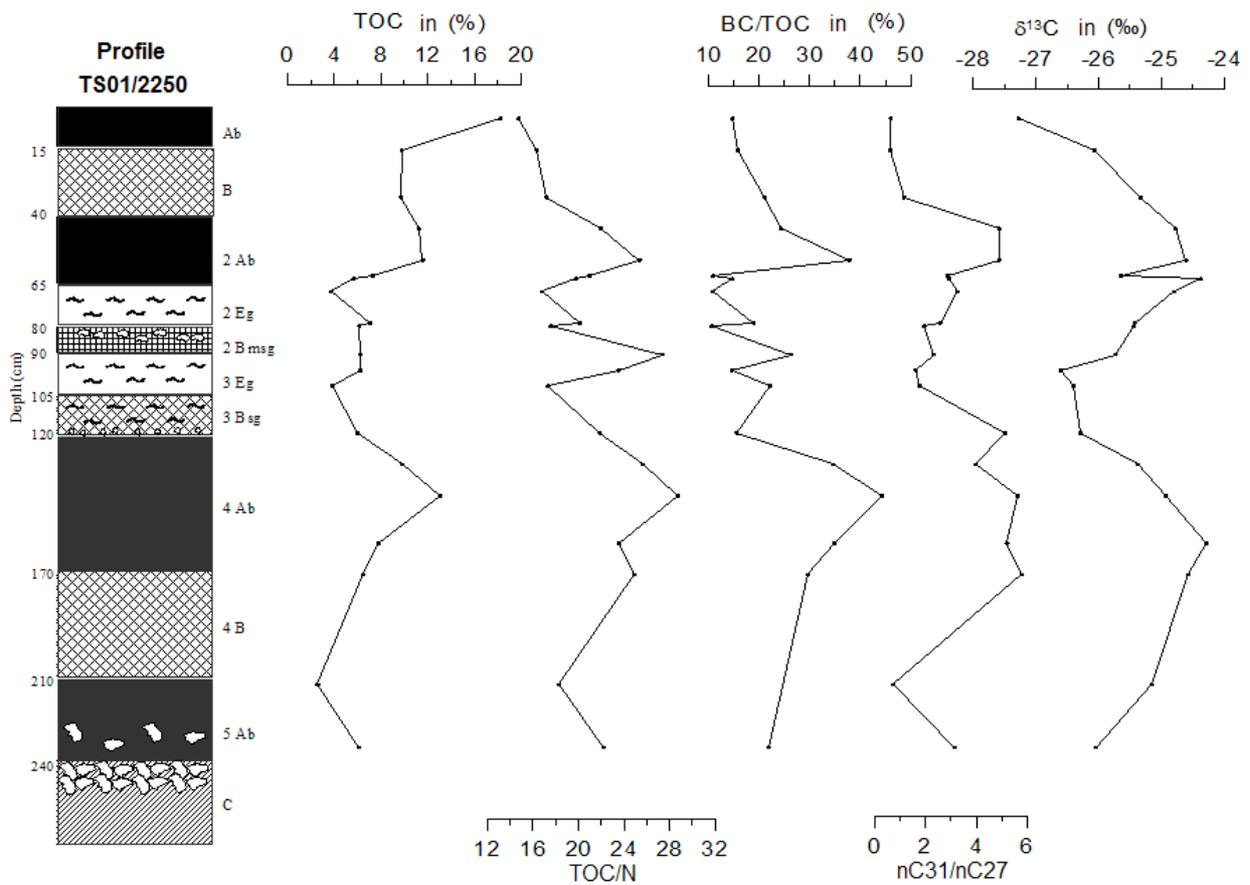
Fig. 1-3: Stratigraphy and geochemical results of profile TS01/2250. Black horizons reveal higher TOC contents and are therefore referred to as Ab horizons. Especially the 2 Ab and 4 Ab horizon are characterized by high TOC/N ratios, maxima in BC, high nC_{31}/nC_{27} ratios and more positive $\delta^{13}C$ values, indicating that these horizons developed under ericaceous vegetation.

Since soils generally reveal lower TOC/N ratios than the covering litter, the observed maxima for our proxy in the Ab horizons cannot be explained by mineralization effects alone. Instead, the high TOC/N ratios in the buried dark layers support the idea, that soil organic matter derived from ericaceous litter.

3.2 Biomarker and stable carbon isotope analyses

Apart from TOC and TOC/N ratios, further proxies like BC, n-alkanes and stable isotopes were applied to characterize the palaeosols of profile TS01/2250 (Fig. 1-3).

3.2.1 Black Carbon (BC)

As demonstrated by Bird and Cali (1998), BC may be a useful tool for reconstructing fire-history. The application of this proxy to the palaeosols of Mt Kilimanjaro was promising, because the Ab horizons often contain charcoal fragments, indicating frequent fire events which are typical for the ericaceous belt but not for the montane zone (Hemp and Beck, 2001). Additionally, BC is a relative stabile C pool (Glaser et al., 2002; Oades, 1995) and could therefore partly explain the wide TOC/N ratios of the Ab horizons.

According to Fig. 1-3, the BC contribution to TOC in soil profile TS01/2250 is astonishing high and varies between 10,6 and 44,4 %. Distinct maxima coincide with the 2 Ab and 4 Ab horizons, indicating frequent fire events during the formation of these horizons. These findings further support hypothesis (ii) that the Ab layers mainly derive from the decline of the ericaceous vegetation during the past.

3.2.2 N-alkanes

Terrestrial plants incorporate n-alkanes with chain-length between nC_{20} and nC_{35} into their leaf-waxes (Kolattukudy, 1976). Plant derived n-alkanes extracted from soils or sediments should exhibit a similar n-alkane pattern as does the former vegetation, which may thus be reconstructed (Cranwell, 1973; Farrimond and Flanagan, 1996b; Ficken et al., 1998). Schwark et al. (2002) for instance, used the dominance of nC_{31} in grasses and nC_{27} in trees, respectively, for the reconstruction of the postglacial to early Holocene vegetation history in the catchment of Lake Steisslingen, Germany.

According to Fig. 1-3 the three Ab horizons of soil profile TS01/2250 are characterized by distinct maxima ($nC_{31}/nC_{27} > 3,5$) while minima with ratios lower than 2 were found for the intercalating B horizons. Fig. 1-4 illustrates the n-alkane pattern of litter and topsoil samples for the soil profiles TS01/3150, representative for the ericaceous belt, and

TS01/2250, representative for the montane zone. Obviously, nC_{27} and nC_{29} dominate in the samples taken from the montane forest and nC_{29} and nC_{31} dominate in the samples from the ericaceous belt. The n-alkane ratio nC_{31}/nC_{27} seems therefore to be a valuable proxy for detecting horizons in the recent montane zone, which developed during the past under ericaceous vegetation. This interpretation of the palaeosol horizons 2 Ab, 4 Ab and 5 Ab is definitely corroborated by palynological analyses from Schlütz (personal communication) who found mainly *Erica excelsa* pollen (> 80%) in the 4 Ab horizon.
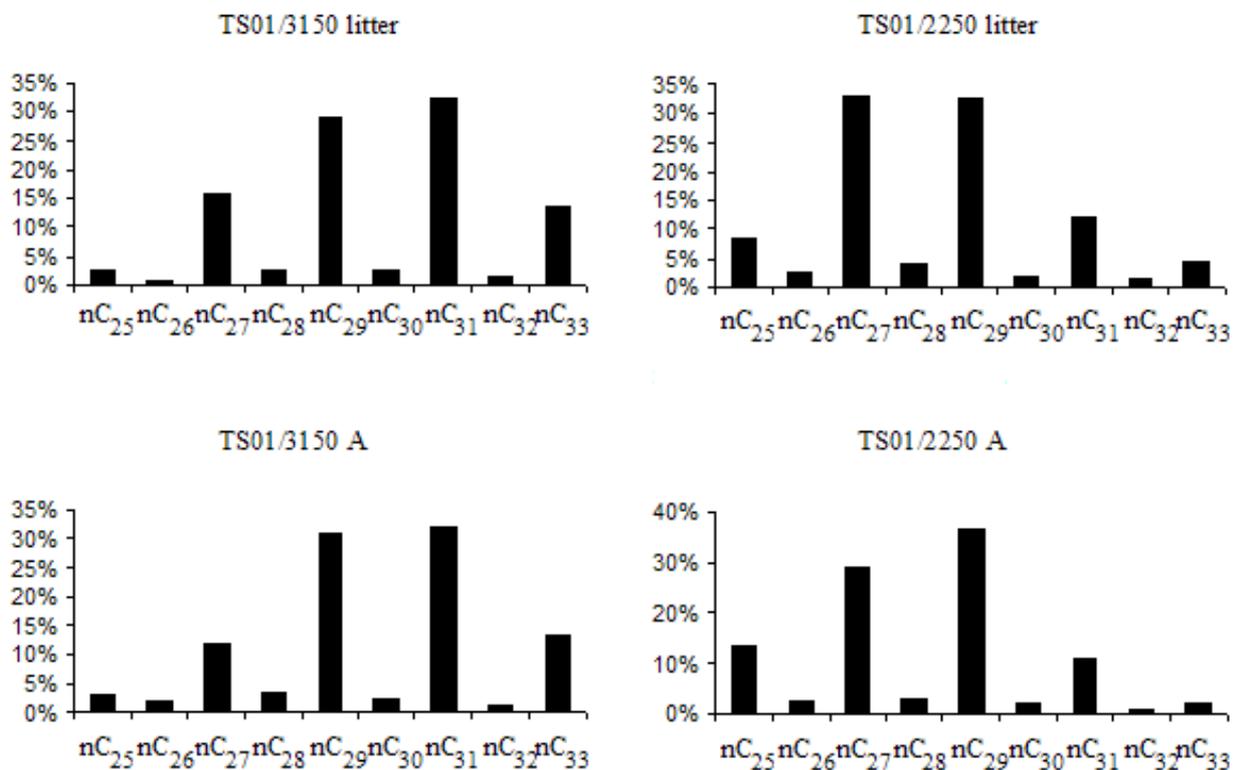
Fig. 1-4: n-Alkane pattern of litter and topsoil samples, collected from soil profile TS01/3150 and from the key profile TS01/2250. The relative abundance of individual n-alkanes to the sum of all n-alkanes from nC_{25} to nC_{33} is plotted. While nC_{29} and nC_{31} dominate in the ericaceous belt, nC_{27} and nC_{29} dominate in the montane forest.

3.2.3 Stable carbon isotopes

Vegetation changes in the tropics may be reconstructed using stable carbon isotopes due to different photosynthetic pathways of C4 and C3 plants (Aucour et al., 1999; Collatz et al., 1998). Nearly all trees, as well as most shrubs and herbs of cold and temperate environments are C3 plants and typically reveal $\delta^{13}C$ values around $-28‰$ (Sage, 2001). C4 plants with $\delta^{13}C$ values around $-14‰$ are generally adapted to higher temperatures, drier climate and lower atmospheric CO_2 concentrations, the latter having occurred during the Last

Glacial Maximum (LGM) (Raynaud et al., 1993). They comprise large numbers of tropical savannah grass and sedge species (graminoids), as well as a range of dicotyledonous herbs and shrubs. However, some panicoid C4 grasses and C4 sedges are able to tolerate low temperatures prevailing in montane environments (Sage et al., 1999). Street-Perrott et al. (1997) explained shifts to more positive $\delta^{13}C$ values (up to about 14‰) in sediments of Sacred Lake, located in 2350 m a.s.l. at Mt. Kenya, with the expansion of C4 grasses during colder and drier climatic conditions characterizing the LGM. Sub-ambient CO_2 and enhanced moisture stress were supposed to have been of profound significance for the competitive advantage of C4 plants during that period.

The $\delta^{13}C$ values of the key soil profile TS01/2250 at Mt. Kilimanjaro stay well within the range typical for the C3 photosynthetic pathway (-27,3‰ to -24,3‰) and give no rise for abundant increase of C4 plants (Fig. 1-3). Nevertheless, the stable carbon isotope signals shift to more positive values in buried A horizons and correlate significantly with other palaeoecologically relevant proxies like the nC_{31}/nC_{29} (R = 0,81) and the nC_{31}/nC_{27} ratios (R = 0,57), respectively. As also the horizons A and 2 Abg of the soil profile TS01/3150 are characterized by more positive $\delta^{13}C$ values (-25,6‰) than the A horizon of profile TS01/2250 (-27,3‰), these results further corroborate hypothesis (ii) that significant environmental changes occurred during the past, which are documented by the buried Ab horizons.

3.3 Palaeopedologic reconstruction of the vegetation history and palaeoclimatic implications

The results discussed so far strongly support our idea that the black palaeosols, frequently occurring in the montane forest belt of the southern slopes at Mt. Kilimanjaro developed under ericaceous vegetation. Nowadays, *Erica excelsa* is the dominant tree species above 2800 m a.s.l.. From palynological studies on East African mountains it is well known that altitudinal shifts of the vegetation zones took place during the past and were mainly controlled by climatic factors like temperature and precipitation (Flenley, 1979b; Hamilton, 1982; Lamb et al., 2003). Accordingly, I propose that the Ab horizons in the montane forest zone document colder and drier periods during the past, when ericaceous vegetation descended several hundreds of meters and gained competitive advantage in an altitude, which is characterized nowadays by broad-leaf montane forest.

In order to establish a chronology for such events, buried Ab horizons of soil profile TS01/2250 and other members of the catena up to 3150 m a.s.l. were dated by a total of 18 radiocarbon analyses. According to Table 1-2 and Fig. 1-5, three calibrated ages around 19.5

Table 1-2: Radiocarbon dates of humic acids and one charcoal sample (HK) of mainly buried A horizons along a soil catena on the southern slopes of Mt. Kilimanjaro (Physical Institute of the University of Erlangen-Nürnberg, Germany). For details of the soil profiles see Fig. 1-5.

sample			targetnumber	conventional ^{14}C (a BP)	calibrated ^{14}C (a BP)	chronology
TS01/3150	2 Ab	60 cm	5052	7020±69	7818±181	**Early Holocene**
TS01/2900	2 Ab	30 cm	4382	6254±61	7152±158	**Early Holocene**
TS01/2700	2 Ab	45 cm	5056	6845±66	7683±155	**Early Holocene**
TS01/2250	B	35 cm	5051	7169±65	7988±108	**Early Holocene**
TS01/2900	2 Ab	65 cm	4389	9387±96	10658±410	**Younger Dryas**
TS01/2700	3 Ab	80 cm	4388	9430±86	10747±342	**Younger Dryas**
TS01/2090	2 Ab	45 cm	4386	9533±89	10870±290	**Younger Dryas**
TS01/2700	3 Ab	125 cm	4384	13833±233	16602±696	**Late Glacial**
TS01/2290	3 Ab	60 cm	5054	13815±122	16594±748	**Late Glacial**
TS01/2250	2 Ab	45 cm	4385	16298±111	19461±540	**LGM**
TS01/2250	2 Ab	60 cm	4390	16613±180	19810±696	**LGM**
TS01/2250	2 Eg	75 cm	5059	16416±155	19588±969	**LGM**
TS01/2290	4 Ab	80 cm	5058	18693±227	-	**LGM**
TS01/2290	4 Ab	95 cm	5063	21196±332	-	**LGM**
TS01/2090	2 Ab	75 cm	4387	15756±132	18829±581	**LGM**
TS01/2250	4 Ab	120 cm	5061	30558±561	-	**MIS 3**
TS01/2250	4 Ab	130 cm	4383	38176±524	-	**MIS 3**
TS01/2250	5 Ab(HK)	235 cm	4301	57804±9260	-	**MIS 3 or 4**

ka BP were obtained for the 2 Ab and the underlying 2 Eg horizons of soil profile TS01/2250, indicating that their organic matter developed during the LGM. Also the lower part of the 2 Ab horizon of soil profile TS01/2090 and the 4 Ab horizon of TS01/2290 were formed during the LGM. These results correlate with ^{36}Cl exposure ages derived from moraine boulders of the Fourth Glaciation on Mt. Kilimanjaro (Shanahan and Zreda, 2000), and with lake level minima of most East African lakes (Gasse, 2000), confirming a cold and dry environment during the LGM. A series of smaller moraines above the LGM deposits record several glacier readvances during the Late Glacial (Shanahan and Zreda, 2000). Although they are not documented in soil profile TS01/2250, dark Ab horizons in other members of the soil catena correlate with these glacial fluctuations. Two calibrated ages around 16.6 ka BP were obtained for the 3 Ab horizon of soil profile TS01/2290 and for the lower part of the 3 Ab horizon of soil profile TS01/2700. In the soil profiles TS/2090, 2700 and 2900 dark buried Ab horizons developed at approximately 10.7 ka BP, indicating a descent of the ericaceous belt

during the Younger Dryas interval. This cold and dry event is also reported from Sacred Lake, Mt. Kenya (Street-Perrott et al., 1997) and from other East African Lakes (Gasse, 2000).
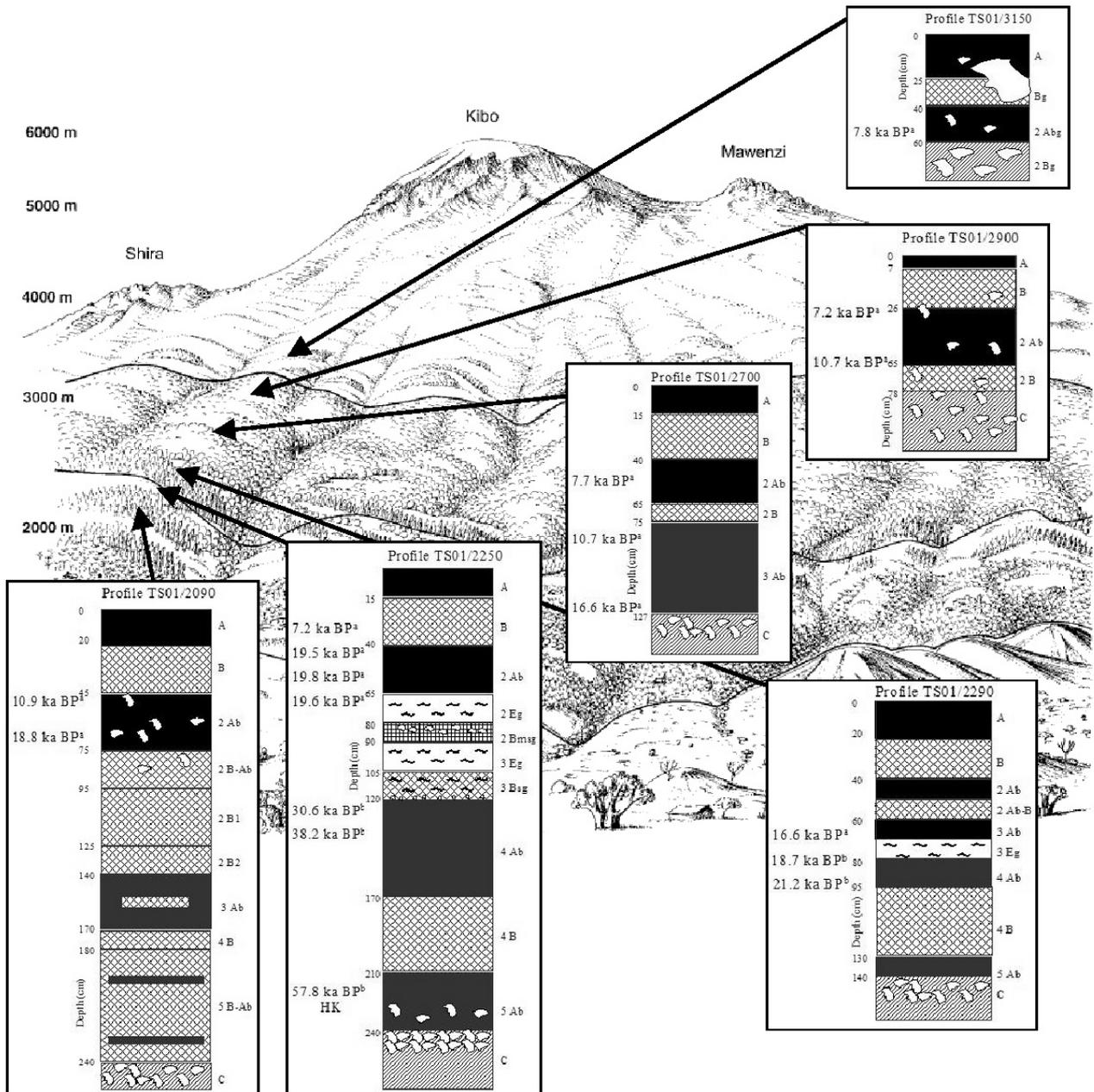
Fig. 1-5: Palaeosol sequences along a catena on the southern slopes of Mt. Kilimanjaro. (redrawn from Hemp and Beck, 2001). 18 radiocarbon ages were obtained mainly for humic acids of soil organic matter (one for charcoal, HK) from buried A horizons. [a] calibrated ^{14}C ages, [b] conventional ^{14}C ages.

Generally, all Ab horizons which developed during the LGM and the Late Glacial are covered by brunified B horizons. The genesis of these B horizons seems therefore to be associated with the ascent of the tree line during the African Humid Period (approximately 10-6 ka BP), which has favored the expansion of the tropical montane forests (Ritchie et al., 1985; Roberts, 1996). During the Early Holocene, North and East Africa experienced a dry spell around 8.4-8 ka BP (Gasse, 2000) and glaciers advanced on Mt. Kenya around 8.6 ka BP (Shanahan and Zreda, 2000). This event is probably documented in the 2 Ab horizons of the soil profiles TS01/2700, TS01/2900 and TS01/3150 (Table 1-2 and Fig. 1-5), the upper members of the catena, although the three calibrated ages obtained for these palaeosols are some hundred years younger (around 7.6 ka BP). The discrepancy may be explained by rejuvenation due to dissolved organic carbon and younger root C inputs. According to these results, the ericaceous belt did not descend lower than approximately 2700 m a.s.l. during the Holocene. B horizons directly below the topsoil A horizons started to develop after 7.6 ka BP at higher altitudes, whereas at lower altitudes their genesis started already after the Younger Dryas or even after the LGM.

Table 1-2 and Fig. 1-5 depict that further palaeosols are buried in the soil profiles TS01/2090-2290 below the LGM-dated horizons. Despite of uncertainties concerning radiocarbon data older than 30-40 ka BP, we assume that these Ab horizons represent cold and dry stages during the Marine Isotope Stages (MIS) 3 and/or 4. Like the LGM, these climatic deteriorations should have been accompanied by vegetation changes in form of a descending ericaceous belt on the southern slopes of Mt. Kilimanjaro.

4. Conclusions

The southern slopes of Mt. Kilimanjaro reveal deep black buried horizons under montane forest in about 2000-2300 m a.s.l.. These Ab horizons are characterized by higher C/N-ratios, higher BC contents, higher n-alkane ratios (C_{31}/C_{27}) and more positive $\delta^{13}C$ values than the intercalating layers. All four geochemical proxies and the preliminary palynological results support the idea that the buried A horizons in the montane forest zone developed under ericaceous vegetation. Since nowadays *Erica excelsa* is dominant only above 2800 m a.s.l., the palaeosols allow the reconstruction of past climatic changes, which caused the descent of the ericaceous belt. Above 2700 m a.s.l., the development of buried A horizons correlates with Late Glacial and Early Holocene glacial readvances around 16.5 ka BP, during the Younger Dryas and at about 7.6 ka BP. Additionally, the lower members of the soil catena

between 2090 m and 2290 m a.s.l. reveal black Ab horizons, which developed during the LGM, between 30-38 ka BP and even before. The palaeosol sequences on the southern slopes of Mt. Kilimanjaro document Late Pleistocene vegetation and climate changes, and thus contribute to a better understanding of the East African palaeoenvironment.

Further palaeopedological work is conducted to refine the spatial and temporal extent of the palaeosols. It would be especially useful to supplement the applied methods with more detailed palynological and charcoal analyses.

Acknowledgements

References

Aucour, A.-M., Hillaire-Marcel, C. and Bonnefille, R., 1999. Sources and accumulation rates of organic carbon in an equatorial peat bog (Burundi, East Africa) during the Holocene: carbon isotope constraints. Palaeogeography, Palaeoclimatology, Palaeoecology, 150: 179-189.

Bird, M.J. and Cali, J.A., 1998. A million-year record of fire in sub-Saharan Africa. Nature, 394: 767-769.

Brodowski, S., Rodionov, A., Haumaier, L. and Zech, W., 2005. Revised black carbon assessment using benzene polycarboxylic acids. Organic Geochemistry, 36: 1299-1310.

Collatz, G.J., Berry, J.A. and Clark, J.S., 1998. Effects of climate and atmospheric CO_2 partial pressure on global distribution of C4 grasses: present, past and future. Oecologia, 114: 441-454.

Cranwell, P.A., 1973. Chain-length distribution of n-alkanes from lake sediments in relation to post-glacial enviromental change. Freshwater Biology, 3: 259-265.

Farrimond, P. and Flanagan, R.L., 1996. Lipid stratigraphy of a Flandrian peat bed (Northumberland, UK): comparison with the pollen record. The Holocene, 6(1): 67-74.

Ficken, K.J., Barber, K.E. and Eglinton, G., 1998. Lipid biomarker, $\delta^{13}C$ and plant macrofossil stratigraphy of a Scottish montane peat bog over the last two millennia. Organic Geochemistry, 28(3/4): 217-237.

Flenley, J.R., 1979a. The Equatorial Rain Forest: a geological history. Butterworths, London.

Flenley, J.R., 1979b. The Late Quaternary vegetational history of the equatorial mountains. Progress in Physical Geography, 3: 488-509.

Gallet, S., Jahn, B., Van Vliet Lanoe, B., Dia, A. and Rossello, E., 1998. Loess geochemistry and its implications for particle origin and composition of the upper continental crust. Earth and Planetary Science Letters, 156: 157-172.

Gasse, F., 2000. Hydrological changes in the African tropics since the Last Glacial Maximum. Quaternary Science Reviews, 19: 189-211.

Glaser, B., Lehmann, J. and Zech, W., 2002. Ameliorating physical and chemical properties of highly weathered soils in the tropics with charcoal - a review. Biology and Fertility of Soils, 35(4): 219-239.

Hamilton, A.C., 1982. Environmental History of East Africa. Academic Press.

Hastenrath, S. and Greischar, L., 1997. Glacier recession on Kilimanjaro, East Africa, 1912-89. Journal of Glaciology, 43(145): 455-459.

Hedberg, O., 1951. Vegetation belts of the East African mountains. Scvensk. Bot. Tidskr., 45: 140-202.

Hemp, A. and Beck, E., 2001. Erica excelsa as a fire-tolerating component of Mt. Kilimanjaro's forests. Phytocoenologia, 31(4): 449-475.

Hemp, A., Hemp, C. and Winter, J.C., 1998. Der Kilimanjaro - Lebensräume zwischen tropischer Hitze und Gletschereis. Natur und Mensch: 5-28.

Huang, Y., Eglington, G., Ineson, P., Latter, P.M., Bol, R. and Harkness, D.D., 1997. Absence of carbon isotope fractionation of individual n-alkanes in a 23-year field decomposition experiment with Calluna vulgaris. Organic Geochemistry, 26(7/8): 497-501.

Irion, R., 2001. The melting snows of Kilimanjaro. Science, 291(5509): 1690-1691.

Klotz, G.e.a., 1989. Hochgebirge der Erde und ihre Pflanzen- und Tierwelt. Urania - Verlag. Leipzig - Berlin.

Kolattukudy, P.E., 1976. Biochemistry of plant waxes. In: Kolattukudy (ed.), Chemistry and Biochemistry of Natural Waxes, Amsterdam: Elsevier, 290-349.

Lamb, H., Darbyshire, I. and Verschuren, D., 2003. Vegetation response to rainfall variation and human impact in central Kenya during the past 1100 years. the Holocene, 13(2): 285-292.

Lehman, J.T., 1998. Environmental Change and Response in East African Lakes. Kluwer Academic Publishers.

Mahaney, W.C., Boyer, M.G. and Rutter, N.W., 1989. Evaluation of amino acid composition as a geochronometer in buried soils on Mount Kenya, East Africa. In: W.C. Mahaney (Editor), Quaternary and Environmental Research on East African Mountain. A.A. Balkema, Rotterdam/Brookfield.

Mohammed, M.U., Bonnefille, R. and Johnson, T.C., 1995. Pollen and isotopic records in Late Holocene sediments from Lake Turkana, Kenya. Palaeogeography, Palaeoclimatology, Palaeoecology, 119: 371-383.

Morris, B., 1970. The Zonal Vegetation of Kilimanjaro. African Wild Life, 24: 157-166.

Oades, J.M., 1995. An overview of processes affecting the cycling of organic carbon in soils. In: C. Sonntag (Editor), The Role of Nonliving Organic Matter in the Earth´s Carbon Cycle. Wiley, Chichester, pp. 293-303.

Odada, E.O. and Olago, D.O., 2002. The East African Great Lakes: Limnology, Palaeolimnology and Biodiversity. Kluwer Academic Publishers.

Osmaston, 1989. Glaciers , glaciations and equilibrium line altitudes on Kilimanjaro. In: W.C. Mahaney (Editor), Quaternary and Environmental Research on East African Mountain. A.A.Balkema, Rotterdam/Brookfield.

Raynaud, D., Jouzel, J.M., Barnola, J.M., Chappellaz, J., Delmas, R.J. and Lorius, C., 1993. The ice record of greenhouse gases. Science, 259: 926-934.

Ritchie, J.C., Eyles, C.H. and Haynes, C.V., 1985. Sediment and pollen evidence for an early to mid-Holocene humid period in the eastern Sahara. Nature, 330: 645-647.

Roberts, N., 1996. The Holocene. Blackwell, Oxford.

Rohr, P.C. and Killingtveit, A., 2003. Rainfall distribution on the slopes of Mt Kilimanjaro. Hydrological Sciences Journal-Journal Des Sciences Hydrologiques, 48(1): 65-77.

Sage, R.F., 2001. Environmental and evolutionary preconditions for the origin of the C4 photosynthetic syndrome. Plant Biology, 3: 202-203.

Sage, R.F., Wedin, D.A. and Li, M., 1999. The biogeography of C4 photosynthesis: patterns and controlling factors. In: R.K. Monson (Editor), C_4 Plant Biology. Academic Press, San Diego, pp. 313-373.

Schrumpf, M., 2004. Biochemical Investigations in Old Growth and Disturbed Forest Sites at Mount Kilimanjaro. Ph.D. Thesis, University of Bayreuth, Germany.

Schwark, L., Zink, K. and Lechtenbeck, J., 2002. Reconstruction of postglacial to early Holocene vegetation history in terrestrial Central Europe via cuticular lipid biomarkers and pollen records from lake sediments. Geology, 30(5): 463-466.

Shanahan, T.M. and Zreda, M., 2000. Chronology of quaternary glaciations in East Africa. Earth and Planetary Science Letters, 177(1-2): 23-42.

Shugart, H.H., French, N.H.F., Kasischke, E.S., Slawski, J.J., Dull, C.W., Shuchman, R.A. and Mwangi, J., 2001. Detection of vegetation change using reconnaissance imagery. Global Change Biology, 7(3): 247-252.

Soil Survey Staff, 2003. Keys to Soil Taxonomy, 9th Edition. United States Department of Agriculture, Natural Resources Conservation Service, Washington.

Street, F.A. and Grove, A.T., 1979. Global Maps of Lake-Level Fluctuations since 30,000 yr B.P. Quaternary Research, 12: 83-118.

Street-Perrott, F.A., Huang, Y., Perrott, R.A., Eglinton, G., Barker, P., Khelifa, L., Harkness, D.D. and Olago, D.O., 1997. Impact of lower atmospheric CO_2 on tropical mountain ecosystems. Science, 278: 1422-1426.

Stuiver, M., Reimer, P.J., Bard, E., Beck, J.W., Burr, G.S., Hughen, K.A., Kromer, B., McCormac, G., Van der Pflicht, J. and Spurk, M., 1998. INTCAL98 Radiocarbon Age Calibration 24.000-0 cal a BP. Radiocarbon, 40: 1041-1083.

Thompson, L.G., Mosley-Thompson, E., Davis, M.E., Henderson, K.A., Brecher, H.H., Zagorodnov, V.S., Mashiotta, T.A., Lin, P.N., Mikhalenko, V.N., Hardy, D.R. and Beer, J., 2002. Kilimanjaro ice core records: Evidence of Holocene climate change in tropical Africa. Science, 298(5593): 589-593.

Trauth, M.H., Deino, A.L., Bergner, A.G. and Strecker, M.R., 2003. East African climate change and orbital forcing during the last 175 kyr BP. Earth and Planetary Science Letters, 206: 297-313.

Zech, W. and Mühle, H., 1989. Über das Alter von Steinlagen (stone lines) in Böden SW-Rwandas. Mitteilgn. Dtsch. Bodenkundl. Gesellsch., 59(2): 1025-1030.

Study 2:

Multi-proxy analytical characterization and palaeoclimatic interpretation of the Tumara Palaeosol Sequence, NE Siberia

Michael Zech [1]*, Roland Zech [1], Wolfgang Zech [1], Bruno Glaser [1], Sonja Brodowski [2] and Wulf Amelung [2]

[1] Institute of Soil Science and Soil Geography, University of Bayreuth, D-95445 Bayreuth, Germany

[2] Institute of Crop Science and Resource Conservation, Soil Science and Soil Ecology, University of Bonn, 53115 Bonn, Germany

* Corresponding author: Michael Zech, Phone: +49 (0)921 552247; Fax: +49 (0)921 552246, Email: michael_zech@gmx.de

Abstract

Northeast Siberia is still lacking a long-term and continuous record for the Quaternary palaeoenvironmental and palaeoclimatic reconstruction. We therefore studied a 15 m high loess-like permafrost palaeosol sequence (the Tumara Palaeosol Sequence, TPS), which developed on a Middle Pleistocene fluvio-glacial terrace of the Tumara River. Various analytical methods were applied to characterize the TPS. Like in typical loess-palaeosol sequences (e.g. in China, Europe etc.), pedogenetic clay formation, mineral weathering and smaller grain sizes are interpreted in terms of warmer and more favorable climatic conditions (interglacials or interstadials). Soil organic matter (SOM), however, reveals an unfamiliar, inverse pattern: High organic carbon contents (> 1%) characterize the dark gray glacial palaeosols, whereas lower contents (≤ 0.5%) are found in the brown interglacial/-stadial palaeosols. This can be explained with permafrost and water logging having inhibited SOM mineralisation during cold periods. D/L-ratios of aspartic acid and lysine turned out to be useful proxies for both SOM aging and palaeotemperature with amino acid racemization being enhanced in interglacials/-stadials palaeosols. In combination with numeric dating results (radiocarbon and luminescence) and in the context of other northern hemispheric records, the simple warm-cold stratigraphy as derived from several developed palaeoenvironmental/-climatic proxies suggests that the TPS represents the last ~240,000 years.

Keywords: Quaternary, NE Siberia, loess-like palaeosol sequence, geochemistry, grain size, magnetic susceptibility, amino acid enantiomers

1. Introduction

Loess and loess-like sediments are valuable archives for the reconstruction of the palaeoenvironment and the palaeoclimate. Not only can loess-palaeosol sequences be considered as terrestrial counterparts to marine and ice core records (e.g. Imbrie et al., 1984; Johnsen et al., 2001; Martinson et al., 1987), they also allow to improve our understanding of how various ecosystems reacted on climate changes in the past. So far, northern hemisphere eolian records have attracted much attention in Europe, Central Siberia, China, Alaska and Midcontinental North America (e.g. Berger, 2003; Chlachula et al., 1997; Frechen and Dodonov, 1998; Heller and Liu, 1982; Kukla, 1987; Muhs and Bettis Ill, 2000; Zöller et al., 2004). A continuous, long-term archive has however not yet been described for NE Siberia, a key region between Greenland and Lake Baikal, Eastern Siberia. There, ice cores (e.g. Dansgaard et al., 1993; Johnsen et al., 2001) and lacustrine sediments (e.g. Karabanov et al., 1998; Prokopenko et al., 2001; Swann et al., 2005), respectively, have been studied intensively and at high-resolution during the last decades.

In this paper, we present and discuss results obtained for the Tumara Palaeosol Sequence (TPS), NE Siberia (Fig. 2-1), in order to evaluate the potential of these loess-like sediments to contribute to the reconstruction of the Quaternary environmental and climatic history of the study area. We specifically address:

- Grain Size Distribution: Nugteren and Vandenberghe (2004) and Porter and An (1995), for instance, have shown that grain size in Chinese loess correlates with wind strength. Coarser sediments document intensified winds entraining larger particles and are therefore often correlated with unstable glacial periods or cold events during glacial-interglacial cycles. On the other hand, clay formation in loess-palaeosol sequences is increased due to enhanced weathering/pedogenesis during warmer and more humid climatic conditions (interglacials/-stadials).

- Geochemical Composition: The geochemistry of loess from different regions can be highly variable, reflecting diverse dust sources (Gallet et al., 1998). Moreover, selective removal of elements during weathering and pedogenesis changes the original input signal and thus allows estimating weathering intensity (Ding et al., 2001; Gallet et al., 1996; Yang et al., 2004). Especially elemental indices or just ratios (e.g. K/Na, K/Ca, Ca/Sr or Ti/Zr) have been established and used successfully to assess changes in provenance and weathering.

- Magnetic Susceptibility (MS): MS may provide a tool for dating by correlation with other profiles and marine records. In Chinese loess-palaeosol sequences this approach is widely and successfully applied (e.g. Heller and Liu, 1982; Heslop et al., 2000; Kohfeld and Harrison, 2003). The concept of magnetic dating there is based on the biotic and abiotic formation and accumulation of ultrafine-grained magnetite during interglacial/–stadial periods coinciding with increased precipitation and enhanced soil formation (An, 2000; Evans and Heller, 2001; Liu et al., 1995; Sartori et al., 2005; Xiuming et al., 1993). On the contrary, in Central Siberia and Alaska higher MS values have been found in glacial loess deposits compared to the interglacial/-stadial soils (Begét, 2001; Chlachula, 2003; Evans et al., 2003). This inverted signature has been attributed to the ability of stronger winds to entrain and transport dense iron oxide particles ('wind vigor model').

- Soil Organic Matter (SOM): Interglacial and interstadial palaeosols typically have higher SOM contents than the intercalating loess sediments (e.g. Muhs et al., 2003b). On the one hand, this is generally attributed to higher organic matter production during warm periods and/or rapid loess accumulation during glacials/stadials (shown for instance by Zander et al. (2003) for the Central Siberian Kurtak Loess record). On the other hand, inhibition of SOM mineralisation (and thus SOM accumulation) due to permafrost and water logging might be worth a more detailed consideration especially in boreal and arctic regions, like e.g. NE Siberia. According to our knowledge, only few palaeosol sequences show an "inverse" SOM pattern with higher organic matter contents correlating with glacial periods and lower ones characterizing interglacial palaeosols (e.g. Zech, 2006). Apart from the standard SOM parameters like total organic carbon (TOC), nitrogen (N) and TOC/N, we will also present amino acid enantiomers as biomarkers, which allow deducing information about both SOM aging and palaeotemperature.

Overall, it should be emphasized that the TPS is not a typical loess- but rather a loess-like palaeosol sequence, i.e. the eolian material in all parts of the profile were subject to pedogenetic processes, and possibly re-worked. Nevertheless, we will show that the analytical results suggest that the TPS is built up of alternating glacial and interglacial/-stadial palaeosols. On the basis of this simple "cold-warm" stratigraphy, the combination with numeric dating results and the comparison with other northern hemispheric records, we will finally propose a tentative chronology for the TPS.

2. Geological setting and Stratigraphy of the Tumara Palaeosol Sequence

The Verkhoyansk Mountains are located in Northeast Siberia and are characterised by boreal continental climate, i.e. short, warm summers and long, cold winters (Müller, 1980) (Fig. 2-1). In Jakutsk, about 300 kilometers south of the Verkhoyansk Mountains, maximum and minimum temperatures are 30 to 38°C and –60 to –70°C, respectively. Westerlies prevail and provide moisture from the Atlantic with annual precipitation being less than 300 mm (Jakutsk: 213 mm/a, Verkhoyansk: 155 mm/a). The extreme continental conditions in the study area are responsible for the formation of 400–600 m thick permafrost and the absence of big glaciers today. Large moraine arcs, however, which can be found in the lowlands west and southwest of the Verkhoyansk Mountains, document several former and extensive piedmont glaciations (Grinenko and Kamaletdinov, 1993). For details on the Russian terminology of the Siberian Quaternary stratigraphy the reader is referred to the literature (e.g. Alekseev et al., 1990; Arkhipov et al., 2000; Arkhipov et al., 1986; Arkhipov et al., 1997; Astakhov, 2004; Grinenko and Kamaletdinov, 1993; Kind et al., 1971; Spektor, 2003).
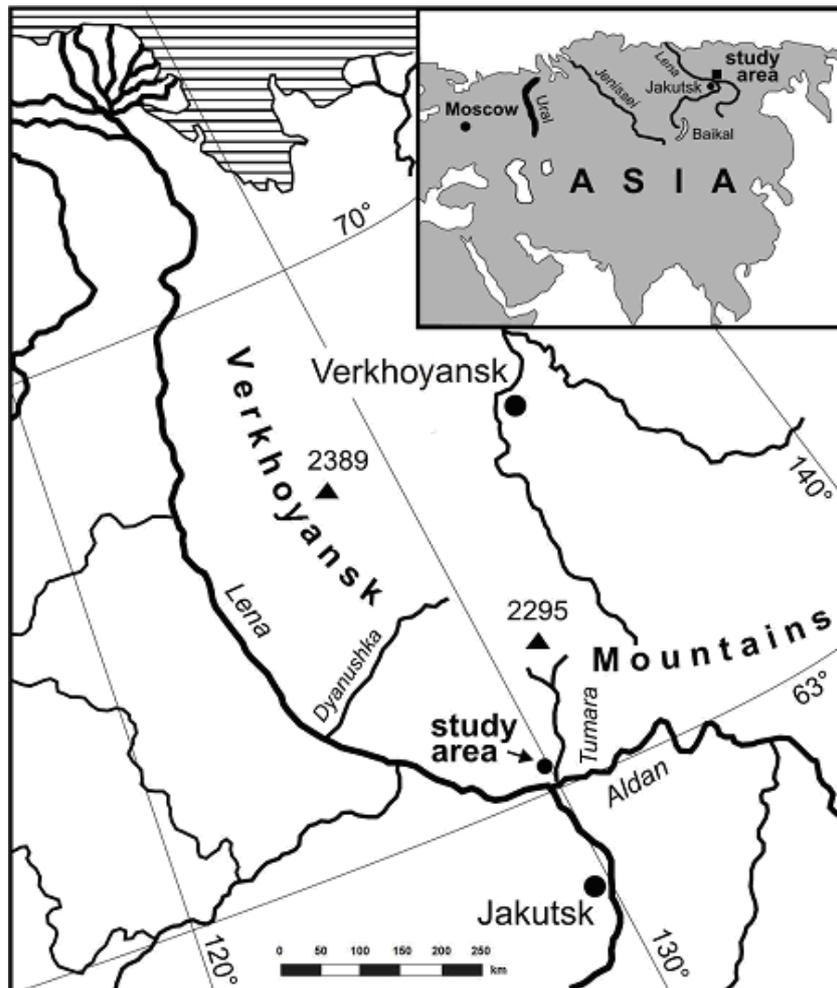
Fig. 2-1: Map showing the location of the study area in Northeast Siberia. The "Tumara Palaeosol Sequence" (TPS) is situated at the right banks of the Tumara River and exposes 15 m of loess-like palaeosols preserved in permafrost.

The southern part of the Verkhoyansk Mountains is drained by the Tumara River (Fig. 2-1). Between the mountains to the north and the debouchure into the Aldan River to the south, the Tumara cuts a ~100 km long transect through Quaternary and Tertiary deposits. Moraines and terraces are typically overlain by several meters of frozen eolian sediments. The investigated loess-like palaeosol sequence, referred to as 'Tumara Palaeosol Sequence' (TPS) (120 m a.s.l., 63°36' N, 129°58' E), is located ~10 km south of the outermost moraine. The lower part of the ~50 m high and several hundred meter long undercut slope exposes yellow tertiary sands, which are rich in fossil woods and trunks. Above (~15-33 m from the surface), fluvio-glacial sandy gravels were deposited during the Middle Pleistocene (Grinenko and Kamaletdinov, 1993). The upper 15 m of the cliff are built up of frozen loess-like sediments, in which brown soil horizons alternate with dark gray ones (Fig. 2-3A). Two thick dark gray layers could easily be traced laterally and formed the basis for the initial stratigraphic division of the TPS into the units A (top, brown), B (dark gray), C (brown), D (dark gray) and E (bottom, brown). Later on, the Units B and C were further subdivided and the A/B boundary was placed 30 cm higher, taking the analytical results into account.

Before describing and sampling the TPS, we cleaned the upper 15 m of the cliff (~100 cm width and 30 cm depth, abseiling from the top was necessary). The following morphological features could be observed (see also Fig. 2-3A): In the lower part of the brown Unit A (0-1.5 m) several thin organic-rich layers marked the transition to a generally dark, silty horizon (Unit B: 1.5–4.8 m). The upper part of Unit B partly revealed hydromorphic features, contained roots especially just above 3 m depth and showed a gray band at ~3.2 m depth. Although color did not change markedly in Unit B, Subunit B2 (3.4–4.0 m) stood out, because it was finer textured and poor in macrofossils, whereas Subunit B3 (4.0–4.8 m) became coarser and rich in macrofossils again. The transition from Unit B to Unit C occurred more or less abruptly and was characterized by a large ice wedge filling protruding into the underlying brown palaeosol (Subunit C1, 4.8–6.7 m). Below, Subunit C2 (6.7–7.8 m) was again darker. At its bottom at ~7.8 m depth a thin coarse-grained layer being rich in concretions could be observed. The generally brown and clayey Subunit C3 (7.8–9.7 m) revealed red-yellow mottles in its upper part and, in contrast to Subunit C1, contained some macrofossils and roots. The underlying Unit D (9.7–12.5 m) was dark gray and rich in roots and wood remnants, resembling Unit B. The lowermost Unit E (12.5–15 m) was composed of a brown horizon in the upper part and a palaeosol complex with alternating humus-rich and

mottled horizons in the lower part. The basis consisted of dark gray fluvio-glacial sandy gravels.

3. Materials and Methods

After cleaning and describing the upper 15 m of the TPS, a total number of 117 samples were taken at 10–20 cm intervals for grain size, geochemical and magnetic analyses. The samples were air dried, sieved (< 2 mm) and stored in plastic bags.

Grain size analyses were performed on a Beckman Coulter LS after removal of organic material with H_2O_2 and removal of carbonates with HCl (10%). Note that laser analyses are not directly comparable with results from the sieve and pipette method (Konert and Vandenberghe, 1997): e.g. 2 µm-particles show up as ~8 µm-particles. We will define reasonable grain size fractions for the TPS based on the grain size distributions later on.

Elemental compositions were obtained using a Philips 2404 X-Ray Fluorescence (XRF) Spectrometer at the University of Greifswald. Major elements are given in mass percent, trace elements are expressed in parts per million (ppm). For calculating correlation coefficients not concerning the Ca and Mg, the elements were corrected for calcium carbonate ($CaCO_3$) and dolomite ($MgCO_3$)(referring to carbonate-free material after correction) according to the Equation (I):

$$\% \text{ X (corrected for carbonates)} = \% \text{ X (measured)} * \left(\frac{100}{100 - \% \, CaCO3 - \% \, MgCO3} \right) \quad \text{(I)}$$

where % $CaCO_3$ and % $MgCO_3$ were calculated from % CO_3 by estimating

$$\frac{\% \, CaCO3}{\% \, MgCO3} \approx \frac{\% \, CaO}{\% \, MgO} \quad \text{(II)}$$

In many loess studies elemental indices or ratios have been proposed in order to assess the weathering intensity of the minerals. For instance, the frequently used chemical index of alteration (CIA) introduced by Nesbitt and Young (1982) is defined as the molar ratio of

$$CIA = \left(\frac{Al2O3}{Al2O3 + CaO * + Na2O + K2O} \right) * 100 \quad \text{(III)}$$

where CaO* is the amount of CaO in silicates. As in this formulation a correction for Ca in carbonates and phosphates (apatite) is necessary but often difficult to accomplish, McLennan (1993) recommended different procedures to estimate CaO*. Our above approximation for $CaCO_3$ and $MgCO_3$ is assumed to be not precise enough for determining CaO*, because leaching should have at least partly influenced our carbonate record and $CaCO_3$ is known to be less resistant to weathering that $MgCO_3$. We therefore used the mean of the calculated CaO* (1.04%) in the equation above estimating Ca in silicates remains constant.

In order to determine the magnetic susceptibility (MS), aliquots of the samples were loosely packed into 8-cc plastic boxes and measured on a Bartington MS2 meter at the University of Bayreuth.

Total organic carbon (TOC) and nitrogen (N) contents were determined following standard laboratory procedures at the Institute of Soil Science and Soil Geography, University of Bayreuth: Removal of carbonates (10% HCl), dry combustion of a finely ground homogeneous 50 mg sub-sample and thermal conductivity detection on a Vario EL elemental analyzer (Elementar, Hanau, Germany). The detection limits of our machine were determined by measuring blanks with increasing net weights of wolfram oxide in tin capsules (~0.0002% for TOC and ~0.007% for N). Carbonate content (CO_3) was calculated by measuring the total carbon content (TC) with a carbonate containing sub-sample and subsequent subtraction of TOC.

Amino acids, mainly bound in proteins, constitute an important N pool in soils (Amelung, 2003). Containing a chiral C atom, they can occur either in the left-handed form (L-enantiomer) or in the right-handed form (D-enantiomer) with living organisms primarily producing the L-enantiomers. The D-amino acids are then generated by racemization – a mainly time-, temperature- and pH-dependent abiotic reaction – from their respective L-enantiomers (Bada, 1985). It has therefore been suggested that D/L-ratios of amino acids can be used for dating. Mahaney and Rutter (1989), for instance, found the ratio D/L-aspartic acid to be a suitable geochronometer in buried soils.

Amino acid enantiomers for 10 selected samples were determined in replication according to the method proposed by Amelung and Zhang (2001). Sample preparation comprised pre-extraction of free and water-soluble amino acids, hydrolysis of protein-bound

amino acids, purification over columns (Dowex W X8) and derivatization. Quantification was carried out on a Saturn GC-MS Workstation at the Institute of Soil Science and Soil Ecology, University of Bonn. Although over 25 amino acid enantiomers were quantified, we only present the results obtained for aspartic acid (Asp) and lysine (Lys), which proved to be most suitable for dating purposes in soils (Amelung, 2003).

As racemization is known to be catalyzed by low pH and high temperatures, both applied during hydrolysis, Amelung and Brodowski (2002) quantified the hydrolysis-induced racemization using deuterium labeling. They could show that less than 10% of D-Asp and D-Lys were formed during the analytical procedure in environmental samples older than 3000 years. We therefore neglect these possible laboratory artifacts.

In order to establish a chronology for the TPS, 16 radiocarbon analyses were carried out for (i) the acid and/or alkali insoluble fractions of soil organic matter, (ii) the hot water soluble and insoluble fraction of a bone collected in 5 m depth and (iii) wood or root remnants. All radiocarbon ages were corrected for the $^{13}C/^{12}C$ ratios. For reasons of simplicity we only refer to uncalibrated ages. Furthermore, four IRSL-ages were obtained for the middle and lower part of the TPS (for more details see Table 2-1).

4. Results and Discussion

4.1 Grain Size Distribution

Most grain size studies only present few selected parameters, like e.g. the fraction below or above 16 μm, the median and maximum grain size, or various ratios (Nugteren and Vandenberghe, 2004; Xiao et al., 1995). Such simplifications may result in loss of information and can be applied for simple grain size distributions only. According to Fig. 2-2A, the loess-like sediments of the TPS are not characterized by uni-modal distributions, but by up to three maxima:

The dominant peak at ~30-50 μm confirms the eolian origin of the material. Important source regions for the long-distance transport are assumed to be in Western and Middle Siberia, whereas the Lena and Aldan River beds should provide dust for the middle-distance transport. Changes in the wind strength are likely responsible for shifts of the grain size maximum, with coarser silt reflecting stronger winds during glacial periods and finer silt reflecting more warmer and more favorable climatic conditions. For further discussions, we

use the 10-40 μm fraction to quantify the fine eolian components and the 40-100 μm fraction to quantify coarser components, respectively.
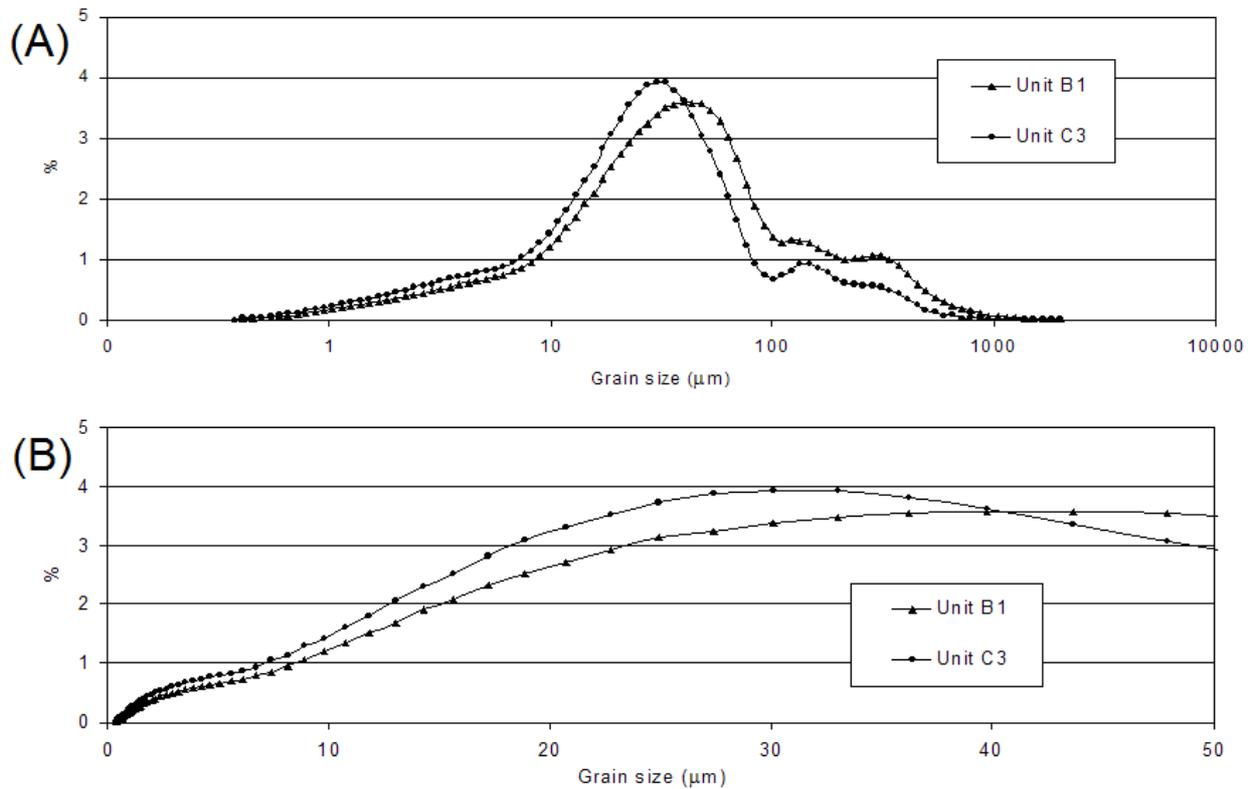
Fig. 2-2: Mean grain size distributions of selected units from the TPS (A) on log-normal scale and (B) on linear scale, respectively.

In most samples two further maxima – although much less pronounced – occur at ~150 μm and ~300 μm (Fig. 2-2A). They probably reflect short-distance transport from the nearby Tumara River bed.

Finally, also pedogenesis influences the grain size distribution due to weathering and clay formation. Fig. 2-2A and 2-2B show a flattening in the grain size distribution below ~8 μm, and we assume that clay formation mainly produced this fraction (which would correspond to the < 2 μm fraction, i.e. the "clay fraction", if sieving and pipette analyses were applied (Konert and Vandenberghe, 1997)).

Fig. 2-3B illustrates the depth functions of selected grain size fractions. The < 2 μm fraction shows values up to 4.5% in the brown Units A, C1, C3 and E, but also in the dark gra y Subunit B2. On the contrary, the dark gray Units B1, B3, C2 and D reveal distinct minima (< 2 μm between 2 and 3%). Comparison of the < 2 μm clay fraction with the 2-6 μm fraction (Fig. 2-2B) reveals a highly significant correlation (correlation coefficient R = 0.93),
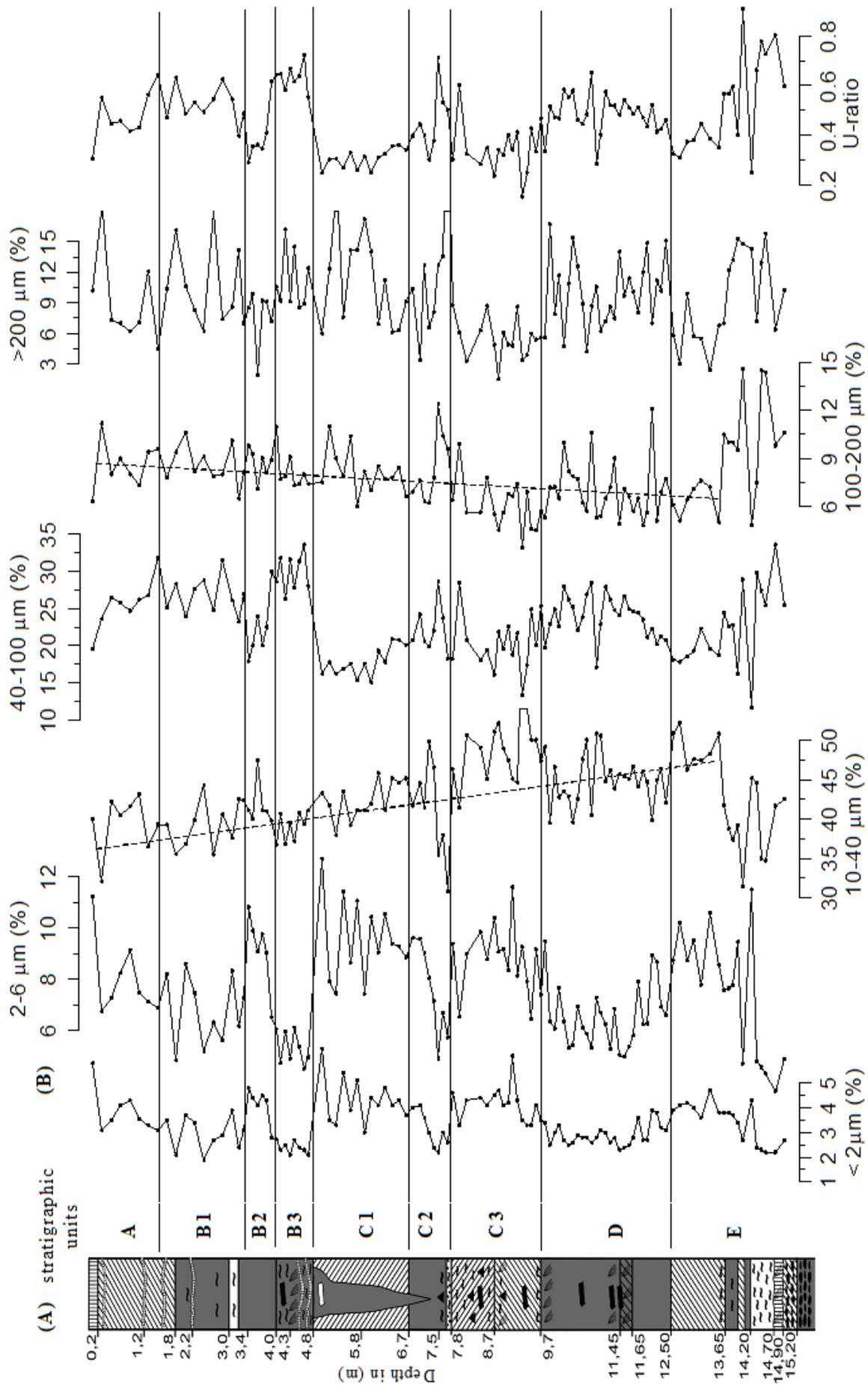
Fig. 2-3: (A) TPS stratigraphy (the legend is given in Fig. 2-7) and (B) depth profiles of selected grain size fractions.

whereas the correlation of the < 6 μm with the 10-40 μm fraction is much lower (R = 0.30). This corroborates that clay formation/pedogenesis dominantly influences the grain size fractions < 6 μm, but barely the fractions > 10 μm. Higher clay contents in loess-palaeosol sequences are typically found in interglacial/-stadial soils. This pattern is, for instance, also reported for the Central Siberian Kurtak Loess Profile (Frechen et al., 2005). Our results thus provide a first hint indicating that the Units A, B2, C1, C3 and E developed during warm and favourable interglacial/-stadial climatic conditions.

As the 10-40 μm fraction correlates only weakly with the clay content (< 6 μm), a sedimentological (i.e. wind strength) rather than a pedological signal is assumed to be recorded in these grain sizes. A general decrease from ~45% to 40% can be observed for the fine and middle silt fraction (10-40 μm) towards the upper parts of the profile (Fig. 2-3B). On the contrary, the coarse silt (40-100 μm) increases from ~20% to 27%, although not continuously. Instead, an abrupt transitions occurs at 4.8 m depth. The ratio of coarse to middle and fine silt (40-100 μm/10-40 μm) accentuates the alternation of coarser and finer silt and additionally reflects the overall increase of coarser particles. When corrected mathematically for this latter trend, the ratio may be regarded as palaeo-wind strength proxy ('U-ratio', used e.g. in Nugteren et al., 2004) adapted to the local conditions at the TPS (Fig. 2-3B). This 'U-ratio' correlates highly significantly with the median calculated for the 10-100 μm fraction (R = 0.95, the fractions < 10 μm and > 100 μm were excluded to minimize the influence of pedogenesis and short-distance sources). Assuming that wind strength variations reflect alternating glacial and interglacial/-stadial periods, our silt grain size results are in good agreement with the above discussed clay formation/pedogenesis proxy (< 6 μm): Accordingly, the Units A, B2, C1, C3 and E developed during more stable interglacial/-stadial periods, whereas the Units B1, B3, C2 and D were deposited during glacial periods with intensified wind strength.

Concerning the sand fractions (short-distance transport), the depth profile of the 100-200 μm fraction reveals no distinct shifts corresponding to stratigraphic unit boundaries, but it shows a general trend to higher contents towards the top of the profile (from ~6% to 10%, Fig. 2-3B). This might be due to varying proximity of the sampling location to the Tumara River bed, which may have contributed increasingly to the local dust load when the cliff edge came closer due to lateral river erosion. Surprisingly, the > 200 μm fraction shows no significant correlation with the 100-200 μm fraction (R = 0.32). This indicates that different

short-distance transport mechanisms might play a role. The very high variability of the coarse sand fraction (~3-15%) points to extreme, but sporadic storm events.

4.2 Geochemical characterization

The major and trace elemental composition of the TPS sediments should corroborate the above grain size results concerning sedimentation and weathering. The concentrations of 26 elements were determined by X-Ray fluorescence analyses (see supplementary material). Almost all elements show distinct variations in their depth profiles, indicating changes in provenance and/or mineral weathering intensity (enrichment or depletion). Here only selected elements can be discussed in more detail (Fig. 2-4 and 2-5).

SiO_2 contents vary – except for the concretion layer at 7.8 m depth – from 59 to 75%, thus being well within the range reported to be typical for loess (Gallet et al., 1998). The highest values occur in the Units A and E. SiO_2 minima at 14.3 m depth and in the Units B1 and D coincide with striking CaO and MgO maxima (Fig. 2-4). The correlation of SiO_2 with CaO + MgO is significant and negative (R = -0.80). CaO and MgO, in turn, correlate significantly and positively with the carbonate content (CO_3) (R = 0.92 and 0.80, respectively), indicating that the SiO_2 variations are mainly controlled by "dilution" of the eolian material with carbonate. Two palaeoenvironmental interpretations are possible:

On the one hand, the carbonate content of the deposited dust may have been variable over time depending on the source areas (Gallet et al., 1998). For instance, Central Alaskan loess contains very low carbonate (Muhs et al., 2003b), whereas the carbonate content is very high in Midcontinental North America loess (Muhs and Bettis Ill, 2000). As most of the eolian material of the TPS is assumed to be derived from long- and middle-distance transport, enhanced carbonate contents in the dust load could be explained with new source areas (e.g. continental shelves) and/or with unweathered carbonate-rich glacial debris being exposed in periglacial regions.

On the other hand, carbonates are rather mobile and affected by pedogenetic processes (Gallet et al., 1996). Varying carbonate contents in the TPS could thus also be the result of weathering and leaching.

Both interpretations are in agreement with the palaeoclimatic proxies deduced from the grain size results and further corroborate the assumption that the stratigraphic units A, B2, C and E were deposited during interglacials, whereas the palaeosols in the Units B1, B3 and D with higher CO_3 contents developed during glacial periods.
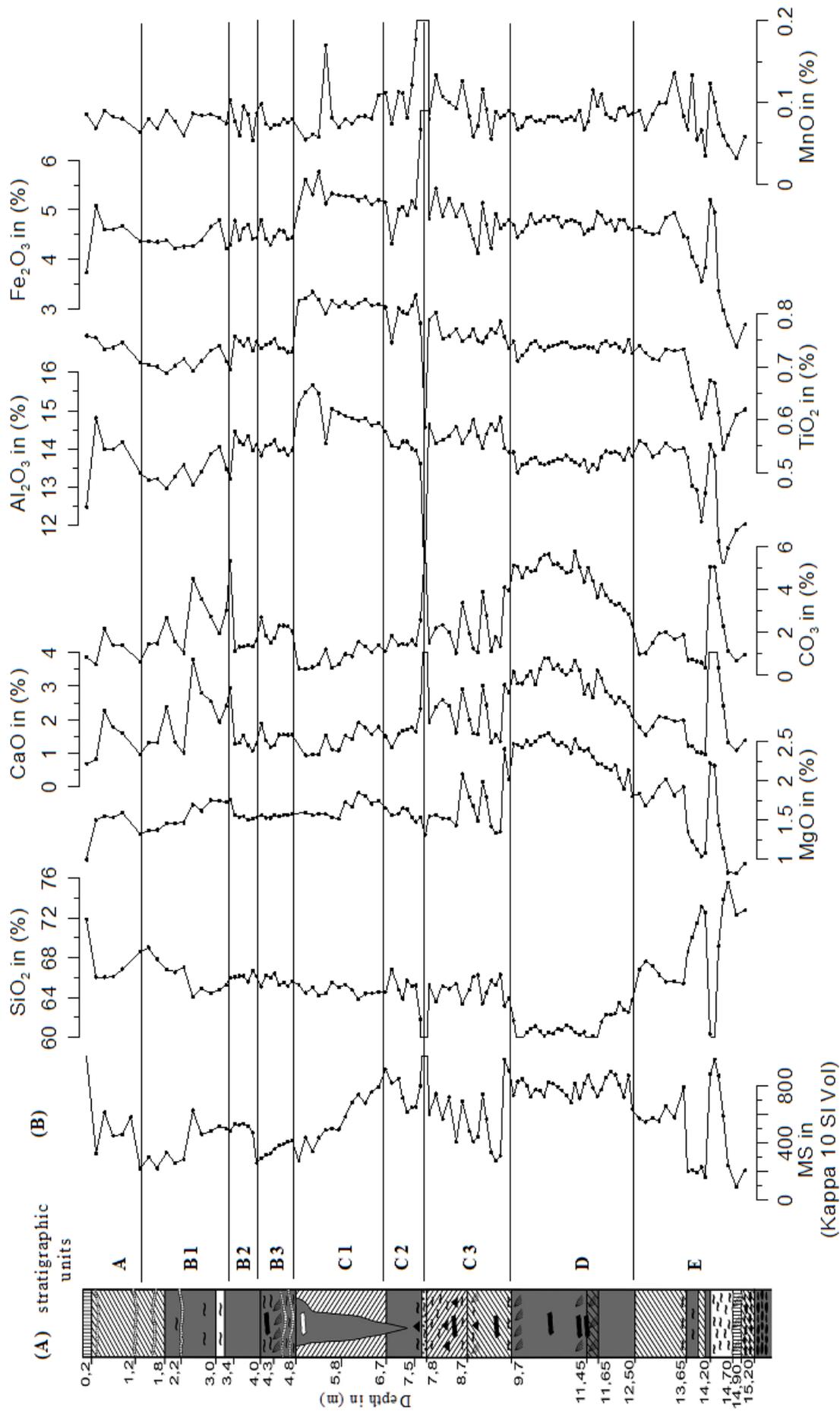
Fig. 2-4: (A) TPS stratigraphy and (B) depth profiles of MS and selected major elements.

Another set of elements, which can be clustered by studying the elemental depth profiles or by using principle component analyses, displays a distinct shift to high contents at the transition from Unit B to C and then a more or less gradually decrease down to Unit E (Al, Ti, Fe, Cr, Ga, Nb and Rb, see also Fig. 2-4). Generally, Al and Ti are considered to be rather immobile and are therefore enriched in palaeosols during mineral weathering (Ding et al., 2001; Muhs and Bettis Ill, 2000; Yang et al., 2004). Their high contents especially in Unit C1 indicate intensive weathering.

On the contrary, Na, Ca and to a lesser degree also K are assumed to be more mobile and are thus often depleted during weathering (Gallet et al., 1998; Yang et al., 2006). As one may therefore expect, Na_2O correlates negatively with Al_2O_3 (R = -0.71, corrected for carbonates). Correlation with SiO_2 is significant and positive (R = 0.77, corrected for carbonates), although Na_2O reveals a distinct shift at 4.8 m depth, which does not occur in the depth profile of SiO_2. Similarly, K_2O – showing no shift at 4.8 m depth in contrast to Al_2O_3 – correlates significantly and positively with Al_2O_3 (R = 0.75, corrected for carbonates).

We used the molar ratios of these elements to assess the weathering intensity of the minerals in the TPS by calculating the CIA (illustrated in Fig. 2-5), which is a frequently used index to estimate the transformation of feldspars to clay minerals. The CIA values for the TPS are well within the range typically found for loess (Gallet et al., 1998). The Subunits C1 and C3 are characterized by the highest values (>63), indicating most intensive weathering, whereas the lowest values are found in Unit E at the transition to the gravel bed (<58). Minor maxima also occur in the Units A, B2 and E (at about 14.2 m depth).

Another promising proxy for estimating weathering intensity could be the Rb/K ratio. We use these elements because Rb substitutes for K in K-feldspars and mica and becomes enriched during weathering (R = 0.91 with Al_2O_3, corrected for carbonates), whereas K is more mobile and preferentially leached. According to Fig. 2-5, the Rb/K ratios for the TPS mainly reflect the variations of the CIA and thus corroborate the idea of most intensive weathering having occurred in the Units A, C1, C3 and at about 14.0 m depth in Unit E.

Like Rb, also Ba is reported to be enriched in palaeosols (Yang et al., 2006). The depth profile of Ba reveals higher values in the brown Units A, C1, C3 and E. Additionally, Ba shows a distinct maximum in Subunit B2 (Fig. 2-5). On the one hand, Ba may reflect an *in situ* enrichment due to selective loss of more mobile elements. On the other hand, Ba may also be an input signal: Firstly, Yang et al. (2006) found higher Ba contents in finer loess fractions compared to coarser ones, and secondly, one may speculate that the Ba content could be influenced by deposition of marine aerosols. The latter idea may arise because
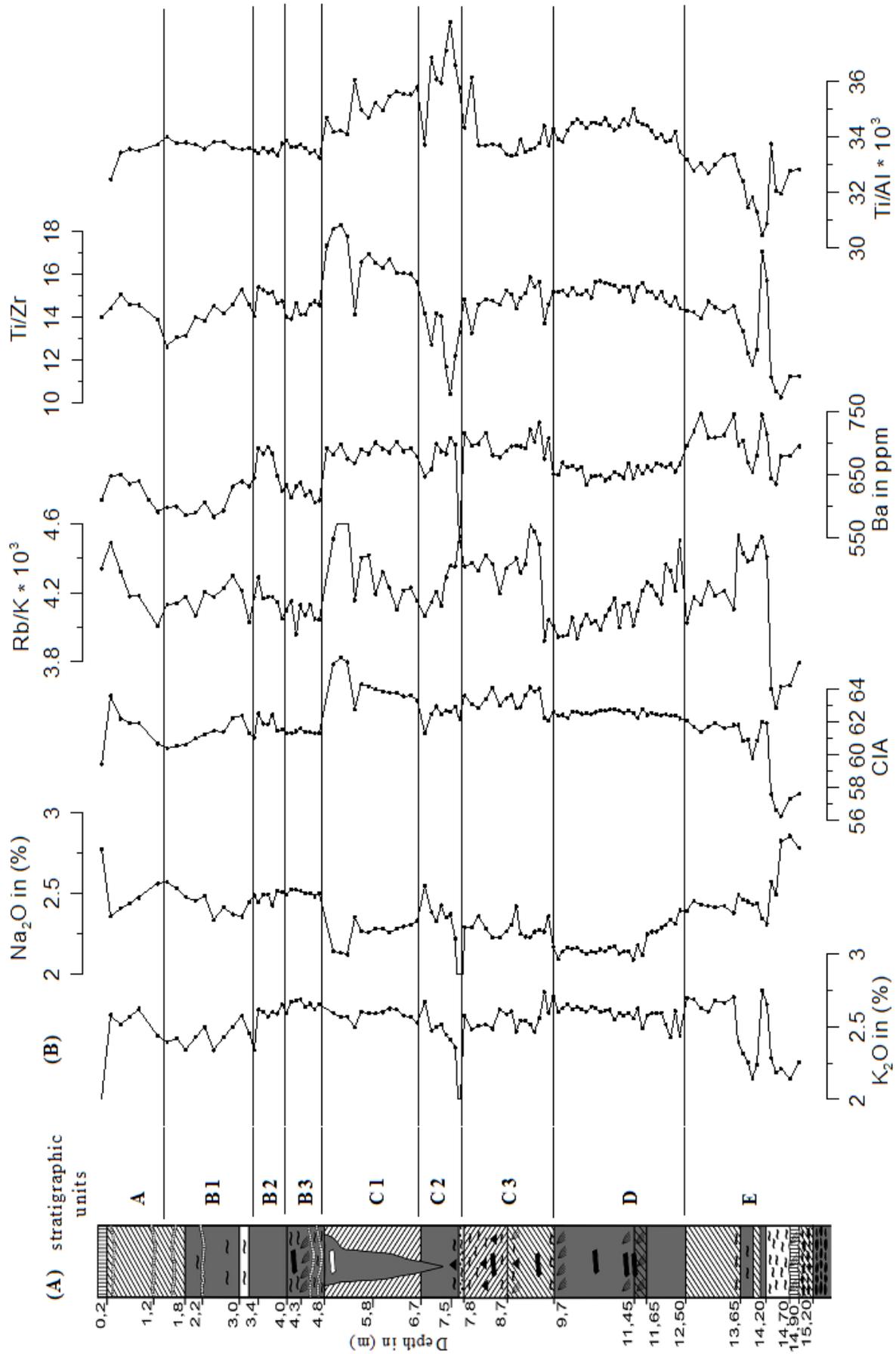
Fig. 2-5: (A) TPS stratigraphy and (B) depth profiles of selected elements and element indices and ratios.

sediment records from the Atlantic Ocean reveal strong fluctuations in the Ba concentration on glacial-interglacial time scales, which have been attributed to variations in deep water circulation (Lea and Boyle, 1990; Martin and Lea, 1998). Although further research is needed to clarify the mechanisms controlling the observed Ba pattern, Ba confirms well the TPS stratigraphy and we will later on use it as one proxy among others for developing a "glacial – interglacial/-stadial" stratigraphy.

Note that in all the above made considerations *in situ* weathering is not the only possible explanation for increased weathering indices and ratios. As partly discussed for the carbonates and barium, also (i) changes in the atmospheric dust source, (ii) increased pre-depositional weathering in the dust source area and (iii) heavy-mineral sorting during eolian transport could be responsible for variations of the elemental composition in the TPS. Provenance studies on unweathered loess traditionally use both cross plot diagrams with major elements (Al_2O_3, SiO_2, Na_2O, K_2O, CaO and MgO), ratios with trace elements and Rare Earth Element distribution patterns (Ding et al., 2001; Gallet et al., 1998; Muhs et al., 2003a). In our study, although we do not compare our elemental results with the elemental composition of possible source areas, depth profiles of ratios with immobile elements are expected to provide information about changes in the original eolian dust composition.

For instance, Ti/Zr ratios in sediments have been used extensively because these elements occur in not easily soluble minerals (Muhs et al., 2003b). The Ti/Zr ratios in the TPS show – apart from fluctuations in Unit E – two abrupt shifts at the unit boundaries B3/C1 and C2/C3 (Fig. 2-5), which hence possibly indicate discordances in the profile. This idea is further corroborated for the lower unit boundary by an iron-manganese concretion layer at 7.8 m depth coinciding with coarser grain sizes and distinct maxima in Fe, Mn, Ce, Co and Y. Besides, the Ti/Al ratios – generally revealing a quite constant signal – are strikingly increased between the two discussed discordances. Although these findings suggest that the loess-like sediments in the Subunits C1 and C2 were deposited under different sedimentological conditions than the rest of the TPS (possibly they are built up with reworked material), a more straight forward interpretation is challenging and should await, for instance, micromorphological analyses. Nevertheless, this special feature has to be kept in mind when discussing the chronology of the TPS.

4.3 Magnetic Susceptibility

MS in loess palaeosol sequences is widely used as a dating tool by correlating it with marine isotope records (Begét, 2001; Chlachula et al., 1997; Evans et al., 2003; Heller and Liu, 1982; Heslop et al., 2000). Fig. 2-4 informs about the MS results for the TPS. Accordingly, except for the concretion layer at 7.8 m depth, which has much higher values, MS in the TPS ranges from ~100 to 1000 (Kappa 10^{-6} SI Vol). There is a high negative correlation with SiO_2 below 7.8 m and above 4.0 m depth (R = -0.82 and R = -0.73, respectively). It might be especially noteworthy that – in contrast to most other proxies – there is no distinct shift in the MS signal at the B3/C1 boundary, but, instead, at the B2/B3 boundary.

The *pedogenetic* magnetoclimatological model, which is generally applied in the Chinese loess palaeosol sequences (Evans and Heller, 2001; Liu et al., 1995; Sartori et al., 2005), could explain high MS values in pedogenetically well developed palaeosols, i.e. in our Units A, C and E. Comparison of the MS signal with the stratigraphy shows that this is not the case.

The applicability of the *wind-vigor* model, which is often used to explain low MS values in palaeosols compared to loess (Begét, 2001; Chlachula, 2003; Evans et al., 2003) can be tested by directly comparing the MS signal with the grain size data: Although high MS values coincide with high U-ratios in Unit D, the two parameters are uncorrelated for both the lower and the upper part of the profile, and also for the whole dataset.

Several studies have shown that pedogenetic processes may not only explain high MS values like in the Chinese loess-palaeosol sequences, but also low MS values as they are often found in other palaeosols around the world (Bidegain et al., 2005; Feng and Khosbayar, 2004; Rousseau et al., 2002). This inverse pattern is especially attributed to the process of "gleying" and the coinciding destruction of magnetic minerals in water logged soils. Recently, Bloemendal and Liu (2005) found that there are also unambiguous discrepancies between magnetic and geochemical proxies for pedogenesis even in Chinese loess. Kohfeld and Harrison (2003) emphasized the often poor correlation between individual magnetic susceptibility records and the marine isotope stratigraphy during the last 150 ka and advised caution when using MS as a dating technique.

Although we noted the negative correlation of the MS record with the SiO_2 content for most parts of the TPS, we are still lacking a straightforward interpretation for this magnetic standard parameter. Further, more advanced magnetic parameters (e.g. frequency dependent

MS) are currently investigated and will hopefully provide more information about type and origin of the magnetic signal.

4.4 Characterization of the Soil Organic Matter

Whereas depending on the study area MS can reveal either a maximum or a minimum in interglacial/interstadial palaeosols, SOM concentrations in loess-palaeosol sequences are widely accepted to be higher in palaeosols than in intercalating loess beds (Antoine et al., 2001; Frechen et al., 2005; Muhs et al., 2003b; Zhang et al., 2003). The depth profiles of TOC, N and TOC/N are illustrated in Fig. 2-6. All parameters display similar variations throughout the profile – with TOC ranging from 0,27% to 2,48% and N ranging from 0,04% to 0,22%, respectively – and reveal abrupt shifts at the transitions from the brown units (C1, C3 and E) to the dark gray units (B, C2 and D). Whereas the former units are generally characterized by lower TOC and N values, the latter ones yield higher values. Strikingly, high TOC values also coincide with higher TOC/N ratios (R = 0.68).
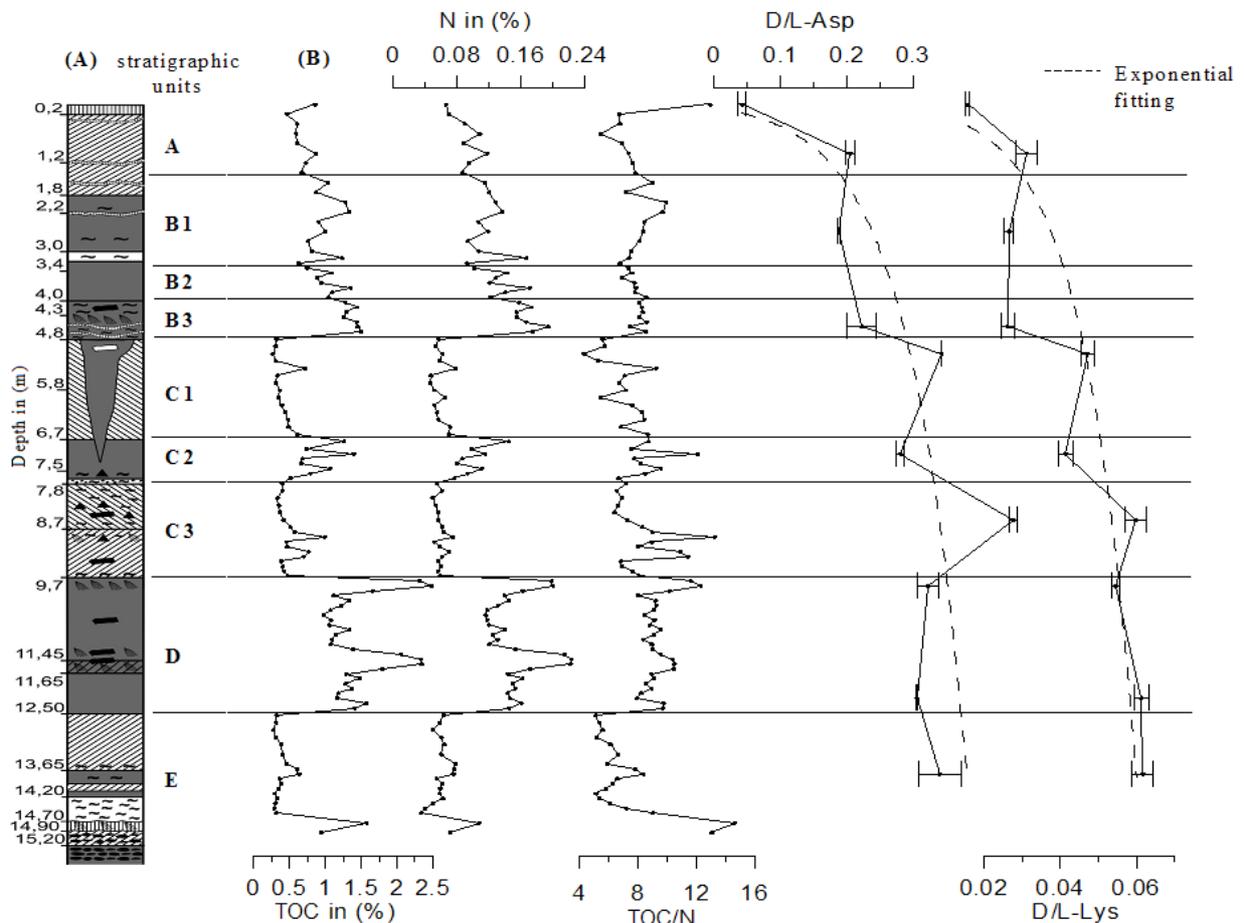
Fig. 2-6: (A) TPS stratigraphy and (B) depth profiles of TOC, N and TOC/N, as well as the D/L-ratios of the amino acids aspartic acid (Asp) and lysine (Lys).

Soil organic matter concentration in loess-palaeosols sequences depends both on organic matter production and on SOM mineralization. Whereas typical loess is very poor in organic matter, TOC concentrations around 0.4% are reported for palaeosols in Alaska, Europe, Central Siberia and China (Antoine et al., 2001; Frechen et al., 2005; Muhs et al., 2003b; Zhang et al., 2003), which are thus well in agreement with the values we find in our brown and more intensively weathered Units A, C1, C3 and E. However, in contrast to typical loess, our intercalating and less intensively weathered palaeosols in the Units B, C2 and D are enriched in SOM. Concerning TOC/N ratios in soils, they may, on the one hand, be influenced by the elemental composition of the litter, which can therefore not be ruled out completely. On the other hand, SOM decomposition is well known to cause lower TOC/N ratios due to the loss of carbon in form of CO_2. Based on the significant positive correlation between TOC and TOC/N in our record, we therefore argue that increased SOM in the dark gray Units B, C2 and D do not indicate enhanced organic matter production but reduced SOM degradation. This interpretation is corroborated by high TOC contents generally coinciding with reduced clay formation and less intensive weathering as inferred from lower clay contents and weathering indices and ratios (Fig. 2-3 and 2-5, respectively).

We suggest permafrost to be a crucial factor for the observed SOM pattern in the TPS. Whereas organic matter production was probably never a limiting factor for the accumulation of SOM due to still relatively warm summers even during the LGM in Siberia (Tarasov et al., 1999), the thickness of the active permafrost layer at our study site presumably strongly depended on the climate: During cold glacial periods the active permafrost layer was thin, thus preventing both SOM in the frozen underground and SOM in the water logged topsoil from being mineralized. On the contrary, during warmer interglacial/-stadial summers soils were characterized by deeper thawing of the permafrost and hence better drainage of the topsoils. Also increased evaporation should have contributed to better aeration of the melted soils, in which consequently SOM mineralization was intensified.

Our interpretation is further corroborated by the stable carbon isotopic composition of the SOM, which is also known to be sensible to mineralisation (isotope results will be published in a separate paper (Zech et al., submitted)). Accordingly, the TOC record constitutes a further proxy for distinguishing between glacial and interglacial/-stadial palaeosols in the TPS with lower TOC values indicating warm and higher TOC values indicating cold periods.

Both temperature and time are main factors controlling amino acid racemization, which may therefore be used to infer information about SOM aging (Amelung, 2003). The

D/L-ratios obtained for aspartic acid (Asp) and lysine (Lys) from selected TPS samples are plotted versus depth in Fig. 2-6 and can be roughly described by exponential fits. In addition, the brown units are generally characterized by higher ratios than the dark gray units. Nevertheless, D/L-ratios overall increase with depth and reveal that the apparent racemization rates are smaller for Lys than for Asp (the latter having higher D/L-ratios). This is in agreement with findings from Amelung (2003), who furthermore emphasized that Lys racemization rates are more or less constant in different soil types. Consequently, we suggest that higher D/L-ratios characterizing the brown Units A, C1 and C3 in our record are the result of higher temperatures during pedogenesis of the respective palaeosols.

5. Towards a chronology for the TPS

Summarizing the above discussion, the analytical results presented so far provide several palaeoenvironmental and palaeoclimatic proxies for the TPS (Fig. 2-7). They indicate that

- the Units A, B2, C1, C3 and E (mainly brown palaeosols) are generally characterized by enhanced SOM mineralisation and pedogenetic clay formation and more intensive mineral weathering. The respective palaeosols likely developed during warmer climatic conditions with relatively weak wind strengths. We hence suggest correlating them with interglacial or interstadial periods. On the contrary,

- the Units B1, B3, C2 and D (dark gray palaeosols) are generally characterized by inhibited SOM mineralisation, reduced pedogenetic clay formation and less intensive mineral weathering. The respective palaeosols likely developed during colder climatic conditions with strong winds. We suggest correlating them with glacial or stadial periods.

Overall, the palaeosols of the TPS thus reflect the alternation of glacials and interglacials/-stadials (Fig. 2-7D). We emphasize that it would be hastily to establish a chronology just based on counting from top to bottom and correlating the palaeosols accordingly with glacials and interglacials, respectively (Penck and Brückner, 1909), or with the marine isotope stages (MIS, Martinson et al., 1987). Several potential weaknesses of our simple "cold-warm" stratigraphy need to be considered: (i) The Subunits C1 and C2 – as deduced from the geochemical results – might consist of reworked material and the respective unit boundaries (B3/C1 and C2/C3) may be erosional discordances. (ii) The lower parts of Unit E may be affected still by fluvial processes as indicated by the high variability in the
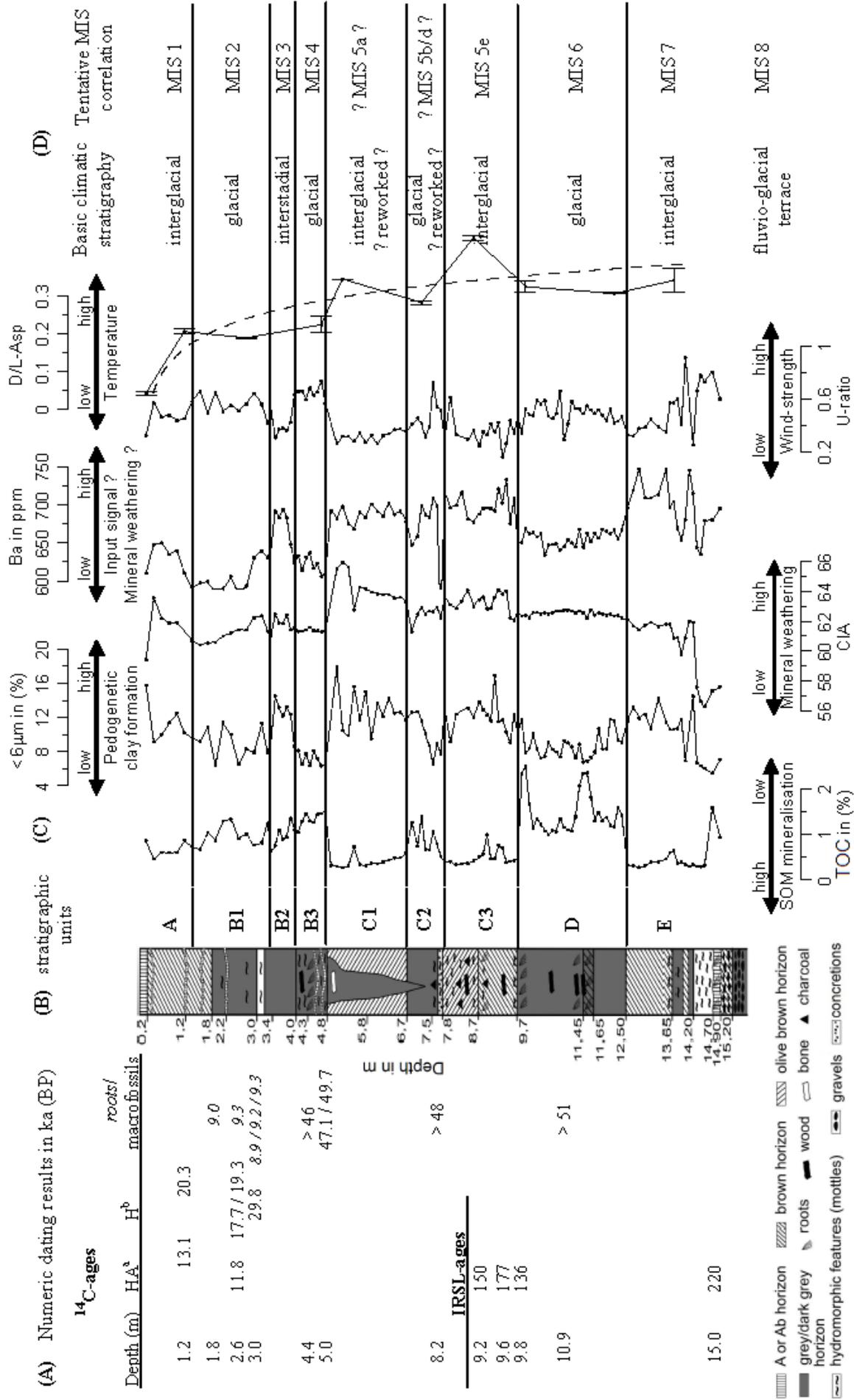
Fig. 2-7: (A) Numeric dating results, (B) TPS stratigraphy and legend, (C) depth profiles of the palaeoenvironmental and palaeoclimatic proxies as inferred from the analytical results and (D) basic climatic stratigraphy and tentative MIS correlation. [a] HA = alkali soluble substances (humic acids), [b] H = alkali insoluble substances (humins).

grain size and geochemical data. (iii) The accumulation rate can not be assumed to be constant *a priori*. (iv) Asynchronous environmental and climate changes could *per se* not be detected in the absence of numeric dating control.

In the following, we present numeric dating results (see Table 2-1 and Fig. 2-7A) and although partly speculative – discuss the TPS in the context of other northern hemispheric records:

- Eleven radiocarbon ages were obtained for the **Units A and B1**. Nevertheless, a precise chronology could not be established, because the radiocarbon ages reveal several inconsistencies: Firstly, alkali soluble substances (humic acids) yield much younger ^{14}C-ages than the respective alkali insoluble substances (humins) (13.1 and 11.8 ka BP versus 20.3 and ~18.5 ka BP at 1.2 and 2.6 m depth, respectively). Secondly, although another humin sample from 3.0 m yielded 29.8 ka BP, the upper ^{14}C-ages are stratigraphically inconsistent. Thirdly, all dated macrofossils from 1.8 to 3.0 m depth are roots of Early Holocene age and likely underestimate the deposition age of the surrounding sediments.

  On the one hand, the inconsistencies of the humin and humic acid ages could be due to dust-transported recalcitrant TOC ($\rightarrow$ too old humin ages). On the other hand, melting of formerly permafrosted palaeosols during warm periods is suggested to mobilize old C-pools. These could/can subsequently be translocated vertically upwards with ascendant soil water, whereas "too young" DOC from the topsoil could penetrate downwards. Concerning the root ages of ~9 ka BP down to 3.0 m depth, they probably document deep melting of the permafrost and rooting during the so-called "Boreal thermal optimum" in Northern Siberia (Andreev et al., 2002).

  Despite of all uncertainties, we tentatively assume that Unit A was deposited during the Holocene, and that Unit B1 corresponds to the global LGM, i.e. the Late Weichselian (15 – 25 ka BP) and the Marine Isotope Stage (MIS) 2, respectively ("Sartan Glaciation" according to the local nomenclature).

- Several analytical parameters reveal abrupt and distinct shifts both for the B1/B2 and the B2/B3 transition. The palaeosol in **Subunit B2** is not developed as strong as the interglacial/-stadial ones in the Units A, C1 or C3, but the palaeoenvironmental proxies indicate that it reflects a climatic amelioration before the onset of the LGM (Fig. 2-7C). Although the existence of the so-called "Karginsky Interstadial" during MIS 3 was recently questioned (Sher et al., 2005), our results are in agreement with findings from other authors reporting that several warm periods occurred during MIS 3. Anderson and Lozhkin (2001),

Table 2-1: Radiocarbon data and infrared stimulated luminescence data obtained for various sample material from the TPS. Analyses were carried out at the Leibniz Laboratory, Kiel (KIA), the Physical Department of the University of Erlangen (Erl.) and the GGA-Institute, Hannover (LUM). All ages are illustrated in stratigraphic position in Fig. 2-7A.

Lab reference	Depth (cm)	Material	Uncalibrated ^{14}C-ages (a BP)
KIA 19138	120	HA[a]	13.052 ± 62
KIA 19138	120	H[b]	20.285 ± 176
KIA 19139	180	Roots	9.022 ± 52
Erl. 6152	260	HA	11.801 ± 69
Erl. 6154	260	H	17.713 ± 90
Erl. 6157	260	H	19.301 ± 128
Erl. 6153	260	Roots	9.272 ± 73
KIA 19140	300	H	29.756 ± 688
Erl. 6155	300	Roots	9.275 ± 79
Erl. 6155	300	Roots	9.240 ± 110
Erl. 6156	300	Roots	8.945 ± 74
Erl. 5203	440	Wood	> 46.0
KIA 18805	500	Bone collagen	47.110 ± 1470
KIA 18805	500	Bone collagen free residue	49.690 ± 2230
Erl. 5203	820	Wood	> 48.0
Erl. 5204	1090	Wood	> 51.0
			IRSL ages (ka)
LUM [c] 240	920		150 ± 14
LUM 206	960		177 ± 13
LUM 239	990		136 ± 10
LUM 204	1495		221 ± 15

[a] HA = alkali soluble substances (humic acids),   [b] H = alkali insoluble substances (humins),
[c] personal communication from M. Frechen.

for instance, inferred warm interstadial conditions between ~30-40 ka BP in Beringia from palynological findings. Frechen and Yamskikh (1999) dated duplicate chernozem-like palaeosols along the river Yenisei, Southern Siberia, to roughly the same time (25 to 35 ka BP). Eventually, MIS 3 climatic warming is also recorded in sediments from Lake Baikal (Swann et al., 2005: 35-39 and 51-54 ka BP) and in Greenland ice cores (Dansgaard et al., 1993: "Denekamp, Hengelo, Glinde and Oerel").

- According to our proxies, **Subunit B3** was deposited during a very pronounced cold period. A wood sample from 4.4 m depth and a bone from the ice wedge filling yielded radiocarbon ages >46 ka BP and ~48 ka BP (Tab. 2-1 and Fig. 2-7). These ^{14}C-ages have to be considered as minimum ages and with great caution, because they are already close to the dating limit of the method. Nevertheless, comparison with other Middle Weichselian records suggests to correlate Subunit B3 (and the ice wedge penetrating into the subjacent C1-palaeosol) with a glacial stage of the Siberian ice sheet dated to ~50-60 ka BP (Svendsen et al., 2004) and the beginning of ice-wedge development in the Lena delta dated to ~60 ka BP (Schirrmeister et al. (2002).

- Many records show that the transition from MIS 5 to MIS 4 coincided with a dramatic climatic deterioration. Discordances in loess-palaoesol sequences are common and often loess accumulation covered well-developed palaeosols at ~65 ka BP (Berger, 2003; Frechen and Dodonov, 1998; Frechen and Yamskikh, 1999; Zander et al., 2003). As mentioned earlier, the **Subunits C1 and C2** may contain reworked material, and we cannot rule out erosional discordances. Nevertheless, we tentatively correlate Subunit C1 with MIS 5a and Subunit C2 with a cold stadial during MIS 5. Presumably corresponding palaeosols are described and dated around ~75 ka BP in Alaska (e.g. Berger, 2003), Europe (e.g. Zöller and Semmel, 2001) and the southern Siberian loess region (Chlachula et al., 2004; Frechen et al., 2005). In all these records, pedogenesis during MIS 5a is much more intensive than during MIS 3. Evidence for pronounced warm interglacial climatic conditions around 80 ka BP also comes from Lake Baikal (Karabanov et al., 1998) and Greenland ice cores (Dansgaard et al., 1993: "Odderade"). Besides, both these archives show that also extreme cold stadials occurred during the Early Weichselian (correlated with MIS 5b and 5d). Eventually, Svendsen et al. (2004) dated the maximum Weichselian extent of the Barents-Kara Ice Sheet to 80–100 ka BP. We therefore tentatively correlate Subunit C2 with this glaciation.

- Two IRSL samples and one wood sample were taken for numeric dating from **Subunit C3** and one IRSL sample from just below the transition to Unit D. According to the

palaeoenvironmental proxies, Subunit C3 is an interglacial palaeosols (Fig. 2-7). Whereas the age for the wood sample was beyond the limit of radiocarbon dating (> 48 ka BP), the IRSL-ages range from 136 to 177 ka BP. Considering the inaccuracies of such old IRSL-ages, discussed for instance in Berger (2003), Subunit C3 represents in all likelihood the Eemian interglacial palaeosol (MIS 5e) ("Kazanzevo Interglacial" in the local nomenclature).

- According to Svendsen et al. (2004), Northern Eurasia experienced an intensive Late Saalian glaciation (130–160 ka BP) prior to the Eemian. Based on the stratigraphic position and the palaeoenvironmental proxies, we propose that **Unit D** developed during this locally called "Tasov Glaciation" (MIS 6). Last but not least, the interglacial/-stadial palaeosol in **Unit E** is tentatively correlated with the preceding "Shirtinsky Interglacial" (presumably MIS 7). This interpretation is corroborated by an IRSL-age of 220 ka BP from 15.0 m depth and by a buried humic-rich horizon covering the brown and weathered gravels at the basis of the TPS.

Overall, the proposed chronology suggests a Middle Pleistocene age (presumably MIS 8) for the fluvio-glacial terrace, on which the TPS developed, and is hence in agreement with the geological map of the study area (Grinenko and Kamaletdinov, 1993). As this terrace is geomorphologically related to the outermost moraine arc in the Tumara Valley, our results indicate that this Middle Pleistocene glaciation was larger than the subsequent glaciations in the Verkhoyansk Mountains. A paper presenting the geomorphological results of two field trips (2002: Tumara Valley and 2003: Djanuska Valley, about 300 km further northwestwards, see Fig. 2-1) is in preparation and supports the idea of progressively smaller glaciations in North and Northeast Siberia during the Weichselian due to increasingly dry conditions. This can be explained with the Scandinavian Ice Sheet having built up and thus having shielded Siberia from the moisture bearing westerlies (Svendsen et al., 2004).

6. Conclusions

Although a lot of studies have provided new insight in the Late Quaternary history of Northeast Siberia during the last years, this region is still lacking a long-term and continuous archive for the reconstruction of the palaeoenvironment and palaeoclimate. The above presented analytical results from the 15 m high TPS, which developed on a Middle Pleistocene fluvio-glacial terrace of the Tumara River, show the potential of the NE-Siberian

loess-like permafrost palaeosol sequences for the reconstruction of the Middle and Late Quaternary palaeoenvironmental and -climatic history of the study area.

In contrast to typical loess-palaeosol sequences found in Alaska, Europe, Southern Central Siberia or China, the loess-like TPS contains no pedogenetically unaltered loess. Instead, it consists of alternating brown, clayey and intensively weathered palaeosols (similar to palaeosols in classical loess regions) and dark gray, organic-rich palaeosols (Fig. 2-7B). Various analyses confirm and refine the basic stratigraphy that could be established during field work (Fig. 2-7C). We briefly summarize the analytical results:

- The grain size distribution reveals a dominance of silt, corroborating the eolian origin of the sediments. Whereas the fraction < 6 μm was shown to be influenced by pedogenetic clay formation, the fine and coarse silt (10-40 and 40-100 μm, respectively) were used to calculate a palaeo-wind strength proxy. The upwards increase of the fine sand fraction probably reflects the approaching cliff edge due to lateral erosion of the Tumara River.

- Geochemical results were discussed both in terms of weathering intensity and changes in provenance. Although the mechanisms causing variations are not always definite (e.g. discussed for CO_3 and Ba), higher CIA values, Rb/K ratios and Ba contents and lower CO_3 contents can be used as proxies for warmer palaeoclimatic conditions. Besides, immobile elements ($\rightarrow$ Ti/Zr and Ti/Al ratios) indicate that the Subunits C1 and C2 may contain reworked material and that there may exist erosional discordances in the profile.

- Concerning MS, neither the *pedogenetic* nor the *wind vigor* magnetoclimatological model alone can explain the observed variations. Pedogenetic processes (e.g. "gleying") are likely responsible for the destruction of the original magnetic signal and thus limit the use of MS for correlation and dating.

- Whereas typical loess contains little SOM, high TOC contents (> 1%) characterize the dark gray loess-like palaeosols in the TPS. Permafrost and water logging were likely responsible for inhibited SOM mineralisation during cold periods.

- Increasing D/L-ratios of the amino acids aspartic acid and lysine reflect SOM aging. Besides, enhanced racemization is documented for the warmer periods, indicating the potential use of the amino acids as palaeo-temperature proxy in palaeosols.

Based on the above analyses, a simple climatic stratigraphy with alternating glacial and interglacial/-stadial palaeosols was developed (Fig. 2-7D). Unfortunately, a high resolution interpretation of the radiocarbon data is limited due to inconsistencies. Nevertheless, in combination with four IRSL ages and in the context of other northern

hemispheric palaeo-records we established a tentative chronology for the TPS, suggesting that it represents the last ~240 ka.

Ongoing work focuses on a more specific characterization of the magnetic properties and on the reconstruction of the palaeovegetation using palynological and biomarker analyses (paper in preparation). A detailed discussion of the carbon and nitrogen isotopic composition will be provided by Zech et al (submitted). Concerning future field trips and research in NE Siberia, further numeric dating control for the TPS will be essential, particularly with more luminescence analyses, and will have to be a outlined in close collaboration with a dating expert. Also micromorphological analyses, especially for the Subunit C1, would be highly desirable.

Acknowledgements

References

Alekseev, M.N., Grinenko, O.V. and Kamaletdinov, V.A., 1990. Neogen and Quaternary deposits of the Nizhnealdanskaya Depression and Middle Lena. Guidebook, Geological Excursion (in Russian), Jakutsk, 43 pp.

Amelung, W., 2003. Nitrogen biomarkers and their fate in soil. Journal of Plant Nutrition and Soil Science, 166: 677-686.

Amelung, W. and Brodowski, S., 2002. In vitro quantification of hydrolysis-induced racemization of amino acid enantiomers in environmental samples using deuterium

labeling and electon impact ionization mass spectrometry. Analytical Chemistry, 74: 3239-3246.

Amelung, W. and Zhang, X., 2001. Determination of amino acid enantiomers in soils. Soil Biology & Biochemistry, 33: 553-562.

An, Z., 2000. The history and variability of East Asian paleomonsoon climate. Quaternary Science Reviews, 19: 171-187.

Anderson, P.M. and Lozhkin, A.V., 2001. The Stage 3 interstadial complex (Karginskii/middle Wisconsinan interval) of Beringia: variations in paleoenvironments and implications for paleoclimatic interpretations. Quaternary Science Reviews, 20: 93-125.

Andreev, A.A., Siegert, C., Klimanov, V.A., Derevyagin, A.Y., Shilova, G.N. and Melles, M., 2002. Late Pleistocene and Holocene Vegetation and Climate on Taymyr Lowland, Northern Siberia. Quaternary Research, 57: 138-150.

Antoine, P., Rousseau, D.D., Zöller, L., Lang, A., Munaut, A.-V., Hatté, C. and Fontugne, M., 2001. High-resolution record of the last Interglacial-glacial cycle in the Nussloch loess-palaeosol sequences, Upper Rhine Area, Germany. Quaternary International, 76/77: 211-229.

Arkhipov, S.A., Gnibidenko, Z.N. and Shelkoplyas, V.N., 2000. Correlation and paleomagnetism of glacial and loess-paleosol sequences on the West Siberian Plain. Quaternary International, 68-71: 13-27.

Arkhipov, S.A., Isayeva, L.L., Bespaly, V.G. and Glushkovo, O., 1986. Glaciation of Siberia and North-East USSR. Quaternary Science Reviews, 5: 475-483.

Arkhipov, S.A., Zykina, V.S., Krukover, A.A., Gnibidenko, Z.N. and Shelkoplyas, V.N., 1997. Stratigraphy and palaeomagnetism of glacial and loess-soil deposits of the West Siberian Plain (in Russian). Journal of Geology and Geophysics, 38(6): 1027-1048.

Astakhov, V., 2004. Middle Pleistocene glaciations of the Russian North. Quaternary Science Reviews, 23(11-13): 1285-1311.

Bada, J.L., 1985. Racemization of amino acids. In: G.C. Barrett (Editor), Chemistry and Biochemistry of Amino Acids. Chapman and Hall, London, New York, pp. 399-414.

Baker, P.A., 2002. Trans-Atlantic Climate Connections. Science, 296: 66-67.

Begét, J.E., 2001. Continuous Late Quaternary proxy climate records from loess in Beringia. Quaternary Science Reviews, 20: 499-507.

Berger, G.W., 2003. Luminescence chronology of late Pleistocene loess-paleosol and tephra sequences near Fairbanks, Alaska. Quaternary Research, 60: 70-83.

Bidegain, J.C., Evans, M.E. and van Velzen, A.J., 2005. A magnetoclimatological investigation of Pampean loess, Argentina. Geophysical Journal International, 160: 55-62.

Chlachula, J., 2003. The Siberian loess record and its significance for reconstruction of Pleistocene climate change in north-central Asia. Quaternary Science Reviews, 22(18-19): 1879-1906.

Chlachula, J., Kemp, R.A., Jessen, C.A. and al., e., 2004. Landscape development in response to climatic change during Oxygen Isotope Stage 5 in the southern Siberian loess region. Boreas, 33(2): 164-180.

Chlachula, J., Rutter, N.W. and M.E., E., 1997. A late Quaternary loess-palaeosol record at Kurtak, Southern Siberia. Canadian Journal of Earth Sciences, 34: 679-686.

Dansgaard, W., Johnsen, S.J., Clausen, H.B., Dahl-Jensen, D., Gundestrup, N.S., Hammer, C.U., Hvidberg, C.S., Steffensen, J.P., Sveinbjörnsdottir, A.E., Jouzel, J. and Bond, G., 1993. Evidence for general instability of past climate from a 250 kyr ice-core record. Nature, 364: 218-220.

Ding, Z.L., Sun, J.M., Yang, S.L. and Liu, T.S., 2001. Geochemistry of the Pliocene red clay formation in the Chinese Loess Plateau and implications for its origin, source

provenance and paleoclimate change. Geochimica et Cosmochimica Acta, 65(6): 901-913.

Evans, M.E. and Heller, F., 2001. Magnetism of loess/palaeosol sequences: recent developments. Earth-Science Reviews, 54: 129-144.

Evans, M.E., Rutter, N.W., Catto, N., Chlachula, J. and Nyvlt, D., 2003. Magnetoclimatology: Teleconnection between the Siberian loess record and North Atlantic Heinrich events. Geology, 31(6): 537–540.

Feng, Z.-D. and Khosbayar, P., 2004. Paleosubarctic Eolian environments along the southern margin of the North American Icesheet and the southern margin of Siberia during the Last Glacial Maximum. Palaeogeography, Palaeoclimatology, Palaeoecology, 212: 265-275.

Filippi, M.L. and Talbot, M.R., 2005. The palaeolimnology of northern Lake Malawi over the last 25 ka based upon the elemental and stable isotopic composition of sedimentary organic matter. Quatenary Science Reviews, 24: 1303-1328.

Frechen, M. and Dodonov, A.E., 1998. Loess chronology of the Middle and Upper Pleistocene in Tadjikistan. Geologische Rundschau, 87: 2-20.

Frechen, M. and Yamskikh, A.F., 1999. Upper Pleistocene loess stratigraphy in the southern Yenisei Sibiria area. Journal of the Geological Society, London, 156: 515-525.

Frechen, M., Zander, A., Zykina, V. and Boenigk, W., 2005. The loess record at the section at Kurtak in Middle Siberia. Palaeogeography, Palaeoclimatology, Palaeoecology, 228: 228-244.

Gallet, S., Jahn, B., Van Vliet Lanoe, B., Dia, A. and Rossello, E., 1998. Loess geochemistry and its implications for particle origin and composition of the upper continental crust. Earth and Planetary Science Letters, 156: 157-172.

Gallet, S., Jahn, B.-m. and Torii, M., 1996. Geochemical characterization of the Luochuan loess-paleosol sequence, China, and paleoclimatic implications. Chemical Geology, 133(1-4): 67-88.

Grinenko, V.S. and Kamaletdinov, V.A., 1993. Geological map of Yakutia (in Russian). VSEGEI, St. Petersburg.

Heller, F. and Liu, T.S., 1982. Magnetostratigraphical dating of loess deposits in China. Nature, 300: 431-433.

Heslop, D., Langereis, C.G. and Dekkers, M.J., 2000. A new astronomical timescale for the loess deposits of Northern China. Earth and Planetary Science Letters, 184(1): 125-139.

Imbrie, J., Hays, J.D., Martinson, D.G., McIntyre, A., Mix, A.C., Morley, J.J., Pisias, N.G., Prell, W.L. and Shackleton, N.J., 1984. The orbital of Pleistocene climate: Support from a revised chronology of the marine ^{18}O record. In: B. Saltzman (Editor), Milankovitch and Climate. Reidel, Dordrecht, pp. 269–305.

Johnsen, S.J., Dahl-Jensen, D., Gundestrup, N., Steffensen, J.P., Clausen, H.B., Miller, H., Masson-Delmotte, V., Sveinbjörnsdottir, A.E. and White, J., 2001. Oxygen isotope and palaeotemperature records from six Greenland ice-core stations: Camp Century, Dye-3, GRIP, GISP2, Renland and NorthGRIP. Journal of Quaternary Science, 16: 299-307.

Karabanov, E.B., Prokopenko, A.A., Williams, D.F. and Colman, S.M., 1998. Evidence from Lake Baikal for Siberian Glaciation during Oxygen-Isotope Substage 5d. Quatenary Research, 50: 46-55.

Kind, N.V., Kolpakov, V.V. and Sulerzhitsky, L.D., 1971. On the age of glaciation in the Verkhoyansk Highlands (in Russian). Izvestiya Academil Nauk SSSR. Ser. Geolog. Kaya, 10: 135-144.

Kohfeld, K.E. and Harrison, S.P., 2003. Glacial-interglacial changes in dust deposition on the Chinese Loess Plateau. Quatenary Science Reviews, 22: 1859–1878.

Konert, M. and Vandenberghe, J., 1997. Comparison of laser grain size analysis with pipette and sieve analysis: a solution for the underestimation of the clay fraction. Sedimentology, 44(3): 523-535.

Kukla, G., 1987. Loess stratigraphy in central China. Quaternary Science Review, 6: 191-219.

Lea, D.W. and Boyle, E.A., 1990. Foraminiferal reconstruction of barium distribution in water masses of the glacial oceans. Paleoceanography, 5: 719-742.

Liu, X., Rolph, T., Bloemendal, J., Shaw, J. and Liu, T., 1995. Quantitative estimates of palaeoprecipitation at Xifeng, in the Loess Plateau of China. Palaeogeography, Palaeoclimatology, Palaeoecology, 113: 243-248.

Mahaney, W.C. and Rutter, N.W., 1989. Amino acid D/L ratio distribution in two Late Quaternary soils in the afroalpine zone of Mount Kenya, East Africa. Catena, 16: 205-214.

Martin, P.A. and Lea, D.W., 1998. Comparison of water mass changes in the deep tropical Altantic derived from Cd/Ca and carbon isotope records: Implications for changing Ba composition of deep Atlantic water masses. Paleoceanography, 13: 572-585.

Martinson, D.G., Pisias, N.G., Hays, J.D., Imbrie, J., Moore, T.C. and Shackleton, N.J., 1987. Age dating and the orbital theory of the ice ages—development of a high-resolution 0 to 300,000-year chronostratigraphy. Quaternary Research, 27: 1–29.

McLennan, S.M., 1993. Weathering and global denudation. Journal of Geology, 101: 295-303.

Muhs, D.R., Ager, T.A., Been, J.M., Bradbury, J.P. and Dean, W.E., 2003a. A late Quaternary record of eolian silt deposition in a maar lake, St. Michael Island, western Alaska. Quaternary Research, 60: 110-122.

Muhs, D.R., Ager, T.A., Bettis Ill, E.A., McGeehin, J., Been, J.M., Beget, J.E., Pavich, M.J., Stafford, J., Thomas W. and Stevens, D.A.S.P., 2003b. Stratigraphy and palaeoclimatic significance of Late Quaternary loess-palaeosol sequences of the Last Interglacial-Glacial cycle in central Alaska. Quaternary Science Reviews, 22(18-19): 1947-1986.

Muhs, D.R. and Bettis Ill, E.A., 2000. Geochemical Variations in Peoria Loess of Western Iowa Indicate Paleowinds of Midcontinental North America during Last Glaciation. Quaternary Research, 53: 49-61.

Müller, M.J., 1980. Handbuch ausgewählter Klimastationen der Erde. Forschungsstelle Bodenerosion. Universität Trier, Mertesdorf.

Nesbitt, H.W. and Young, G.M., 1982. Early Proterozoic climates and plate motions inferred from major chemistry of lutites. Nature, 299: 715-717.

Nugteren, G. and Vandenberghe, J., 2004. Spatial climatic variability on the Central Loess Plateau (China) as recorded by grain size for the last 250 kyr. Global and Planetary Change, 41: 185-206.

Nugteren, G., Vandenberghe, J., van Huissteden, J.K. and Zhisheng, A., 2004. A Quaternary climate record based on grain size analysis from the Luochuan loess section on the Central Loess Plateau, China. Global and Planetary Change, 41(3-4): 167-183.

Penck, A. and Brückner, E., 1909. Die Alpen im Eiszeitalter. Tauchnitz, Leipzig.

Porter, S.C. and An, Z., 1995. Correlation between climate events in the North Atlantic and China during the last glaciation. Nature, 375: 305-308.

Prokopenko, A.A., Karabanov, E.B., Williams, D.F., Kuzmin, M.I., Khursevich, G.K. and Gvozdkov, A.A., 2001. The detailed record of climatic events during the past 75,000 yrs BP from the Lake Baikal drill core BDP-93-2. Quaternary International, 80-81: 59-68.

Rousseau, D.D., Antoine, P., Hatté, C., Lang, A., Zöller, L., Fontugne, M., Othman, D.B., Luck, J.M., Moine, O., Labonne, M., Bentaleb, I. and Jolly, D., 2002. Abrupt

millennial climatic changes from Nussloch (Germany) Upper Weichselian eolian records during the Last Glaciation. Quaternary Science Reviews, 21: 1577-1582.

Sartori, M., Evans, M.E., Heller, F., Tsatskin, A. and Han, J.M., 2005. The last glacial/interglacial cycle at two sites in the Chinese Loess Plateau: Mineral magnetic, grain-size and 10Be measurements and estimates of palaeoprecipitation. Palaeogeography, Palaeoclimatology, Palaeoecology, 222: 145– 160.

Sher, A.V., Kuzmina, S.A., Kuznetsova, T.V. and Sulerzhitsky, L.D., 2005. New insights into the Weichselian environment and climate of the East Siberian Arctic, derived from fossil insects, plants, and mammals. Quaternary Science Reviews, 24: 533-569.

Spektor, V.V., 2003. Genesis of cryolithogenic complexes of the Lena and Amga rivers interfluve high plain. Abstract of the dissertation. Jakutsk, Permafrost Institute SB RAS.

Svendsen, J.I., Alexanderson, H., Astakhov, V.I., Demidov, I., Dowdeswell, J.A., Funder, S., Gataullin, V., Henriksen, M., Hjort, C. and Houmark-Nielsen, M., 2004. Late Quaternary ice sheet history of northern Eurasia. Quaternary Science Reviews, 23(11-13): 1229-1271.

Swann, G.E.A., Mackay, A.W., Leng, M.J. and Demory, F., 2005. Climate change in Central Asia during MIS 3/2: a case study using biological responses from Lake Baikal. Global and Planetary Change, 46: 235-253.

Tarasov, E., Peyron, O., Guiot, J., Brewer, S., Volkova, S., Bezusko, L.G., Dorofeyuk, N.I., Kvavadze, V., Osipova, I.M. and Panova, N.K., 1999. Last Glacial Maximum climate of the former Soviet Union and Mongolia reconstructed from pollen and plant macrofossil data. Climate Dynamics, 15: 227-240.

Xiao, J., Porter, S.C., An, Z., Kumai, H. and Yoshikawa, S., 1995. Grain Size of Quartz as an Indicator of Winter Monsoon Strength on the Loess Plateau of Central China during the Last 130,000 Yr. Quaternary Research, 43(1): 22-29.

Xiuming, L., Shaw, J., Tungsheng, L. and Heller, F., 1993. Magnetic susceptibility of the Chinese loess-palaeosol sequence: environmental change and pedogenesis. Journal of Geological Society, London, 150: 583-588.

Yang, S., Ding, F. and Ding, Z., 2006. Pleistocene chemical weathering history of Asian arid and semi-arid regions recorded in loess deposits of China and Tajikistan. Geochimica et Cosmochimica Acta, 70: 1695-1709.

Yang, S.Y., Li, C.X., Yang, D.Y. and Li, X.S., 2004. Chemical weathering of the loess deposits in the lower Changjiang Valley, China, and paleoclimatic implications. Quaternary International, 117: 27-34.

Zander, A., Frechen, M., Zykina, V. and Boenigk, W., 2003. Luminescence chronology of the Upper Pleistocene loess record at Kurtak in Middle Siberia. Quaternary Science Reviews, 22: 999-1010.

Zárate, M.A., 2003. Loess of southern South America. Quaternary Science Reviews, 22: 1987-2006.

Zech, M., 2006. Evidence for Late Pleistocene climate changes from buried soils on the southern slopes of Mt. Kilimanjaro, Tanzania. Palaeogeography, Palaeoclimatology, Palaeoecology, accepted.

Zech, M., Zech, R. and Glaser, B., submitted. A 240,000-year stable carbon and nitrogen isotope record from a loess-like palaeosol sequence in the Tumara Valley, Northeast Siberia. Chemical Geology.

Zhang, Z., Zhao, M., Lu, H. and Faiia, A.M., 2003. Lower temperature as the main cause of C4 plant declines during the glacial periods on the Chinese Loess Plateau. Earth and Planetary Science Letters, 214(3-4): 467-481.

Zöller, L., Rousseau, D.D., Jäger, K.D. and Kukla, G., 2004. Last interglacial, Lower and Middle Weichselian - a comparative study from the Upper Rhine and Thuringian loess areas. Zeitschrift für Geomorphologie N.F., 48(1): 1-24.

Zöller, L. and Semmel, A., 2001. 175 years of loess research in Germany - long records and "unconformities". Earth-Science Reviews, 54: 19-28.

Study 3:

A 240,000-year stable carbon and nitrogen isotope record from a loess-like palaeosol sequence in the Tumara Valley, Northeast Siberia

Michael Zech[*], Roland Zech and Bruno Glaser

Institute of Soil Science and Soil Geography, University of Bayreuth, D-95440 Bayreuth, Germany

* Corresponding author: Michael Zech, Phone: +49 (0)921 552247; Fax: +49 (0)921 552246;
   Email: michael_zech@gmx.de

Abstract

A 15 m loess-like palaeosol sequence located in the Tumara Valley southwest of the Verkhoyansk Mountains was investigated to reconstruct the Late Quaternary environmental history of Northeast Siberia. Total organic carbon (TOC) and total nitrogen (N) show several distinct and abrupt shifts during the last 240 ka. Both proxies have generally low values (<0.5% and <0.06%, respectively) in brown and weathered horizons, which indicates accelerated soil organic matter (SOM) degradation during periods of favorable climatic conditions. On the contrary, dark horizons in the permafrost profile are characterized by higher TOC and N contents (≥1% and ≥0.12%, respectively). They probably correlate with cold glacial periods, when water logging conditions and preservation of SOM were favoured due to extensive permafrost. The natural abundance of ^{13}C in bulk SOM ($\delta^{13}C_{TOC}$)range from approximately -29‰ to -24‰ and show distinct shifts in concert with TOC. Based on the negative correlations of $\delta^{13}C_{TOC}$ with TOC ($R^2 = 0.49$; n = 117) and TOC/N ($R^2 = 0.51$; n = 117), we suggest that variations of $\delta^{13}C_{TOC}$ in the Tumara Profile are intensively controlled by SOM degradation. Additionally, also water stress and changes of the atmospheric CO_2 signal should have influenced our stable carbon isotope record. Contrariwise, $\delta^{15}N$ – ranging from about +1‰ to +6‰ – showed no significant correlations with our SOM degradation proxies TOC and TOC/N. We therefore assume that processes like denitrification, N fixation, nitrogen losses by frequent fire events and changes in the atmospheric ^{15}N deposition contributed to an opening of the N cycle and are thus responsible for the observed $\delta^{15}N$ signal of the Tumara Profile.

1. Introduction

The reconstruction of past climate changes is necessary for a better understanding of the climate system and for the prediction of the future. High-resolution and long records are available from ice-cores and deep-sea sediments (e.g. Lisiecki and Raymo, 2005; McManus et al., 1999; NGRIP members, 2004; Schulz et al., 1998; Siegenthaler et al., 2005). Comparable terrestrial archives are lake sediments (e.g. Karabanov et al., 1998; Last and Smol, 2001; Prokopenko et al., 2001) and loess and loess-like deposits (e.g.: Chlachula, 2003; Liu et al., 1999; Muhs et al., 2003; Rousseau et al., 2002). As only a large number of records allows to investigate regional aspects of past climate and environmental changes, the need and search for further archives especially from hitherto less intensively studied areas is obvious. Here we present results of geochemical (total organic carbon and nitrogen), grain size (clay content) and stable isotope analyses ($\delta^{13}C_{TOC}$ and $\delta^{15}N$) from the Tumara Profile. This loess-like palaeosol sequence in the southwest of the Verkhoyansk Mountains probably spans the last 240 ka (Zech et al., submitted).

Within the last decades stable isotope techniques have become an increasingly important tool for current and past ecologic and climatic studies. The natural abundance of ^{13}C in bulk soil organic matter (SOM) is influenced by the input signal of the vegetation and by pedogenetic effects. Specifically, we will discuss our $\delta^{13}C_{TOC}$ record in terms of (i) the photosynthetic pathway of the surrounding vegetation (C3/C4 metabolic pathway), (ii) water stress, (iii) changes in the atmospheric CO_2 concentration and its isotopic signal, (iv) SOM degradation and (v) methanogenesis. Of course, it is sometimes difficult to disentangle the contribution of all these various factors and therefore especially interpretations of smaller carbon isotopic shifts may be controversial and speculative. Concerning the $\delta^{13}C_{TOC}$ record of the Tumara Profile, we will show that valuable information can be obtained in combination with TOC and the TOC/N ratio.

In contrast to the natural abundance of ^{13}C, which is widely used in palaeoecologic studies, $\delta^{15}N$ analyses have been applied much less so far. Wolfe et al. (1999), for example, studied lake sediments in arctic Russia and found that the natural abundance of ^{15}N reflects the Mid-Holocene transition from forest to tundra vegetation in the catchment. The authors suggest that higher rates of biogeochemical reworking due to warmer climate are responsible for the isotopic enrichment of sediments derived from forest soils, whereas more negative $\delta^{15}N$ values are typical for tundra soils and lower temperatures. Another example comes from Ethiopia, where Eshetu and Högberg (2000) found isotope enrichment in soils under

relatively young or disturbed forests compared with soils from forests that were established several hundred years ago. The authors explained this difference with a land-use caused opening of the N cycle, which led to nitrogen losses and fractionating processes.

According to our knowledge, the here presented study is the first one that applies $\delta^{15}N$ analyses at high resolution in a loess-like palaeosol sequence. We will discuss the $\delta^{15}N$ variations with respect to (i) SOM degradation, (ii) biological and chemical denitrification, (iii) N fixation, (iv) N uptake by plants, (v) nitrogen losses by frequent fire events and (vi) changes in the atmospheric deposition of ^{15}N.

2. Geological setting, stratigraphy and chronology of the Tumara Profile

The investigated loess-like palaeosol sequence, referred to as 'Tumara Profile' (120 m a.s.l., 63°36' N, 129°58' E), is located about 300 km north of Jakutsk at the banks of the Tumara River, which drains part of the southern Verkhoyansk Mountains (Fig. 3-1). The study area is characterized by a boreal climate with a pronounced dry winter season (Jakutsk: 213 mm/a, Verkhoyansk: 155 mm/a)(Müller, 1980). Between the mountains to the north and the debouchure into the Aldan River to the south, the Tumara River cuts a 100 km long transect through Quaternary and Tertiary deposits. Moraines and terraces are typically overlain by several meters of frozen aeolian sediments. Note that in the study area we do not deal with "classical loess" as we find it e.g. in China or Western and Southeast Europe. Similar to aeolian records from Middle Siberia, where the loess is often colluvially reworked or pedogenetically imprinted (Chlachula, 2003; Frechen et al., 2005), our sediments are influenced by pedogenetic and/or cryogenetic processes. Depending on the climatic conditions – glacial or interglacial/interstadial – one can expect that either water saturated pedogenetic conditions prevailed in a thin active permafrost layer with water logging, or weathering processes (e.g. clay mineral formation) and SOM degradation dominated in well aerated and warm surface soils.

Already Kind et al. (1971) reported that the Verkhoyansk Mountains have experienced three major glacial advances during the Upper Pleistocene: the Zyryan during the Early Weichselian, the Zhigansk during the Middle Weichselian and – synchronous with the global Last Glacial Maximum (LGM) – the Sartan Glaciation during Marine Isotope Stage (MIS) 2. More recently, Svendsen et al. (2004) reconstructed four glaciations for northern Eurasia: (1) the Late Saalian (>140 ka), (2) the Early Weichselian (100–80 ka), (3) the Middle Weichselian (60–50 ka) and (4) the Late Weichselian (25–15 ka). This palaeoclimatic history

can be expected to be recorded in the loess-like palaeosol sequences covering the oldest moraines and terraces in the study area.
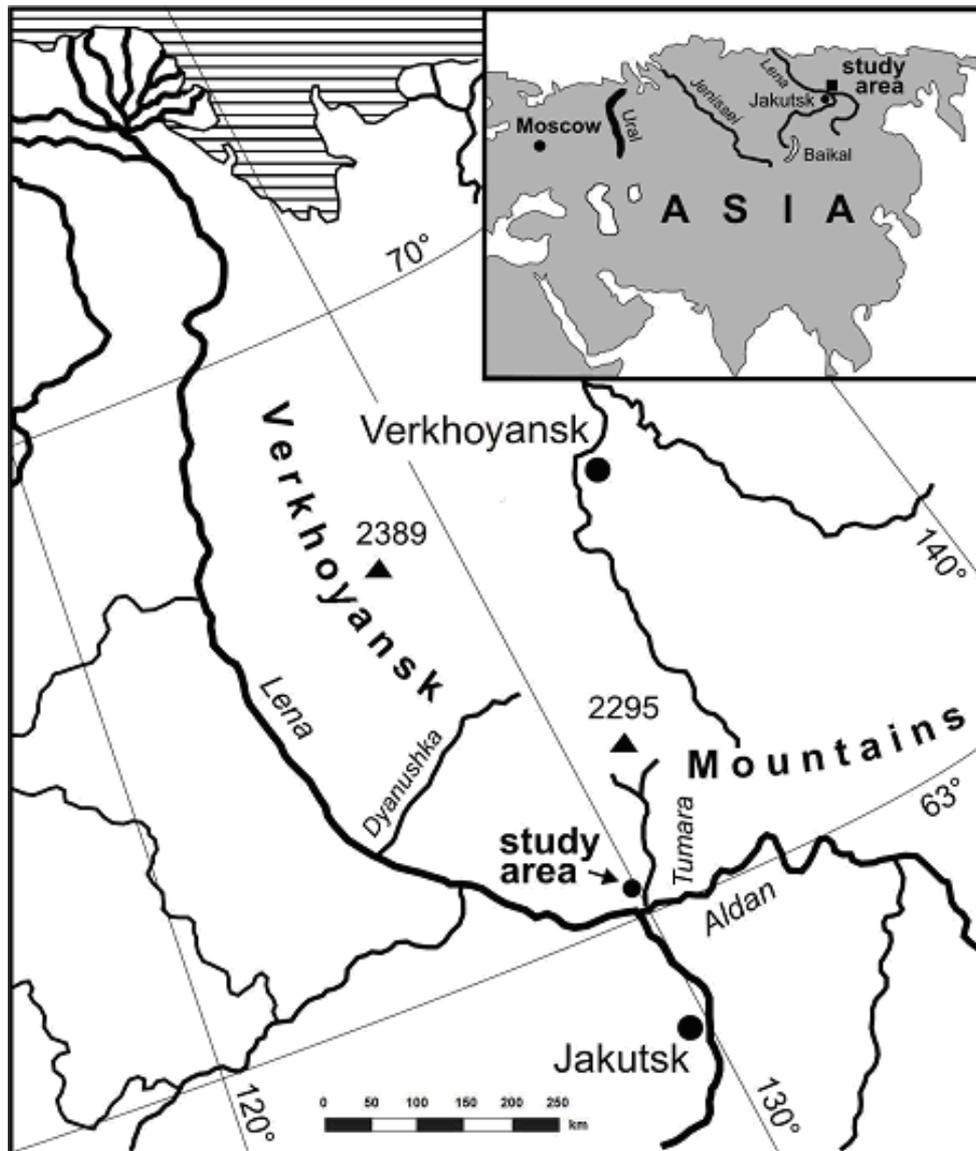
Fig. 3-1: Location of the study area in Northeast Siberia. The upper 15 m of an undercut slope of the Tumara River is the frozen loess-like palaeosol sequence referred to as 'Tumara Profile'. From Zech et al. (submitted).

The Tumara Profile, which was sampled during field work in summer 2002, is exposed at an ~60 m high undercut slope of the Tumara River. It is situated several kilometers outside the outermost moraine arc and the surrounding vegetation is taiga. The stratigraphy of the sampled profile is illustrated in Fig. 3-2B: In the lower part of the brown Unit A (0 - 1.8 m) several thin organic-rich layers mark the transition to a dark, silty horizon (1.8 – 4.8 m). This Unit B partly reveals hydromorphic features, is rich in macrofossils and has a gray band at ~3 m depth. The division in three subunits is suggested by Zech et al. (submitted) and based

on geochemical and granulometric results. A large ice-wedge protrudes from Subunit B3 (4.0 – 4.8 m) into the underlying intensively weathered, brown palaeosol (Subunit C1, 4.8 – 6.7 m). Subunit C2 is less weathered and slightly darker; a thin pebble layer in ~7.7 m depth may indicate a discontinuity. Subunit C3 (7.8 – 9.7 m) is again generally brown and more clayey than C2; its upper part is rich in red-yellow mottles. Unit D (9.7 – 12.5 m) is a thick dark horizon, resembling Unit B. The lowermost Unit E (12.5 – 15 m) is composed of a brown horizon in the upper part and a partly mottled palaeosol complex in the lower part. The basis consists of dark gray fluvioglacial sandy gravels. A more detailed description is given in Zech et al. (submitted).

According to the chronology discussed in Zech et al. (submitted), the Tumara Profile spans the last 240,000 years (Fig. 3-2D). The authors developed different palaeopedologic proxies (TOC, clay content, "U-ratio", weathering indices and D/L-amino acids) indicating warm interglacial/interstadial climatic conditions or cold glacial ones. Accordingly, the brown palaeosols revealing generally low TOC but increased clay contents characterise warm and favourable periods with enhanced SOM degradation and clay mineral production. On the contrary, SOM accumulation and reduced brunification are characteristic for dark palaeosol, which developed during cold/glacial periods. The palaeopedologic proxies were used to derive a "warm vs. cold stratigraphy", in which the numeric dating results were be embedded and allow a tentative correlation with marine isotope stages (MIS). A short summary of the chronological proposal of Zech et al. (submitted) is given in the following:

Despite of inconsistencies in the radiocarbon ages, the Holocene is supposed to be represented by the brunified Unit A (Fig. 3-2). Presumably, ^{14}C ages are overestimated for instance by the deposition of "too old" recalcitrant windblown carbon or by mobilisation and vertical translocation of "too old" carbon with ascending water from underlying and formerly permafrosted palaeosols.

Although several radiocarbon ages of approximately 9 ka BP were derived for roots down to 3 m depth (Fig. 3-2A), Subunit B1 is supposed to have been deposited during MIS 2. Note that this inconsistency among the datable materials does not necessarily belittle the chronological and palaeoenvironmental interpretation, but may enrich it: probably, the warm Late Glacial and Early Holocene summers caused an intensive thawing of the active permafrost layer and allowed roots to penetrate this depth (3 m). This is in agreement with the so-called Boreal thermal optimum reported by Andreev et al. (2002) for Northern Siberia.

The Subunits B2 and B3 can tentatively be correlated with MIS 3 and 4 (Fig. 3-2D). The three radiocarbon ages around 48 ka BP at the basis of Unit B are expected to be minimum ages. Cold glacial conditions during the early MIS 3 – from 50 to 60 ka BP according to Svendsen et al. (2004) – likely provoked the epigenetic ice-wedge to protrude into the underlying brown palaeosol, which is supposed to corresponds to MIS 5a. Subunit C2 probably represents the Early Weichselian glaciation of Svendsen et al. (2004) (MIS 5b) and overlies the Eemian soil (MIS 5e: Subunit C3), for which 3 IRSL ages were obtained (136, 150 and 177 ka). Based on the comparison of the Tumara Profile with other northern hemispheric records and another IRSL age from Unit E (220 ka), Zech et al. (submitted) correlate Unit D with MIS 6 and Unit E with MIS 7, respectively.

3. Materials and Methods

After cleaning the upper 15 m of the Tumara Profile (100 cm width and 30 cm depth), a total number of 117 samples were taken at 10 to 20 cm intervals. The samples were air dried, sieved (<2 mm) and stored in plastic bags. Analyses were performed following standard laboratory procedures at the Institute of Soil Science and Soil Geography, University of Bayreuth. Total organic carbon (TOC) and total nitrogen (N) were determined after removal of carbonate (10% HCl) by dry combustion of a finely ground homogeneous 50 mg sub-sample followed by thermal conductivity detection on a Vario EL elemental analyser (Elementar, Hanau, Germany). The detection limits of our machine were calculated by measuring blanks with increasing net weights of wolfram oxide in tin capsules (~0.0002% for TOC and ~0.007% for N).

The δ^{13}C and δ^{15}N values of the bulk organic matter (OM) were obtained by dry combustion of decalcified subsamples on a Carlo Erba NC 2500 elemental analyzer coupled with a Delta^{plus} continuous-flow isotope ratio mass spectrometer (Thermo Finnigan MAT, Bremen, Germany) via a Conflow II interface (Thermo Finnigan MAT, Bremen, Germany). Sucrose (ANU, IAEA, Vienna, Austria), $CaCO_3$ (NBS 19, Gaithersburg, USA), and ammoniumsulfate (N1 and N2, both IAEA, Vienna, Austria) were used as calibration standards. Natural abundances of carbon and nitrogen stable isotopes are expressed in the usual δ-scale in parts per thousand according to the equation

$$\delta_{sample}\ (‰) = \left(\frac{R_{sample} - R_{standard}}{R_{standard}} \right) \times 1000,$$

where R_{sample} and $R_{standard}$ are the $^{13}C/^{12}C$ or $^{15}N/^{14}N$ abundance ratios of a sample or a standard, respectively. Precision was determined by measuring known standards in replication (~0,15‰ for $\delta^{13}C$ and ~0.25‰ for $\delta^{15}N$). Grain size analyzes were performed on a Beckman Coulter particle size analyzer after removal of OM with H_2O_2 (30%) and removal of carbonate with HCl (10%).

4. Results and Discussion

The depth-profiles of TOC, N, TOC/N, $\delta^{13}C_{TOC}$, $\delta^{15}N$ and the clay content are illustrated in Fig. 3-2C. All parameters show distinct shifts for most transitions between brown and dark gray horizons and therefore corroborate the stratigraphic units deduced from field observations.

4.1 Carbon and nitrogen contents

The organic carbon and nitrogen contents display similar variations throughout the profile and range from 0,27% to 2,48% and from 0,04% to 0,22%, respectively (Fig. 3-2C). Several abrupt shifts occur at the transitions from the brown units (C1, C3 and E) to the dark gray units (B, C2 and D), with TOC and N being generally low in the former and high in the latter ones. High TOC and N values also coincide with higher TOC/N ratios (Fig.3- 2C).

On the one hand, the elemental composition of litter may influence the TOC/N ratio in soils and cannot be completely ruled out. On the other hand, decomposition of SOM lowers the TOC/N ratio due to the loss of carbon in form of CO_2. However, we assume that the latter effect dominates in our record and hence TOC and TOC/N are appropriate proxies for SOM degradation. As one may expect, reduced SOM degradation generally coincides with reduced weathering, the latter being inferred from lower clay contents in the Units B1, B3, C2 and D. Vice versa, the brown units are characterised by higher clay contents (increased weathering) and lower TOC and TOC/N ratios (intensive SOM degradation).

With regard to the chronostratigraphy (Fig. 3-2D), our findings show that warm climatic conditions during MIS 1, 3, 5 and 7 favored SOM degradation and weathering (Units A, C and E), whereas during the cold periods MIS 2, 4, 5b/d and 6 weathering and SOM degradation were reduced (Units B1, B3, C2 and D).

The comparison with northern hemispheric loess records reveals that there is a striking difference between the Tumara Profile and European or Chinese loess profiles. In the Tumara
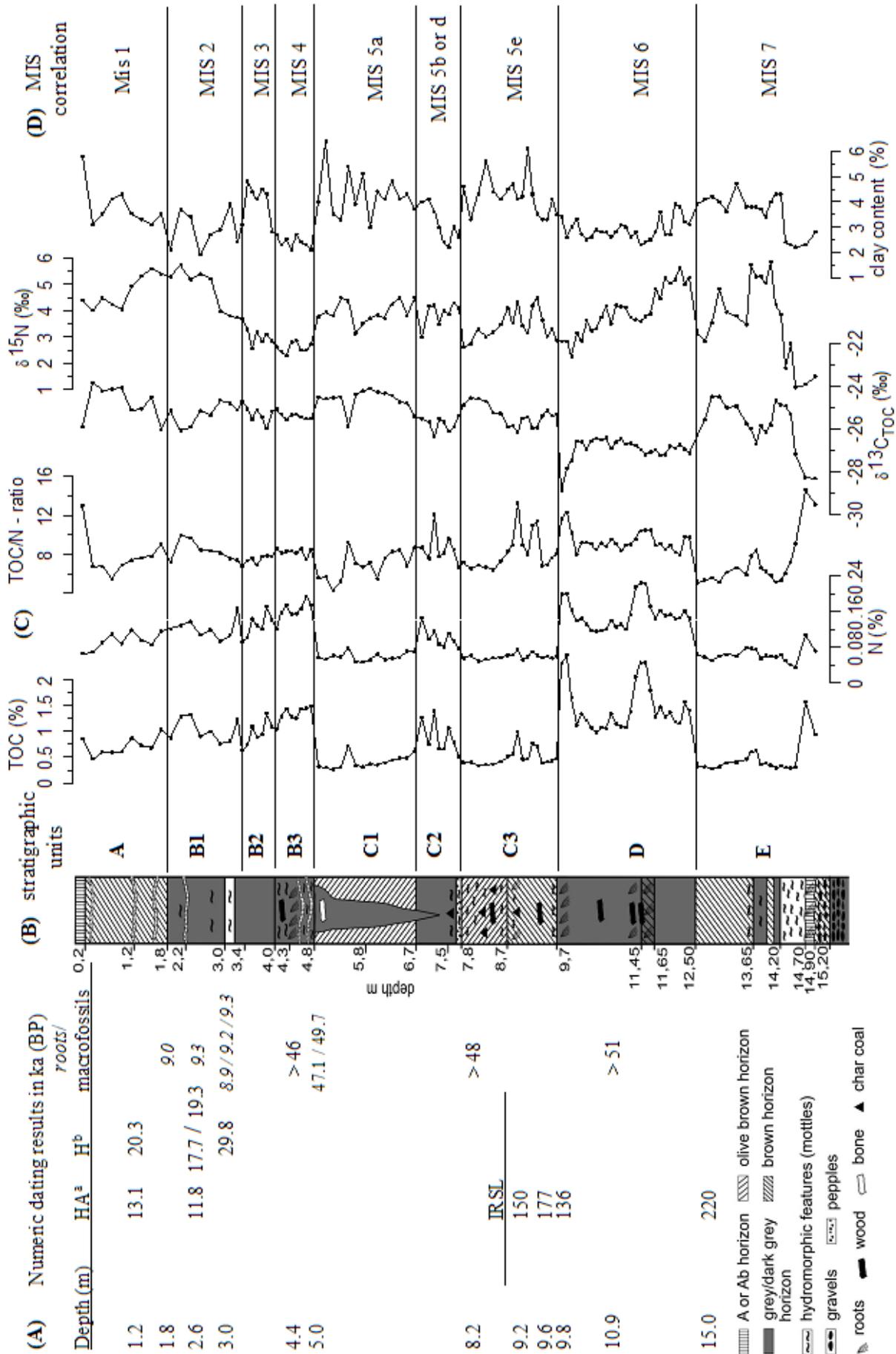
Fig. 3-2: (A) Numeric dating results in ka BP, (B) stratigraphy, (C) depth profiles of the analysed parameters (TOC, N, TOC/N, $\delta^{13}C_{TOC}$, $\delta^{15}N$ and clay content) and (D) correlation of the stratigraphic units with marine oxygen isotope stages (MIS). Modified after Zech et al. (submitted).

Profile high TOC values correlate with glacial periods. In Europe and China, on the contrary, the interglacial and interstadial palaeosols are often enriched in OM indicating higher biomass production, increased moisture availability and low dust accumulation rates (Bronger, 2003; Fink, 1962; Hatté et al., 1999; Zöller et al., 2004). This difference can be explained with permafrost being a crucial factor for pedogenetic processes in Northeast Siberia. Whereas biomass production was probably never a limiting factor for the accumulation of OM due to still relatively warm summers even during the LGM in Siberia (Tarasov et al., 1999), pedogenetic conditions at our study site presumably differed depending on the climate: during cold glacial periods water logging conditions prevailed in the thin active permafrost layer and inhibited SOM degradation in the topsoil. On the contrary, warmer summers during the interstadials and interglacials were characterised by both deeper melting of the permafrost and hence better drainage and increased evaporation. As in these better aerated topsoils SOM mineralisation was intensified, TOC can not only be interpreted as "warm vs. cold" proxy in our record, but also as proxy for the degree of SOM degradation. This will be of importance when discussing the natural abundance of ^{13}C in the following paragraphs.

4.2 Natural abundance of ^{13}C

According to Fig. 3-2C, δ^{13}C values obtained for bulk SOM range from –28.9‰ to –23.9‰. They display systematic variations throughout the profile with more negative values coinciding with TOC maxima (Units D, C2 and B). Besides, there is a general tendency towards more positive $\delta^{13}C_{TOC}$ values in the younger sediments over the whole profile.

Numerous processes can potentially influence the natural abundance of SOM ^{13}C in soils and/or sediments. This makes a palaeoenvironmental reconstruction with bulk $\delta^{13}C_{TOC}$ values alone sometimes speculative. On the one hand, δ^{13}C variations of the deposited OM have to be taken into consideration. On the other hand, pedogenetic processes can lead to isotopic fractionation, too. Both aspect will be discussed in the following for the $\delta^{13}C_{TOC}$ record of the Tumara Profile.

In many studies, varying contributions of **C3 versus C4 plants** were found to be responsible for changing stable carbon isotope compositions in loess-palaeosol sequences or other palaeoenvironmental archives (e.g.: Aucour et al., 1999; Freitas et al., 2001; Liu et al., 2005b; Wang and Follmer, 1998; Wang et al., 2000). These studies are based on the fact that the photosynthetic pathway of C3 plants produces rather depleted δ^{13}C values of approximately -27‰ (O´Leary, 1988). On the contrary, the C4 metabolism, which is more

competitive under drier and/or warmer conditions and lower atmospheric CO_2 concentrations, leads to plant $\delta^{13}C$ values around -14‰ (Collatz et al., 1998). As one may expect, in the Tumara Profile all $\delta^{13}C_{TOC}$ values are well within the range of SOM derived from C3 vegetation. The absence of C4 plants is typical for temperate and cold environments and has the advantage that other ecological factors affecting $\delta^{13}C_{TOC}$ in sediments can be investigated more easily.

One of the main environmental factors known to control the $\delta^{13}C$ in plants is **water stress**. Plants react on it with stomata narrowing, which results in lower intercellular CO_2 concentrations, reduced isotope fractionation and thus more positive $\delta^{13}C$ values of the synthesized organic compounds (Farquhar et al., 1982; O'Leary, 1995; Schliesser, 1995). Recently, Liu et al. (2005a) and Stevenson et al. (2005) have shown for plants and soils, respectively, that $\delta^{13}C$ decreases (up to 5‰) with increasing rainfall along precipitation gradients in arid regions of China and the USA. Hatté and Guiot (2005) used this relationship to reconstruct the palaeoprecipitation by using the isotopic signal of loess OM in the Nußloch loess sequence (Rhine Valley, Germany). A key assumption for their modelling is the absence of pedogenesis in typical loess. According to the authors, this implies that the dry glacial environment favoured the degradation of OM without distortion of the isotopic signal.

Reminding our interpretation of TOC and N for the Tumara Profile (reduced SOM degradation in water logged active permafrost layers versus enhanced SOM degradation in well aerated active permafrost layers), the more positive $\delta^{13}C_{TOC}$ values in the generally OM-depleted Units A, C1, C3 and E could also be interpreted in terms of water stress. In these units, water could have become a limiting factor for plants during the growing season, whereas no water stress should have occurred during the deposition of the water logged Units B, C2, and D. Furthermore, this mechanism could explain the general tendency towards more positive $\delta^{13}C_{TOC}$ values in the younger sediments. On the one hand, the thus deduced increasing aridity of the study site during the Late Quaternary can be seen in a large-scale context, as e.g. Svendsen et al. (2004) reported that the Northern Siberian ice sheets got progressively smaller during the last four glaciations (covering the last 160,000 years) and this can be explained with decreasing precipitation. On the other hand, one may not forget the local setting being characterised by the Tumara cliff edge, which approached our study site during the Late Quaternary. Accordingly, wind exposure increased and plants hence should have suffered more and more water stress.

Another important environmental factor, which is supposed to influence $\delta^{13}C$ of plants, is the **CO_2 concentration** in the atmosphere. Lower CO_2 concentrations during

glacials (~100 ppm, e.g. Petit et al., 1999) lead to reduced isotopic fractionation, resulting in $\delta^{13}C$ values that are 0,02‰ more positive per 1 ppm CO_2 (Feng and Epstein, 1995). In the Tumara Profile, however, the dark glacial deposits (Units B, C2 and D) would have to be enriched. As this is not the case, we conclude that the changing atmospheric CO_2 concentration does not explain but rather dampens the observed $\delta^{13}C_{TOC\ g}$ signal. Concerning the **carbon isotope signature** of the atmospheric CO_2, which can be measured on air trapped in ice cores, only minor changes (0.3 ± 0.2‰) have been reported for glacial-interglacial transitions (Leuenberger et al. (1992). They can therefore be neglected.

Whereas according to Hatté and Guiot (2005) **SOM degradation** does not influence the $\delta^{13}C_{TOC}$ signal in typical loess records, such fractionation can certainly not be ruled out for our loess-like palaeosol sequence, which is characterised by the alteration of different pedogenetic conditions. Many soil studies reported increasing ^{13}C abundance with soil depth being correlated with a decrease of TOC and with age of SOM despite the absence of C3-C4 shifts (Andreux et al., 1990; Balesdent et al., 1993; Bol et al., 1999; Chen et al., 2002; Krull et al., 2002; Nadelhoffer and Fry, 1988; Stevenson, 1997). Although the exact mechanisms are not yet well understood, this pattern is mainly attributed to SOM decomposition. Note that there are also studies of aquatic sediments, peat bogs and litter decay revealing no ^{13}C enrichment or even ^{13}C depletion in more degraded OM in contrast to well preserved OM (Balesdent et al., 1993; Benner et al., 1987; Meyers and Ishiwatari, 1993; Pancost et al., 2003; Spiker and Hatcher, 1984; Van Kaam-Peters et al., 1998). According to Balesdent and Mariotti (1998), these apparently divergent results can however be reconciled in an OM decomposition model considering both a ^{13}C enrichment due to OM degradation (e.g. by microbial respiration) and a slower because inhibited decay of ^{13}C-depleted compounds (e.g. lignin) during certain steps of OM decomposition. Reviewing the literature, we conclude that OM degradation in soils – and hence also in our loess-like palaeosol sequence – can account for a ^{13}C enrichment of up to 2-3‰ in temperate and boreal environments.

We tried to assess the SOM degradation effect on $\delta^{13}C_{TOC}$ in the Tumara Profile by applying cross-plot-analyses. As outlined above, TOC and TOC/N can be used as proxies for SOM degradation in our study. A significant positive correlation between TOC and TOC/N (R^2_{total} = 0.46, n = 117) corroborates our previous TOC interpretation (low TOC contents are caused by SOM degradation as indicated by coinciding low TOC/N ratios) and also holds true for most individual stratigraphic units (Fig. 3-3A). Correlation coefficients range from R^2 = 0.06 (n = 8, Subunit B3) to R^2 = 0.95 (n = 16, Subunit C3). Trendlines with slopes of ~2 are
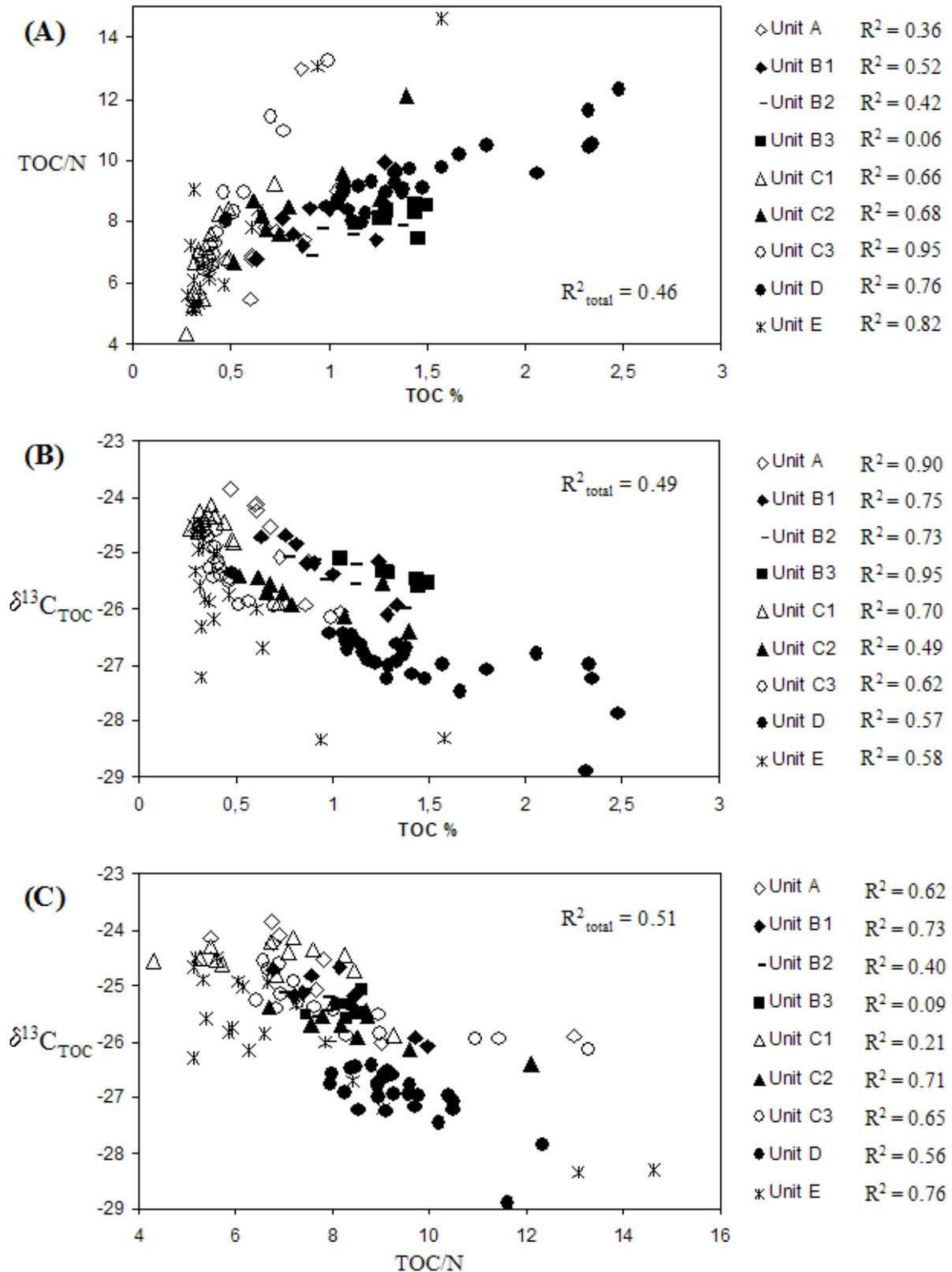
Fig. 3-3: Correlation between TOC, TOC/N and $\delta^{13}C_{TOC}$ (n = 117): (A) TOC vs. TOC/N (R^2_{total} = 0.46), (B) TOC vs. $\delta^{13}C_{TOC}$ (R^2_{total} = 0.49) and (C) TOC/N vs. $\delta^{13}C_{TOC}$ (R^2_{total} = 0.51). Correlation coefficients for individual stratigraphic units are given in the legend. The highly significant correlations indicate that $\delta^{13}C_{TOC}$ in the Tumara Profile is intensively influenced by SOM degradation.

characteristic for the dark organic-rich units, whereas the slopes are much steeper for the intensively weathered brown units (~10). Both TOC and TOC/N are negatively correlated with $\delta^{13}C_{TOC}$ (R^2_{total} = 0.49 and R^2_{total} = 0.51, respectively, see Fig. 3-3B and C). The correlation coefficients for the individual stratigraphic units range from R^2 = 0.09 (TOC/N vs. $\delta^{13}C_{TOC}$ in Subunit B3, n = 8) to R^2 = 0.95 (TOC/N vs. $\delta^{13}C_{TOC}$ in Subunit B3, n = 8). We conclude that most likely SOM degradation exerted a dominant control on TOC, TOC/N and likewise on $\delta^{13}C_{TOC}$ of the Tumara Profile.

Our interpretation is in agreement with findings from other permafrost soils in Siberia: Pfeiffer and Jansen (1993) and Gundelwein (1998) found more negative $\delta^{13}C$ values in hydromorphic, humic-rich soils in comparison to well drained soils that were enriched in ^{13}C. The authors explained their findings with differences in the SOM decomposition and with anaerobic SOM transformation processes, although climatically induced variations of the plant communities were not completely ruled out (Gundelwein, 1998). The data of Schirrmeister et al. (2002), who studied Ice Complex deposits in the Laptev Sea region, Northern Siberia, reveal the same negative correlation between TOC and TOC/N versus $\delta^{13}C_{TOC}$ as our results do. Their 60 ka record, however, shows two distinctive differences compared to our record: firstly, lower TOC contents and more positive $\delta^{13}C_{TOC}$ values for MIS 2 sediments and TOC maxima and $\delta^{13}C_{TOC}$ minima for Holocene and MIS 3 layers (i.e. that is the direct opposite signal in the Tumara Profile); secondly, the TOC contents in the peaty Ice Complex deposits are by factor 10 higher than in our loess-like profile. This likely reflects the different environmental conditions at the two study sites, although similar mechanisms could be responsible for the $\delta^{13}C_{TOC}$ signals.

Another relevant process that might be important when explaining fluctuations of $\delta^{13}C_{TOC}$ values is **methanogenesis**. Methane emitted from wetlands is strongly depleted in ^{13}C (Bréas et al., 2001). This readily leads to ^{13}C enrichment of soils. Several studies determined methane production rates for various environments (Whiting and Chanton, 1993). Generally, methanogenic bacteria are suppressed by oxygen and high CH_4 emissions only occur when the groundwater table and the soil temperature are high (>10°C) (Dunfield et al., 1993; Svensson, 1984). According to our interpretation, these two conditions rather exclude each other at our study site. Either the soils were well drained during warm periods, or water logged during cold periods. We therefore assume that methanogenesis is less important than water stress and SOM degradation for the observed $\delta^{13}C_{TOC}$ variations in the Tumara Profile.

4.3 Natural abundance of ^{15}N

The δ^{15}N values of the Tumara Profile vary from +1‰ and +6‰ and are well within the range typically found in soils (Nadelhoffer and Fry, 1988). The Units A and C generally reveal smaller δ^{15}N fluctuations around +4‰, whereas distinct long-term trends occur in the organic-rich Units B and D. The largest variations occur in the lowermost Unit E (Fig. 3-2C).

Typically, δ^{15}N is higher in soils compared to the surrounding vegetation and increases with soil depth (Nadelhoffer and Fry, 1988). This points to an isotopic enrichment during **SOM degradation**. We can test this effect on our δ^{15}N record in a similar way as previously performed for $\delta^{13}C_{TOC}$. Interestingly, no significant correlation can be found between δ^{15}N and any of the other organic parameters (TOC, TOC/N and $\delta^{13}C_{TOC}$), which are controlled by SOM degradation. Other processes of the N cycle apparently exert a dominant control on the nitrogen isotopic composition in the Tumara Profile.

It is well-known that **denitrification** strongly discriminates against the heavier ^{15}N isotope and causes a preferential emission of ^{14}N in form of N_2 and N_2O. This results in more positive δ^{15}N values in the remaining SOM. Dörsch et al. (1993), for instance, found significant N_2O emissions especially during melting after frost periods – probably due to short-term but strongly increased microbial activity. Papen and Butterbach-Bahl (1999) confirmed the importance of freeze/thaw cycles and emphasized that also the forest type greatly influences the N_2O release. Their beech control site released 4-5 times more N_2O than their spruce control site. Chemical denitrification, as opposed to biological denitrification, might play a role at temperatures just below 0°C. Christianson and Cho (1983) measured N_2 emissions and showed that the chemical denitrification generally decreases with temperature, however, at –3.5°C it suddenly increases again and reaches values as they are typical for ~20°C. They explained this temperature anomaly with higher solute concentration of NO_2^- in the unfrozen interfacial water, which exists at temperatures as low as –40°C.

We tentatively conclude that the very positive δ^{15}N values in the lower parts of the Units A and D as well as in Unit B1 and partly in Unit E may be caused by extraordinarily frequent freeze/thaw cycles having occurred in these sediments (Fig. 3-2C). At least for the Units A and B1 the numeric dating result support this idea. Several ^{14}C ages around 9 ka BP – obtained for roots down to 3 m depth – indicate a regular and deep melting of the active permafrost layer during the warm summers of the Late Glacial and Early Holocene climatic optimum. However, the δ^{15}N pattern for the whole profile is not consistent with the alternating brown and dark gray palaeosols. Therefore denitrification is unlikely to be the only process responsible for the observed nitrogen isotopic composition.

As mentioned before, vegetation changes may affect the biological denitrification. Additionally, vegetation changes could influence the nitrogen isotopic composition of soils especially when atmospheric nitrogen is fixed. **N fixation** is well-known to cause more negative $\delta^{15}N$ values of the biomass and hence also of the SOM. Benson and Silvester (1993) reported that in cold environments N-fixation by actinomycetes (*Francia*), living in symbiosis with trees and shrubs, especially alnus, may be underestimated. Apart from N-fixation, further differences in the **N uptake** have to be considered when interpreting $\delta^{15}N$ variations in plants. For example the arctic sedge *Eriophorum vaginatum*, gets up to 60% of their nitrogen in form of free amino acids instead of inorganic NO_3^- and NH_4^+ (Chapin III et al., 1993). This confirms that different soil nitrogen sources contribute to the wide range of $\delta^{15}N$ values found in various plant species collected from tundra ecosystems – e.g. very low values (-8 to -6‰) in *Picea* and ericaceous species and even positive values in sedges and grasses (Nadelhoffer et al., 1996; Schulze et al., 1994). Accordingly, apart from SOM degradation N-uptake by plants is often accounted when interpreting ^{15}N enrichment with soil depth. However, on the one hand, we have no stable surface in our accumulating loess-like sediments – making considerations concerning this isotopic depth gradient difficult. On the other hand, we argue that the N uptake by plants (N fixation is not included here) should not have the potential to alter the $\delta^{15}N$ signal if the N cycle remains closed and all plant material converts again into SOM by decomposition.

Therefore, other mechanisms leading to gains/losses of depleted/enriched N pools should be further investigated. For instance, frequent **fire events** could have contributed significantly to an open N cycle and thus to a preferential loss of isotopically lighter plant OM. Apart from nitrogen losses, also changes in the nitrogen input by dry and wet **atmospheric deposition** have to be considered. Rain contains significant amounts of dissolved nitrogen (as NO_3^-, NO_2^- and NH_4^+) with relatively low $\delta^{15}N$ values (Heaton, 1987; Paerl and Fogel, 1994), whereas aeolian dust containing SOM is relatively enriched in ^{15}N. The distinctive shift from low $\delta^{15}N$ values in Unit B2 and 3 to very positive values in Unit B1 could thus indicate decreasing wet and increasing dry nitrogen deposition. This would confirm the trend towards more arid conditions in Siberia in the course of the last glacial cycle (Hubberten et al., 2004; Svendsen et al., 2004). Whether changing atmospheric ^{15}N deposition contributed to the observed trend in Unit D or the large variations in Unit E is however even more speculative.

5. Conclusions

In this study we presented the carbon and nitrogen contents and the respective isotopic compositions of a probably ~240,000 years old loess-like palaeosol sequence in the Tumara Valley, Northeast Siberia. In contrast to European and Chinese loess records, glacial and stadial soils in the Tumara Profile are characterised by higher TOC and N contents than the interglacial and interstadial ones. Water logging conditions likely favoured the preservation of SOM during cold periods with extensive permafrost. The highly significant correlations between TOC, TOC/N, $\delta^{13}C_{TOC}$ and the clay content suggest that all these parameters reflect the alternation of accelerated and reduced SOM degradation/weathering. Although probably intensively controlled by SOM degradation, the $\delta^{13}C_{TOC}$ record should have also been influenced by water stress and the atmospheric CO_2 signal.

The interpretation of $\delta^{15}N$ is more speculative. SOM degradation probably affects the nitrogen isotopic composition, but the lack of a significant correlation with TOC, TOC/N or $\delta^{13}C_{TOC}$ indicates that additional processes of the N cycle played a crucial role. For instance, denitrification, depending on temperature and on the frequency of freeze/thaw cycles, causes ^{15}N enrichment of soils and in all likelihood influenced the $\delta^{15}N$ record of the Tumara Profile. Vegetation changes should not have contributed significantly to the observed $\delta^{15}N$ variations, if they were not accompanied by an opening of the N cycle. On the contrary, N fixation and nitrogen losses by fire events had the potential to alter the $\delta^{15}N$ pattern. Eventually, dry and wet atmospheric N deposition should be further investigated because of their different isotopic signal.

Both $\delta^{13}C_{TOC}$ and $\delta^{15}N$ are subjected to pedogenetic processes, which have to be considered carefully when deriving palaeoclimatic information from SOM stable isotopic variations. The application of compound-specific isotope analyses on degradation-resistant biomarkers could be a promising methodological approach in order to disentangle the influence of SOM degradation on $\delta^{13}C_{TOC}$. Palynological work for the Tumara Profile is in progress.

Acknowledgements

References

Andreev, A.A. et al., 2002. Late Pleistocene and Holocene Vegetation and Climate on Taymyr Lowland, Northern Siberia. Quaternary Research 57, 138-150.

Andreux, F., Cerri, C., Vose, P.B., Vitorello, V.A., 1990. Potential of stable isotope, ^{15}N and ^{13}C methods for determining input and turnover in soils. In: Harrison, A.F., Ineson, P., Heal, O.W. (Eds.), Nutrient Cycling in Terrestrial Ecosystems. Elsevier Applied Science, London, pp. 259-275.

Aucour, A.-M., Hillaire-Marcel, C., Bonnefille, R., 1999. Sources and accumulation rates of organic carbon in an equatorial peat bog (Burundi, East Africa) during the Holocene: carbon isotope constraints. Palaeogeography, Palaeoclimatology, Palaeoecology 150, 179-189.

Balesdent, J., Girardin, C., Mariotti, A., 1993. Site-related δ^{13}C of tree leaves and soil organic matter in a temperate forest. Ecology 74 (6), 1713-1721.

Balesdent, J., Mariotti, A., 1998. Measurement of SOM turnover using ^{13}C natural abundance. In: Boutton, T.W., Yamasaki, S. (Eds.), Mass spectrometry of soils. Marcel Dekker, Inc., New York.

Benner, R., Fogel, M.L., Sprague, E.K., Hodson, R.E., 1987. Depletion of 13C in lignin and its implications for stable carbon isotope studies. Nature 329, 708.

Benson, D.R., Silvester, W.B., 1993. Biology of Francia strains: Environmental, ecological, and management effects. Microbiol. Rev. 57, 293-319.

Bol, R.A., Harkness, D.D., Huang, Y., Howard, D.M., 1999. The influence of soil processes on carbon isotope distribution and turnover in the British uplands. European Journal of Soil Science 50, 41-51.

Bréas, O., Guillou, C., Reniero, F., Wada, E., 2001. The global methane cycle: isotopes and mixing ratios, sources and sinks. Isotopes Environ. Health Stud. 37, 257-379.

Bronger, A., 2003. Correlation of loess-paleosol sequences in East and Central Asia with SE Central Europe: towards a continental Quaternary pedostratigraphy and paleoclimatic history. Quaternary International 106-107, 11-31.

Chapin III, F.S., Moilanen, L., Kielland, K., 1993. Preferential use of organic nitrogen for growth by a non-mycorrhizal artic sedge. Nature 361, 150-153.

Chen, Q. et al., 2002. Soil organic matter turnover in the subtropical mountainous region of south China. Soil Science 167 (6), 401-415.

Chlachula, J., 2003. The Siberian loess record and its significance for reconstruction of Pleistocene climate change in north-central Asia. Quaternary Science Reviews 22 (18-19), 1879-1906.

Christianson, C.B., Cho, C.M., 1983. Chemical Denitrification of Nitrite in Frozen Soils. Soil. Sci. Soc. Am. J. 47, 38-42.

Collatz, G.J., Berry, J.A., Clark, J.S., 1998. Effects of climate and atmospheric CO_2 partial pressure on global distribution of C4 grasses: present, past and future. Oecologia 114, 441-454.

Dörsch, P., Flessa, H., Beese, F., 1993. Jahreszeitliche N_2O-Emmisionsspitzen nach Bodenfrost. Mitteilungen Bodenkundliche Gesellschaft 72, 495-498.

Dunfield, P.R., Knowles, R., Dumont, R., Moore, T.R., 1993. Methane poduction and consumption in temperate and subarctic peat soils: Response to temperature and pH. Soil Biol. Biochem. 25, 321-326.

Eshetu, Z., Högberg, P., 2000. Effects of land use on ^{15}N natural abundance of soils in Ethiopian highlands. Plant and Soil 222, 109-117.

Farquhar, G.D., O'Leary, M.H., Berry, J.A., 1982. On the relationship between carbon isotope discrimination and the intercellular carbon dioxide concentration in leaves. Australian Journal of Plant Physiology 9, 121-137.

Feng, X., Epstein, S., 1995. Carbon isotopes of trees from arid environments and implications for reconstructing atmospheric CO_2 concentration. Geochimica et Cosmochimica Acta 59, 2599-2608.

Fink, J., 1962. Die Gliederung des Jungpleistozäns in Österreich. Mitteilungen Geologische Gesellschaft Wien 54, 1-25.

Frechen, M., Zander, A., Zykina, V., Boenigk, W., 2005. The loess record from the section at Kurtak in Middle Siberia. Palaeogeography, Palaeoclimatology, Palaeoecology 228, 228-244.

Freitas, H.A. et al., 2001. Late Quaternary Vegetation Dynamics in the Southern Amazon Basin Inferred from Carbon Isotopes in Soil Organic Matter. Quaternary Research 55, 39-46.

Gundelwein, A., 1998. Eigenschaften und Umsetzung organischer Substanz in Nordsibirischen Permafrostböden. Hamburger Bodenkundliche Arbeiten 39, 1-162.

Hatté, C. et al., 2001. δ^{13}C of Loess Organic Matter as a Potential Proxy for Paleoprecipitation. Quaternary Research 55, 33-38.

Hatté, C. et al., 1999. New chronology and organic matter δ^{13}C paleoclimatic significance of Nußloch loess sequence (Rhine Valley, Germany). Quaternary International 62, 85-91.

Hatté, C., Guiot, J., 2005. Palaeoprecipitation reconstruction by inverse modelling using the isotopic signal of loess organic matter: application to the Nußloch loess sequence (Rhine Valley, Germany). Climate Dynamics 25, 315-327.

Heaton, T.H.E., 1987. ^{15}N/^{14}N ratios of nitrate and ammonium in rain at Pretoria, South Africa. Atmos. Environ. 21, 843-852.

Hubberten, H.W. et al., 2004. The periglacial climate and environment in northern Eurasia during the Last Glaciation. Quaternary Science Reviews 23 (11-13), 1333-1357.

Karabanov, E.B., Prokopenko, A.A., Williams, D.F., Colman, S.M., 1998. Evidence from Lake Baikal for Siberian Glaciation during Oxygen-Isotope Substage 5d. Quaternary Research 50, 46-55.

Kind, N.V., Kolpakov, V.V., Sulerzhitsky, L.D., 1971. On the age of glaciations in the Verkhoyansk Highlands. Izvestiya Academii Nauk SSSR. Ser. Geologicheskaya 10, 135-144.

Krull, E.S., Bestland, E.A., Gates, W.P., 2002. Soil organic matter decomposition and turnover in a tropical ultisol: evidence from δ^{13}C, δ^{15}N and geochemistry. Radiocarbon 44 (1), 93-112.

Last, W.M., Smol, J.P. (Eds.), 2001. Tracking Environmental Change Using Lake Sediments, 2. Kluwer Academic Publishers, Dordrecht, The Netherlands.

Leunenberger, M., Siegenthaler, U., Langway, C.C., 1992. Carbon isotope composition of atmospheric CO_2 during the last ice age from Antarctica ice core. Nature 357, 488-490.

Lin, B.R., An, Z., 1991. Preliminary research on stable isotopic compositions of Chinese loess. In: Tingsheng, L. (Ed.), Loess, Environment and Global Change. Science Press, Beijing, China, 124-131.

Lisiecki, L.E., Raymo, M.E., 2005. A Pliocene-Pleistocene stack of 57 globally distributed benthic δ^{18}O records. Paleoceanography 20, doi:10.1029/2004PA001071.

Liu, T., Ding, Z., Rutter, N.W., 1999. Comparison of Milankovitch periods between continental loess and deep sea records over the last 2.5 Ma. Quaternary Science Reviews 18, 1205-1212.

Liu, W. et al., 2005a. δ^{13}C variation of C3 and C4 plants across an Asian monsoon rainfall gradient in arid northwestern China. Global Change Biology 11, 1094-1100.

Liu, W. et al., 2005b. Did an extensive forest ever develop on the Chinese Loess Plateau during the past 130 ka?: a test using soil carbon isotopic signatures. Applied Geochemistry 20, 519-527.

McManus, J.F., Oppo, D.W., Cullen, J.L., 1999. A 0.5-Million-Year Record of Millennial-Scale Climate Variability in the North Atlantic. Science 283, 971-975.

Meyers, P.A., Ishiwatari, R., 1993. Lacustrine organic geochemistry - an overview of indicators of organic matter sources and diagenesis in lake sediments. Organic Geochemistry 20 (7), 867-900.

Muhs, D.R. et al., 2003. Stratigraphy and palaeoclimatic significance of Late Quaternary loess-palaeosol sequences of the Last Interglacial-Glacial cycle in central Alaska. Quaternary Science Reviews 22 (18-19), 1947-1986.

Müller, M.J., 1980. Handbuch ausgewählter Klimastationen der Erde. Forschungsstelle Bodenerosion. Universität Trier, Mertesdorf.

Nadelhoffer, K. et al., 1996. ^{15}N natural abundances and N use by tundra plants. Oecologia 107, 386-394.

Nadelhoffer, K.J., Fry, B., 1988. Controls on natural Nitrogen-15 and Carbon-13 abundances in soil organic matter. Soil Sci. Soc. Am. J. 52, 1633-1640.

NGRIP members, 2004. High-resolution record of Northern Hemisphere climate extending into the last interglacial period. Nature 431, 147-151.

O´Leary, M.H., 1988. Carbon isotopes in photosynthesis. Bioscience 38, 328-336.

O'Leary, M.H., 1995. Environmental effects on carbon isotope fractionation in terrestrial plants. In: Wada, E., Yokoyama, T., Minagawa, M., Ando, T., Fry, B.D. (Eds.), Stable Isotopes in the Biosphere. Kyoto University Press, Japan, pp. 79-91.

Paerl, H.W., Fogel, M.L., 1994. Isotopic characterization of atmospheric nitrogen inputs as sources of enhanced primary production in coastal Atlantic Ocean waters. Mar. Biol. 119, 635-645.

Pancost, R.D., Baas, M., van Geel, B., Damsté, J.S.S., 2003. Response of an ombrotrophic bog to a regional climate event revealed by macrofossil, molecular and carbon isotope data. The Holocene 13 (6), 921-932.

Papen, H., Butterbach-Bahl, K., 1999. A 3-year continuous record of nitrogen trace gas fluxes from untreated and limed soil of a N-saturated spruce and beech forest ecosystem in Germany. J. Geophys. Res. 104, 18487-18503.

Petit, J.R. et al., 1999. Climate and atmospheric history of the past 420,000 years from the Vostoc ice core, Antarctica. Nature 399, 429-436.

Pfeiffer, E.M., Jansen, H., 1993. δ^{13}C-analysis of permafrost soil samples of NE-Siberia. Proc. of the 3rd Symp. on the Joint Siberian Permafrost Studies between Japan and Russia, 8-13.

Prokopenko, A.A. et al., 2001. The detailed record of climatic events during the past 75,000 yrs BP from the Lake Baikal drill core BDP-93-2. Quaternary International 80-81, 59-68.

Rousseau, D.-D. et al., 2002. Abrupt millennial climatic changes from Nussloch (Germany) Upper Weichselian eolian records during the Last Glaciation. Quaternary Science Reviews 21, 1577-1582.

Schirrmeister, L., Siegert, C., Kunitzky, V.V., Groote, P.M., Erlenkeuser, H., 2002. Late Quaternary ice-rich permafrost sequences as a paleoenvironmental archive for the Laptev Sea Region in northern Siberia. Int. J. Earth Sciences 91, 154-167.

Schliesser, G.H., 1995. Parameters determining carbon isotope ratios in plants. In: Frenzel, B. (Ed.), Problems of stable isotopes in tree-rings, lake sediments and peat bogs as climate evidence for the Holocene. Palaeoclimate Res. 15, 71-96.

Schulz, H., von Rad, U., Erlenkeuser, H., von Rad, U., 1998. Correlation between Arabian Sea and Greenland climate oscillations of the past 110,000 years. Nature 393, 54-57.

Schulze, E.-D., Chapin III, F.S., Gebauer, G., 1994. Nitrogen nutrition and isotope differences among life forms at the northern treeline of Alaska. Oecologia 100, 406-412.

Siegenthaler, U. et al., 2005. Stable Carbon Cycle-Climate Relationship During the Late Pleistocene. Science 310, 1313-1317.

Spiker, E.C., Hatcher, P.G., 1984. Carbon isotope fractionation of sapropelic organic matter during early diagenesis. Organic Geochemistry 5 (4), 283-290.

Stevenson, B.A., 1997. Stable carbon and oxygen isotopes in soils and paleosols of the Palouse loess, eastern Washington state: modern relationships and applications for paleoclimatic research. Ph.D. Dissertation. Colorado State University, Fort Collins, Colorado.

Stevenson, B.A., Kelly, E.F., McDonald, E.V., Busacca, A.J., 2005. The stable carbon isotope composition of soil organic carbon and pedogenic carbonates along a bioclimatic gradient in the Palouse region, Washington State, USA. Geoderma 124, 37-47.

Svendsen, J.I. et al., 2004. Late Quaternary ice sheet history of northern Eurasia. Quaternary Science Reviews 23 (11-13), 1229-1271.

Svensson, B.H., 1984. Different temperature optima fot methane formation when enrichments from acid peat are supplemented with acetate or hydrogen. Appl. Env. Microbiol. 48, 389-394.

Tarasov, E. et al., 1999. Last Glacial Maximum climate of the former Soviet Union and Mongolia reconstructed from pollen and plant macrofossil data. Climate Dynamics 15, 227-240.

Van Kaam-Peters, J.M.E., Schouten, S., Köster, J., Damsté, J.S.S., 1998. Controls on the molecular and carbon isotopic composition of organic matter deposited in a Kimmeridgian euxinic shelf sea: Evidence for preservation of carbohydrates through sulfurisation. Geochimica and Cosmochimica Acta 62 (19/20), 3259-3283.

Wang, H., Ambrose, S.H., Liu, C.L.J., Follmer, L.R., 1997. Paleosol stable isotope evidence for early hominid occupation of east asian temperate environments. Quaternary Research 48, 228-238.

Wang, H., Follmer, L.R., 1998. Proxy of monsoon seasonality in carbon isotopes from paleosols of the southern Chinese Loess Plateau. Geology 26 (11), 987-990.

Wang, H., Follmer, L.R., Liu, C.-L.J., 2000. Isotope evidence of paleo-El Niño-Southern Oscillation cycles in loess-paleosol record in the central United States. Geology 28 (9), 771-774.

Whiting, G.J., Chanton, J.P., 1993. Primary production control of methane emission from wetland. Nature 364, 794-795.

Wolfe, B.B., Edwards, T.W.D., Aravena, R., 1999. Changes in carbon and nitrogen cycling during tree-line retreat recorded in the isotopic content of lacustrine orgenic matter, western Taimyr Peninsula, Russia. The Holocene 9, 215-222.

Zech, M. et al., submitted. Multi-proxy analytical characterisation and palaeoclimatic interpretation of the Tumara Palaeosol Sequence, NE Siberia. Quaternary Research.

Zöller, L., Rousseau, D.D., Jäger, K.D., Kukla, G., 2004. Last interglacial, Lower and Middle Weichselian - a comparative study from the Upper Rhine and Thuringian loess areas. Z. Geomorph. N. F. 48 (1), 1-24.

Study 4:

Reconstruction of NE Siberian vegetation history based on cuticular lipid biomarker and pollen analyses

Michael Zech [1*], Andrei Andreev [2]

[1] Institute of Soil Science and Soil Geography, University of Bayreuth, D-95445 Bayreuth, Germany

[2] Alfred Wegener Institute for Polar and Marine Research, Research Unit Potsdam, 14473 Potsdam, Germany

* Corresponding author: Michael Zech, Phone: +49 (0)921 552247; Fax: +49 (0)921 552246; Email: michael_zech@gmx.de

Boreas

To be submitted

Abstract

In this paper we present lipid biomarker (n-alkanes) and pollen data obtained for the 15 m high loess-like permafrost "Tumara Palaeosol Sequence" (TPS), NE Siberia. The alkane ratio $(nC_{31} + nC_{29})/nC_{27}$ is used as proxy for grasses/herbs versus trees. Both biomarker and pollen results indicate that trees dominated during formation of the lower half of the sequence. Then, various and mainly treeless grass/herb communities prevailed, before reforestation started at ~2.3 m depth. The palaeoclimatic interpretation of these palaeobotany findings with the best modern analogue (BMA) method, which calculates transfer functions based on the comparison of recent pollen spectra with modern climate conditions, seems to be in disagreement with the climatic stratigraphy inferred from a multi-proxy palaeopedologic approach. Different climatic parameters probably exert dominant control over palaeobotany and pedogenic history, respectively. Complementary, rather than contradicting palaeo-environmental information can thus be inferred.

1. Introduction

In order to better predict the response of various ecosystems to global warming it is essential to know how palaeobotany reacted to climate changes in the past. Both vegetation and climate history in Arctic Russia have previously been reconstructed using pollen analyses (e.g. Alekseev, 1997; Andreev et al., 2004; Andreev et al., 1997; Andreev et al., 2001b; Andreev et al., 2002a; Ilyashuk et al., 2006; Klimanov, 1984; Klimanov and Andreev, 1992; Tarasov et al., 1998). However, many studies lack sufficient age control and/or long-term continuous records. Methodologically, palynology is limited to archives allowing conservation of pollen. Furthermore, long-distance transport and variable pollination rates may cause discrepancies between standing vegetation and corresponding pollen distributions (Faegri and Iversen, 1989).

Whereas the natural abundance of stable carbon isotopes can only be applied in tropical and subtropical archives, where changes in the photosynthetic pathway (C3 versus C4) are recorded (Boutton, 1996), biomarker analyses could be a promising complementary method to palynology in temperate (Farrimond and Flanagan, 1996; Ficken et al., 1998), alpine (Zech, 2006) and boreal study areas like NE Siberia. For instance, n-alkanes are important constituents of cuticular plant leaf waxes (Kolattukudy, 1976). They are deposited with the litter and buried subsequently in soils, where they are exceptionally resistant to degradation (Cranwell, 1981; Meyers and Ishiwatari, 1993). Hence, they should store information about the former standing vegetation. Short- and mid-chain n-alkanes are valuable biomarkers for lacustrine-derived organic matter (Bourbonniere et al., 1997; Ficken et al., 2000; Zech et al., submitted-a; Zhang et al., 2004). On the other hand, long-chain n-alkanes (nC_{27}, nC_{29} and nC_{31}) dominate in terrestrial plants. As different plants reveal characteristic n-alkane patterns, the distribution of these biomarkers in sediments has been used in palaeoenvironmental studies to reconstruct vegetation changes (Cranwell, 1973; Nott et al., 2000; Schwark et al., 2002; Zech, 2006; Zech et al., submitted-a).

In this paper we present n-alkane biomarker and pollen results obtained for the "Tumara Palaeosol Sequence" (TPS) in NE Siberia. The main objectives are (i) to evaluate the potential of long-chain n-alkanes as biomarkers in permafrost palaeosol sequences, (ii) to contribute to the reconstruction of the vegetation history in the study area and (iii) to compare the results with the climatic chronostratigraphy, which is based on multi-proxy pedological analysis (Zech et al., submitted-b).

2. Materials and Methods

2.1 Geographical setting

The loess-like permafrost palaeosol sequence TPS (120 m a.s.l., 63°36' N, 129°58' E) is located about 300 km north of Jakutsk at the banks of the Tumara River, which drains part of the southern Verkhoyansk Mountains (for details see Zech et al., submitted-b). Between the mountains to the north and the debouchure into the Aldan River to the south, the Tumara River cuts a 100 km long transect through Quaternary and Tertiary deposits. It thereby passes also large moraine arcs, which are abundant in the western and southern Verkhoyansk Forelands and which document several former piedmont glaciations (Kind, 1975; Kolpakov, 1979; Stauch et al., 2006). Today no glaciers exist, although climate is characterised by short, warm summer and long, cold winter seasons. In Jakutsk, maximum and minimum temperatures are 30-38°C and −60 to −70°C (Müller, 1980). Annual precipitation, mainly brought by the westerlies, is too low (Jakutsk: 213 mm/yr, Verkhoyansk: 155 mm/yr). The extreme continental conditions cause the formation of 400 – 600 m thick permafrost. Concerning vegetation, larch forests typically cover the southern and western forelands of the Vekhoyansk Mountains (Anderson and Lozhkin, 2001).

2.2 The Tumara Palaeosol Sequence

Approximately 10 km south of the outermost moraine arc a 50-60 m high cliff is exposed on the orographically right river bank. Its lower part consists of yellow tertiary sand with embedded fossil woods and trunks. Superjacent are gray Early Pleistocene sands and pebbles (Grinenko and Kamaletdinov, 1993). Between ~15-33 m from the surface, Mid Pleistocene fluvio-glacial sandy gravels were deposited. The upper 15 m of the exposure are referred to as "TPS" and consist of frozen dark gray loess-like sediments intercalated by brown soil horizons (Fig. 4-1B). A detailed description and discussion of the chronology is provided by Zech et al. (submitted-b). Briefly, both morphological features and analytical results allow distinguishing the stratigraphic units A, B1-3, C1-3, D and E. The dark gray Units B, C2 and D are characterized by higher organic carbon contents than the brown, more intensively weathered Units A, C1, C2 and E (Fig. 4-1C). Based on a multi-proxy analytical approach (geochemistry, grain size distribution and characterization of the soil organic matter), numeric dating results (Fig. 4-1A) and the comparison with other northern hemispheric records, a simple glacial - interglacial/-stadial climatic stratigraphy can be established (glacial conditions: thin active permafrost layer, water logging → less weathering, organic matter preservation; versus interglacial/-stadial: warmer, aerated top soil → more

intensive weathering and organic matter decomposition). A tentative correlation with the marine isotope stages (MIS, see also Fig. 4-1D) is proposed by Zech et al. (submitted-b). Accordingly, the palaeopedologic results suggest that the TPS spans the last ~240 ka. The unit boundaries B/C and C2/C3 possibly reflect discordances and the Units C1 and C2 may contain reworked material.

2.3 Alkane and pollen analyses

After cleaning and describing the upper 15 m of the TPS, a total number of 117 samples were taken at 10–20 cm intervals for geochemical and pollen analyses from the frozen deposits. The samples were air dried, sieved (<2 mm) and stored in plastic bags. Furthermore, several plant samples were collected for biomarker analyses.

Sample preparation of n-alkanes from soil and plant samples was carried out at the University of Bayreuth. We adopted the method described by Bourbonniere et al. (1997): Free lipids were extracted with methanol/toluene (7/3) using Soxhlet apparatuses. Then, concentrated lipid extracts were given on columns filled with deactivated (5%) silica gel (2 g) and deactivated (5%) aluminum oxide (2 g). n-Alkanes were eluted with 45 ml hexane/toluene (85/15). Quantification was performed on an HP 6890 GC equipped with a flame ionisation detector (FID). Deuterated n-alkanes (d_{42}-n-C_{20} and d_{50}-n-C_{24}) were added as internal and recovery standards, respectively.

Pollen analyses were carried out at the Alfred Wegener Institute for Polar and Marine Research, Potsdam. A standard HF technique was used for pollen preparation (Berglund and Ralska-Jasiewiczowa, 1986). The relative frequencies of pollen taxa were calculated from the sum of the terrestrial pollen taxa.

Recently, the best modern analogue (BMA) method (Guiot, 1990) was applied for quantitative Late Pleistocene and Holocene climatic reconstruction in Arctic Russia (Andreev et al., 2004; Andreev and Klimanov, 2000; Andreev et al., 2003a; Andreev et al., 2003b). It uses transfer functions, which are calculated by comparison of recent pollen spectra with modern climate conditions. Although not quantitatively, we use the BMA method as described in the above references to infer palaeoclimatic information from the reconstructed TPS vegetation.

3. Results

3.1 n-Alkane patterns

All analysed plant and soil samples were dominated by long-chain n-alkanes ranging from nC_{25} to nC_{33} (0.89 to 29.88 μg/g soil and 0.10 to 2.74 mg/g TOC, respectively) and
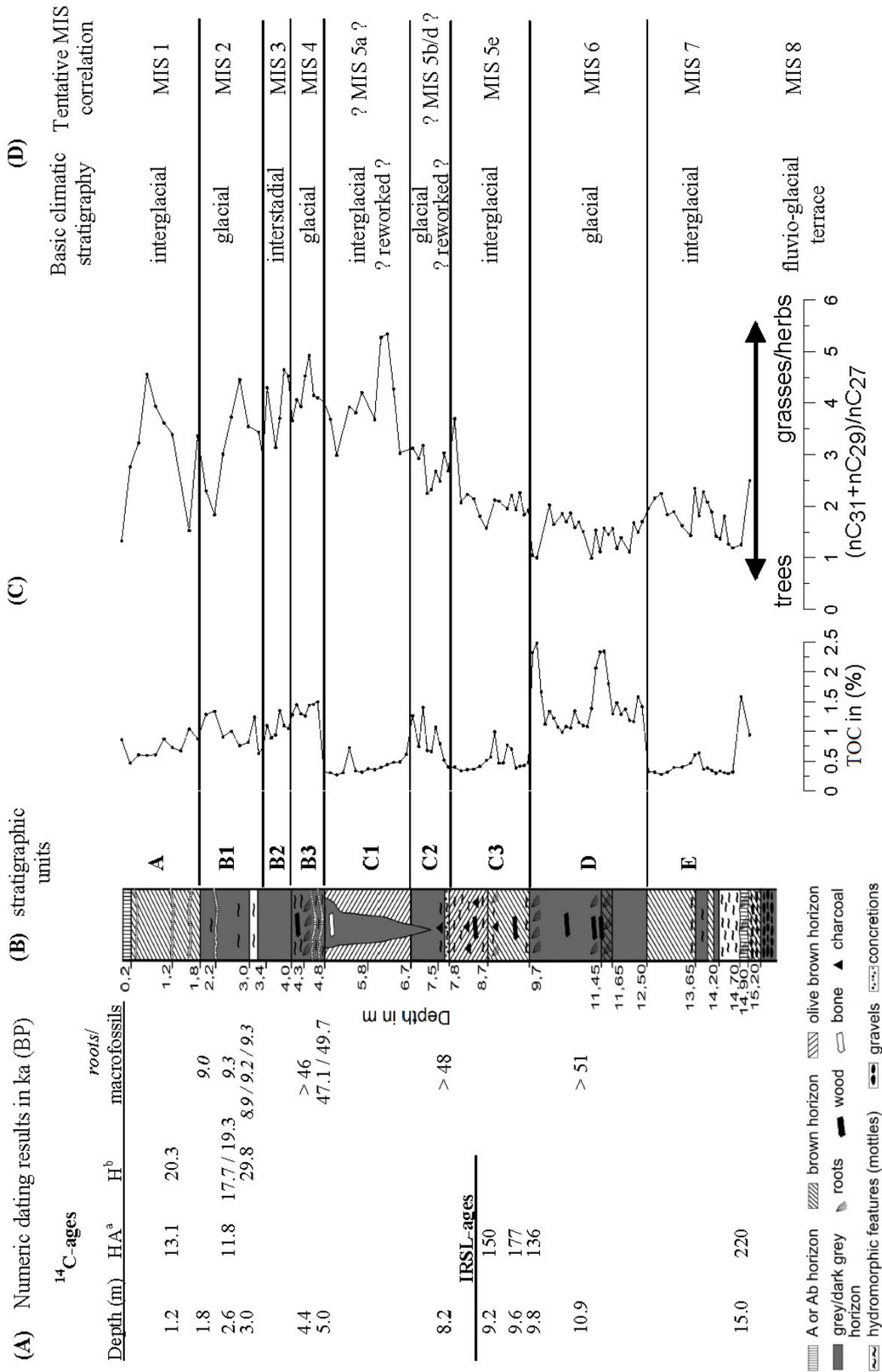
Fig. 4-1: (A) Numeric dating results, (B) stratigraphy, (C) TOC and biomarker proxy ratio $(nC_{31} + nC_{29})/nC_{27}$ and (D) climatic stratigraphy as deduced from a multi-proxy pedological approach and tentative MIS correlation for the TPS (modified after Zech et al., submitted-b).

revealed a strong odd-over-even-predominance. Such n-alkane patterns are typical for epicuticular plant leaf waxes (Kolattukudy, 1976). Concerning the modern plant samples, they are either dominated by nC_{27} (trees), nC_{29} (*Carex* → Cyperaceae) or nC_{31} (Poaceae and herbs). This is in agreement with findings from other authors (Cranwell, 1973; Nott et al., 2000; Schwark et al., 2002; Zech et al., submitted-a) and can be illustrated in a ternary diagram (Fig. 4-2): Whereas trees cluster close to nC_{27}, *Carex* is localized close to nC_{29} and Poaceae/herbs cluster close to nC_{31}. Fig. 4-2 also depicts that the cluster formed by the sediment samples from Unit D is well separated from the cluster formed by the Units B2 and B3, with the former one being closer to nC_{27} and the latter one being closer to nC_{31}. These results suggest that trees dominated the vegetation cover during formation of Unit D, but that a mainly treeless steppe-like vegetation with grasses and herbs prevailed during formation of Unit B. In order to illustrate the varying contribution of grasses/herbs versus trees/shrubs at higher temporal resolution, we calculated the alkane ratio $(nC_{31} + nC_{29})/nC_{27}$ and plotted it versus depth in Fig. 4-1C. Accordingly, the lower half of the profile developed under tree-dominated vegetation, the upper half of the TPS under grasses and herbs. Reforestation started only at ~2.3 m depth and was again interrupted by a treeless phase documented within in the uppermost meter.
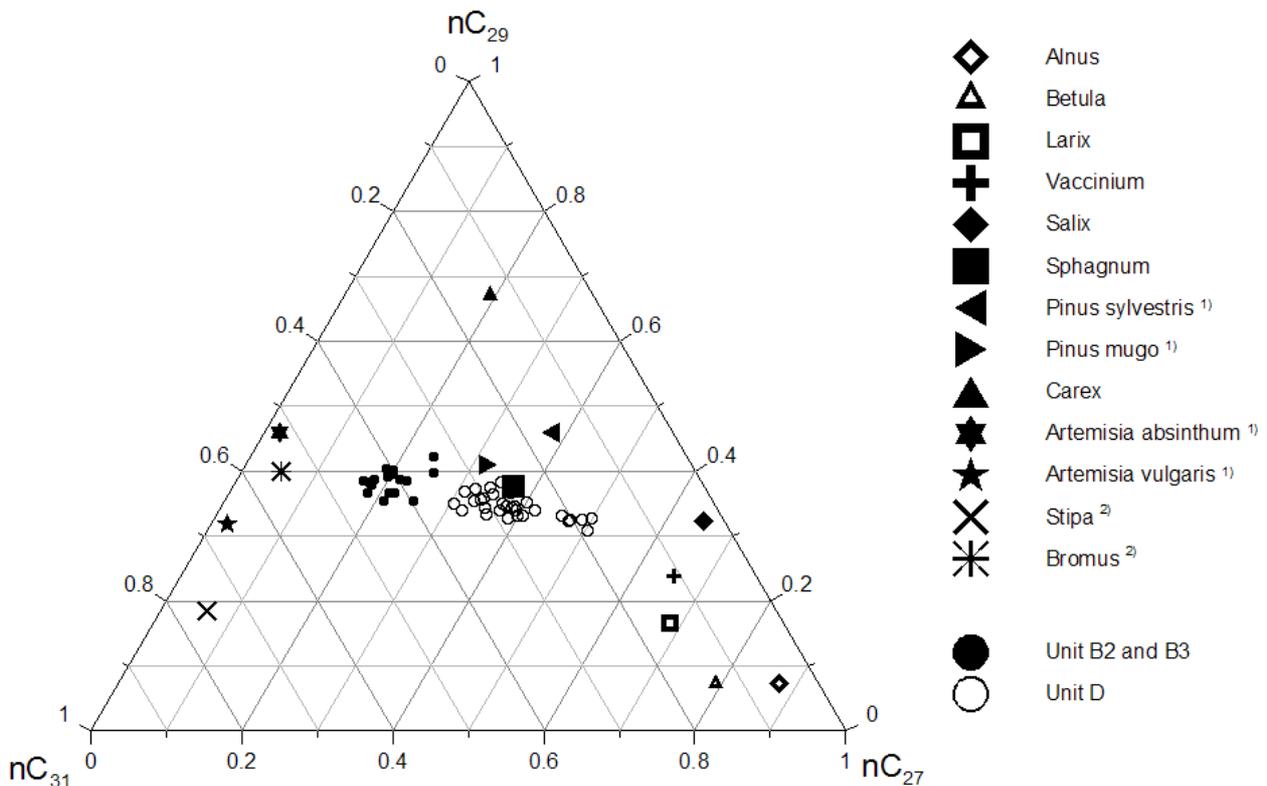
Fig. 4-2: Ternary diagram with the alkanes nC_{27}, nC_{29} and nC_{31} for plant samples and sediment samples from the Tumara Profile. [1] From Schwark et al. (2002), [2] own unpublished data from other study sites

3.2 Pollen diagram

Ten pollen zones (PZ) were distinguished independently from pedological features and can be described as follows (Fig. 4-3):

- Cyperaceae with few Poaceae and *Salix* dominate in the lowermost sample (PZ-I). Pollen concentration is high. Presumably, open sedge-grass dominated vegetation with few willow stands was typical for the study area.

- PZ-II contains high amounts of tree (*Larix, Picea, Pinus*) and shrub (*Betula* sect. *Nanae, Alnus fruticosa*) pollen, as well as *Sphagnum* spores. Larch forest with some spruce should have dominated with dwarf birch and shrub alder growing under the trees. Wet habitats with Cyperaceae and *Sphagnum* were also common.

- Rather high amounts of tree and shrub pollen and *Sphagnum* spores also dominate the spectrum of PZ-III. However, pollen of Chenopodiaceae, Cichoriaceae, Caryophyllaceae, *Thalictru*m (in the uppermost sample) markedly increase and higher amounts of *Selaginella rupestris* spores are notable in this zone.

- Few pollen are preserved in PZ-IV. On the one hand this could indicate scarce vegetation cover. On the other hand, the absence of palynomorphs could be the result of intense pollen degradation during this period.

- PZ-V contains rather high pollen concentrations again, especially from Cyperaceae, Poaceae, Caryophyllaceae, Chenopodiaceae and Artemisia. Treeless, steppe like vegetation should have covered the study area.

- Rather high amounts of *Betula* sect *Albae, Salix* and Cyperaceae pollen characterize PZ-VI. Open birch and larch forests and steppe like associations should have occurred, but *Larix* pollen are easily corroded (Andreev et al., 2001a)

- Cyperaceae, Poaceae, Caryophyllaceae, Cichoriaceae, and Thalictrum dominate the PZ-VII. Treeless herb communities covered the study area during this time.

- PZ-VIII is characterized by rather high amounts of *Alnus fruticosa* and *Pinus sylvestris*.

- Pollen of *Betula* sect *Albae* and *Salix* contribute largely to the spectrum of PZ-IX except for the transition to PZ-X, where Asteraceae and Ranunculaceae pollen markedly increase.

- PZ-X contains high amounts of *Betula sect. Albae* and *Pinus sylvestris*. We assume that the study area during PZ-IX and PZ-X intervals was also partly covered by *Larix* forests, but *Larix* pollen could be corroded.
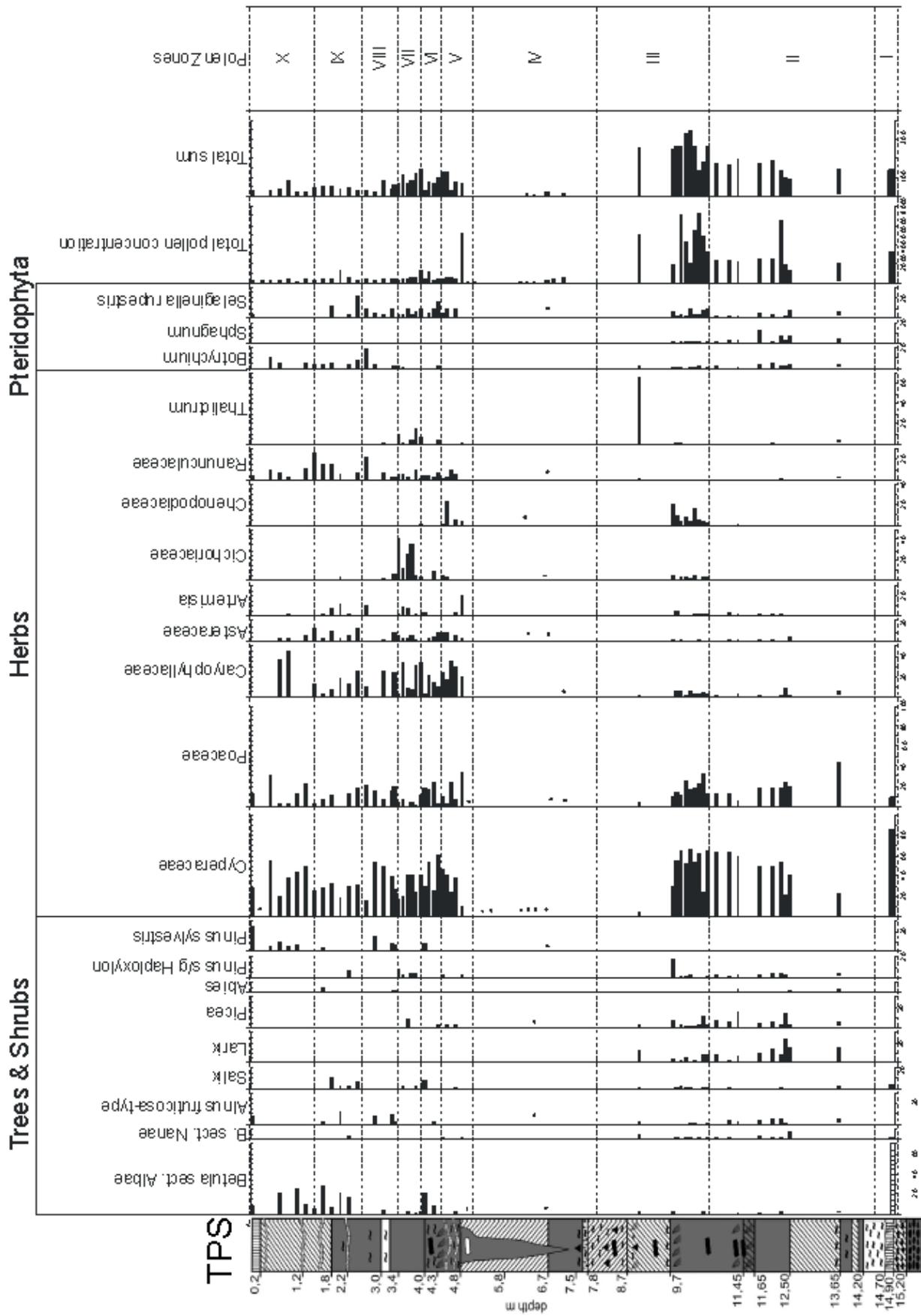
Fig. 4-3: Pollen percentage diagram of the TPS.

4. Discussion

4.1 Comparison of alkane and pollen results

Both presented methods – biomarkers analysis and palynology – have advantages but also limitations when deducing palaeobotanical information (Faegri and Iversen, 1989; Farrimond and Flanagan, 1996; Ficken et al., 1998): The biomarkers store the signal of the formerly standing vegetation and are available even when organic matter content (TOC) is low (due to increased SOM degradation like in Unit C, see Fig. 4-1C). On the other hand, the biomarker signal may be not representative for a whole region but only for a small study area, where the vegetation might have been influenced by local site peculiarities (e.g. water logging in thermokarst depressions, proximity to the cliff edge, etc.). Furthermore, a detailed differentiation of diverse vegetation types beyond tree versus grasses/herbs on the basis of the alkanes nC_{27}, nC_{29} and nC_{31} is challenging.

Although pollen principally have the potential for a high vegetational differentiation and provide a signal, which is not restricted to standing vegetation, the mid- and long-distance transport of pollen may also lead to misinterpretations: *Pinus sylvestris,* for example, should have come to Central Yakutia not until ~6 ka BP (e.g. Andreev et al., 1997 and references therein). But respective pollen are already present in PZ-VI to VIII, i.e. much earlier than ~9 ka BP according to the numeric dating results (Fig. 4-1A). Furthermore, one may be tempted to correlate pollen spectra of the TPS with other pollen records: The pollen spectra of PZ-I, for instance, is similar to those found for late Saalian interstadial deposits in Northern Yakutia dated around 200 ka (e.g. Andreev et al., 2004 and references therein). However, the validity of such correlations may be questioned as it is well known that both the interstadial and glacial vegetation exhibited significant regional variations in the East Siberian Arctic (e.g. Anderson and Lozhkin, 2001; Sher et al., 2005). Eventually, pollen spectra can be severely adulterated or even not be available at all if pollen were corroded due to oxygenating soil conditions: Almost no pollen were preserved in Unit C. *Larix* pollen, which should be rather abundant in Holocene deposits, were not detected in PZ-X. This discrepancy is even observed in pollen spectra under modern larch forests (Andreev et al., 2001a).

Despite of the above mentioned limitations, comparison between biomarker and pollen results for the TPS shows that both data sets are generally in good agreement. This firstly corroborates the validity of the proposed biomarker proxy ratio $(nC_{31} + nC_{29})/nC_{27}$. Secondly,

as vegetation depends on climate, palaeoclimatic conditions can be tentatively reconstructed using the BMA method.

4.2 Palaeoclimatic interpretation of the alkane and pollen results

The Units D and E are characterized by low n-alkane ratios indicating tree dominance (Fig. 4-1C). This is corroborated by rather abundant arboreal pollen contents (Fig. 4-3). Such spectra, especially when there are *Larix* pollen preserved, are generally supposed to reflect interglacial environmental conditions. Considering the available IRSL ages (Fig. 4-1A) and their uncertainties, the co-author of this paper (i) suggests to correlate PZ-1 with the Late Saalian Interstadial, which is described as a warm and wet period between 200 and 170 ka BP in Northern Yakutia (Andreev et al., 2004), (ii) assumes an erosive hiatus between PZ-I and PZ-II and (iii) correlates PZ-II with the Eemian (Kazantsevo) Interglacial. Note, that conversely, the multi-proxy palaeopedological approach conducted by the first author (Zech et al., submitted-b) rather indicates that Unit D reflects glacial conditions (Fig. 4-1D). This and the following discrepancies will be discussed later on.

Only few pollen are preserved in the middle part of the TPS. This corroborates the pedological finding that the Units C1 and C2 may be composed of reworked material. Concerning the biomarker proxy, it indicates a more or less gradual replacement of trees by grasses and herbs. According to the BMA method, such a vegetational change reflects a palaeoclimatic deterioration. It could correspond to the Early Weichselian, for which erosive environmental conditions were reported from Northern Yakutia (Schirrmeister et al., 2003; Schirrmeister et al., 2002).

Both biomarker and pollen results show that herbs contributed largely to the vegetation cover in the upper part of the TPS (Fig. 4-1C and 4-3). However, neither the minor fluctuations of the n-alkane proxy in the Units B2 and B3 nor the pollen seem to confirm the pedologically based interpretation of Unit B2 as interstadial (Fig. 4-1D). A marked reforestation, which is also corroborated by the biomarker proxy, is recorded only above 2.3 m depth (*Salix* and *Betula sect. Albae*) and could reflect the Boelling/Alleroed warming (Andreev et al., 2002b). Again, this is in disagreement with the palaeopedological findings that still indicate glacial conditions. *Pinus sylvestris* starts at 1.2 m depth, probably corresponding to the Boreal warming ~6 ka BP (Andreev et al., 1997). Climatic deterioration in the study area around 4 ka BP (Andreev et al., 2001a; Popp et al., 2006) is recorded by a marked increase of the biomarker proxy in the uppermost meter of the TPS (Fig. 4-1C) and an

increase of Cyperaceae, Poaceae, Caryophyllaceae and Ranunculaceae pollen at ~0.6 m depth (Fig. 4-3).

4.3 Palaeovegetation versus pedogenic/glacial history

As mentioned above, the palaeoclimatic implications derived from the reconstructed vegetation history often seem to be in disagreement with the climatic stratigraphy proposed by Zech at al. (submitted-b), which is based on a multi-proxy palaeopedological approach. A critical discussion of the BMA method and the palaeopedological findings, respectively, may help to understand these apparent discrepancies:

Concerning the BMA method, mean July temperature and the annual sum of days with mean-temperatures above 5°C were shown to have the most definite effect on Arctic vegetation (e.g. Andreev et al., 2003b; Kaplan, 2001). In the extreme continental climate prevailing in the study area, other climatic parameters than these two may, however, be more important for both glacial advances and pedogenetic conditions. Glacier mass balance, for instance, mainly depends on precipitation under (semi-)arid continental conditions. Actually, increasing aridity during the last glacial cycle has been suggested to be responsible for the progressively smaller Northern Siberian Weichselian Ice Sheets compared to the Scandinavian Ice Sheet (Svendsen et al., 2004). Aridity also explains the absence of extensive ice sheets in NE Siberia during the Late Quaternary and the absence of glaciers in the Verkhoyansk Mountains today. Weathering and soil development likewise depend on moisture availability. Note that water logging in the top soils during glacials might not only be caused by precipitation changes but also by a thinner active permafrost layer and by reduced evapotranspiration. Hence, even during glacial conditions, which were inferred e.g. for Unit D (see Fig. 4--1), forests could have prevailed at least in refugium areas (Brubaker et al., 2005) provided that the vegetation period was warm and long enough. Accordingly, correlating the vegetation history with the pedogenic/glacial history may be invalid for NE Siberia. The two methodological approaches may provide complementary rather than contradicting palaeo-environmental information.

An alternative explanation for the discrepancies could be that the pedological conditions in the TPS do not only reflect climate changes, but mainly temporally and spatially variable microhabitat conditions: For instance, one may speculate that Unit D did not develop during cold glacial conditions (as suggested by Zech et al., submitted-b), but instead during the warm Kazantsevo Interglacial in a depression affected by water logging (suggestion of the co-author based on the pollen data). Subsequently, Unit C3 accumulated during the end of the

Kazantsevo when lateral erosion of the approaching Tumara River had – by chance – caused better drainage of the study site. The Early Weichselian would be documented by the deposition of reworked material (Units C1 and C2), before thermokarst activity during the relatively warm Karginsky Interstadial may have created again a depression with water logging (beginning of Unit B, PZ-V) .

At the current state of knowledge, we cannot completely rule out the latter interpretation, i.e. varying geomorphological/pedological conditions due to river erosion and thermokarst activity, but the lateral extent of the stratigraphic units over several hundred meters suggests that weathering and soil development are climatically-driven regional processes, rather than local ones.

5. Conclusions

A biomarker proxy ratio, $(nC_{31} + nC_{29})/nC_{27}$, has been defined on the basis of own and previously published n-alkane patterns of plants. It provides an approximate measure for organic matter input from grasses/herbs and trees/shrubs, respectively. Comparison of alkane and pollen data obtained for the TPS shows that both datasets are generally in good agreement, thus validating the proposed biomarker proxy ratio. The vegetation history recorded in the TPS can be reconstructed as follows: The lower half of the TPS developed under tree/shrub vegetation, whereas grass/herb-derived pollen and alkanes predominate in the upper half of the TPS. Reforestation started again at ~2.3 m depth. These findings - when interpreted qualitatively according to the BMA method - seem to be in disagreement with the previously proposed climatic stratigraphy for the TPS based on a multi-proxy pedological approach (Zech et al., submitted-b). However, the pedological and palaeobotany results could be reconciled when considering that different climatic parameters may exert dominant control over vegetation on the one hand and weathering/soil development on the other hand: The palaeovegetation in the strongly continental climate of NE Siberia may have depended mainly on the length of the growing season and on the summer temperatures, whereas soil moisture conditions (aeration vs. water logging) may have been more important for pedogenesis.

Future work should focus on the establishment of a better chronology for the TPS. Especially, more luminescence dating would be highly desirable.

Acknowledgements

References

Alekseev, M.N., 1997. Palaeogeography and geochronology in the Russian Eastern Arctic during the second half of the Quaternary. Quaternary International 41/42, 11-15.

Anderson, P.M., Lozhkin, A.V., 2001. The Stage 3 interstadial complex (Karginskii/middle Wisconsinan interval) of Beringia: variations in paleoenvironments and implications for paleoclimatic interpretations. Quaternary Science Reviews 20, 93-125.

Andreev, A.A. et al., 2004. Late Saalian and Eemian palaeoenvironmental history of the Bol'shoy Lyakhovsky Island (Laptev Sea region, Arctic Siberia). Boreas 33, 319-348.

Andreev, A.A., Klimanov, V.A., 2000. Quantitative Holocene climatic reconstruction from Arctic Russia. Journal of Paleolimnology 24, 81-91.

Andreev, A.A., Klimanov, V.A., Sulerzhitsky, L.D., 1997. Younger Dryas pollen records from central and southern Yakutia. Quaternary International 41/42, 111-117.

Andreev, A.A., Klimanov, V.A., Sulerzhitsky, L.D., 2001a. Vegetation and climate history of the Yana River lowland, Russia, during the last 6400 yr. Quaternary Science Reviews 20, 259-266.

Andreev, A.A. et al., 2001b. Late Pleistocene Interstadial Environment on Faddeyevskiy Island, East-Siberian Sea, Russia. Arctic, Antarctic and Alpine Research 30, 28-35.

Andreev, A.A. et al., 2002a. Palaeoenvironmental changes in northeastern Siberia during the Upper Quaternary - evidence from pollen records of the Bykovsky Peninsula. Polarforschung 70, 13-25.

Andreev, A.A. et al., 2002b. Late Pleistocene and Holocene Vegetation and Climate on the Taymyr Lowland, Northern Siberia. Quaternary Research 57, 138-150.

Andreev, A.A., Tarasov, P.E., Klimanov, V.A., Hubberten, H.-W., 2003a. Russian Arctic lakes as climatic archives: pollen-based reconstructions of the Late Quaternary climate. Terra Nostra 6, 17-21.

Andreev, A.A. et al., 2003b. Vegetation and climate changes on the northern Taymyr, Russia during the Upper Pleistocene and Holocene reconstructed from pollen records. Boreas 32, 484-505.

Berglund, B.E., Ralska-Jasiewiczowa, M., 1986. Pollen analysis and pollen diagrams. In: Berglund, B. (Ed.), Handbook of Holocene Palaeoecology and Palaeohydrology. Interscience, New York, pp. 455-484.

Bourbonniere, R.A. et al., 1997. Biogeochemical marker profiles in cores of dated sediments from large north American lakes. In: Eganhouse, R.P. (Ed.), Molecular Markers in Environmental Geochemistry. Acs Symposium Series, Washington D.C., pp. 133-150.

Boutton, T.W., 1996. Stable Carbon Isotope Ratios of Soil Organic Matter and Their Use as Indicators of Vegetation and Climate Change. In: Yamasaki, S. (Ed.), Mass Spectrometry of Soils. Marcel Dekker, Inc., New York, pp. 47-82.

Brubaker, L.B., Anderson, P.M., Edwards, M.E., Lozhkin, A.V., 2005. Beringia as a glacial refugium for boreal trees and shrubs: new perspectives from mapped pollen data. Journal of Biogeography 32, 833-848.

Cranwell, P.A., 1973. Chain-length distribution of n-alkanes from lake sediments in relation to post-glacial environmental change. Freshwater Biology 3, 259-265.

Cranwell, P.A., 1981. Diagenesis of free and bound lipids in a terrestrial detritus deposited in a lacustrine sediment. Organic Geochemistry 3, 79-89.

Faegri, K., Iversen, J., 1989. Textbook of Pollen Analysis. Wiley, Chichester.

Farrimond, P., Flanagan, R.L., 1996. Lipid stratigraphy of a Flandrian peat bed (Northumberland, UK): comparison with the pollen record. The Holocene 6 (1), 69-74.

Ficken, K.J., Barber, K.E., Eglinton, G., 1998. Lipid biomarker, $\delta^{13}C$ and plant macrofossil stratigraphy of a Scottish montane peat bog over the last two millennia. Organic Geochemistry 28 (3/4), 217-237.

Ficken, K.J., Li, B., Swain, D.L., Eglinton, G., 2000. An n-alkane proxy for the sedimentary input of submerged/floating freshwater aquatic macrophytes. Organic Geochemistry 31, 745-749.

Grinenko, V.S., Kamaletdinov, V.A., 1993. Geological map of Yakutia (in Russian). VSEGEI, St. Petersburg.

Guiot, J., 1990. Methodology of the last climatic cycle reconstruction in France from pollen data. Palaeogeography, Palaeoclimatology, Palaeoecology 80, 49-69.

Ilyashuk, B.P., Andreev, A.A., Bobrov, A.A., Tumskoy, V.E., Ilyashuk, E.A., 2006. Interglacial history of a palaeo-lake and regional environment: a multi-proxy study of a permafrost deposit from Bol`shoy Lyakhovsky Island, Arctic Siberia. Journal of Paleolimnology 35, 855-872.

Kaplan, J.O., 2001. Geophysical Applications of Vegetation Modeling. Ph.D. dissertation Thesis, University Lund. 113 pp.

Kind, N.V., 1975. Glaciations in the Verkhoyansk Mountains and their place in the radiocarbon geochronology of the Siberian Late Anthropogene. Biuletyn Peryglacjalny 2, 41-54.

Klimanov, V.A., 1984. Paleoclimatic reconstruction based on the information-statistical method. In: Barnosky, C.W. (Ed.), Late Quaternary Environments of the Soviet Union. University of Minnesota Press, Minneapolis, pp. 297-303.

Klimanov, V.A., Andreev, A.A., 1992. Correlation analysis of surface pollen spectra from Yakutia. Izvestiya Akademii Nauk USSR, Seria Geograficheskaya 5, 82-93 (in Russian).

Kolattukudy, P.E., 1976. Biochemistry of plant waxes. In: Kolattukudy (ed.), Chemistry and Biochemistry of Natural Waxes, Amsterdam: Elsevier, 290-349.

Kolpakov, V.V., 1979. Glacial and periglacial topography of the Verkhoyansk glacial area and new radiocarbon dates. In: Muzins, A.I. (Ed.), Regionalnaya Geomorpholigiya Rayonov Novogo Osvoeniya, Moscow, pp. 83-98 (in Russian).

Meyers, P.A., Ishiwatari, R., 1993. Lacustrine organic geochemistry - An overview of indicators of organic matter sources and diagenesis in lake sediments. Organic Geochemistry 20, 867-900.

Müller, M.J., 1980. Handbuch ausgewählter Klimastationen der Erde. Forschungsstelle Bodenerosion. Universität Trier, Mertesdorf.

Nott, C.J. et al., 2000. n-Alkane distribution in ombrotrophic mires as indicators of vegetation change related to climatic variation. Organic Geochemistry 31, 231-235.

Popp, S. et al., 2006. Palaeoclimate Signals as Inferred from Stable-isotope Composition of Ground Ice in the Verkhoyansk Foreland, Central Yakutia. Permafrost and Periglacial Processes 17, 119-132.

Schirrmeister, L. et al., 2003. Late Quaternary history of the accumulation plain north of the Chekanovsky Ridge (North East Yakutia). Polar Geography 27 (4), 277-319.

Schirrmeister, L. et al., 2002. Paleoenvironmental and paleoclimatic records from permafrost deposits in the Arctic region of Northern Siberia. Quaternary International 89, 97-118.

Schwark, L., Zink, K., Lechtenbeck, J., 2002. Reconstruction of postglacial to early Holocene vegetation history in terrestrial Central Europe via cuticular lipid biomarkers and pollen records from lake sediments. Geology 30 (5), 463-466.

Sher, A.V., Kuzmina, S.A., Kuznetsova, T.V., Sulerzhitsky, L.D., 2005. New insights into the Weichselian environment and climate of the East Siberian Arctic, derived from fossil insects, plants, and mammals. Quaternary Science Reviews 24, 533-569.

Stauch, G., Lehmkuhl, F., Frechen, M., 2006. Luminescence chronology from the Verkhoyansk Mountains (North-Eastern Siberia). quaternary Geochronology in press.

Svendsen, J.I. et al., 2004. Late Quaternary ice sheet history of northern Eurasia. Quaternary Science Reviews 23 (11-13), 1229-1271.

Tarasov, P.E. et al., 1998. Present-day and mid-Holocene biomes reconstructed from pollen and plant macrofossil data from the former Soviet Union and Mongolia. Journal of Biogeography 25 (6), 1029-1053.

Zech, M., 2006. Evidence for Late Pleistocene climate changes from buried soils on the southern slopes of Mt. Kilimanjaro, Tanzania. Palaeogeography, Palaeoclimatology, Palaeoecology accepted.

Zech, M., Zech, R., de Morrás, H., Moretti, L., Glaser, B., submitted-a. Late Quaternary environmental changes in Misiones, subtropical NE Argentina, deduced from multi-proxy geochemical analyses in a palaeosol-sediment sequence. Quaternary International.

Zech, M. et al., submitted-b. Multi-proxy analytical characterisation and palaeoclimatic interpretation of the Tumara Palaeosol Sequence, NE Siberia. Quaternary Research.

Zhang, Z. et al., 2004. A hydrocarbon biomarker record for the last 40 kyr of plant input to Lake Heqing, southwestern China. Organic Geochemistry 35, 595-613.

Study 5:

Late Quaternary environmental changes in Misiones, subtropical NE Argentina, deduced from multi-proxy geochemical analyses in a palaeosol-sediment sequence

Michael Zech[1]*, Roland Zech[2], Bruno Glaser[1], Héctor de Morrás[3] and Lucas Moretti[3]

[1] Institute of Soil Science and Soil Geography, University of Bayreuth, D-95440 Bayreuth, Germany

[2] Institute of Geography, University of Bern, 3012 Bern, Switzerland

[3] INTA-CIRN, Instituto de Suelos, 1712 Castelar, Buenos Aires, Argentina

* Corresponding author: Michael Zech, Phone: +49 (0)921 552247; Fax: +49 (0)921 552246; Email: michael_zech@gmx.de

Abstract

A 4.5 m long sediment core from a small basin in the Province of Misiones, NE Argentina, was analyzed in a multi-proxy geochemical approach (major and minor elemental composition, TOC, N, HI, OI, $\delta^{13}C_{TOC}$ and n-alkanes) in order to contribute to the reconstruction of the Late Quaternary environmental and climate history of subtropical South America. The results of the elemental analyses and radiocarbon dating indicate different sediment provenances for Unit A – the Holocene, Unit B – the Late Glacial and the Last Glacial Maximum (LGM), and Unit C – the 'Inca Huasi' wet phase (before ~40 ka BP). A sedimentary hiatus after ~40 ka BP is interpreted as a pronounced pre-LGM dry phase with landscape erosion/deflation. Multi-proxy geochemical characterization of the soil organic matter (SOM) shows that especially (i) the natural abundance of ^{13}C of bulk SOM ($\delta^{13}C_{TOC}$) (ii) the alkane ratio nC_{31}/nC_{27} and (iii) lacustrine-derived short- and mid-chain alkanes are valuable proxies for the reconstruction of the palaeoenvironment. A transition from C3 tree dominance to C4 grass dominance is recorded at the end of the 'Inca Huasi' wet phase. In Unit B, the ratio nC_{31}/nC_{27} documents forest expansion at the beginning of a lateglacial wet phase. More positive $\delta^{13}C_{TOC}$ values in Unit A reflect the increasing contribution of C4 grasses and/or CAM plants to the SOM during the Holocene and a human impact on the formation of this unit may be possible. Our results are in good agreement with other tropical/subtropical palaeoenvironmental records and highlight the importance and temporal variability of the palaeo-South American Summer Monsoon (SASM).

1. Introduction

Late Quaternary environmental and climate changes in and around tropical and subtropical South America can be reconstructed at high resolution using marine records, lacustrine sediments, speleothems and ice cores (e.g. Behling et al., 2000; Cruz et al., 2005; Fritz et al., 2004; Salgado-Labouriau, 1997; Thompson et al., 2005). Although not at the same temporal resolution, colluvial deposits and palaeosol-loess sequences constitute important terrestrial counterparts (e.g. Kemp et al., 2006; Kröhling and Iriondo, 1999; Zárate, 2003). In order to derive reliable information about the palaeoenvironmental conditions during sedimentation and to assess post-depositional changes, various geochemical analytical methods are already available and constantly being improved.

During the last few decades the application of stable carbon isotope techniques on soil organic matter ($\delta^{13}C_{TOC}$) in palaeosols contributed significantly to a better understanding of the palaeoenvironment, particularly the reconstruction of the vegetation history. The stable carbon isotopes allow differentiating between vegetation types, which followed the C3 or the C4 photosynthetic pathway (Aucour et al., 1999; Freitas et al., 2001; Liu et al., 2005; Wang et al., 2000): More positive $\delta^{13}C$ values (approximately −14‰) are characteristic for C4 savannah grasses and more negative $\delta^{13}C$ values (approximately −28‰) are found in trees and C3 grasses. Hence, changes in the carbon isotopic composition in soil or peat profiles or loess-palaeosol sequences can reflect expansion and retreat of forests versus savannah grasslands.

Further information about the palaeovegetation can be obtained from certain compounds that serve as 'biomarkers' (Glaser and Zech, 2005; Huang et al., 1996; Lichtfouse, 1998; Street-Perrott et al., 2004). Such 'biomarkers' ideally originate from certain (groups of) organisms (e.g. higher plants, lacustrine organism, microorganisms, etc.) and are exceptionally resistant to degradation. Schwark et al. (2002) and Zech (2006), for instance, used plant leaf wax-derived long-chain n-alkanes (nC_{27}, nC_{29} and nC_{31}) in lacustrine sediments and palaeosols, respectively, to reconstruct vegetation histories.

In this study, we present results from multi-proxy geochemical analyses that were carried out on palaeosol-sediment samples obtained from a 4.5 m deep core from Misiones, NE Argentina (Fig. 5-1). We specifically aim at:

- the establishment of a chronostratigraphy, using the major and minor elemental composition combined with radiocarbon dating,

- the characterization of the soil organic matter (SOM), using standard geochemical parameters like total organic carbon content (TOC), TOC/N ratio, $\delta^{13}C_{TOC}$ and the hydrogen and oxygen index (HI and OI, respectively), and

- the reconstruction of the vegetation history, using $\delta^{13}C_{TOC}$ and n-alkanes as biomarkers.

Based on these results and in the context of other palaeoenvironmental findings, we will then try to draw a conclusive picture of the Late Quaternary environmental and climate changes in Misiones, NW Argentina.

2. Regional setting and modern climate

The Province of Misiones in NE Argentina (25 – 28°S, 53 – 56°W , 100 – 800 m a.s.l.) lies between the Rivers Paraná and Uruguay and comprises an area of about 30,000 km^2 (Margalot, 1985) (Fig. 5-1). Its geological basement is formed by basalts of the Serra Geral Formation which flooded the Paraná Basin during the lower Cretaceous (Zeil, 1986). According to Iriondo and Kröhling (2004), loess of Late Pleistocene-Holocene age (the so-called Oberá Formation) mantles the Province of Misiones and neighboring areas of Brazil and Paraguay with a typical thickness between 3 and 8 m. On the contrary, Morrás et al. (2005) suggested that in situ weathering rather than eolian transport is the source for the soil parent material. The existence of this 'tropical loess' is still discussed controversially (Iriondo et al., this issue; Morrás et al., this issue).

The original vegetation cover in Misiones mainly consisted of mesophytic subtropical forests with large proportions of evergreen species (Hueck and Seibert, 1972). Current land use converted large areas into commercial plantations with non-native *Pinus* (190,000 hectares) and *Eucalyptus* (15,000 hectares). The native timber tree, *Araucaria angustifolia (Bert) O. Ktze* covers 20,000 hectares (Fernández et al., 1999).

The South American climate is characterized by three dominant circulation regimes (Fig. 5-1): (i) The westerlies, which provide Pacific moisture to the southwest (Patagonia), (ii)

the SE trades, which advect moisture to regions near the Atlantic coast (NE Argentina, Uruguay and SE-Brazil), and (iii) the South American Summer Monsoon (SASM) and the South Atlantic Convergence Zone (SACZ), respectively, which result in an austral summer precipitation maximum in tropical/subtropical South America (Cerveny, 1998; Gan et al., 2004; Vera et al., 2002; Zhou and Lau, 1998). Misiones receives the highest rainfalls of Argentina except for the southern cordillera (mean annual precipitation ~1700 mm). This is due to the combined influence of high summer and winter precipitation as illustrated in Fig. 5-1 and manifests in a double rainy season (Prohaska, 1976).
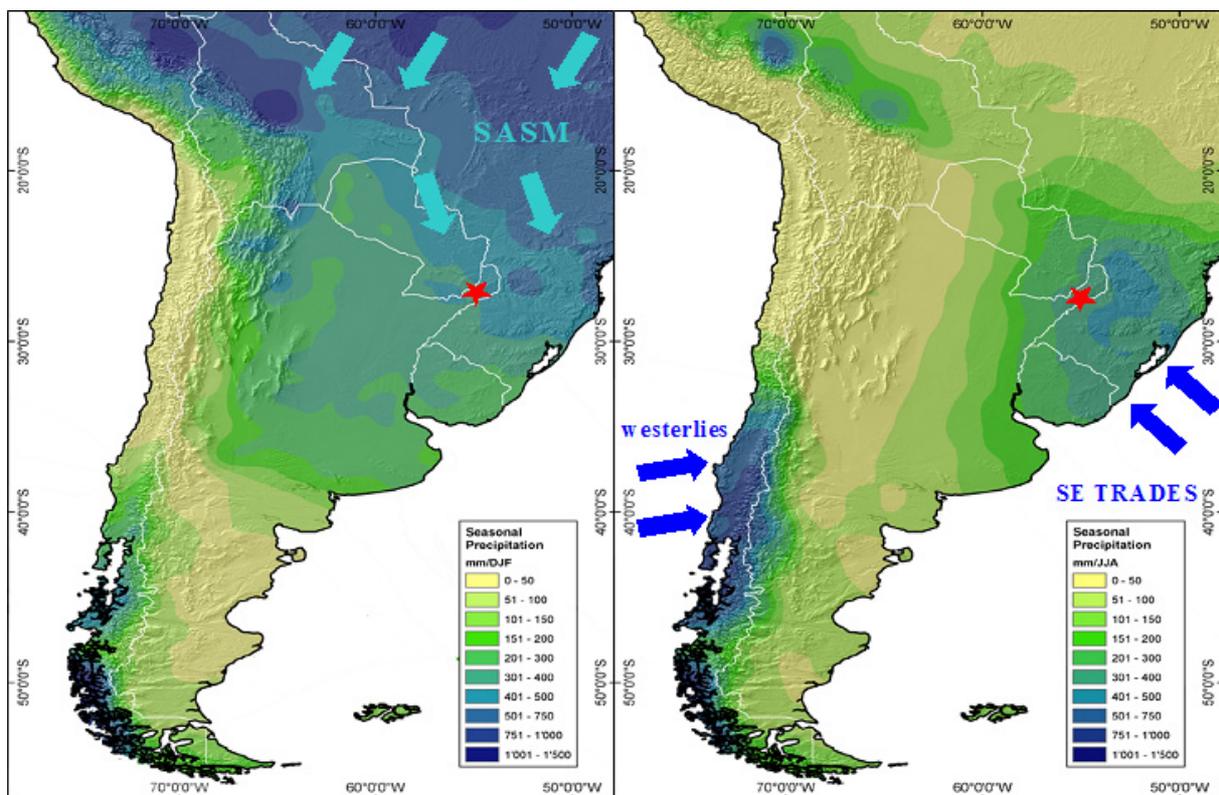
Fig. 5-1: Location of the Province of Misiones in NE-Argentina and seasonal atmospheric circulation patterns providing moisture to the study area (★). Left: rainfall during austral summer (DJF, December January February), SASM = South American Summer Monsoon. Right: rainfall during austral winter (JJA = July June August) (courtesy of J.-H. May)

3. Materials and Methods

In September 2004, a 4.5 m long sediment core ('Arg. D4') was taken with a piston corer from a weakly flooded small basin located northeast of the city Oberá (27°23'35''S; 55°31'52''W; 330 m a.s.l., see Fig. 5-1). Before sub-sampling the core at 5 cm intervals for geochemical analysis, we documented color, grain size and soil morphological features in the

field (see also Fig. 5-2 a): The upper 60 cm were characterized by black, intensively rooted, silty fine sand. Below, an abrupt change to very dense, light gray, mottled clay could be observed. At about 1.4 m depth the compact sediments became darker again with embedded gray, mottles between 1.7 and 2.5 m depth. A light gray silty layer from 2.5 - 2.9 m depth with an intercalated thin humus band separated these deposits from underlying dark sediments, which continued down to 3.2 m depth. From 3.2 - 3.6 m depth the mottled and now coarser grained material became paler again. Below, we found very dense light gray sediments with hydromorphic features (from 3.6 to 4.0 m depth) covering the reddish brown and probably saprolytic parent material at 4.0 + m depth.

Geochemical analyses were done on air-dried, homogenized sample aliquots. Small amounts of carbonate (<1%) were present from 30 – 100 cm depth and in the light gray band between 2.5 and 2.9 m depth. **Major and minor elemental compositions** were determined using a Philips 2404 X-ray fluorescence spectrometer. The weathering indices A and B were calculated according to Kronberg and Nesbitt (1981) following the equations:

$$\text{Weathering index A} = \frac{SiO_2 + Na_2O + K_2O + CaO}{Al_2O_3 + SiO_2 + Na_2O + K_2O + CaO}$$

$$\text{Weathering index B} = \frac{Na_2O + K_2O + CaO}{Al_2O_3 + Na_2O + K_2O + CaO}$$

Total organic carbon (TOC) and **total nitrogen (N)** were measured using dry combustion of a finely ground, homogeneous and decalcified 50 mg sub-sample followed by thermal conductivity detection on a Vario EL elemental analyzer (Elementar, Hanau, Germany). The detection limits of our machine were calculated by measuring blanks with increasing net weights of wolfram oxide in tin capsules (~0.0002% for C and ~0.007% for N).

Further information about the elemental composition of the OM was obtained by Rock-Eval pyrolysis ($\rightarrow$ **Hydrogen and Oxygen Index, HI and OI**). The analytical procedure comprises progressive heating of sediment samples and measurements of the amounts of hydrocarbons that escape at different temperatures. This method was initially developed to measure both the free hydrocarbon content and the hydrocarbons released by thermal conversion of kerogen in rock and sediment samples (Espitalie et al., 1985). The HI estimates the amount of hydrogen contained in the sedimentary OM (expressed as mg

hydrocarbons $\times$ g^{-1} TOC), whereas the OI represents the amount of oxygen in mg $CO_2 \times$ g^{-1} TOC. These parameters hence roughly correspond to the H/C and O/C ratios of OM.

Several authors used the Rock-Eval pyrolysis to characterize lake sediments and interpreted the HI and OI in terms of origin of the OM and/or degree of OM oxidation (Ariztegui et al., 2001; Filippi and Talbot, 2005; Lüniger and Schwark, 2002). Recently, Disnar et al. (2003) applied this technique to a variety of soil profiles and found the parameters HI and OI to be diagnostic for SOM alteration.

The natural abundance of ^{13}C of bulk SOM (**δ^{13}C$_{TOC}$**) was measured using dry combustion of 40 mg decalcified sub-samples with a Carlo Erba NC 2500 elemental analyzer coupled to a Delta^{plus} continuous flow isotope ratio mass spectrometer (IRMS) via a Conflow II interface (Thermo Finnigan MAT, Bremen, Germany). Sucrose (CH-6, IAEA, Vienna, Austria) and $CaCO_3$ (NBS 19, Gaithersburg, USA) were used as calibration standards. Natural abundances of stable carbon isotopes are expressed in the usual δ-scale in parts per thousand according to the equation:

$$\delta_{sample}\ (‰) = \left(\frac{R_{sample} - R_{standard}}{R_{standard}} \right)\ \times\ 1000,$$

where R_{sample} and $R_{standard}$ are the ^{13}C/^{12}C abundance ratios of a sample or a standard, respectively. Precision was determined by measuring known standards in replication (~0,15‰ for δ^{13}C and 0.25‰ for δ^{15}N).

For the extraction of **n-alkanes**, an accelerated solvent extractor (Dionex ASE 200) was used. Free lipids were extracted with methanol/toluene (7/3) at 9×10^6 Pa and a temperature of 120° C, followed by n-alkane separation on columns with deactivated (5%) aluminum oxide (2 g) above deactivated (5%) silica gel (2 g) and 45 ml hexane/toluene (85/15) as elution solvent (Bourbonniere et al., 1997). For quantification, an HP 6890 GC equipped with a flame ionization detector (FID) and deuterated n-alkanes (d$_{42}$-n-C$_{20}$ and d$_{50}$-n-C$_{24}$) as internal standards were used.

Long-chain n-alkanes (nC$_{25}$-nC$_{33}$) with a pronounced odd-over-even predominance of carbon atoms are incorporated in cuticular plant leaf-waxes (Collister et al., 1994; Kolattukudy, 1976). As they are assumed to be relatively resistant to degradation (Cranwell, 1981; Meyers and Ishiwatari, 1993) they are used as biomarkers in palaeoenvironmental

studies (e.g. Bourbonniere et al., 1997; Ficken et al., 1998; Glaser and Zech, 2005). We will use the n-alkane pattern in our palaeosol-sediment record in order to distinguish between OM derived from grasses versus OM derived from trees. Several studies have shown that nC_{31} dominates in most grasses/herbs, whereas nC_{27} dominates in most trees/shrubs and used this difference for the reconstruction of the palaeovegetation (Cranwell, 1973; Nott et al., 2000; Schwark et al., 2002). Furthermore, it is well known that the short-chain alkanes nC_{17}, nC_{18} and nC_{19} in lake sediments are mainly from algal origin (Bourbonniere et al., 1997; Meyers and Ishiwatari, 1993) and recently Ficken at al. (2000) and Zhang et al. (2004) reported that the mid-chain alkanes nC_{23} and nC_{25} in lake sediments originate mainly from submerged plants.

Fifteen AMS **radiocarbon ages** were obtained for acid and/or alkali insoluble fractions extracted from 8 samples of the core Arg. D4 and two samples deriving from other sediment cores taken in the study area (Arg. 03/P2 and Arg. 03/D2). All radiocarbon ages were corrected for the $^{13}C/^{12}C$ ratio and additionally calibrated with quickcal2005 vers.1.4 (http://www.calpal-online.de). Both uncalibrated and calibrated ages are given in Table 5-1. For reasons of simplicity we only refer to calibrated ages in the text and in Fig. 5-2 and 5-3.

4. Results and Discussion

In the following, we first present the results of the X-ray fluorescence analyses and the radiocarbon ages aiming at the establishment of a chronostratigraphy for our palaeosol-sediment record. Then, we characterize the SOM based on the parameters TOC, TOC/N, $\delta^{13}C_{TOC}$, HI and OI. Subsequently, the n-alkane biomarker data are presented and used to reconstruct the vegetation history.

4.1 Chronostratigraphy

The depth functions of most major and minor elements show distinct shifts at 60 and 290 cm depth, respectively. This is illustrated exemplarily in Fig. 5-2A, where the ratio of the weathering indices A and B (according to Kronberg and Nesbitt (1981)) is plotted versus depth. These results suggest that the sedimentary material is not homogeneous but stratified. This can be corroborated by plotting SiO_2 versus $Na_2O + K_2O$ (Fig. 5-2B) and SiO_2 versus Al_2O_3 (Fig. 5-2C). Such cross-plot diagrams are frequently used to evaluate the transformation of feldspars to clay minerals (Garrels and Mackenzie, 1971; McLennan, 1993)

(A)

(B)
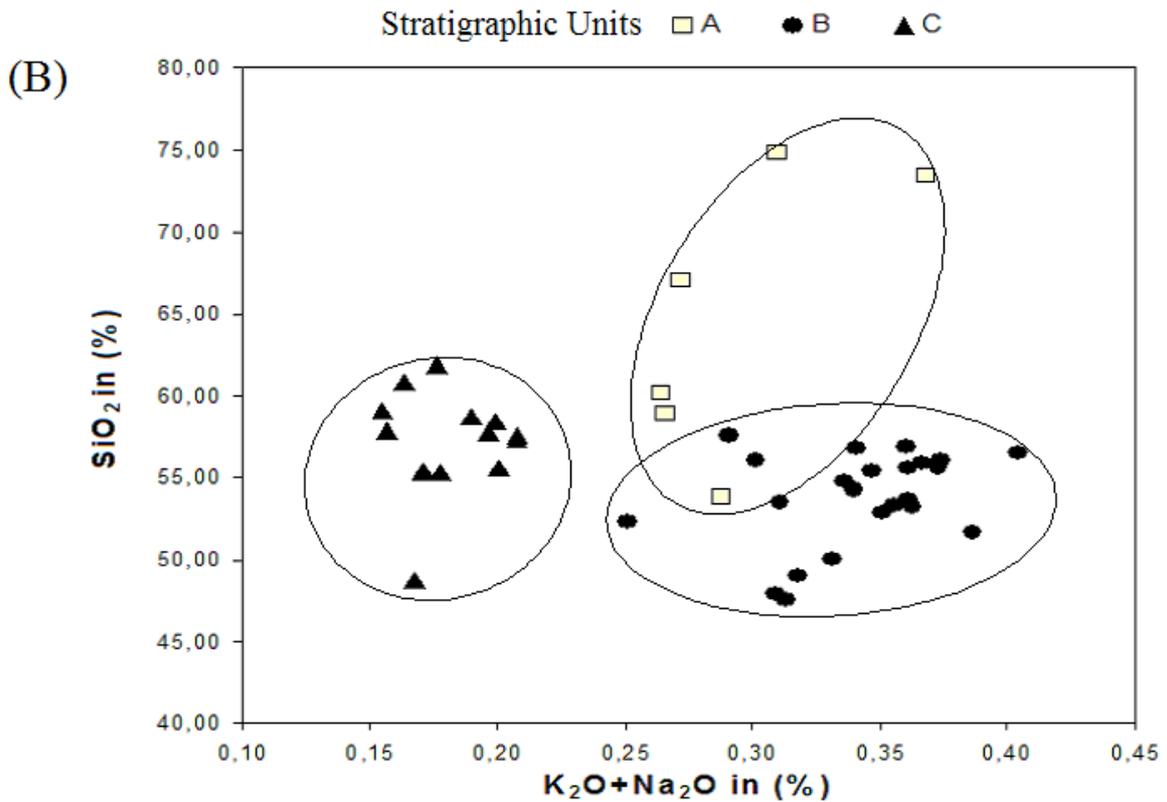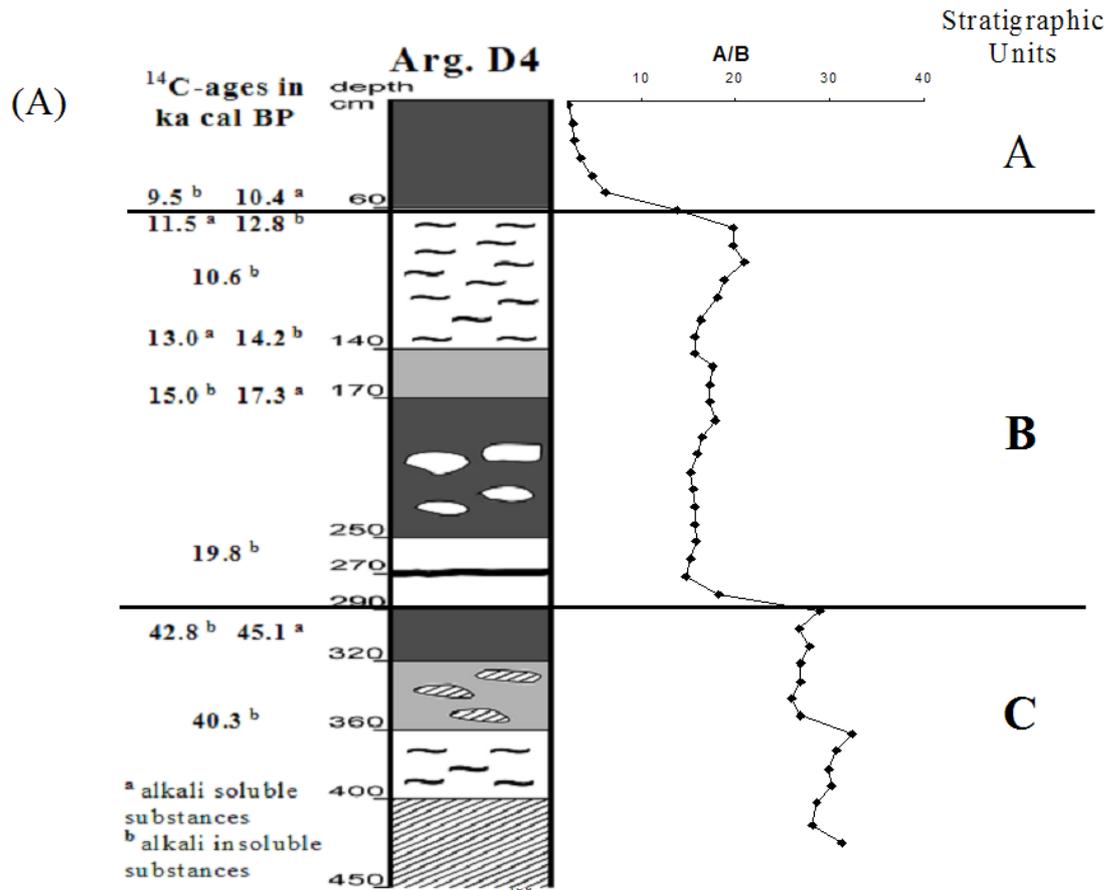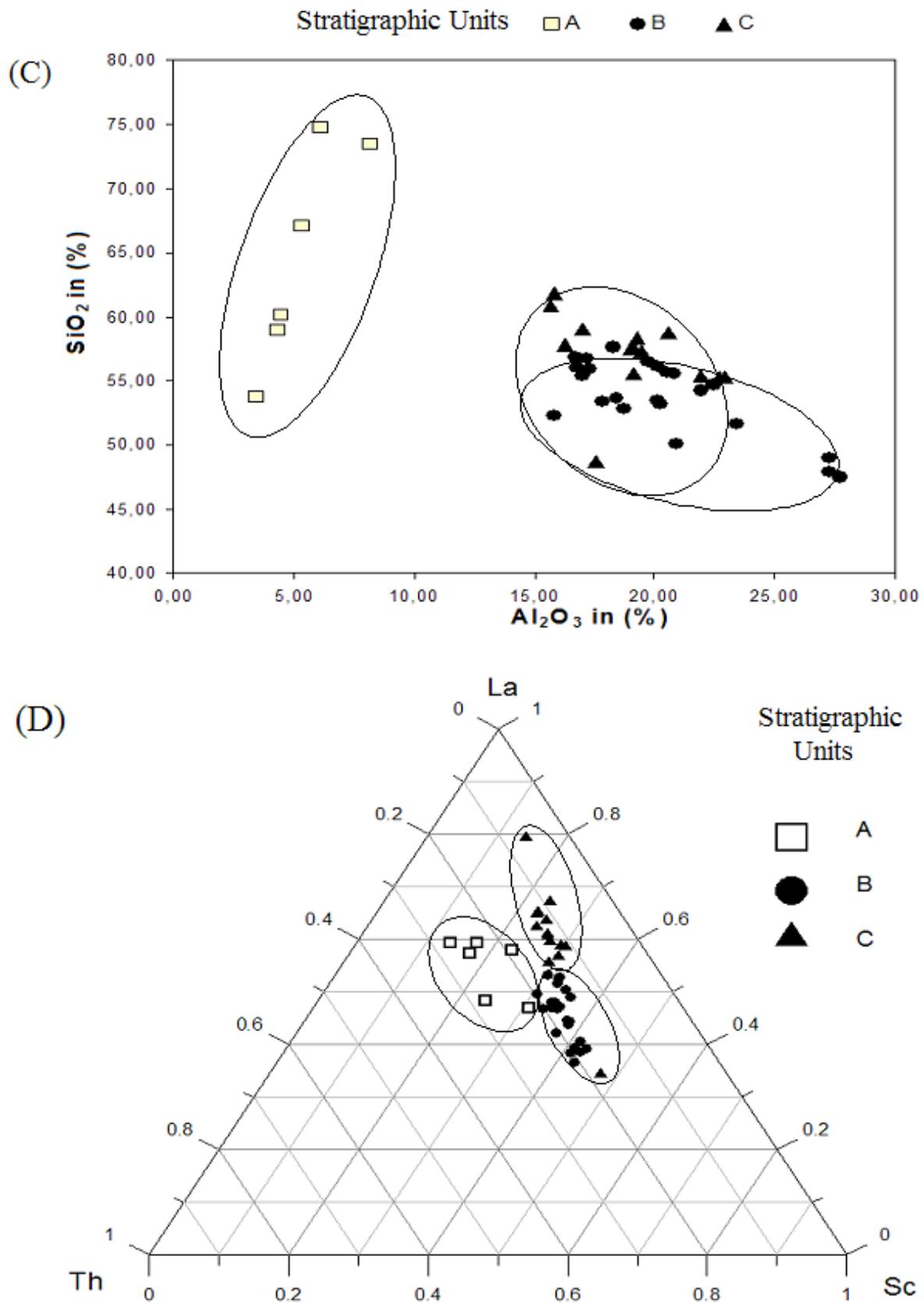
Fig. 5-2: (A) Schematic stratigraphy and numeric dating results for the sediment core Arg. D4, depth function for the ratio of the weathering indices A and B, and subdivision of the core into the stratigraphic units A, B and C. (B) Cross-plot diagrams for SiO_2 versus $Na_2O + K_2O$, and (C) SiO_2 versus Al_2O_3. (D) Ternary diagram for the immobile trace elements Sc, Th and La.

and to depict compositional variability of sitly material (Gallet et al., 1998; Muhs et al., 2004). Similar diagrams can be plotted for immobile trace elements, which also allow identification of different sources of sediments (Muhs et al., this issue). In Fig. 5-2D, for example, a ternary diagram for the elements Sc, Th and La is shown. All these diagrams depict well discernable clusters for the samples from 0 – 60 cm, 60 – 290 cm and 290 – 425 cm depth. These findings suggest distinguishing at least three stratigraphic units (A, B and C, see Fig. 5-2), which indicates that the core comprises several periods of sedimentation.

Erosive discordances in eolian sediments in northern Argentina have previously been described and seem to be common features (Iriondo and Kröhling, 2004; Kemp et al., 2006; Zárate, 2003). We therefore interpret the abrupt shifts in the elemental composition as erosive events – possibly by means of deflation – which may have truncated the palaeosol-sediment sequence under study before sedimentation proceeded.

To provide a chronological framework for the palaeoenvironmental events recorded in our sediment core, eight soil samples were dated by radiocarbon analyses. The ^{14}C-ages obtained for alkali soluble and/or alkali insoluble substances are illustrated in Fig. 5-2 and 5-3 and listed in Table 5-1. Two samples from the lowermost Unit C yielded calibrated ages between 40.3 and 45.1 ka cal BP, five samples from Unit B gave ^{14}C-ages between 10.6 and 19.8 ka cal BP. Humic acids at the bottom of Unit A were 10.4 ka old, whereas alkali insoluble substances from the same sample yielded an age of 9.5 ka cal BP. Considering the uncertainties of radiocarbon dating in sediments (Geyh and Schleicher, 1991), all ages are more

Overall, the numeric dating results (i) confirm the distinction of at least three stratigraphic units and (ii) allow the establishment of a tentative chronostratigraphy: the sediments of Unit C were deposited at/before ~40 ka BP, i.e. likely during Marine Isotope Stage (MIS) 3, Unit B represents the Last Glacial Maximum (LGM) and the Late Glacial, and Unit A started to developed during the Early Holocene. or less consistent despite of two minor age inversions (10.6 and 40.3 ka cal BP).

4.2 Characterization of the organic matter

The depth functions of TOC, TOC/N, δ^{13}C$_{TOC}$, HI, OI and the alkane ratio nC$_{31}$/nC$_{27}$ are shown in Fig. 5-3. **TOC** decreases sharply below 30 cm depth in Unit A. High TOC values around 15% in the upper decimeters indicate considerable recent biomass production.

Table 5-1: Radiocarbon dates (KIA: Leibniz Laboratory, University of Kiel, Germany; Poz: Poznan radiocarbon Laboratory, Poland; Erl: Physical Department of the University of Erlangen, Germany). Calibration was outlined with quickcal2005 vers.1.4 (http://www.calpal-online.de).

Sample	Lab.number	Depth (cm)	Material	uncalibrated ^{14}C (a BP)	calibrated ^{14}C (a cal BP)	Chronostratigraphic Interpretation
Arg.04/D4/6B	KIA30161	57.5	HA [a]	9255±40	10422±78	**Early Holocene**
Arg.04/D4/6B	KIA30161	57.5	H [b]	8470±45	9495±26	**Early Holocene**
Arg.04/D4/8A	KIA26094	72.5	HA	10025±60	11548±169	**Late Glacial**
Arg.04/D4/8A	KIA26094	72.5	H	10890±50	12847±81	**Late Glacial**
Arg.04/D4/10A	KIA26095	92.5	H	9384±45	10620±53	**Late Glacial**
Arg.04/D4/14	KIA26096	135	HA	11069±193	13006±187	**Late Glacial**
Arg.04/D4/14	KIA26096	135	H	12149±50	14190±237	**Late Glacial**
Arg.04/D4/18A	KIA26097	172.5	H	12654±55	15022±294	**Late Glacial**
Arg.04/D4/18A	KIA26097	172.5	HA	13908±105	17302±125	**LGM/Late Glacial**
Arg.04/D4/26B	Poz-12818	257.5	H	16490±90	19809±292	**LGM**
Arg.04/D4/31B	Poz-12925	307.5	H	37900±900	42817±609	**MIS 3**
Arg.04/D4/31B	Poz-15662	307.5	HA	41400±1300	45134±1271	**MIS 3**
Arg.04/D4/36B	Poz-12926	357.5	H	34500±600	40332±853	**MIS 3**
Arg.03/P2	Erl-6147	240	H	14368±102	17700±235	**LGM/Late Glacial**
Arg.03/D2	Erl-6148	140	H	30460±284	35682±307	**MIS 3**

[a] HA = alkali soluble substances (humic acids), [b] H = alkali insoluble substances (humines)

In the Units B and C the values range from 0.21 - 5.1% with TOC being higher than 2% from 1.5 - 2.5 m depth. Distinct TOC minima around 1.0 and 3.8 m depth coincide with sediments characterized by hydromorphic features. These horizons also depict low **TOC/N** ratios, which vary in concert with TOC in Unit C (R = 0.87, n = 26) and Unit B (R = 0.85, n = 43). On the contrary, TOC and TOC/N correlate negatively in Unit A (R = -0.89, n = 12).

Apart from the observation that the transition from Unit A to B reveals a distinct shifts in the TOC/N ratios and therefore confirms the stratigraphy, a more detailed and straight-forward interpretation of TOC and TOC/N concerning the palaeoenvironmental conditions is challenging, because both proxies are subject to various factors influencing them. The TOC content mainly depends both on primary production and on SOM mineralization. Also low TOC/N ratios may on the one hand indicate intensive SOM mineralization and hence the release of CO_2. On the other hand, lacustrine phytoplankton is characterized by low TOC/N ratios (e.g.: Silliman et al., 1996) and could have become an important source for OM when a
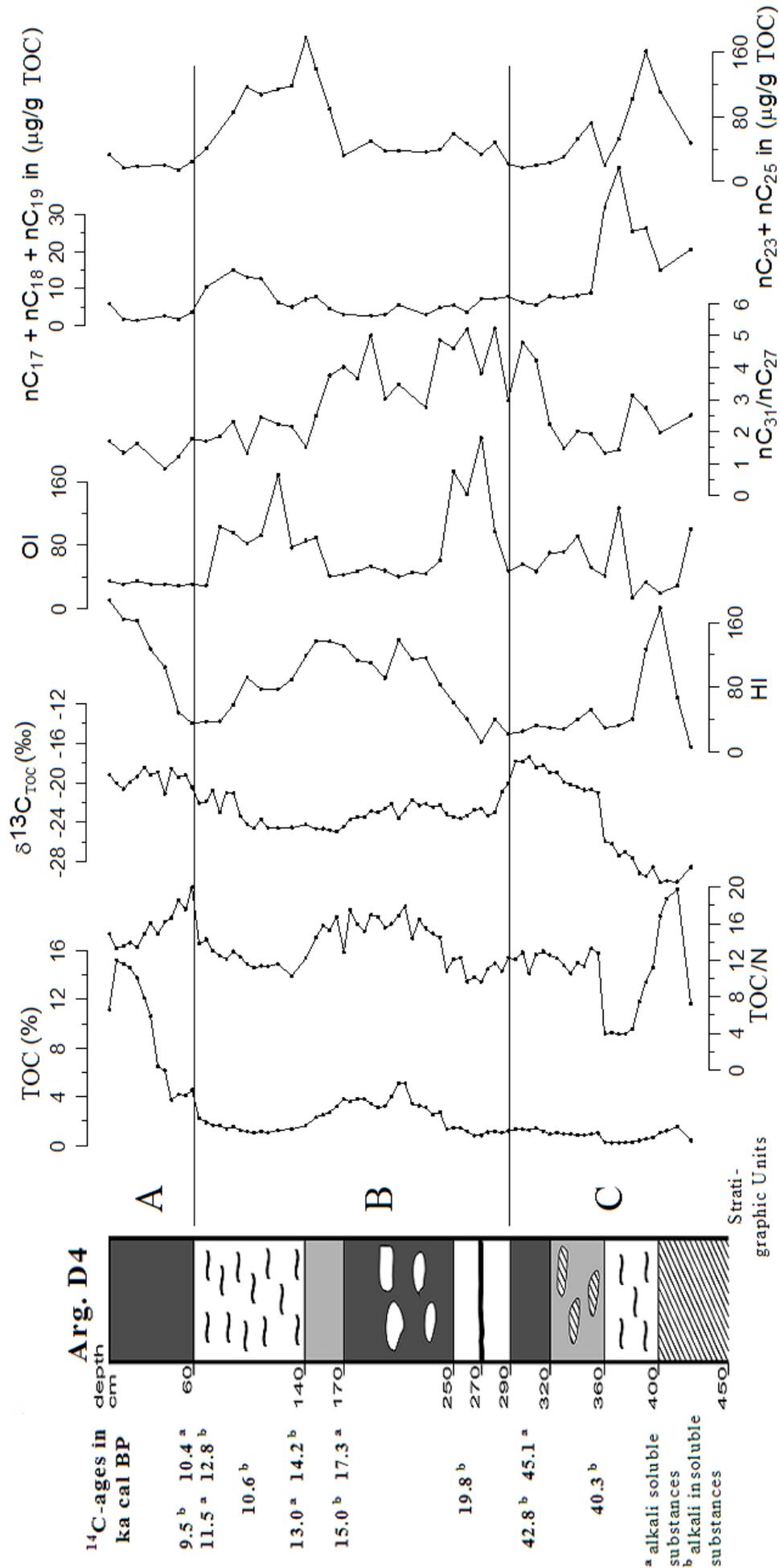
Fig. 5-3: Left: Schematic stratigraphy and numeric dating results for the sediment core Arg. D4, and stratigraphic subdivision. Right: Depth-functions for TOC, TOC/N, $\delta^{13}C_{TOC}$, HI, OI and the biomarker proxies nC_{31}/nC_{27}, $nC_{17} + nC_{18} + nC_{19}$ and $nC_{23} + nC_{25}$.

shallow lake possibly developed under more humid conditions (at around 1 m depth and from 3.6 to 4.0 m depth).

Further palaeoenvironmental information can be derived from the stable carbon isotopic composition of the OM ($\delta^{13}C_{TOC}$). It varies between -30‰ and -18‰ (Fig. 5-3). Unit C shows a general upward trend from the most negative to the most positive values in our palaeosol-sediment sequence and a sudden shift of almost 5‰ at 3.6 m depth. The lower meter of Unit B has $\delta^{13}C$ values around -23‰. From 1.7 - 1.0 m depth the values are ~ -25‰ and the upper decimeters of Unit B reveal the transition to again more positive values as observed in Unit A (~ -20‰).

Principally, smaller $\delta^{13}C$ variations in plants and sediments can be caused both by environmental factors like water stress or changes in the atmospheric CO_2 (concentration and isotopic signature) and by pedogenetic processes like SOM degradation or methanogenesis (discussed in details e.g. in Zech et al., submitted). However, the pronounced trends of several per mille in our record can only be interpreted in terms of photosynthetic pathway changes of the surrounding vegetation, which also allow palaeoclimatic implications as it is well known that the C4 grasses are especially competitive under relatively drier/warmer conditions (Collatz et al., 1998). Accordingly, $\delta^{13}C$ in Unit C (Fig. 5-3) documents that C3 vegetation first dominated during MIS 3 and was then replaced increasingly by C4 savannah grasses or succulent plants using the *Crassulacean* acid metabolism (CAM). The $\delta^{13}C_{TOC}$ results for Unit A and B indicate that changes of the photosynthetic pathway (C3/C4/CAM) occurred in the study area also since the LGM. Whereas the C3 photosynthetic pathway dominated from 1.0 - 2.9 m depth, C4 savannah grasses and/or CAM plants started to expand since the Holocene. For reasons of simplicity the subsequent discussions neglect the CAM plants and are restricted to the C3 and C4 photosynthetic pathway.

Fig. 5-3 illustrates the HI and OI depth functions in our core, showing distinct variations: The HI values range from 7 – 187 and are especially increased in the uppermost decimeters of Unit A, from 1.5 - 2.5 m depth in Unit B and in the lowermost decimeters of Unit C. They correlate with TOC (R = 0.64; n = 43) and TOC/N (R = 0.42; n = 43) indicating that OM in these TOC enriched horizons is less degraded than the more dehydrogenated OM at approximately 0.7 m depth and in the upper part of Unit C. In the course of humus degradation, the dehydrogenation (HI decreases) is progressively followed by a gain in oxygen (OI increase). OI values obtained for Arg. D4 range from 14 – 215 with OI maxima

occurring both in the uppermost and lowermost decimeters of Unit B (Fig. 5-3). This could indicate that the SOM between 0.6 and 1.5 m and between 2.5 and 2.9 m depth is intensively degraded. However, as already mentioned, small amounts of carbonate (<1%) were detected both in the light gray horizon from 2.5 to 2.9 m depth and from 0.3 to 1.0 m depth. Therefore, an inorganic contamination of our OI signal has to be accounted.

4.3 Lacustrine biomarkers

The concentrations of short-chain alkanes are generally low in our record (<10 μg $\sum$(nC$_{15}$-nC$_{19}$) × g TOC^{-1}). However, we found distinctly increased values (>15 μg) in the uppermost decimeters of Unit B and in the lower part of Unit C coinciding with low TOC/N ratios (Fig. 5-3). As it is well known that the alkane pattern of many algae are dominated by short-chain homologs (Bourbonniere et al., 1997; Meyers and Ishiwatari, 1993), these results point to lacustrine conditions presumably having prevailed during the deposition of these sediments. This interpretation is furthermore corroborated by mid-chain alkane maxima ($\sum$(nC$_{23}$, nC$_{25}$)) occurring in these horizons (Fig. 5-3): Recently, these homologs were found to dominate the alkane pattern of submerged plants in lakes and were consequently used in a proxy ratio (P$_{aq}$) to reconstruct lake histories (Ficken et al., 2000; Zhang et al., 2004). Although these findings are important for the palaeoenvironmental and palaeoclimatic interpretation of Arg. D4, SOM in our record nevertheless predominantly originates from terrestrial plants.

4.4 n-Alkane ratio nC$_{31}$/nC$_{27}$ as proxy for the palaeovegetation

Typical GC-FID chromatograms for n-alkanes extracted from higher plant samples in Misiones are shown in Fig. 5-4. They reveal the tree- and shrub-characteristic predominance of nC$_{27}$ and nC$_{29}$ for (A) *Prosopis sp*. and the grass- and herb-characteristic predominance of the alkane nC$_{31}$ for (B) *Setaria sp.*. A ternary diagram with the alkanes nC$_{27}$, nC$_{29}$ and nC$_{31}$ therefore depicts a typical cluster for most grass samples close to nC$_{31}$, whereas most trees/shrubs cluster close to nC$_{27}$ (Fig. 5-5). Our results are hence in agreement with findings from other authors using these two n-alkanes for the reconstruction of palaeovegetation (Cranwell, 1973; Farrimond and Flanagan, 1996; Schwark et al., 2002).

Fig. 5-3 illustrates the depth-function for the alkane ratio nC$_{31}$/nC$_{27}$ obtained for our core Arg. D4. The ratio ranges from 0.9 - 5.2 and serves as a proxy for grasses and herbs versus trees and shrubs. The increase of C4-savannah-grasses in Unit C, which was already deduced from the δ^{13}C$_{TOC}$, is corroborated by our biomarker results showing a trend to a
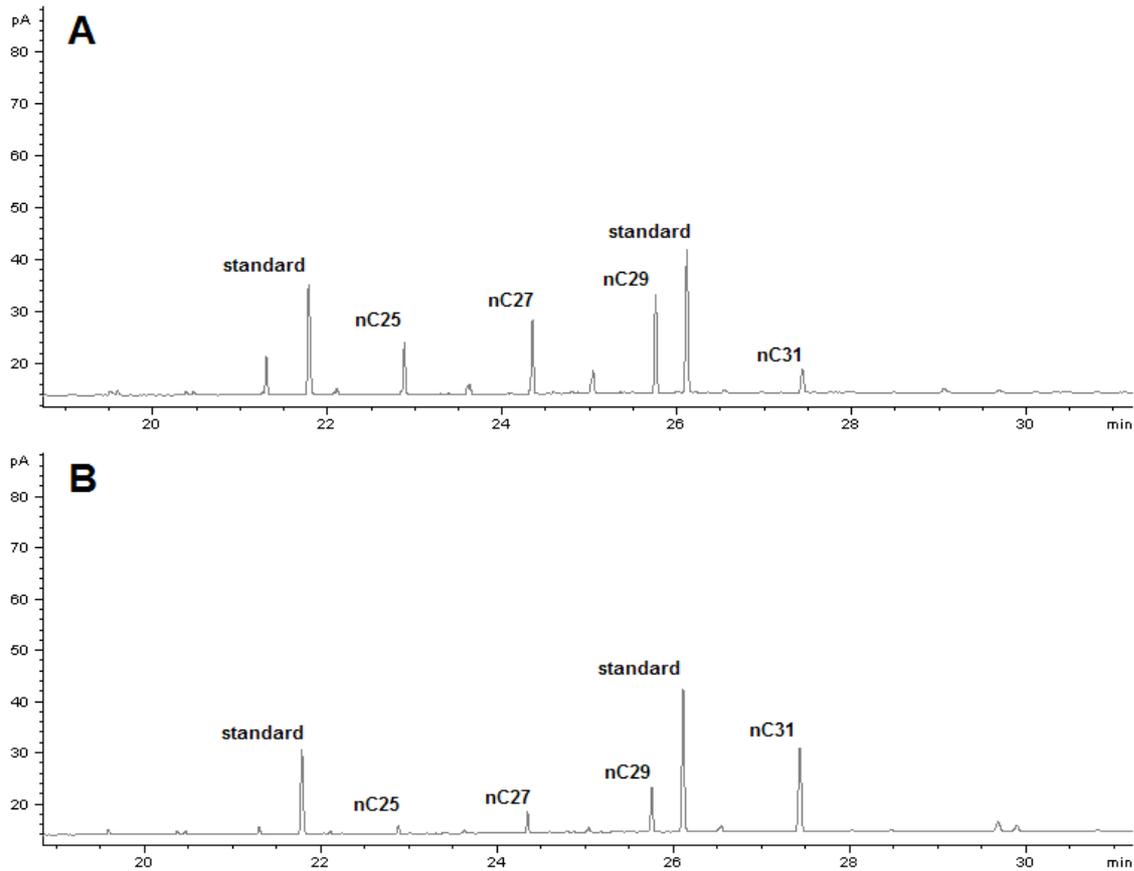
Fig. 5-4: GC-FID chromatograms for (A) the shrub sample *Prosopis sp.* and (B) the grass sample *Setaria sp.*.
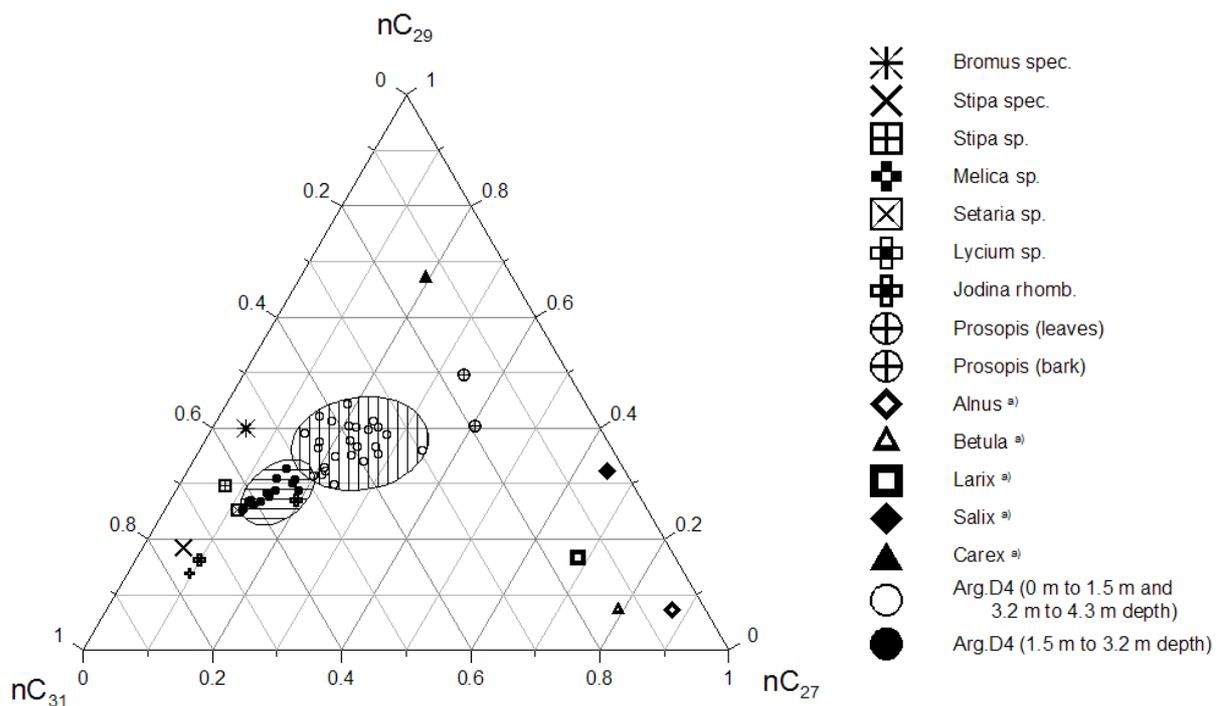
Fig. 5-5: Ternary diagram with the n-alkanes nC_{27}, nC_{29} and nC_{31} for plant samples and Arg. D4 sediment samples (in shaded clusters). Whereas grasses cluster close to nC_{27}, trees and shrubs cluster closer to nC_{29} and nC_{31}. [a] Own data from another study site

wider ratio of nC_{31}/nC_{27}. The opposite trend from Unit B to A reflects the re-expansion of forests since the LGM. Although according to the biomarker results trees and shrubs already contributed to the SOM around 18 ka cal BP, a marked forest retreat is indicated by the alkane ratio from 2.0 – 1.6 m depth. Ratios from 0.9 - 2.4 above 1.5 m depth document a mixed tree/grass vegetation cover since the Late Glacial and suggest that grasses did not re-expanded significantly since then. The increasing $\delta^{13}C_{TOC}$ values in Unit A would therefore have to be interpreted as suppression of C3 grasses by C4 grasses in the tree-grass-landscape rather than as increasing dominance of grasslands over forests.

5. Synthesis: Late Quaternary palaeoenvironmental and palaeoclimate evolution

In the following, we discuss the results of our multi-proxy analyses in a synthesized view and in the context with other findings in order to tentatively describe the Late Quaternary palaeoenvironmental and palaeoclimatic evolution of the study area.

Unit C : The 'Inca Huasi' wet phase (~ >40 ka BP)

Unit C likely documents a period of stable environmental conditions during MIS 3 before ~ 40 ka BP. Note that the chronostratigraphy of our core 'Arg D4' is corroborated by other cores in the study area (a ^{14}C age of 35.7 ka cal BP was obtained for the depression Arg. 03/D2 from a buried humic-rich horizon (Table 5-1)). The vegetation at that time was first dominated by C3 plants with a preponderance of forests (low $\delta^{13}C_{TOC}$ values and low nC_{31}/nC_{27}). Possibly, even lacustrine conditions occurred in the depression (lacustrine biomarkers), indicating rather humid conditions. The end of the humid period is documented in the upper part of Unit C by a considerable increase of $\delta^{13}C_{TOC}$ and the alkane ratio nC_{31}/nC_{27}, indicating expansion of C4 savannah grasslands.

Comparison with other findings corroborates our interpretation of Unit C: For instance, Behling et al. (2004) and Salgado-Labouriau (1997) found palynological evidence for humid and relatively stable environmental conditions in southern Brazil during MIS 3. Evidence for a wet phase in tropical/subtropical South America between ~ 40 and 50 ka BP also comes from recently published speleothem records from SE Brazil (Cruz et al., in press; Cruz et al., 2005; Wang et al., in press) and lake sediments from the Bolivian Altiplano (Baker et al., 2001; Fritz et al., 2004; Placzek et al., 2006) (Fig. 5-6). Following the argumentation of Placzek et al. (2006), we suggest to use their terminology for the respective

wet phase, i.e. 'Inca Huasi', in order to avoid confusion with the formerly used term 'Minchin' (Minchin sensu Baker and Fritz corresponds to 'Inca Huasi'). From a palaeoclimatological point of view, the 'Inca Huasi' wet phase can be explained with an intensification and/or southward shift of the South American Summer Monsoon (SASM), favored by increased austral summer insolation (Fig. 5-6).

C3 – C2 Hiatus: A pre-LGM dry phase (~ 40 – 20? ka BP)

In our sediment core Arg. D4 both the ^{14}C results and the elemental composition indicate a hiatus between Unit C and B. Sedimentary gaps are actually quite common in tropical/subtropical South America; most pedosedimentary records are discontinuous and dry conditions with intensive erosion and deflation have been inferred (e.g. Iriondo and Kröhling, 2004; Kemp et al., 2006; Zárate, 2003). Palynological findings provide evidence for the replacement of forests by savannah and grasslands due to much drier conditions in South Brazil (Behling, 2002). These changes in the vegetation cover, of course, negatively affected the overall landscape stability: Eolian activity, for example, has been documented in the southern Chaco (Iriondo, 1999) and the Paraná river basin (Stevaux, 2000), and fluvial records along the Andean Piedmont indicate the development of braided river systems with coarse gravel-beds (May et al., in press). Very dry conditions after ~ 40 ka BP are also found in the speleothem records in SE Brazil and on the Altiplano (Fig. 5-6).

Unit B: The LGM and the subsequent Lateglacial wet phase (~20 – 11 ka BP)

Sedimentation and soil development in core Arg. D4 started again ~ 20 ka cal BP and continued during the Late Glacial (Fig. 5-3). This is corroborated by a [14]Cage of 17.7 ka cal BP, which was obtained for a humic-rich horizon in another small basin in the study area (Arg. 03/P2, see Table 5-1). Our geochemical proxies for the lower part of Unit B indicate accumulation of mainly C3-derived, relatively degraded OM during the LGM (~ 250 - 290 cm depth). During the LGM/Late Glacial transition (middle part of Unit B from ~ 170 – 250 cm depth) the SOM is still mainly C3-derived but much better preserved. Evidence for the expansion of forests during the Lateglacial (above 170 cm: ~16 ka BP) comes from the decreasing nC_{31}/nC_{27} ratios. This vegetation change presumably documents increasing precipitation, which is confirmed by other biomarker proxies, too. Also the high clay content (~ 70%) and the pronounced hydromorphic features in the uppermost part of Unit B (140-60 cm) indicate that again lacustrine conditions could have occurred in the small basin during the Late Glacial. The low TOC values, TOC/N ratios and HI values point to a reduced OM input and/or again more intensive SOM degradation.
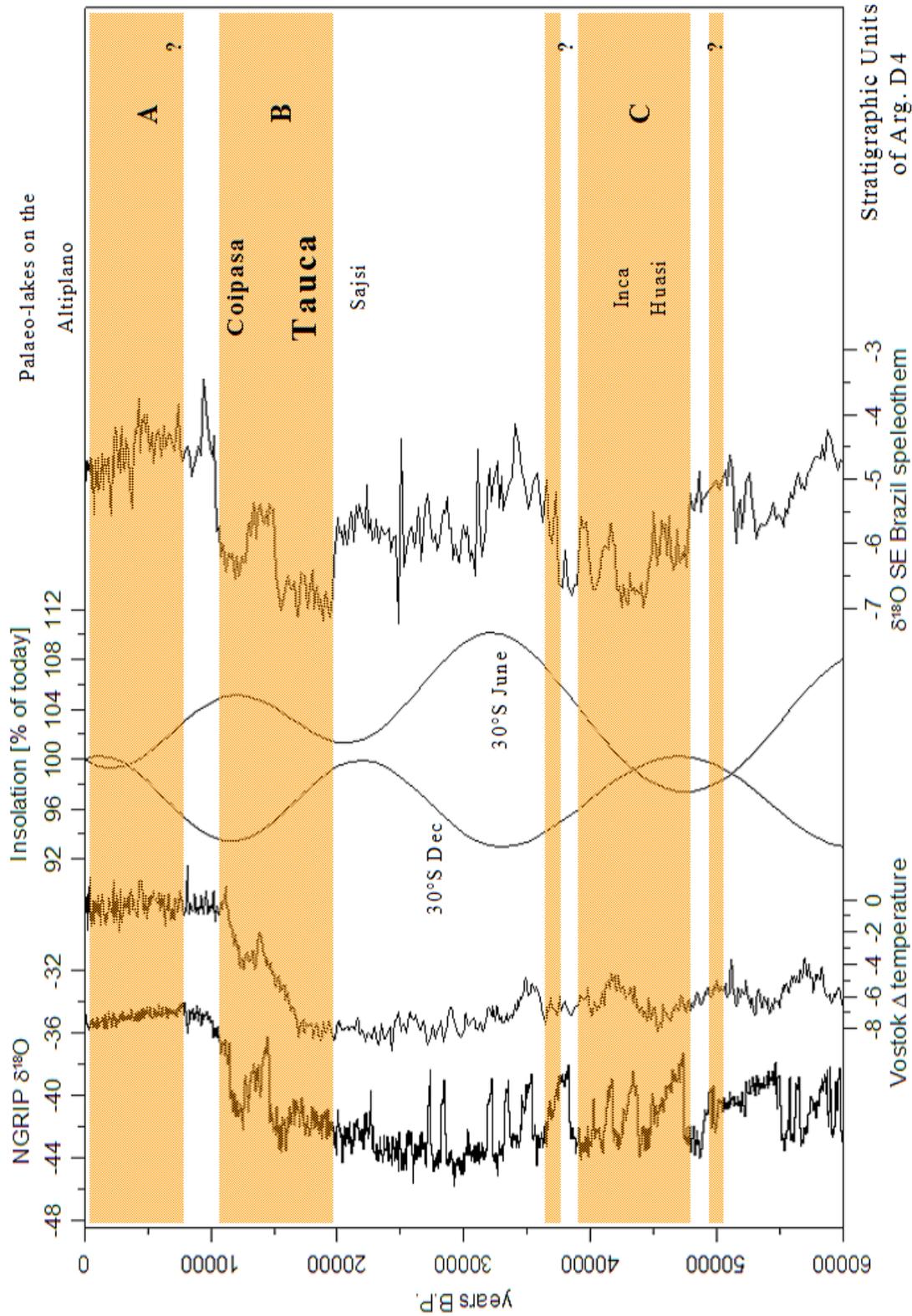
Fig. 5-6: Palaeoclimatic context for the sediment core Arg. D4 (periods of sedimentation are illustrated in brown shaded bars, stratigraphic units are given on the right). a, NGRIP δ¹⁸O record as temperature proxy for Greenland (NGRIP members, 2004). b, Temperature deviation from present conditions in Antarctica derived from the Vostoc deuterium record (Petit et al., 1999). c, Insolation changes normalized to present conditions for austral summer (30°S Dec) and austral winter (30°S June) (Berger and Loutre, 1991). d, Speleothem δ¹⁸O record from SE Brazil as proxy for the intensification of the SASM and the southward shift of the ITCZ (= more negative values) (Cruz et al., in press). e, Reconstructed palaeo-lakes from shoreline deposits on the Bolivian Altiplano (Placzek et al., 2006).

Our results and the interpretation are in good agreement with other palaeoenvironmental findings: Increased precipitation during the LGM and the LGM/Late Glacial transition and hence the stabilization of the landscape due to denser vegetation can be inferred from the oxygen isotope composition in the SE Brazilian stalagmites (→ intensification of the SASM) as well as from the lake sediment studies on the Altiplano. Also wet conditions during the Late Glacial are evident from the speleothem records and the lake sediments on the Altiplano ('Tauca and Coipasa' wet phase, Placzek 06; see also Fig. 5-6), but also from numerous other archives. Palynological and isotopic studies, for example, show lateglacial forest expansion in NE Brazil and southern Amazon (Behling et al., 2000; Freitas et al., 2001) and cloud forests became fully developed in the Subandean Ranges of Eastern Bolivia (Mourguiart and Ledru, 2003). Besides, the transformation of the fluvial systems (from braided- to meander-river-systems) indicates geomorphic stability, and consequently soil development began e.g. along the Andean piedmont (May et al., in press). In the Central Andes, lake transgression phases and corresponding glacial advances at that time can be traced as far south as 30°S, i.e. far beyond the present limit of the SASM (Geyh et al., 1999; Grosjean et al., 2001; Zech et al., 2006).

From a palaeoclimatic point of view, the prominent lateglacial wet phase in tropical/subtropical South America is related to a massive intensification and southward shift of the tropical circulation (Baker et al., 2001; Cruz et al., 2005; Wang et al., in press). Although on orbital time-scales monsoonal circulations are certainly controlled by summer insolation and resulting ocean-continental temperature and pressure gradients e.g. (Clemens et al., 1991; Gasse, 2000), the high-resolution and well-dated speleothem records clearly show that on the millennial and centennial time-scales other influencing factors must play an important role (Cruz et al., in press; Wang et al., in press). Recent modeling studies describe and emphasize the possible role of high-latitude boundary conditions, like snow and ice cover, or the thermohaline circulation (Chiang and Bitz, 2005; Clement et al., 2004; Zhang and Delworth, 2005). These models suggest that the intertropical convergence zone (ITCZ) can be rapidly shifted southward as a result of cold conditions in the northern hemisphere, as they occurred e.g. during the Late Glacial. The southward shift of the ITCZ, which is strictly speaking a marine phenomenon, corresponds to a southward shift and an intensification of the SASM/SACZ, thus explaining increased summer precipitation over large parts of South America.

Unit A: Loess deposition versus slope debris during the Holocene

The clay-rich and probably lacustrine deposits in Unit B are covered by 60 cm of almost pure silt and find sand in Unit A, which also shows a distinctly different elemental composition. This indicates changing environmental conditions since the beginning of the Holocene. Our record lacks sufficient resolution to document environmental changes in the course of the Holocene, but two possible interpretations seem to be plausible:

a) Following the suggestion of Iriondo and Kröhling (2004), Unit A could be interpreted as Holocene loess with a different sediment provenance compared to earlier eolian components contributing to our palaeosol-sediment record. Organic matter started to accumulate (increasing TOC) and SOM degradation is not as advanced as during the Lateglacial (increasing HI and low OI).

The palaeoclimatic interpretation in this scenario is that overall precipitation reduced due to the northward shift and weakening of the tropical circulation (Cruz et al., in press; Placzek et al., 2006; Wang et al., in press). Hence, new dust sources in the more arid regions west of our study area were created. At the same time, in our basin Arg. D4 probably seasonally shallow-inundated, rather swampy conditions prevailed during the Holocene period. In contrast to the proposed late glacial lacustrine conditions, the basin was likely stocked all the time with dust catching vegetation. We suggest that the annual seasonality was reduced due to increased winter precipitation (SE trades). Intensification of the SE trades may be explained (i) by the post-glacial sea-level rise → flooding of the Argentinean shelf → proximity to the ocean, and (ii) by high winter insolation → changes in the ocean-continent temperature and pressure gradient → increased moisture advection. At least for the Early Holocene, there is palaeopedological and palynological evidence for increased austral winter precipitation from the eastern Argentinean grasslands (Mancini et al., 2005; Prieto, 2000; Zech, this issue).

b) The second possible interpretation of Unit A is that these upper 60 cm of our palaeosol-sediment record mainly represent slope debris coming from the catchment of the depression. One may also doubt whether Unit A has necessarily to be interpreted palaeoclimatically. On the one hand, several authors report that seasonal climate with a long annual dry period established during the Middle Holocene and fires became very frequent in tropical and subtropical South America (Behling et al., 2004; Freitas et al., 2001; Mayle et al., 2004). On the other hand, Behling et al. (2004) suggested for the close-by southern Brazil

human occupation being responsible for frequent fires after 7.4 ka cal BP and Iriarte (2006) found a mid Holocene drying trend in southeastern Uruguay coinciding with major organizational changes in settlement, subsistence and technology of the pre-Hispanic populations. In both scenarios – be it climatically driven or human-induced – a destabilization of the slopes in our study area can be expected. Note that the ^{14}C ages obtained for the bottom of Unit A (Early Holocene) do not contradict this interpretation as they would probably overestimate the real deposition age due to the input of "too old" SOM from the eroded soils in the catchment.

6. Conclusions

Our results show that a multi-proxy approach provides much more detailed information than the standard geochemical parameters alone. The alkane ratio nC_{31}/nC_{27}, for example, turned out to be a powerful tool for reconstructing vegetation changes in terms of grass/herbs versus trees/shrubs, whereas short- and mid-chain alkanes can be used to detect lacustrine-derived OM.

The combination of all geochemical analyses allows a tentative reconstruction of the palaeoenvironmental conditions in Misiones, i.e. in brief: stable landscape conditions, forest cover and subsequent transition to C4 grasslands (Unit C: before ~40 ka BP); landscape instability, erosive hiatus (Unit C – Unit B boundary); re-onset of sedimentation, first C3 grassland, then transition to C3 grass tree savannah and lacustrine conditions (Unit B: LGM and Late Glacial); and, finally, holocene sedimentation with increasing OM contribution from C4 and/or CAM plants (Unit A).

Our palaeoclimatic interpretation is in good agreement with fluvial, palynological, speleothem and lacustrine data from tropical/subtropical South America and suggests that variations in the intensity and/or latitudinal shifts of the tropical circulation (SASM and SACZ) play an important role for the palaeoenvironmental conditions: The sediment core Arg. D4 likely records (i) the 'Inca Huasi' wet phase (~ >40 ka BP), (ii) a dry phase of pronounced landscape instability and erosion during the pre-LGM, (iii) the transition from intermediate environmental conditions during the LGM to the pronounced lateglacial wet phase, which probably documents the phase of the most intensive and southward shifted tropical circulation, and (iv) finally, the establishment of the holocene atmospheric circulation pattern.

Ongoing research now focuses on palynological work in order to confirm the reconstructed vegetation history. Furthermore, compound-specific stable carbon isotope analyis of n-alkanes were engaged in order to validate the $\delta^{13}C_{TOC}$ interpretation in terms of C3-C4 vegetation changes. Results will be published elsewhere.

Acknowledgements

References

Amelung, W., Cheshire, M.V. and Guggenberger, G., 1996. Determination of neutral and acidic sugars in soil by capillary gas-liquid chromatography after trifluoroacetic acid hydrolysis. Soil Biology and Biochemistry, 28: 1631-1639.

Ariztegui, D., Chondrogianni, C., Lami, A., Giulizzoni, P. and Lafargue, E., 2001. Lacustrine organic matter and the Holocene paleoenvironmental record of Lake Albano (central Italy). Journal of Paleolimnology, 26: 283-292.

Aucour, A.-M., Hillaire-Marcel, C. and Bonnefille, R., 1999. Sources and accumulation rates of organic carbon in an equatorial peat bog (Burundi, East Africa) during the Holocene: carbon isotope constraints. Palaeogeography, Palaeoclimatology, Palaeoecology, 150: 179-189.

Baker, P.A., Rigsby, C.A., Seltzer, G.O., Fritz, S.C., Lowenstein, T.K., Bacher, N.P. and Veliz, C., 2001. Tropical climate changes at millennial and orbital timescales on the Bolivian Altiplano. Nature, 409: 698-701.

Behling, H., 2002. South and southeast Brazilian grasslands during Late Quaternary times: a synthesis. Palaeogeography, Palaeoclimatology, Palaeoecology, 177: 19-27.

Behling, H., Arz, H.W., Pätzold, J. and Wefer, G., 2000. Late Quaternary vegetational and climate dynamics in northeastern Brazil, inferences from marine core GeoB 3104-1. Quaternary Science Reviews, 19: 981-994.

Behling, H., Pillar, V., Orlóci, L. and Bauermann, S.G., 2004. Late Quaternary Araucaria forest, grassland (Campos), fire and climate dynamics, studied by high-resolution pollen, charcoal and multivariate analysis of the Cambará do Sul core in southern Brazil. Palaeogeography, Palaeoclimatology, Palaeoecology, 203: 277-297.

Berger, A.L. and Loutre, M.F., 1991. Insolation values for the climate of the last 10 million years. Quaternary Science Reviews, 10(4): 297-317.

Bourbonniere, R.A., Telford, S.L., Ziolkowski, L.A., Lee, J., Evans, M.S. and Meyers, P.A., 1997. Biogeochemical marker profiles in cores of dated sediments from large North American lakes. In: R.P. Eganhouse (Editor), Molecular Markers in Environmental Geochemistry, ACS Symposium Series. American Chemical Society, Washington, DC, pp. 133-150.

Cerveny, R.S., 1998. Present Climates of South America. In: J.E. Hobbs, J.A. Lindesay and B. H.A. (Editors), Climates of the Southern Continents: Present, Past and Future. Wiley & Sons.

Chiang, J. and Bitz, C., 2005. Influence of high latitude ice cover on the marine Intertropical Convergence Zone. Climate Dynamics, 25(5): 477-496.

Clemens, S.C., Prell, W.L., Murray, D., Shimmield, G. and Weedon, G., 1991. Forcing mechanisms of the Indian Ocean monsoon. Nature, 353: 720-725.

Clement, A.C., Hall, A. and Broccoli, A.J., 2004. The importance of precessional signals in the tropical climate. Climate Dynamics, 22(4): 327-341.

Collatz, G.J., Berry, J.A. and Clark, J.S., 1998. Effects of climate and atmospheric CO_2 partial pressure on global distribution of C4 grasses: present, past and future. Oecologia, 114: 441-454.

Collister, J.W., Rieley, G., Stern, B., Eglington, G. and Fry, B., 1994. Compound-specific δ^{13}C analyses of leaf lipids from plants with differing carbon dioxide metabolism. Organic Geochemistry, 21: 619-627.

Cranwell, P.A., 1973. Chain-length distribution of n-alkanes from lake sediments in relation to post-glacial environmental change. Freshwater Biology, 3: 259-265.

Cranwell, P.A., 1981. Diagenesis of free and bound lipids in terrestrial detritus deposited in lacustrine sediments. Organic Geochemistry, 3: 79-89.

Cruz, F.W., Burns, S.J., Karmann, I., Sharp, W.D. and Vuille, M., in press. Reconstruction of regional atmospheric circulation features during the Late Pleistocene in subtropical Brazil from oxygen isotope composition of speleothems. Earth and Planetary Science Letters.

Cruz, F.W., Burns, S.J., Karmann, I., Sharp, W.D., Vuille, M., Cardoso, A.O., Ferrari, J.A., Dias, P.L. and Viana, O., 2005. Insolation-driven changes in atmospheric circulation over the past 116,000 years in subtropical Brazil. Nature, 434: 63-65.

Disnar, J.R., Guillet, B., Keravis, D., Di-Giovanni, C. and Sebag, D., 2003. Soil organic matter (SOM) characterization by Rock-Eval pyrolysis: scope and limitations. Organic Geochemistry, 34: 327-343.

Espitalie, J., Deroo, J. and Marquis, F., 1985. Rock-Eval Pyrolysis and its Applications. Institut Francais du Pétrole: Report 33578.

Farrimond, P. and Flanagan, R.L., 1996. Lipid stratigraphy of a Flandrian peat bed (Northumberland, UK): comparison with the pollen record. The Holocene, 6(1): 67-74.

Feng, X., 2002. A theoretical analysis of carbon isotope evolution of decomposing plant litters and soil organic matter. Glob. Biogeochem. Cycles, 16: 1-10.

Fernández, R.A., Lupi, A.M. and N., P., 1999. Aptitud de las tierras para la implantación de bosques. Provincia de Misiones. Yvyraretá, 9.

Ficken, K.J., Barber, K.E. and Eglinton, G., 1998. Lipid biomarker, δ^{13}C and plant macrofossil stratigraphy of a Scottish montane peat bog over the last two millennia. Organic Geochemistry, 28(3/4): 217-237.

Ficken, K.J., Li, B., Swain, D.L. and Eglinton, G., 2000. An n-alkane proxy for the sedimentary input of submerged/floating freshwater aquatic macrophytes. Organic Geochemistry, 31: 745-749.

Filippi, M.L. and Talbot, M.R., 2005. The palaeolimnology of northern Lake Malawi over the last 25 ka based upon the elemental and stable isotopic composition of sedimentary organic matter. Quatenary Science Reviews, 24: 1303-1328.

Freitas, H.A., Pessenda, L.C., Aravena, R., Gouveia, S.E., Ribeiro, A.S. and Boulet, R., 2001. Late Quaternary Vegetation Dynamics in the Southern Amazon Basin Inferred from Carbon Isotopes in Soil Organic Matter. Quaternary Research, 55: 39-46.

Fritz, S.C., Baker, P.A., Lowenstein, T.K., Seltzer, G.O., Rigsby, C.A., Dwyer, G.S., Tapia, P.M., Kimberly, K.A., Ku, T.-L. and Luo, S., 2004. Hydrologic variation during the last 170,000 years in the southern hemisphere tropics of South America. Quaternary Research, 61: 95-104.

Gallet, S., Jahn, B., Van Vliet Lanoe, B., Dia, A. and Rossello, E., 1998. Loess geochemistry and its implications for particle origin and composition of the upper continental crust. Earth and Planetary Science Letters, 156: 157-172.

Gan, M.A., Kousky, V.E. and Ropelewski, C.F., 2004. The South American monsoon circulation and its relationship to rainfall over West-Central Brazil. Journal of Climate, 17: 47-66.

Garrels, R.M. and Mackenzie, F.T., 1971. Evolution of Sedimentary Rocks. Norton, New York, 397 pp.

Gasse, F., 2000. Hydrological changes in the African tropics since the Last Glacial Maximum. Quaternary Science Reviews, 19: 189-211.

Geyh, M.A., Grosjean, M., Nunez, L. and Schotterer, U., 1999. Radiocarbon Reservoir Effect and the Timing of the Late-Glacial/Early Holocene Humid Phase in the Atacama Desert (Northern Chile). Quaternary Research, 52: 143–153.

Geyh, M.A. and Schleicher, H., 1991. "Absolute Age Determination". Springer, New York.

Glaser, B., 2005. Compound-specific stable-isotope (δ^{13}C) analysis in soil science. Journal of Plant Nutrition and Soil Science, 168: 633-648.

Glaser, B. and Amelung, W., 2002. Determination of ^{13}C natural abundance of amino acid enantiomers in soil: methodological considerations and first results. Rapid Communications in Mass Spectrometry, 16: 891-898.

Glaser, B. and Zech, W., 2005. Reconstruction of climate and landscape changes in a high mountain lake catchment in the Gorkha Himal, Nepal during the Late Glacial and Holocene as deduced from radiocarbon and compound-specific stable isotope analysis of terrestrial, aquatic and microbial biomarkers. Organic Geochemistry, 36: 1086-1098.

Grosjean, M., van Leeuwen, J.F.N., van der Knaap, W.O., Geyh, M.A., Ammann, B., Tanner, W., Messerli, B. and Veit, H., 2001. A 22,000 14C yr BP sediment and pollen record of climate change from Laguna Miscanti 231S, northern Chile. Global and Planetary Change, 28: 35–51.

Gross, S. and Glaser, B., 2004. Minimization of foreign carbon addition during derivatization of organic molecules for compound-specific δ^{13}C analysis of soil organic matter. Rapid Communications in Mass Spectrometry, 18: 2753-2764.

Huang, Y., Bol, R., Harkness, D.D., Ineson, P. and Eglington, G., 1996. Post-glacial variations in distributions, ^{13}C and ^{14}C contents of aliphatic hydrocarbons and bulk organic matter in three types of British acid upland soils. Organic Geochemistry, 24(3): 273-287.

Huang, Y., Eglington, G., Ineson, P., Latter, P.M., Bol, R. and Harkness, D.D., 1997. Absence of carbon isotope fractionation of individual n-alkanes in a 23-year field decomposition experiment with Calluna vulgaris. Organic Geochemistry, 26(7/8): 497-501.

Huang, Y., Street-Perrott, F.A., Metcalfe, S.A., Brenner, M., Moreland, M. and Freeman, K.H., 2001. Climate change as the dominant control on glacial-interglacial variations in C_3 and C_4 plant abundance. Science, 293: 1647-1651.

Hueck, K. and Seibert, P., 1972. Vegetationskarte von Südamerika. Vegetationsmonographien der einzelnen Großräume, Band II a. Gustav Fischer Verlag, Stuttgart.

Iriarte, J., 2006. Vegetation and climate change since 14,810 ^{14}C yr B.P. in southeastern Uruguay and implications for the rise of early Formative societies. Quaternary Research, 65: 20-32.

Iriondo et al., this issue.

Iriondo, M., 1999. Climatic changes in the South American plains: Records of a continent-scale oscillation. Quaternary International, 57/58: 93-112.

Iriondo, M. and Kröhling, D.M., 2004. The parent material as the dominant factor in Holocene pedogenesis in the Uruguay River Basin. Revista Mexicana de Ciencias Geológicas, 21(1): 175-184.

Kemp, R.A., Zárate, M.A., Toms, P., King, M., Sanabria, J. and Arguello, G., 2006. Late Quaternary paleosols, stratigraphy and landscape evolution in the Northern Pampa, Argentina. Quaternary Research, ??

Kolattukudy, P.E., 1976. Biochemistry of plant waxes. In: Kolattukudy (ed.), Chemistry and Biochemistry of Natural Waxes, Amsterdam: Elsevier, 290-349.

Kröhling, D.M. and Iriondo, M., 1999. Upper Quaternary Palaeoclimates of the Mar Chiquita area, North Pampa, Argentina. Quaternary International, 57/58: 149-163.

Kronberg, B.I. and Nesbitt, H.W., 1981. Quantification of weathering soil chemistry and soil fertility. Journal of Soil Science, 32: 453-459.

Lichtfouse, E., 1998. Isotope and Biosynthetic Evidence for the Origin of Long-Chain Aliphatic Lipids in Soils. Naturwissenschaften, 85: 76-77.

Liu, W., Huang, Y., An, Z., Clemens, S.C., Li, L., Prell, W.L. and Ning, Y., 2005. Summer monsoon intensity controls C4/C3 plant abundance during the last 35 ka in the Chinese Loess Plateau: Carbon isotope evidence from bulk organic matter and individual leaf waxes. Palaeogeography, Palaeoclimatology, Palaeoecology, 220: 243-254.

Lüniger, G. and Schwark, L., 2002. Characterisation of sedimentary organic matter by bulk and molecular geochemical proxies: an example from Oligocene maar-type Lake Enspel, Germany. Sedimentary Geology, 148: 275-288.

Mancini, M.V., Paez, M.M., Prieto, A.R., Stutz, S., Tonello, M. and Vilanova, I., 2005. Mid-Holocene climatic variability reconstruction from pollen records (32°–52°S, Argentina). Quaternary International, 132: 47-59.

Margalot, J.A., 1985. Geografía de Misiones. Industria Gráfica del Libro, Buenos Aires, 236 pp.

May, J.-H., Zech, R. and Veit, H., in press. Late Quaternary paleosol-sediment-sequences and landscape evolution along the Andean piedmont, Bolivian Chaco. Geomorphology.

Mayle, F.E., Beerling, D.J., Gosling, W.D. and Bush, M.B., 2004. Responses of Amazonian ecosystems to climatic and atmospheric carbon dioxide changes since the Last Glacial Maximum. DOI 10.1098/rstb.2003.1434.

McLennan, S.M., 1993. Weathering and global denudation. Journal of Geology, 101: 295-303.

Meyers, P.A. and Ishiwatari, R., 1993. Lacustrine organic matter geochemistry - an overview of indicators of organic matter sources and diagenesis in lake sediments. Organic Geochemistry, 20(7): 867-900.

Morrás et al., this issue.

Morrás, H., Moretti, L., Píccolo, G. and Zech, W., 2005. New hypotheses and results about the origin of stonelines and subsurface structured horizons in ferrallitic soils of Misiones, Argentina. Geophysical Research Abstracts, 7: 05522.

Mourguiart, P. and Ledru, M.-P., 2003. Last Glacial Maximum in an Andean cloud forest environment (Eastern Cordillera, Bolivia). Geology, 31(3): 195-198.

Muhs, D.R., Ager, T.A., Bettis III, E.A., McGeehin, J., Been, J.M., Begét, J.E., Pavich, M.J., Stafford Jr., T.W. and Stevens, S.P., 2004. Stratigraphy and palaeoclimatic significance of Late Quaternary loess–palaeosol sequences of the Last Interglacial–Glacial cycle in central Alaska. Quaternary Science Reviews, 22: 1947-1986.

Muhs et al., this issue.

NGRIP members, 2004. High-resolution record of Northern Hemisphere climate extending into the last interglacial period. Nature, 431: 147-151.

Nott, C.J., Xie, S., Avsejs, L.A., Maddy, D., Chambers, F.M. and Evershed, R.P., 2000. n-Alkane distributions in ombrotrophic mires as indicators of vegetation change related to climatic variation. Organic Geochemistry, 31: 231-235.

Petit, J.R., Jouzel, J., Raynaud, D., Barkov, N.I., Barnola, J.-M., Basile, I., Bender, M., Chappellaz, J., Davis, M., Delaygue, G., Delmotte, M., Kotlyakov, V.M., Legrand, M., Lipenkov, V.Y., Lorius, C., Pépin, L., Ritz, C., Saltzman, E. and Stievenard, M., 1999. Climate and atmospheric history of the past 420,000 years from the Vostoc ice core, Antarctica. Nature, 399: 429-436.

Placzek, C., Quade, J. and Patchett, P.J., 2006. Geochronology and stratigraphy of late Pleistocene lake cycles on the southern Bolivian Altiplano: Implications for causes of tropical climate change. Geological Society of America Bulletin, 118(5-6): 515-532.

Prieto, A.R., 2000. Vegetational history of the Late glacial–Holocene transition in the grasslands of eastern Argentina. Palaeogeography, Palaeoclimatology, Palaeoecology, 157: 167-188.

Prohaska, F., 1976. The Climate of Argentina, Paraquay and Uruquay. In: W. Schwertfeger (Editor), Climates of Central and South America. Elsevier Scientific Publishing Company, Amsterdam.

quickcal2005 ver.1.4, http://www.calpal-online.de. - Copyright 2003-2005, CalPal Authors.

Salgado-Labouriau, M.L., 1997. Late Quaternary palaeoclimate in the savannas of South America. Journal of Quaternary Science, 12(5): 371-379.

Schmitt, J., Glaser, B. and Zech, W., 2003. Amount-dependent isotopic fractionation during compound-specific isotope analysis. Rapid Communications in Mass Spectrometry, 17: 970-977.

Schwark, L., Zink, K. and Lechtenbeck, J., 2002. Reconstruction of postglacial to early Holocene vegetation history in terrestrial Central Europe via cuticular lipid biomarkers and pollen records from lake sediments. Geology, 30(5): 463-466.

Silliman, J.E., Meyers, P.A. and Bourbonniere, R.A., 1996. Record of postglacial organic matter delivery and burial in sediments of Lake Ontario. Organic Geochemistry, 24: 463-472.

Stevaux, J.C., 2000. Climatic events during the Late Pleistocene and Holocene in the Upper Parana River: Correlation with NE Argentina and South-Central Brazil. Quaternary International, 72: 73-85.

Street-Perrott, F.A., Ficken, K.J., Huang, Y. and Eglington, G., 2004. Late Quaternary changes in carbon cycling on Mt. Kenya, East Africa: an overview of the δ^{13}C record in lacustrine organic matter. Quaternary Science Reviews, 23: 861-879.

Thompson, L.G., Davis, M.E., Mosley-Thompson, E., Lin, P.-N., Henderson, K.A. and Mashiotta, T.A., 2005. Tropical ice core records: evidence for asynchronous glaciation on Milankovitch timescales. Journal of Quaternary Science, 20(7-8): 723-733.

van Dongen, B.E., Schouten, S. and Sinninghe Damasté, J.S., 2002. Carbon isotope variability in monosaccharides and lipids of aquatic algae and terrestrial plants. Marine Ecology Progress Series, 232: 83-92.

Vera, C.S., Vigliarolo, P.K. and Berbery, E.H., 2002. Cold season synoptic-scale waves over subtropical South America. Monthly Weather Review, 130: 684-699.

Wang, H., Follmer, L.R. and Liu, C.-L.J., 2000. Isotope evidence of paleo-El Niño-Southern Oscillation cycles in loess-paleosol record in the central United States. Geology, 28(9): 771-774.

Wang, X., Auler, A.S., Edwards, R.L., Cheng, H., Ito, E. and Solheid, M., in press. Interhemispheric anti-phasing of rainfall during the last glacial period. Quaternary Science Reviews.

Zárate, M.A., 2003. Loess of southern South America. Quaternary Science Reviews, 22: 1987-2006.

Zech, M., 2006. Evidence for Late Pleistocene climate changes from buried soils on the southern slopes of Mt. Kilimanjaro, Tanzania. Palaeogeography, Palaeoclimatology, Palaeoecology, accepted.

Zech, M. and Glaser, B., to be submitted. Improved compound-specific $\delta^{13}C$ analysis of n-alkanes for the application in a palaeoenvironmental study. Rapid Communications in Mass Spectrometry.

Zech, M., Zech, R. and Glaser, B., submitted. A 240,000-year stable carbon and nitrogen isotope record from a loess-like palaeosol sequence in the Tumara Valley, Northeast Siberia. Chemical Geology.

Zech, R., Kull, C. and Veit, H., 2006. Late Quaternary glacial history in the Encierro Valley, northern Chile (29°S), deduced from ^{10}Be surface exposure dating. Palaeogeography, Palaeoclimatology, Palaeoecology, 234: 277-286.

Zech, W., this issue.

Zeil, W., 1986. Südamerika. Geologie der Erde Band 1. Ferdinand Enke Verlag, Stuttgart.

Zhang, R. and Delworth, T.L., 2005. Simulated Tropical Response to a Substantial Weakening of the Atlantic Thermohaline Circulation. Journal of Climate, 18(12): 1853-1860.

Zhang, Z., Zhao, M., Yang, X., Wang, S., Jiang, X., Oldfield, F. and Eglinton, G., 2004. A hydrocarbon biomarker record for the last 40 kyr of plant input to Lake Heqing, southwestern China. Organic Geochemistry, 35: 595-613.

Zhou, J.Y. and Lau, K.-M., 1998. Does a monsoon climate exist over South America? Journal of Climate, 11: 1020-1040.

Study 6:

Improved compound-specific δ^{13}C analysis of n-alkanes for the application in palaeoenvironmental studies

Michael Zech* and Bruno Glaser

Institute of Soil Science and Soil Geography, University of Bayreuth, D-95440 Bayreuth, Germany

* Corresponding author: Michael Zech, Phone: +49 (0)921 552247; Fax: +49 (0)921 552246; Email: michael_zech@gmx.de

Abstract

In this paper we present an optimized method for compound-specific stable carbon isotope (δ^{13}C) analysis of n-alkanes. Concerning the sample preparation, the traditionally used Soxhlet extraction was replaced by accelerated solvent extraction (ASE). δ^{13}C values of individual n-alkanes – measured on a GC-C-IRMS – were firstly drift-corrected with regularly discharged pure CO_2 pulses as reference gas and, secondly, corrected for the amount dependence of the δ^{13}C values by co-analyzing standards with varying analyte concentrations. Finally, the δ^{13}C values were calibrated against two internal standards.

The improved method was applied to selected sediment samples from a palaeoenvironmental study in subtropical NE Argentina. Results show that the δ^{13}C values of all long-chain n-alkanes (nC_{27}, nC_{29}, nC_{31} and nC_{33}), representing biomarkers for terrestrial plants, correlate significantly with δ^{13}C of bulk organic matter ($\delta^{13}C_{TOC}$). The latter is hence corroborated as proxy for C3-C4 vegetation changes. Furthermore, the δ^{13}C variations are higher for nC_{31} and nC_{33} than for nC_{27} and nC_{29}, indicating that the former n-alkanes mainly derive from C3 and/or C4 grasses, whereas the latter homologs mainly derive from C3 plants (trees and shrubs). Except for the lowermost part of the sediment core, the δ^{13}C values of the mid-chain alkanes nC_{23} and nC_{25} do not reflect the terrestrial δ^{13}C pattern, thus indicating that they are probably mainly of lacustrine origin.

Keywords: CSIA; n-alkanes; drift correction, amount dependence; palaeoenvironment; biomarkers.

1. Introduction

During the last decades, stable carbon isotope (δ^{13}C) analysis has become a valuable tool with a wide range of applications spanning from forensic to organic geochemistry (Benson et al., 2006; Meier-Augenstein, 1999). In palaeoenvironmental studies, one of the most utilized phenomena is the δ^{13}C difference between C3 and C4 plants, the latter being characterized by values of ~ -27‰ and ~ -13‰, respectively (Boutton, 1996). Accordingly, many authors used δ^{13}C variations in soils, sediments and loess palaeosol sequences for reconstructing C3-C4 vegetation changes during the past (Aucour et al., 1999; Freitas et al., 2001; Liu et al., 2005c; Wang and Follmer, 1998; Wang et al., 2000). However, when interpreting smaller δ^{13}C variations, changing palaeoclimatic conditions (Hatté and Guiot, 2005; Liu et al., 2005a; Stevenson et al., 2005) and isotope fractionation processes during soil organic matter (SOM) decomposition (Balesdent et al., 1993; Bol et al., 1999; Glaser and Zech, 2005; Nadelhoffer and Fry, 1988; Zech et al., submitted-b) may have to be considered as well. Recently, Chen et al. (2002) and Krull et al. (2002) even explained δ^{13}C enrichments of several per mil in tropical and subtropical soils with SOM decomposition instead of C3-C4 changes and argued with intense weathering and high organic matter turnover rates. Also Xie et al. (2004a) and Glaser and Zech (2005) pointed to the restricted utility of δ^{13}C of bulk SOM (δ^{13}C$_{TOC}$) as proxy for palaeovegetation and hence questioned the reliability of reconstructed C3-C4 vegetation changes when based on δ^{13}C$_{TOC}$. Concerning the responsible mechanisms for isotope fractionation during SOM decomposition, Balesdent and Mariotti (1998) suggested a model, in which ^{13}C-depleted or -enriched carbon pools are differently prone to decay. Hence, more reliable δ^{13}C input signatures may be derived from individual C pools such as n-alkanes.

n-Alkanes are important constituents of natural waxes (Kolattukudy, 1976). As they are highly resistant to biochemical degradation and diagenesis (Cranwell, 1981), they can be found e.g. in terrestrial and lacustrine sediments where they may serve as biomarkers: Long-chain homologs (> nC$_{27}$) with a strong odd-over-even predominance (OEP) are characteristic for higher plant leaf waxes, short-chain homologs (nC$_{15}$-nC$_{19}$) indicate aquatic sources (Bourbonniere et al., 1997; Meyers and Ishiwatari, 1993). Furthermore, nC$_{31}$ and nC$_{33}$ were mainly found in grasses and herbs, whereas nC$_{27}$ and nC$_{29}$ were reported to dominate in trees and shrubs (Cranwell, 1973; Farrimond and Flanagan, 1996; Nott et al., 2000; Schwark et al., 2002; Zech et al., submitted-a). Combining δ^{13}C with n-alkane analysis may have even more potential.

Since the commercial availability of facilities for compound-specific stable isotope ratio measurements such as GC-C-IRMS systems, $\delta^{13}C$ values for individual n-alkanes have been reported in numerous studies, mainly focusing on SOM characterization and on reconstruction of palaeoenvironments and palaeoclimate (Collister et al., 1994; Glaser and Zech, 2005; Lichtfouse et al., 1998; Street-Perrott et al., 2004; Xie et al., 2004b; Yamada and Ishiwatari, 1999; Zhang et al., 2003). Unfortunately, often little information is given about desirable $\delta^{13}C$ corrections concerning for instance "amount dependence", although the latter analytical problem for compound-specific $\delta^{13}C$ measurements was already reported by several authors (e.g. Glaser and Amelung, 2002; Hall et al., 1999). However, if such corrections are not made, data interpretation may give misleading results.

The objectives of this study were therefore to improve the compound-specific $\delta^{13}C$ analysis of n-alkanes and to apply this method to samples from a palaeoenvironmental study in order to validate n-alkanes as terrestrial plant-derived biomarkers. Specifically, we aimed at (i) optimizing the sample preparation for n-alkanes from sediment samples, (ii) introducing correction factors for $\delta^{13}C$ drifts occurring during individual measurements, (iii) introducing correction factors for amount dependence of $\delta^{13}C$ measurements as determined by co-analyzing standards of varying analyte concentrations, and (iii) comparing the $\delta^{13}C$ values of individual n-alkanes with $\delta^{13}C_{TOC}$.

2. Materials and Methods

2.1 n-Alkane standards

For method evaluation and calibration of the $\delta^{13}C$ results we used n-alkane standard solutions (nC_8-nC_{20} and nC_{21}-nC_{40}, respectively, Fluka) and deuterated n-alkanes: n-tetracosane-d_{50} and n-eicosane-d_{42} (D, 98%, Cambridge Isotope Laboratories, Inc., USA) were added to the samples as internal standard before extraction and as recovery standard before measurement, respectively. Both standards were additionally used for calibration of measured compound-specific $\delta^{13}C$ values of n-alkanes (calibration against certified international standards via EA-IRMS). For this aim, we determined the stable carbon isotope compositions of the standard n-alkanes by continuous-flow elemental analysis (EA)-IRMS linking a Carlo Erba CN 2500 (Thermo Finnigan MAT) to a Delta^{plus} isotope ratio mass spectrometer (Thermo Finnigan MAT) via a Conflow II interface (Thermo Finnigan MAT). During these measurements, three pulses of CO_2 (99.7% purity; Riessner) were directly discharged into the isotope ratio mass spectrometer for 20 seconds as reference gas for drift

correction. Calibration was performed using the certified standards sucrose (CH-6, IAEA, Vienna, Austria, $\delta^{13}C$ = -10.47‰) and $CaCO_3$ (NBS 19, Gaithersburg, USA, $\delta^{13}C$ = +1.95‰). Also the $\delta^{13}C$ values of the deuterated alkanes n-triacontane-d_{62} and n-nonadecane-d_{40} (99.3 and 99.0 atom% D, respectively, both CDN Isotopes, Canada) were determined using EA-IRMS as outlined above. These two standards were added to the samples before GC-C-IRMS measurement and served for quality control.

2.2 Sediment samples

For the application of the CSIA method to a palaeoenvironmental study, we selected eleven sediment samples from a 4.5 m long core ("Arg. D4"), which was taken in September 2004 with a piston corer from a weakly flooded small basin located northeast of the city Oberá, Province of Misiones, NE Argentina (27°23'35''S; 55°31'52''W; 330 m a.s.l.). The color and morphological features of the core were described in the field before sub-sampling the core at 5 cm intervals for geochemical and grain size analyses. A detailed profile description and presentation of palaeoenvironmental data is given by Zech et al. (submitted-a). Important criteria for selecting samples from this location were that both the sedimentological and palaeoenvironmental history have been studied intensively and that bulk $\delta^{13}C_{TOC}$ varies in a wide range from –17.4‰ to –30.1‰. According to Zech et al. (submitted-a), biomarker (quantified n-alkanes) and $\delta^{13}C_{TOC}$ results for "Arg. D4" indicate:

- a transition from C3 tree dominance with probably also lacustrine conditions to C4 grass dominance in the lowermost stratigraphic Unit C (representing the end of the 'Inca Huasi' wet phase during the Marine Isotope Stage (MIS) 3),

- C3 grass dominance in the lower part of Unit B (representing the LGM), forest re-expansion in the middle part (beginning of the late glacial wet phase) and probably again lacustrine influence in the upper part of Unit B and

- increasing contribution of C4 grasses and/or CAM plants to the SOM in Unit A (Holocene).

The total organic carbon contents (TOC) for the selected samples range from 0.52% to 13.75% (sample 41A and 3A, respectively).

2.3 Sample preparation for n-alkane analysis

Soil samples were air-dried and sieved <2 mm. The analytical procedure for the isolation of the n-alkanes was adopted from Bourbonniere et al. (1997) and originally comprised (i) Soxhlet extraction (2 × 24 h) with azeotropic toluene/methanol after addition of

deuterated n-tetracosane (d_{50}-n-C_{24}) as internal standard, (ii) concentration of the extract and saponification of co-eluted esters, (iii) fractionation of extracted lipids on aluminum oxide/silica gel (both 5% deactivated) columns with hexane/toluene (85:15) as eluent, (iv) addition of deuterated n-eicosane (d_{42}-n-C_{20}, recovery standard) to the eluted and concentrated hydrocarbon fraction and (v) quantification of the n-alkanes by injection into an HP 6890 GC equipped with a flame ionization detector (FID). Detailed recovery, blind and spike tests showed that this method exhibits several deficiencies and suggested that analytical improvements were necessary. Specifically, we replaced the Soxhlet extraction by accelerated solvent extraction (ASE, with 9×10^6 Pa and 120°C), amended the recovery and determined possible sources of contamination.

2.4 Instrumentation

All compound-specific δ¹³C experiments and measurements were performed using a GC-C-IRMS system consisting of a Trace GC 2000 gas chromatograph (Thermo Finnigan MAT, Bremen, Germany) equipped with a split-splitless (S/SL) injector. In the latter, deactivated glass liners (5% dimethylchlorsilane in toluene for at least one week) were used without glass wool packing. Injection was performed using an autosampler (AS 2000; Thermo Finnigan MAT) with a 10 mL syringe with 70 mm needle length (IVA, Meerbusch, Germany). Chromatographic separation was conducted with a fused silica BPX5 column (60 m × 0.250 mm × 0.25 μm, SGE, Ringwood, Victoria, Australia). The temperature of the combustion and the reduction ovens were set to 940°C and 600°C, respectively. Helium (99.996% purity; Riessner, Lichtenfels, Germany) was used as carrier gas. Isotope ratios were measured using a Delta^{plus} isotope ratio mass spectrometer (Thermo Finnigan MAT).

All measurements were carried out at a constant gas flow of 1.5 mL min^{-1}. The injected amount was 3.0 mL (splitless injection, 2 min splitless time), the temperature of the injector was 300°C and the oven temperature was 120°C at the injection time. The temperature was held at 120°C for 1 min. Then it was raised to 310°C at 4°C min^{-1} and held isothermal for 80 min resulting in a total oven runtime of 128.5 min.

During all sample and standard measurements, 10 pulses of CO_2 (99.7% purity; Riessner, Lichtenfels, Germany) were directly discharged into the isotope ratio mass spectrometer for 20 seconds as reference gas ("ref" in Fig. 6-1) for the calculation of relative δ¹³C values and drift correction during measurements
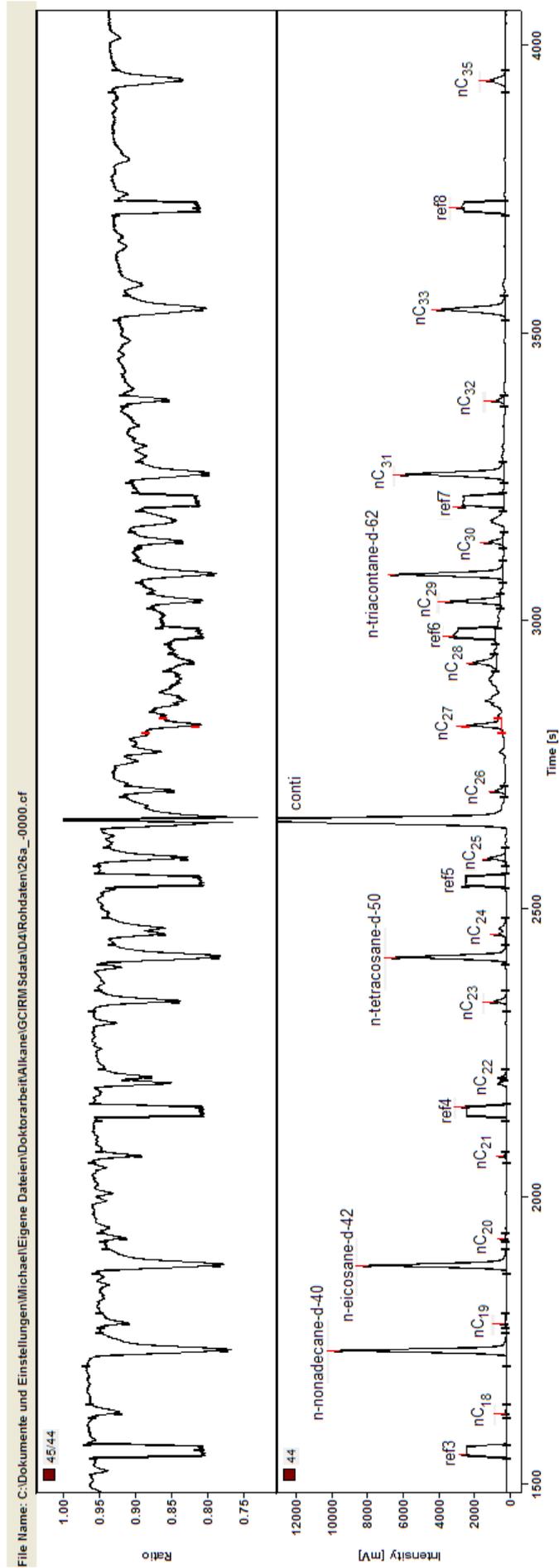
Fig. 6-1: Typical GC-C-IRMS chromatogram for individual n-alkanes, internal standards and reference gas (ref) of a sediment sample with m/z 44 intensity given below and m/z ratio 45/44 given above.

2.5 Optimization of the GC-C-IRMS results

In contrast to conventional dual inlet systems and IRMS systems connected to an elemental analyzer (EA), direct calibration and testing of a GC-C-IRMS system with a primary standard is not possible (Werner and Brand, 2001). Furthermore, GC-C-IRMS technique is prone to unintended isotope fractionation in many parts of the system and at many steps of the analytical procedure. In the sequence of analysis these potential isotope fractionation factors can occur during (i) sample preparation and derivatization, (ii) injection, (iii) chromatography, (iv) combustion, (v) open split passage, (vi) ionization in the IRMS, (vii) the procedure of calibration with external and internal standards, and (viii) peak integration and calculation of the $\delta^{13}C$ value (Schmitt et al., 2003).

An advantage when focusing on n-alkanes as analytes is the fact that isotope fractionation during derivatization does not need to be considered, as n-alkanes are already GC-compatible. However, relatively high temperatures and long run times are necessary and may involve errors. We found that (i) marked $\delta^{13}C$ drifts occurred during individual measurements and (ii) amount dependence of the $\delta^{13}C$ values adulterated our compound-specific isotope results. In order to improve the reliability of the $\delta^{13}C$ results we developed and carried out respective correction factors. These corrections are however independent from chromatographic optimization concerning for instance split ratio and/or oven temperature program, which have to be adjusted additionally to guaranty optimal peak separation.

3. Results and Discussion

3.1 Optimized sample preparation

Recovery tests revealed that ~70% of the internal standard were lost between saponification and column fractionation. In more detail, the analytical steps in-between comprised firstly heating of the concentrated Soxhlet extract in 1 mL of 0.5M KOH in methanol (100°C for 10 minutes in 5 mL reactivials^{TM}), secondly cooling to room temperature and thirdly addition of 1 mL saturated NaCl solution. Finally, the hydrocarbons were extracted with 1 mL of hexane and added on the columns for purification of the n-alkanes. In further tests the liquid-liquid extraction with hexane turned out to be much more efficient if the preceding NaCl addition was omitted. Additionally, losses of the internal standard were reduced by extracting twice with 3 mL of hexane. Recovery with this improved method yielded generally >80% for the investigated sediment samples.
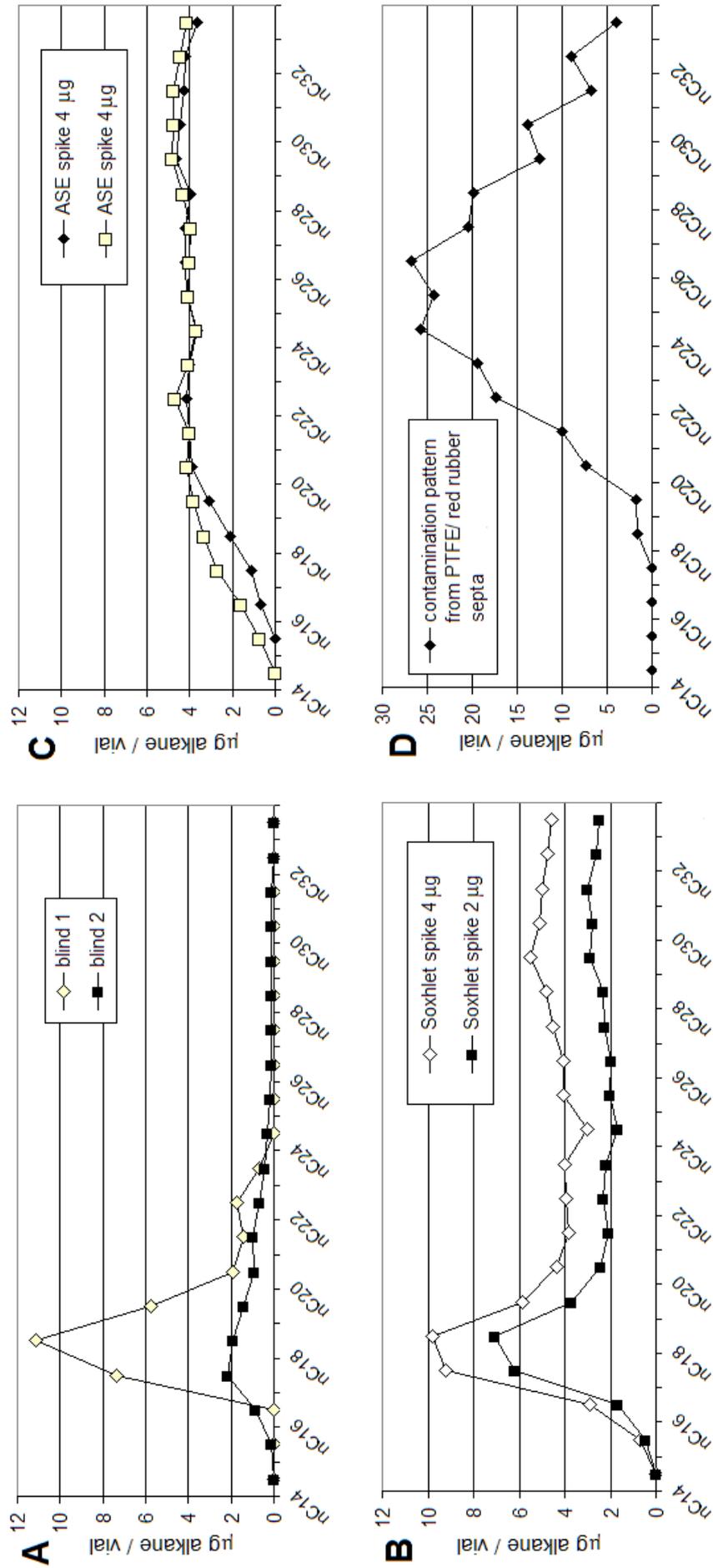
Fig. 6-2: Blind and spike tests for Soxhlet extraction (A and B, respectively) and (C) accelerated solvent extraction (ASE). (D) Contamination pattern of PTFE/red rubber septa.

Blind and spike tests showed that a contamination with short-chain n-alkanes, especially with the homologs nC_{17}, nC_{18} and nC_{19}, occurred during the sample preparation (Fig. 6-2A and 6-2B). This contamination occurred in the Soxhlet extraction step and ranged from 2 μg/vial up to 10 μg/vial for the individual n-alkanes. We assume that the cellulose extraction timbles (Schleicher & Schuell, Whatman) caused this contamination. Although it could have been circumvented by pre-rinsing the cellulose filters with an organic solvent or by using heated glass fibre extraction timbles, the Soxhlet extraction was time-consuming anyway and we therefore tested the applicability of an accelerated solvent extractor instead (Dionex ASE 200). The rest of the analytical procedure remained the same as described above. Although we found no contamination during ASE extraction, spike tests revealed that the recovery for the short-chain homologs remained unsatisfactory (Fig. 6-2C). These results suggest considerable caution when interpreting (i) the n-alkane ratio (nC_{27} + nC_{29} + nC_{31})/(nC_{15} + nC_{17} + nC_{19}) in terms of "terrestrial vs. aquatic" proxy as proposed by Bourbonniere et al. (1997) and Meyers and Ishiwatari (1993) and (ii) the compound-specific δ^{13}C results of "aquatic" n-alkanes, if respective recovery and blind tests are lacking. In the following, we used the ASE method as it was more convenient and only focused on the reliably extracted mid- and long-chain homologs.

Finally, we found that also a contamination of the samples with compounds from the crimp cap septa for the GC vials has to be considered. This contamination is septa- and time-dependent. The former is important because the initially used caps with clear PTFE/red rubber septa (Agilent Technologies) cause a contamination with long-chain n-alkanes as soon as the PTFE coating is pierced during the first injection (Fig. 6-2D). The time dependence is of relevance, because in order to reduce shift effects during quadruplicate GC-C-IRMS measurements, the samples were not injected one by one fourfold at once, but the whole sequence containing all standards and all samples was repeated. This procedure resulted in intervals of up to several days for one sample until it was measured again. To avoid an adulteration of our isotope results, we alternatively used black viton septa, which we put in hexane for at least one week. Despite the fact that also these septa caused contamination (see "conti" peak and background elevation between nC_{27} and nC_{29} in Fig. 6-1), they were preferable as they did at least not contain n-alkanes.

3.2 Correction factors for the GC-C-IRMS results

3.2.1 Drift-correction with CO_2

In many GC-C-IRMS studies pure CO_2 with a (more or less) constant stable isotope composition is used for relative calibration by introducing it as reference gas at defined times during each run (Werner and Brand, 2001). CO_2 is thereby directly injected via a reference gas open split into the carrier gas stream entering the IRMS and allows on/off experiments with a minimum of fractionating processes before detection. Under stable conditions, Schmitt et al. (2003) found that standard deviations of ten replicate measurements for our IRMS system were usually <0.02‰. However, experiments with varying CO_2 pressure caused $\delta^{13}C$ shifts of >1‰.

During our measurements we often observed significant $\delta^{13}C$ shifts of the reference gas within one measurement (Fig. 6-3). This phenomenon was not observed in previous studies focusing on sugars, amino sugars, amino acids and lignin phenols (Glaser and Amelung, 2002; Glaser and Gross, 2005; Gross and Glaser, 2004; Sauheitl et al., 2005; Schmitt et al., 2003) and may be attributed to the high temperature and the long run time, which are necessary when working with hardly volatile long-chain n-alkanes. These shifts made it impossible to simply calibrate the analytes with one of the reference gas peaks or with one of the internal standards. Also a drift correction by interpolating between two or three reference gas peaks as outlined by the above mentioned authors would still have been too imprecise. We therefore discharged 10 pulses of pure CO_2 during each run (Fig. 6-3). For the subsequent calibration with the software of the workstation (Isodat NT, version 2.0, Thermo Electron), we first calculated "relative" $\delta^{13}C$ values for all peaks by calibrating against the reference gas peak "ref 2" (assigning it a $\delta^{13}C$ value of -42‰). Then we made a drift correction for each n-alkane peak by interpolating from one reference gas peak to the other and assigning each reference gas peak a $\delta^{13}C$ value of -42‰ (Fig. 6-3).

3.2.2 Correction for amount dependence

As pointed out by several authors (Glaser and Amelung, 2002; Hall et al., 1999; Schmitt et al., 2003), $\delta^{13}C$ values of individual compounds may depend on the injected sample amount. Following the suggestion of these authors, we therefore co-analyzed all alkane standards (external and internal standards) with varying concentrations and plotted the drift-corrected $\delta^{13}C$ values versus the peak areas (shown for n-tetracosane and n-eicosane in Fig. 6-4). Accordingly, polynomial functions were found to describe best the amount-dependent isotope fractionation of the standards. As for the deuterated standards (solids)
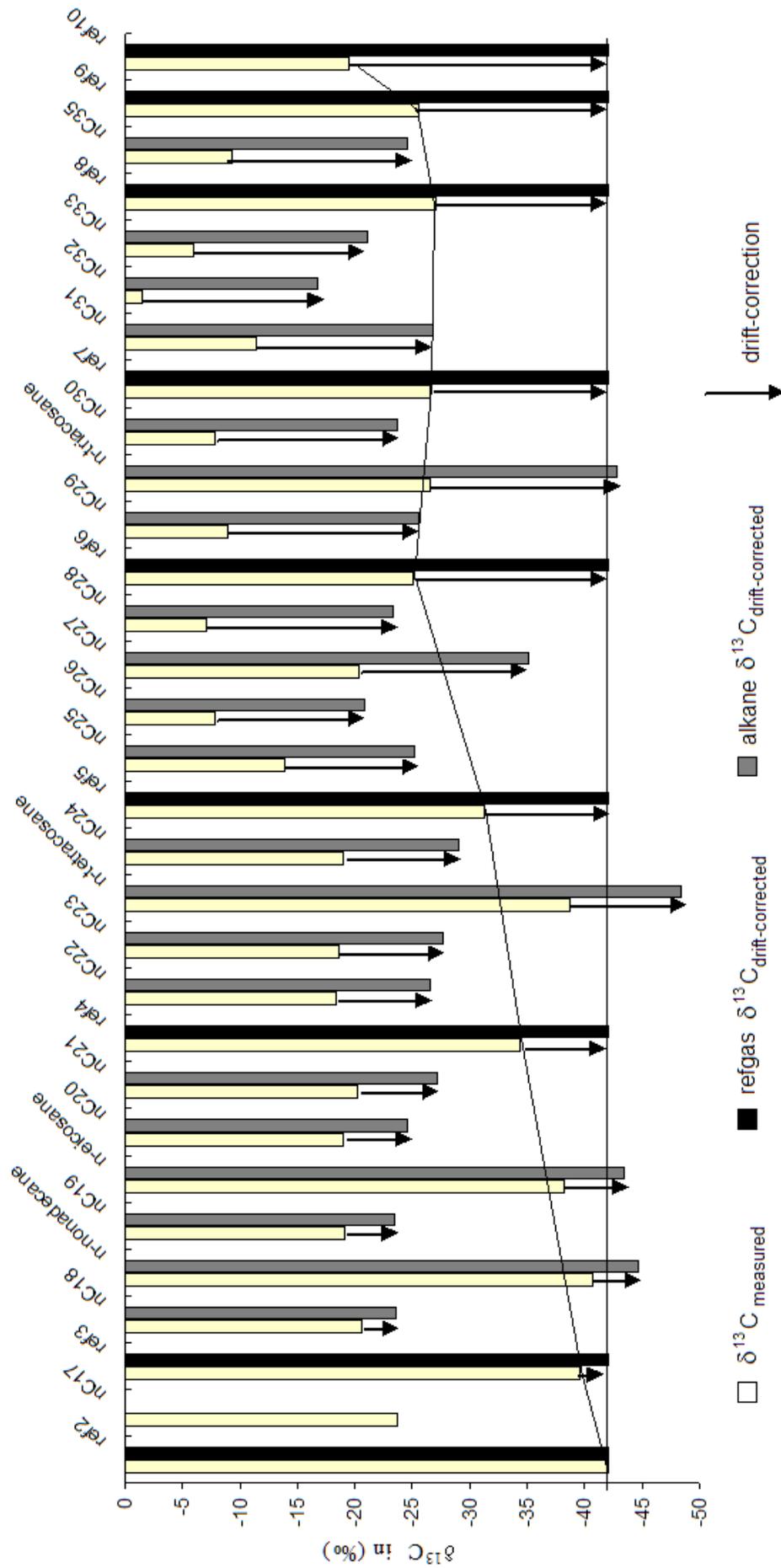
Fig. 6-3: Drift correction for a sediment sample with pure CO_2 as reference gas, which is discharged into the IRMS in regular intervals during all measurements. The solid lines illustrate the interpolation between the reference gas peaks.
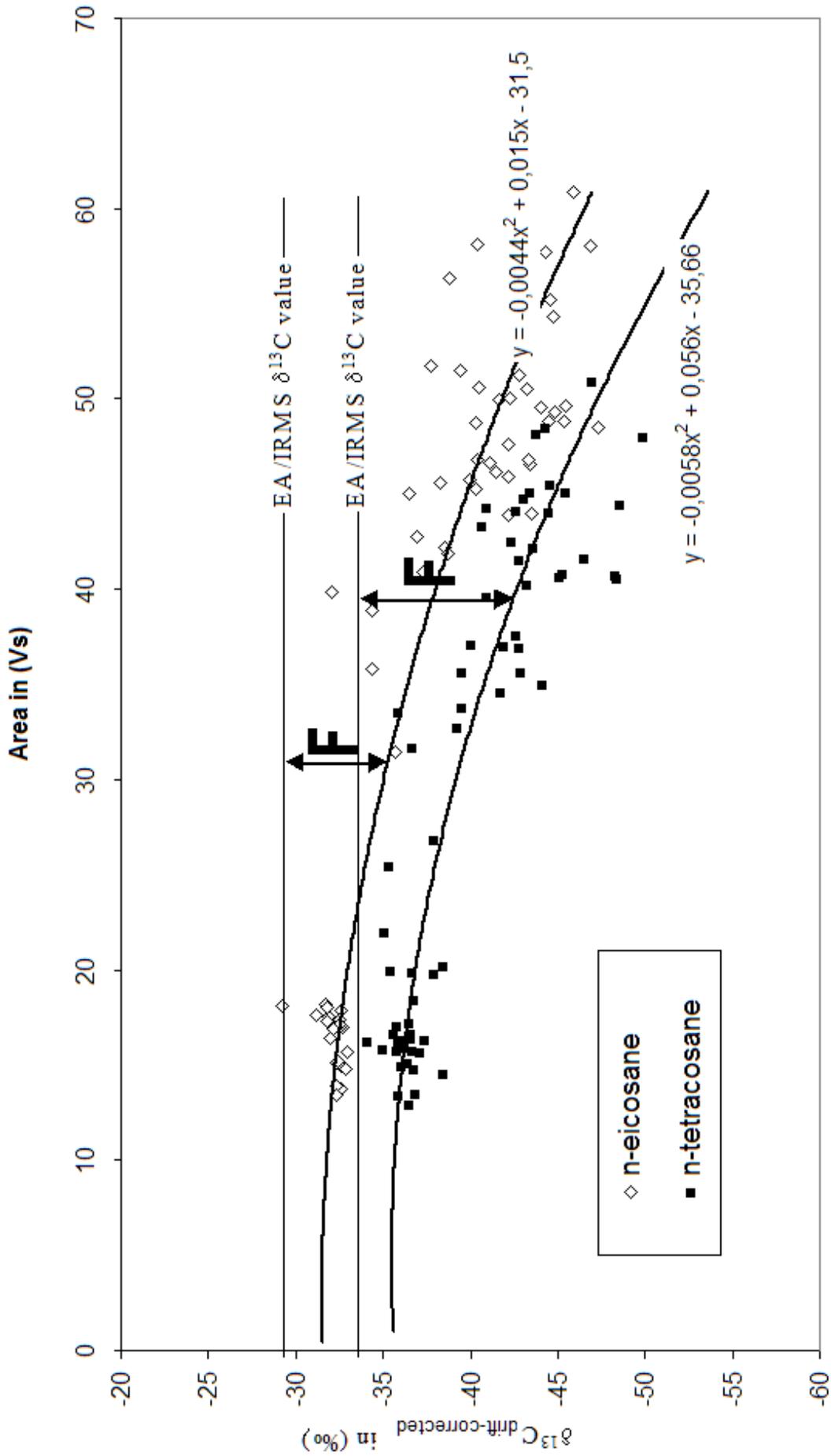
Fig. 6-4: Amount dependence of the drift-corrected GC-C-IRMS $\delta^{13}C$ values for the standards n-tetracosane-d$_{50}$ and n-eicosane-d$_{42}$. The amount-dependent correction factor "F" is the difference between the drift-corrected GC-C-IRMS $\delta^{13}C$ value and the EA-IRMS $\delta^{13}C$ value and is calculated for each analyte and in each sample individually.

absolute (EA-IRMS) δ^{13}C values were available, mathematical corrections for their drift-corrected GC-C-IRMS δ^{13}C values could be made according to Equation (1):

$$\delta^{13}\text{C}_{\text{amount-corrected}} = \delta^{13}\text{C}_{\text{drift-corrected}} - \text{F}, \tag{1}$$

where F is a term, which calculates the amount-dependent δ^{13}C difference between the drift-corrected GC-C-IRMS δ^{13}C value and the EA-IRMS δ^{13}C value for a certain alkane (Fig. 6-4).

On the other hand, EA-IRMS measurements with the liquid n-alkane standard solutions nC_8-nC_{20} and nC_{21}-nC_{40} were not possible. However, we estimated their EA-IRMS δ^{13}C values by assuming that the y-axis intersection points of their polynomial functions are ~2‰ more negative than their EA-IRMS δ^{13}C values (likewise as the deuterated standards, see Fig. 6-4). Hence, mathematical corrections for the amount-dependent isotope fractionation could be outlined for all standards and all analytes.

3.2.3 Calibration against certified standards

The drift- and amount-corrected δ^{13}C values were still "relative" δ^{13}C values and not yet calibrated against certified standards. As the "absolute" δ^{13}C values of the deuterated internal and recovery standards have been determined *ex ante* by EA-IRMS measurements, we could calculate a correction factor for the difference between $\delta^{13}\text{C}_{\text{deut.Std.}}$ (EA) and $\delta^{13}\text{C}_{\text{deut.Std.}}$ (GC) – the latter already being drift- and amount-corrected – according to Equation (2):

$$\Delta_{\text{deut.Std.}} = \delta^{13}\text{C}_{\text{deut.Std.}}\,(\text{EA}) - \delta^{13}\text{C}_{\text{deut.Std.}}\,(\text{GC}) \tag{2}$$

Absolute δ^{13}C values for all n-alkanes could then be calculated according to Equation (3) (Barrie and Prasser, 96):

$$\delta^{13}\text{C}_{\text{alkane}} = \delta^{13}\text{C}_{\text{alkane}}\,(\text{GC}) + \Delta_{\text{deut.Std.}} + \frac{(\delta^{13}\text{C}_{\text{alkane}}\,(\text{GC}) \times \Delta_{\text{deut.Std.}})}{1000} \tag{3}$$

where $\delta^{13}\text{C}_{\text{alkane}}$ (GC) = drift- and amount-corrected δ^{13}C value of the individual alkanes.

For our 11 palaeoenvironmental samples we calibrated all n-alkanes both against the standards n-tetracosane and n-eicosane and then calculated the mean of both in order to increase the accuracy of the δ^{13}C values.

3.2.4 Accuracy and precision of δ^{13}C values of individual n-alkanes obtained by GC-C-IRMS measurements

As the deuterated standards n-nonadecane and n-triacontane were added to all samples, they could be used as quality standards. Their respective EA-IRMS measurements (calibration against certified standards) gave δ^{13}C values of -28.47 ± 0.05‰ and -33.34 ± 0.06‰, respectively. On the other hand, GC-C-IRMS measurements revealed drift-corrected and calibrated δ^{13}C values of -34.57 ± 0.67‰ and -30.54 ± 0.46‰, respectively, thus accuracy was unsatisfying. Only when the δ^{13}C values were additionally corrected for amount dependence (Fig. 6-4), accuracy improved significantly to -29.44 ± 0.38‰ and −35.35 ± 0.47‰ for n-nonadecane-d_{40} and n-triacontane-d_{62}, respectively. Although the optimized GC-C-IRMS method yielded δ^{13}C values that are still too negative, correction for amount dependence gave results that were much closer to the accurate EA-IRMS values than uncorrected results (difference of 0.87‰ and 2.01‰ versus 5.91‰ and 2.80‰ for n-nonadecane-d_{40} and n-triacontane-d_{62}, respectively). This finding suggests considerable caution when interpreting published δ^{13}C values of n-alkanes, which lack information on accomplished correction procedures.

Standard errors for the quadruplicate measurements of the analytes in the sediment samples from Arg. D4 range from 0.27 − 2.83‰ and are given in Table 6-1 and shown in Fig. 6-5.

Table 6-1: Drift- and amount-corrected δ^{13}C values (‰) ± standard error for individual n-alkanes from the sediment core Arg. D4 after calibration against d_{50}-n-C_{24} and d_{42}-n-C_{20}.

Sample	nC_{23}	nC_{25}	nC_{27}	nC_{29}	nC_{31}	nC_{33}
3A	-26.59 ± 2.19	-25.67 ± 1.57	-27.01 ± 2.70	-22.64 ± 2.56	-25.41 ± 2.21	-21.59 ± 1.32
8A	-28.01 ± 2.17	-23.92 ± 1.81	-24.81 ± 1.58	-20.48 ± 1.54	-22.24 ± 0.75	-18.99 ± 1.56
12A	-27.95 ± 1.80	-28.50 ± 2.72	-27.82 ± 1.83	-26.98 ± 1.55	-29.97 ± 1.72	-28.36 ± 1.71
18A	-27.03 ± 1.43	-26.03 ± 1.04	-28.76 ± 1.33	-28.11 ± 1.01	-28.20 ± 1.12	-26.14 ± 1.32
22A	-29.24 ± 0.89	-25.85 ± 1.16	-28.84 ± 0.58	-26.86 ± 0.27	-28.39 ± 0.63	-23.13 ± 0.62
26A	-29.22 ± 1.75	-29.35 ± 1.57	-30.21 ± 1.43	-29.74 ± 1.01	-32.89 ± 0.99	-27.29 ± 2.14
29A	-31.32 ± 1.82	-29.09 ± 0.72	-29.50 ± 1.61	-29.28 ± 1.67	-30.62 ± 1.43	-27.41 ± 2.19
34A	-30.84 ± 1.46	-27.83 ± 2.21	-29.47 ± 1.24	-26.94 ± 1.83	-27.16 ± 1.12	-25.55 ± 1.43
36A	-29.17 ± 2.83	-25.63 ± 1.24	-27.17 ± 1.66	-26.82 ± 1.04	-25.28 ± 0.93	-22.47 ± 1.20
40A	-34.38 ± 1.38	-30.30 ± 1.21	-32.96 ± 0.61	-35.73 ± 0.71	-40.49 ± 0.95	-37.71 ± 1.33
41A	-36.17 ± 0.72	-34.39 ± 2.55	-34.79 ± 1.51	-35.41 ± 2.65	-37.57 ± 0.79	-37.77 ± 0.66
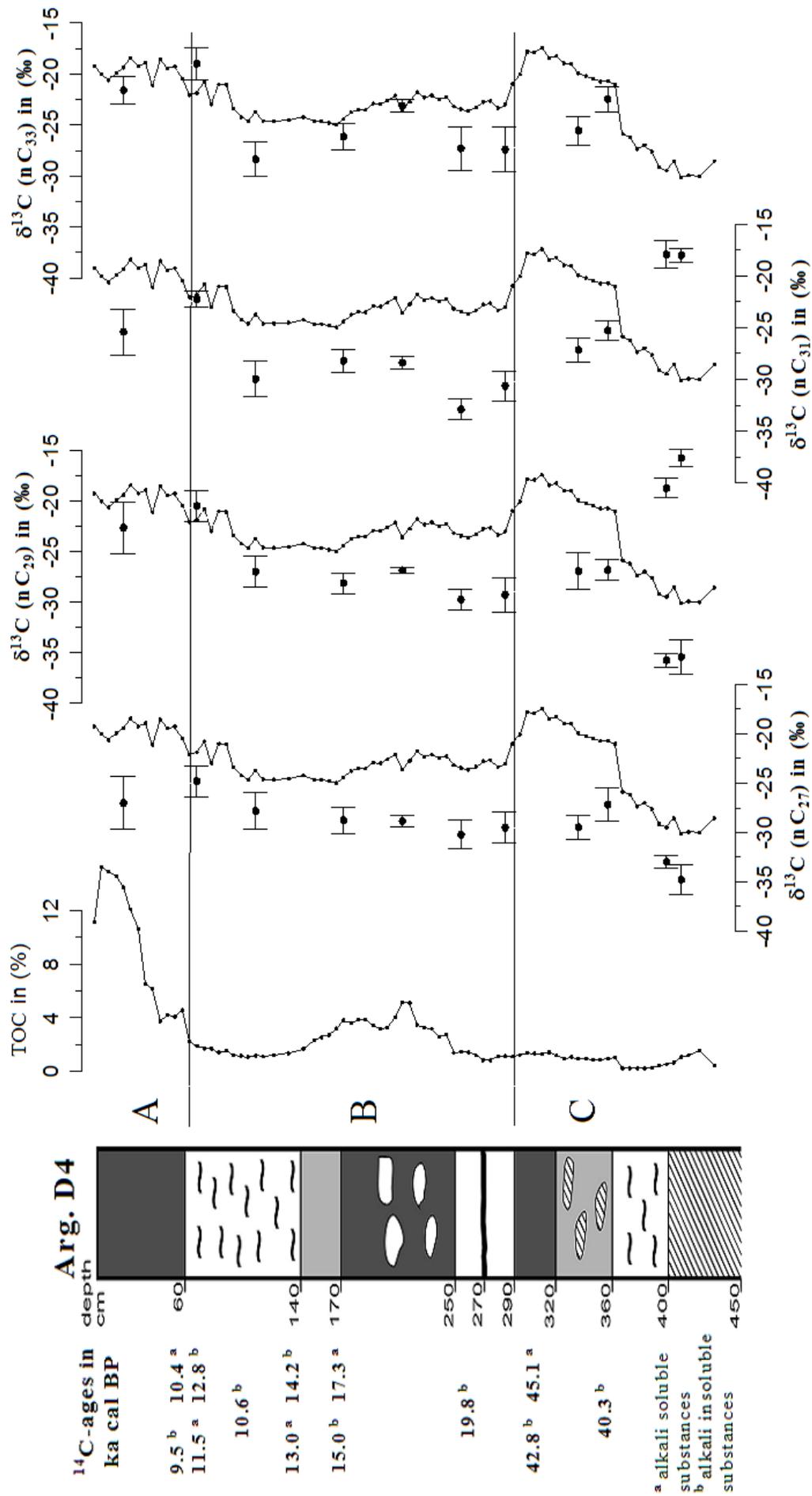
Fig. 6-5: Stratigraphy of the sediment core "Arg. D4" (from Zech et al., submitted-a) and δ¹³C values of individual terrestrial plant-derived n-alkanes (circles with error bars) in comparison with δ¹³C$_{TOC}$ (solid lines). Capital letters to the right of the profile indicate stratigraphic units.

3.3 Interpretation of $\delta^{13}C$ values of individual n-alkanes in the sediment core Arg. D4

Table 6-1 informs about the $\delta^{13}C$ values of the individual n-alkanes obtained for the 11 selected sediment samples from core "Arg. D4". Additionally, the $\delta^{13}C$ values for the long-chain n-alkanes nC_{27}, nC_{29}, nC_{31} and nC_{33} are plotted versus profile depth along with bulk $\delta^{13}C_{TOC}$ in Fig. 6-5. It is obvious that the $\delta^{13}C$ values of the individual n-alkanes corroborate the major $\delta^{13}C_{TOC}$ variations. Correlation coefficients range from 0.82 (nC_{27}) to 0.89 (nC_{33}). This is in agreement with findings from Chinese loess-palaeosol sequences (Liu et al., 2005b) and suggests that $\delta^{13}C_{TOC}$ in our sediment core is poorly adulterated by SOM decomposition and may hence be interpreted as proxy for C3-C4 vegetation changes as practiced by Zech et al. (submitted-a).

Fig. 6-5 also reveals that n-alkanes are isotopically depleted in comparison to bulk SOM. Also this is in agreement with findings from other authors (Glaser, 2005; Glaser and Zech 2005; van Dongen et al., 2002) and confirms that a selective removal of certain ¹³C-enriched or -depleted carbon pools principally has to be considered when interpreting $\delta^{13}C_{TOC}$ variations in soils and sediments.
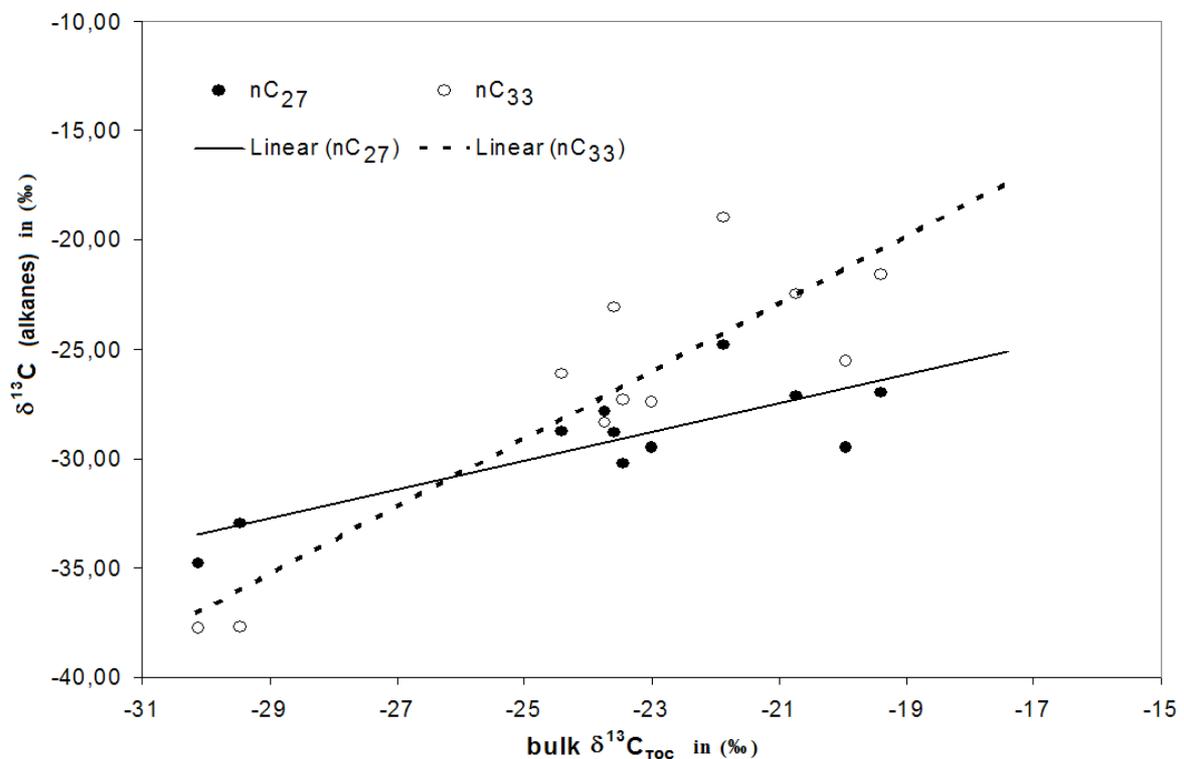
Fig. 6-6: Relationship between $\delta^{13}C_{TOC}$ and $\delta^{13}C$ of individual n-alkanes. Steeper trend lines for nC_{31} and nC_{33} than for nC_{27} and nC_{29} indicate higher sensitivity of the former n-alkanes to C3-C4 vegetation changes.

Furthermore, individual the n-alkanes exhibit variable amplitudes in their $\delta^{13}C$ variations, ranging from ~ –25‰ to -35‰ (nC_{27}), ~ -20‰ to -36‰ (nC_{29}), ~ -22‰ to -40‰ (nC_{31}) and ~ -19‰ to -38‰ (nC_{33}). This is also illustrated in Fig. 6-6 (steeper trendline for nC_{33} compared to nC_{27}) and can be explained with different origins of individual n-alkanes as indicated by Zech et al. (submitted-a): Whereas nC_{27} and nC_{29} mainly derived from trees and shrubs, i.e. from C3 plants, nC_{31} and nC_{33} mainly derived from grasses and herbs, i.e. from C3 and/or C4 plants. The longer-chain n-alkanes are therefore particularly sensitive biomarkers for detecting C3-C4 vegetation changes.

The $\delta^{13}C$ values of the mid-chain alkanes nC_{23} and nC_{25} (data not shown) – the latter originating from terrestrial plants, submerged lacustrine plants and microorganisms – only confirm the distinct $\delta^{13}C_{TOC}$ and $\delta^{13}C_{\text{long-chain alkanes}}$ shifts in Unit C. For the rest of the profile they show a poor correlation with $\delta^{13}C_{TOC}$ (R = -0.03 and R = 0.29, respectively, in comparison to R > 0.51 for nC_{29}, nC_{31} and nC_{33}). This indicates that the alkanes nC_{23} and nC_{25} are not suitable proxies for tracing C3-C4 vegetation changes. As the notably negative $\delta^{13}C$ values in the lower part of Unit C are reflected in both bulk SOM and all individual n-alkanes (and also in neutral sugars, own unpublished data) originating from different sources, they can only partly be explained with C3-C4 vegetation changes. Hence, other palaeoenvironmental factors influencing the reported $\delta^{13}C$ record in unit C need to be considered. For instance, $\delta^{13}C$ in C3 plants is well known to be species-dependent and to become more negative when water stress plays no role and/or when atmospheric CO_2 partial pressure is high. A more detailed interpretation (e.g. that the lowermost part of Unit C might correspond to the last interglacial) remains however speculative.

4. Conclusions

In this study we presented an optimized method for CSIA of individual n-alkanes in soils and sediments. Our CSIA results for n-alkanes suggest that measured $\delta^{13}C$ values should be corrected before calibration against a standard: Firstly, we propose a drift-correction with regularly introduced CO_2 pulses as reference gas, secondly, we propose a correction for the amount dependence of the GC-C-IRMS results by co-analyzing standards with varying analyte concentrations. The latter correction is especially important when focusing on palaeoenvironmental samples with often strongly varying analyte concentrations. Finally,

calibration against two instead of one internal standard should further improve the accuracy of $\delta^{13}C$ values.

The $\delta^{13}C$ values of all plant-derived long-chain n-alkanes in the investigated sediment core "Arg. D4" correlate significantly with $\delta^{13}C_{TOC}$. This finding suggests that $\delta^{13}C_{TOC}$ is poorly adulterated by SOM decomposition and may be used as proxy for reconstructing C3-C4 vegetation changes. However, this might not be the case in other soils or sediments with a higher SOM decomposition overprint. Furthermore, $\delta^{13}C$ variations of the alkanes nC_{31} and nC_{33} are distinctly larger than those of the alkanes nC_{27} and nC_{29}. This corroborates that the former n-alkanes mainly derive from C3 and/or C4 grasses, whereas the latter ones mainly originate from C3 plants. $\delta^{13}C$ values of mid-chain n-alkanes poorly correlate with $\delta^{13}C_{TOC}$, corroborating an origin from submerged plants.

Future work should focus on optimizing the method also for the short-chain n-alkanes and on analyzing also deuterium in alkanes, the latter being a promising complementary palaeoclimatic proxy (Sachse et al., 2004; Sauer et al., 2001).

Acknowledgements

References

Aucour, A.-M., Hillaire-Marcel, C. and Bonnefille, R., 1999. Sources and accumulation rates of organic carbon in an equatorial peat bog (Burundi, East Africa) during the Holocene: carbon isotope constraints. Palaeogeography, Palaeoclimatology, Palaeoecology, 150: 179-189.

Balesdent, J., Girardin, C. and Mariotti, A., 1993. Site-related $\delta^{13}C$ of tree leaves and soil organic matter in a temperate forest. Ecology, 74(6): 1713-1721.

Balesdent, J. and Mariotti, A., 1998. Measurement of SOM turnover using ^{13}C natural abundance. In: S. Yamasaki (Editor), Mass spectrometry of soils. Marcel Dekker, Inc., New York.

Benson, S., Lennard, C., Maynard, P. and Roux, C., 2006. Forensic applications of isotope ratio mass spectrometry - A review. Forensic Science International, 157: 1-22.

Bol, R.A., Harkness, D.D., Huang, Y. and Howard, D.M., 1999. The influence of soil processes on carbon isotope distribution and turnover in the British uplands. European Journal of Soil Science, 50: 41-51.

Bourbonniere, R.A., Telford, S.L., Ziolkowski, L.A., Lee, J., Evans, M.S. and Meyers, P.A., 1997. Biogeochemical marker profiles in cores of dated sediments from large north American lakes. In: R.P. Eganhouse (Editor), Molecular Markers in Environmental Geochemistry. Acs Symposium Series, Washington D.C., pp. 133-150.

Boutton, T.W., 1996. Stable Carbon Isotope Ratios of Soil Organic Matter and Their Use as Indicators of Vegetation and Climate Change. In: T.W. Boutton and S. Yamasaki (Editors), Mass Spectrometry of Soils. Marcel Dekker, Inc., New York, pp. 47-82.

Chen, Q., Shen, C., Peng, S., Sun, Y., Yi, W., Li, Z. and Jiang, M., 2002. Soil organic matter turnover in the subtropical mountainous region of south China. Soil Science, 167(6): 401-415.

Collister, J.W., Rieley, G., Stern, B., Eglinton, G. and Fry, B., 1994. Compound-specific δ^{13}C analyses of leaf lipids from plants with differing carbon dioxide metabolism. Organic Geochemistry, 21: 619-627.

Cranwell, P.A., 1973. Chain-length distribution of n-alkanes from lake sediments in relation to post-glacial environmental change. Freshwater Biology, 3: 259-265.

Cranwell, P.A., 1981. Diagenesis of free and bound lipids in a terrestrial detritus deposited in a lacustrine sediment. Organic Geochemistry, 3: 79-89.

Farrimond, P. and Flanagan, R.L., 1996. Lipid stratigraphy of a Flandrian peat bed (Northumberland, UK): comparison with the pollen record. The Holocene, 6(1): 67-74.

Freitas, H.A., Pessenda, L.C., Aravena, R., Gouveia, S.E., Ribeiro, A.S. and Boulet, R., 2001. Late Quaternary Vegetation Dynamics in the Southern Amazon Basin Inferred from Carbon Isotopes in Soil Organic Matter. Quaternary Research, 55: 39-46.

Glaser, B., 2005. Compound-specific stable-isotope (δ^{13}C) analysis in soil science. Journal of Plant Nutrition and Soil Science, 168: 633-648.

Glaser, B. and Amelung, W., 2002. Determination of ^{13}C natural abundance of amino acid enantiomers in soil: methodological considerations and first results. Rapid Communications in Mass Spectrometry, 16: 891-898.

Glaser, B. and Gross, S., 2005. Compound-specific δ^{13}C analysis of individual amino sugars - a tool to quantify timing and amount of soil microbial residue stabilization. Rapid Communications in Mass Spectrometry, 19: 1409-.

Glaser, B. and Zech, W., 2005. Reconstruction of climate and landscape changes in a high mountain lake catchment in the Gorkha Himal, Nepal during the Late Glacial and Holocene as deduced from radiocarbon and compound-specific stable isotope analysis of terrestrial, aquatic and microbial biomarkers. Organic Geochemistry, 36: 1086-1098.

Gross, S. and Glaser, B., 2004. Minimization of carbon addition during derivatization of monosaccharides for compound-specific δ^{13}C analysis in environmental research. Rapid Communications in Mass Spectrometry, 18: 2753-2764.

Hall, J.A., Barth, J.A.C. and Kalin, R.M., 1999. Routine Analysis by High Precision Gas Chromatography/Mass Selective Detector/Isotope Ratio Mass Spectrometry to 0.1 Parts Per Mil.

Hatté, C. and Guiot, J., 2005. Palaeoprecipitation reconstruction by inverse modelling using the isotopic signal of loess organic matter: application to the Nußloch loess sequence (Rhine Valley, Germany). Climate Dynamics, 25: 315-327.

Kolattukudy, P.E., 1976. Biochemistry of plant waxes. In: Kolattukudy (ed.), Chemistry and Biochemistry of Natural Waxes, Amsterdam: Elsevier, 290-349.

Krull, E.S., Bestland, E.A. and Gates, W.P., 2002. Soil organic matter decomposition and turnover in a tropical ultisol: evidence from δ^{13}C, δ^{15}N and geochemistry. Radiocarbon, 44(1): 93-112.

Lichtfouse, E., Chenu, C., Baudin, F., Leblond, C., Silva, M., Behar, F., Derenne, S., Largeau, C., Wehrung, P. and Albrecht, P., 1998. A novel pathway of soil organic matter formation by selective preservation of resistant straight-chain biopolymers: chemical and isotope evidence. Organic Geochemistry, 28(6): 411-415.

Liu, W., Feng, X., Ning, Y., Zhang, Q., Cao, Y. and An, Z., 2005a. $\delta^{13}C$ variation of C3 and C4 plants across an Asian monsoon rainfall gradient in arid northwestern China. Global Change Biology, 11: 1094-1100.

Liu, W., Huang, Y., An, Z., Clemens, S.C., Li, L., Prell, W.L. and Ning, Y., 2005b. Summer monsoon intensity controls C_4/C_3 plant abundance during the last 35 ka in the Chinese Loess Plateau: Carbon isotope evidence from bulk organic matter and individual leaf waxes. Palaeogeography, Palaeoclimatology, Palaeoecology, 220: 243-254.

Liu, W., Yang, H., Cao, Y., Ning, Y., Li, L., Zhou, J. and An, Z., 2005c. Did an extensive forest ever develop on the Chinese Loess Plateau during the past 130 ka?: a test using soil carbon isotopic signatures. Applied Geochemistry, 20: 519-527.

Meier-Augenstein, W., 1999. Applied gas chromatography coupled to isotope ratio mass spectrometry. Journal of Chromatography A, 842: 351-371.

Meyers, P.A. and Ishiwatari, R., 1993. Lacustrine organic geochemistry - An overview of indicators of organic matter sources and diagenesis in lake sediments. Organic Geochemistry, 20: 867-900.

Nadelhoffer, K.J. and Fry, B., 1988. Controls on natural Nitrogen-15 and Carbon-13 abundances in soil organic matter. Soil Sci. Soc. Am. J., 52: 1633-1640.

Nott, C.J., Xie, S., Avsejs, L.A., Maddy, D., Chambers, F.M. and Evershed, R.P., 2000. n-Alkane distribution in ombrotrophic mires as indicators of vegetation change related to climatic variation. Organic Geochemistry, 31: 231-235.

Sachse, D., Radke, J. and Gleixner, G., 2004. Hydrogen isotope ratios of recent lacustrine sedimentary n-alkanes record modern climate variability. Geochimical et Cosmochimica Acta, 68(23): 4877-4889.

Sauer, P.E., Eglinton, T., Hayes, J.M., Schimmelmann, A. and Sessions, A., 2001. Compound-specific D/H ratios of lipid biomarkers from sediments as a proxy for environmental and climatic conditions. Geochimical et Cosmochimica Acta, 65(2): 213-222.

Sauheitl, L., Glaser, B. and Bol, R.A., 2005. Short-term dynamics of slurry-derived plant and microbial sugars in a temperate grassland soil as assessed by compound-specific $\delta^{13}C$ analyses. Rapid Communications in Mass Spectrometry, 19: 1437-1446.

Schmitt, J., Glaser, B. and Zech, W., 2003. Amount-dependent isotopic fractionation during compound-specific isotope analysis. Rapid Communications in Mass Spectrometry, 17: 970-977.

Schwark, L., Zink, K. and Lechtenbeck, J., 2002. Reconstruction of postglacial to early Holocene vegetation history in terrestrial Central Europe via cuticular lipid biomarkers and pollen records from lake sediments. Geology, 30(5): 463-466.

Stevenson, B.A., Kelly, E.F., McDonald, E.V. and Busacca, A.J., 2005. The stable carbon isotope composition of soil organic carbon and pedogenic carbonates along a bioclimatic gradient in the Palouse region, Washington State, USA. Geoderma, 124: 37-47.

Street-Perrott, F.A., Ficken, K.J., Huang, Y. and Eglinton, G., 2004. Late Quaternary changes in carbon cycling on Mt. Kenya, East Africa: an overview of the $\delta^{13}C$ record in lacustrine organic matter. Quaternary Science Reviews, 23: 861-879.

van Dongen, B.E., Schouten, S. and Sinninghe Damasté, J.S., 2002. Carbon isotope variability in monosaccharides and lipids of aquatic algae and terrestrial plants. Marine Ecology Progress Series, 232: 83-92.

Wang, H. and Follmer, L.R., 1998. Proxy of monsoon seasonality in carbon isotopes from paleosols of the southern Chinese Loess Plateau. Geology, 26(11): 987-990.

Wang, H., Follmer, L.R. and Liu, C.-L.J., 2000. Isotope evidence of paleo-El Niño-Southern Oscillation cycles in loess-paleosol record in the central United States. Geology, 28(9): 771-774.

Werner, R.A. and Brand, W.A., 2001. Referencing strategies and techniques in stable isotope ratio analysis. Rapid Communications in Mass Spectrometry, 15: 501-519.

Xie, S., Guo, J., Huang, J., Chen, F., Wang, H. and Farrimond, P., 2004a. Restricted utility of δ^{13}C of bulk organic matter as a record of paleovegetation in some loess–paleosol sequences in the Chinese Loess Plateau. Quaternary Research, 62: 86-93.

Xie, S., Nott, C.J., Avsejs, L.A., Maddy, D., Chambers, F.M. and Evershed, R.P., 2004b. Molocular and isotopic stratigraphy in an ombotrophic mire for paleoclimate reconstruction. Geochimical et Cosmochimica Acta, 68(13): 2849-2862.

Yamada, K. and Ishiwatari, R., 1999. Carbon isotopic composition of long-chain n-alkanes in the Japan Sea sediments: implications for paleoenvironmental changes over the past 85 kyr. Organic Geochemistry, 30: 367-377.

Zech, M., Zech, R., de Morrás, H., Moretti, L. and Glaser, B., submitted-a. Late Quaternary environmental changes in Misiones, subtropical NE Argentina, deduced from multi-proxy geochemical analyses in a palaeosol-sediment sequence. Quaternary International.

Zech, M., Zech, R. and Glaser, B., submitted-b. A 240,000-year stable carbon and nitrogen isotope record from a loess-like palaeosol sequence in the Tumara Valley, Northeast Siberia. Chemical Geology.

Zhang, Z., Zhao, M., Lu, H. and Faiia, A., 2003. Lower temperature as the main cause of C_4 plant declines during the glacial periods on the Chinese Loess Plateau. Earth and Planetary Science Letters, 214: 467-481.

Acknowledgements/Dank

Ich danke allen, die mir während meiner Doktorzeit zur Seite standen ganz herzlich. Mein spezieller Dank gilt:

Herrn Prof. Dr. Ludwig Zöller, der mir als Doktorvater die Möglichkeit gab, an der Universität Bayreuth zu promovieren. Seine vorbildliche Betreuung lies mir stets den nötigen Freiraum und sorgte zugleich für motivierenden Ansporn.

Herr Prof. Dr. Bernd Huwe, Herr Prof. Dr. Georg Guggenberger und Herr Prof. Dr. Wulf Amelung leisteten wichtige organisatorische Hilfestellungen und die Arbeiten an ihren Lehrstühlen bzw. ihren Abteilungen trugen wesentlich zur vorliegenden Dissertation bei.

Herr PD. Dr. habil. Bruno Glaser stand jederzeit für fachliche Diskussionen bereit, betreute mich im Labor äußerst engagiert und las mehrere Manuskripte Korrektur. Seine wissenschaftlichen wie menschlichen Qualitäten waren mir stets Vorbild und Stütze.

Die Mitarbeiter/-innen der Lehrstühle Geomorphologie, Bodenphysik und Bodenkunde, namentlich zu nennen sind hier v.a. Frau Gabriele Wittke, Frau Evelin Löbl, Frau Tanja Gonter, Frau Ilse Thaufelder, Frau Martina Haider, Frau Marcela Weiß, Frau Katja Poxleitner, Frau Karin Jeschke, Frau Iris Schmiedinger, Herr Dr. Ludwig Haumaier, Herr Dr. Markus Fuchs, Herr Dr. Ulrich Hambach und Herr Manfred Fischer, ermöglichten es mir in einer äußerst angenehmen Arbeitsatmosphäre an der Universität Bayreuth zu arbeiten. In fruchtbaren Diskussionen halfen sie mir über manche Schwierigkeiten hinweg.

Die Studenten/-innen der „Bodenkunde-Familie", namentlich Claudia Hörold, Christina Brösike, Theresa Wittmann, Leopold Sauheitl, Korbinian Freier, Carsten Prasse und Björn Buggle begleiteten mich auf Höhen und Tiefen und ihnen sei herzlich gedankt für die fachliche wie nichtfachliche Unterstützung.

Meine Geschwister und meine Eltern boten mir Rückhalt in guten wie in schlechten Zeiten. Sie unterstützten mich in meiner beruflichen wie persönlichen Weiterentwicklung wo und wann immer sie konnten.

Überlaß`es der Zeit

Erscheint Dir etwas unerhört,
Bist Du im Herzen tief empört,
Bäume nicht auf, versuch`s nicht im Streit,
Berühr`es nicht, überlaß`es der Zeit.

Am ersten Tag wirst Du Dich feige schelten,
Am zweiten läßt Du Dein Schweigen gelten,
Am Dritten hast Du`s überwunden,
Alles ist wichtig, nur auf Stunden.

Ärger ist Zehren und Lebensvergifter,
Zeit ist Balsam und Friedensstifter.

Theodor Fontane

Declaration/Erklärung

Hiermit erkläre ich, dass ich diese Arbeit selbständig verfasst und keine anderen als die angegebenen Quellen und Hilfsmittel verwendet habe. Ich erkläre ferner, dass ich an keiner anderen Hochschule als der Universität Bayreuth ein Promotionsverfahren begonnen habe.

Bayreuth, Oktober 2006